Development of Graphene-Based Adsorbents for Removal of Heavy Metals from Tannery Effluents

By

Sobur Ahmed

A Dissertation

Submitted to the Dept. of Applied Chemistry and Chemical Engineering

University of Dhaka

in Partial Fulfilment of the Requirements for

the Degree of Doctor of Philosophy

December 2022

DECLARATION

It is hereby declared that this thesis or any part of it has not been submitted elsewhere for the award of any degree or diploma.

Signature of the Candidate

Sobur Ahmed

Registration Number: 25

Session: 2019-2020 (Reregistration)

CERTIFICATION

This is to certify that the thesis entitled "**Development of Graphene-based Adsorbent for Removal of Heavy Metals from Tannery Effluents**" being submitted by Sobur Ahmed, Registration No. 25, Session: 2019-2020, Department of Applied Chemistry and Chemical Engineering, University of Dhaka, in partial fulfillment of the requirement for the degree of Doctor of Philosophy, is an original study of the author carried out under our joint supervisions. No part of this thesis has been submitted before to any other University or institute for the award of any degree or diploma.

Supervisor

(Dr. Md. Nurnabi)
Professor and Chairman
Applied Chemistry and Chemical Engineering
University of Dhaka

Co-Supervisor

(Dr. Md. Zahangir Alam)
Professor
Applied Chemistry and Chemical Engineering
University of Dhaka

Co-Supervisor

(Dr. Tasrina Rabia Choudhury)
Principal Scientific Officer
Atomic Energy Center
Bangladesh Atomic Energy Commission
Dhaka

Dedicated

To

My Beloved Teachers, Parents and Family

Acknowledgement

First, I wish to express my gratitude to the most gracious, merciful Almighty Allah, since without his blessings it would impossible to complete the PhD research work.

Heartiest gratitude goes to my honorable supervisors Professor Dr. Md. Nurnabi, Chairman of the Department of Applied Chemistry and Chemical Engineering, Professor Dr. Md. Zahangir Alam, Department of Applied Chemistry and Chemical Engineering, University of Dhaka and Dr. Tasrina Rabia Choudhury, Principal Scientific Officer, Atomic Energy Center, Bangladesh Atomic Energy Commission, Dhaka for giving me the opportunity, courage and trusts that boosting me to perform this research work. It is a great pleasure to express my sincere and deep gratefulness to them for their immense guidance, information, and practical suggestion to finish this thesis work and to write the dissertation.

I owe my heartfelt thanks to all faculty members of the Department of Applied Chemistry and Chemical Engineering, University of Dhaka, for their lab support and cooperation throughout my research.

My sincere thanks to Professor Dr. Mohammed Mizanur Rahman, Director, Institute of Leather Engineering and Technology, University of Dhaka, for providing incredible support during the completion of this dissertation.

I am very grateful to all the Office staffs, Librarian, Lab personnel specially Mr. Mazharul Islam for their cooperation.

Special thanks to Dr. Dewan Md. Mahmudunnabi, my spouse and daughter for their support and passionate inspiration that helped me to complete this research work.

December, 2022 Author

Abstract

Water, an essential part of the life cycle, is seriously affected during industrial, domestic and agricultural activities. Tannery effluents contain a huge amount of toxic metal ions, organic and inorganic pollutants that pose high risks to the environmental ecosystem and human beings. Heavy metals, which are non-biodegradable and frequently accumulate in the environment, need special consideration among the numerous pollutants found in water since they can cause harm even at low concentrations. Adsorption has outperformed other technologies in terms of efficiency and economic viability, particularly when it comes to removing contaminants from diluted solutions. In this regard, substantial research is being conducted on novel graphene-based adsorbents.

In this framework, the feasibility of using graphene-based adsorbents graphene oxide (GO) and calcium alginate-graphene oxide (CA-GO) composite beads for the removal of chromium(III), copper(ii) and cadmium(II) for the aqueous solution and tannery effluents has been studied.

This thesis is divided into five chapters, such as Chapter 1 (Introduction), Chapter 2 (Literature Review), Chapter 3 (Materials and Method), Chapter 4 (Results and Discussion) and Chapter 5 (Conclusions).

Chapter 1 describes the background, problem statement, objectives, conceptual framework and thesis outlines of the study.

Chapter 2 reviews the literature on water pollution and pollutants, tannery effluents, physicochemical parameters of tannery effluents, heavy metals occurrence in the environment, metal pollutants, different technologies of heavy metal removal and graphene-based adsorbents.

Chapter 3 represents information on the materials which were used in this research. This chapter also represents different methods, equations and models used for the research.

Chapter 4 is related to the main research work and is divided into two parts.

Part 1 narrates the synthesis of graphene oxide (GO), its characterization and its application for the removal of chromium(III), copper(II) and cadmium(II) from aqueous solutions. Here graphite powder was used to prepare GO by modified Hummer's method. The prepared GO was characterized by FTIR, Raman spectroscopy, SEM, XRD, XPS and BET analysis. The adsorption capacity of GO was found to be 366.3 mg/g for Cr(III) at pH 4.0, 193.05 mg/g for Cu(II) at pH 6.0 and 231.48 mg/g for Cd(II) at pH 7.0.

Part 2 describes the preparation, characterization and application of calcium alginate-graphene oxide (CA-GO) composite beads for heavy metals like chromium(III), copper(II) and cadmium(II) removal form an aqueous solution. The CA-GO composite beads were prepared using the ratio of sodium alginate and GO (10:1) and 6% $CaCl_2$ w/w solution. Characterization of CA-GO was carried out by FTIR, SEM, XRD and spectrum analysis. The adsorption capacity of CA-GO is 90.58 mg/g for Cr(III) at pH 4.5, 108.57 mg for Cu(II) at pH 6.0 and 134.77 mg/g for Cd(II) at pH 7.0.

Finally, the conclusion and further scope of work are presented in chapter 5.

From these results, it is realized that the prepared adsorbents showed significant adsorption capacity for heavy metal removal from aqueous solution and tannery effluents.

The distribution of adsorbate (heavy metals) on the adsorbent (GO, CA-GO) surface was explained by Langmuir and Freundlich isotherm models. It was observed that the adsorption was followed both the models, preferably the Langmuir model.

The pseudo-first-order and pseudo-second-order reaction kinetic models were used to analyze the experimental data. Analyzing the kinetic parameters, it was observed that the pseudo-second-order kinetic models contributed better correlation for most of the metals and adsorbents.

The thermodynamic analyses were also carried out for all adsorbents. It was observed that the adsorptions were physical and spontaneous at lower temperatures in most cases.

The regeneration of the used GO and CA-GO composite beads was studied and found that the used adsorbents can be regenerated. The regenerated adsorbents showed significant adsorption capacity for removing heavy metals such as chromium, copper and cadmium from aqueous solution.

Table of Contents

List of Tables

List of Figures

List of Abbreviations

AAS	Atomic Adsorption Spectroscopy
AC	Activated Carbon
BET	Brunauer-Emmett-Teller
BOD	Biochemical Oxygen Demand
CA-GO	Calcium Alginate-Graphene Oxide
COD	Chemical Oxygen Demand
FESEM	Field Emission Scanning Electron Microscopy
FTIR	Fourier Transform Infrared Spectroscopy
ICP-MS	Inductively Coupled Plasma Mass Spectrometry
IUPAC	International Union of Pure and Applied Chemistry
GO	Graphene Oxide
LCA	Low-Cost Adsorbent
SA	Sodium Alginate
SA-GO	Sodium-alginate-GO
SEM	Scanning Electron Microscopy
TDS	Total Dissolved Solids
TSS	Total Suspended Solids
XRD	X-Ray Diffraction
ZPC	Zeta Potential Charge

Chapter 1

Introduction

1.1. Research background

Leather production from animal hides/skins has been one of the oldest manufacturing methods since the beginning of human civilization to meet the demand for garments and foot covering [1, 2]. According to Sundar et al. (2011), the marvelous fiber texture of leather is still unmatched by any other manmade fabrics and other poromeric materials [3]. Moreover, the premium quality of leather and its associated products such as shoes, leather garments, gloves, etc. are unique, very much comfortable, and hygienic to use as daily commodities [4]. As a result, the leather industry has always been an important business sector as well as a source of employment for many countries [3, 5]. Despite having a significant economic contribution, the leather industry is recognized as a potential pollutant-generating industry. In the process of per ton wet salted hides/skins, 500 kg chemicals, 15-50 m^3 water, and 2600-11700 kW energy are consumed that yielding only 200-250 kg finished leather remaining 72 kg chemicals inside and release 600-750 kg of various solid wastes (both tanned and untanned) and 30-35 m^3 effluents [5–7]. These effluents have no further possible application and need proper treatment before discharging them into the environment, as they contain a significant quantity of heavy metals, such as Cr, Cu, Cd, Fe, Pb, etc., colorants, and other organic and inorganic pollutants that create toxicological problems for both environment and living species and decrease the quality of water as well [8, 9]. As a major pollutants toxicity of heavy metals is becoming an issue for ecological, nutritional, and environmental causes. Any metallic elements with high density, which is toxic (non-biodegradable) and poisonous even at low concentration is referred to as “heavy metals” [10]. Tannery effluents contain a various toxic heavy metals, including Cr, Cd, Co, Pb, Ni, Se and As [11]. Moreover, excess water wastage in leather production might cause a higher rate of water consumption and a decrease in groundwater level too, since most of the required water is lifted from underground [12]. Scientists have reported that the disposal of untreated chromium enriched tannery effluents discharged from chrome-tanning and re-chroming operations deposit a notable amount of chromium complexes into water streams which causes river pollution in many parts of the world [13–15]. Tanneries are one of the most extensive users of chromium salts. Ninety percent of the leather industries use chromium as ‘Basic chromium sulfate’ [$Cr(OH)(SO_4)$], a partially neutralized trivalent chromium salt for tanning of leather as chrome-tanned leathers show exceptional shrinkage temperature and few distinctive properties (smooth grain, good elasticity, and resistance to atmospheric

influences) [16]. Previous studies showed that the pickled pelts uptake only 60% of the employed chromium salts and the residual 40% of them remained unreacted and completely discharged with wastewater, ranging between 2656 and 5420 mg/L that is much beyond its threshold limits in both surface water (0.1 mg/L) and industrial effluents (5 mg/L) [17–20]. A substantial quantity of heavy metals, for example chromium, cadmium, copper, iron, lead, barium, etc. are discharged through wastewater during leather production [21]. Scholars observed that the metal loaded tannery effluents are one of the most common routes to introduce chromium after a volcanic eruption, sedimentation, and land filling of industrial sludge from effluent treatment plants. These metal ions are first deposited into soil from leachates and become stable after reacting with organic soil matters/inorganic anions (nitrates and phosphates) and turns into less mobilized species [22]. These species are highly biocompatible and stored into vegetative or reproductive parts of different plant species through bioaccumulation, then can affect human health and even causing mortality during long-term intake of such plants as a daily diet [23–25]. Paul et al. (2013) [7] found that in Bangladesh the estimated amount of originated tannery effluents was 20,000 m^3 per day when the tanneries were densely located at Hazaribagh area and the untreated effluents were directly discharged into the Buriganga river while passing the sewers line that completely destroyed the river ecosystem, reduced its water quality and had lower the living standard of the surrounding areas than satisfactory level. Also, the experimental studies of Alam et al. (2019) [26] and Al-Mizan et al. (2020) [27] have reported that the spatial concentration of chromium was measured in soil resulting in a higher pollution load index (PLI), in groundwater, and in some cultivated vegetables at Hazaribagh which is of beyond level than the prescribed oral reference dosage (Cr(III) 1.5 mg/kg/day, and Cr(VI) 3×10^{-3} mg/kg/day) of daily metal intake by the US Environmental Protection Agency (USEPA) while possessing a significant threat to both carcinogenic and non-carcinogenic health risks, even after several years of tannery relocation from this area. In the previous study, author investigated the metal contents, such as chromium and cadmium in tannery effluents contaminated soil and found that they exceeded the permissible limits (Cr=100 mg/kg Dw and Cd=1.5 mg/kg Dw) recommended by DoE (2015) [28]. Therefore, proper treatment of chromium and other heavy metals containing tannery effluents should be of paramount interest to protect the environment and for the sustainability of this age-old industry [26, 29]. At present, several conventional and advanced wastewater treatment techniques (WWTTs) had been subjected to employ for remediation of toxic metals, proteinous

particulates, refractory wastages (dyes and pigments), and other persistent organic pollutants (phthalates, polyphenols, etc.) from tannery effluents [30]. The methods like ion-exchange, chemical oxidation and reduction, membrane filtration, chemical precipitation, coagulation-flocculation, adsorption, biological treatment, electrochemical methods, etc. were developed for heavy metals removal from wastewater. A majority of those methods required sophisticated equipment and selective components (bacterial/fungal strains, chemical agents), which increase both machine maintenance and effluent treatment expenses, resulting in a promotion of the manifestation for economical and highly effective treatment technologies for the remediation of industrial effluents [31]. Adsorption is considered as the most capable of all WWTTs owing to its operational simplicity, inexpensiveness, noticeable removal capacity of wide-ranged chemicals from a very dilute aqueous solution, and less secondary waste formation [32]. Activated carbons, zeolites, activated alumina, nanomagnetic materials, silica gels, polymeric organic resins (POR), and molecular sieves are some common and market available adsorbents that are used for the detoxification of different industrial effluents [33].

In recent times, graphene and graphene oxide (GO), a novel type of carbon materials has drawn massive interests of research for the treatment of wastewater as they exhibit huge adsorption capability towards different adsorbates. GO, a sheet materials have huge specific surface area and several functional groups, for instance hydroxyl, carbonyl and epoxide, linked to its surface that is just one atom thick [34]. Heavy metals like Cd^{+2}, Co^{+2}, and Pb^{+2} from wastewater can be eliminated by using GO [35–37]. However, the GO is expensive and has some limitation in application as its dispersibility in aqueous media and biotoxicity to human cell. It has also tendency to aggregate in aqueous solution resulting in a reduced surface area which decrease the adsorption capacity. Hence, developing eco-friendly graphene-based adsorbents, such as calcium alginate-graphene oxide composite can be a solution to these problems which will be attractive as well as viable to apply.

1.2. Problem statement

The presence of various emerging contaminants and persistent pollutants at a higher concentration than their minimal acceptance limit causes water pollution that increases the probability of breaking out severe water-borne diseases in different regions of the world.

For this reason, scientific community is very concern for developing low-cost, efficient and eco-friendlier WWTTs for degrading toxic organic pollutants and heavy metals. Although the conventional biological and chemical wastewater treatment methods are vastly employed for large-scale treatment of industrial effluents, these techniques possess certain drawbacks. For example, biological wastewater treatment processes are effective for large-scale treatment effluents containing both organic and inorganic substances, they produce toxic residues/secondary pollutants which requires further sophisticated treatment for decontamination before their disposal.

1.3. Rationale

The availability of pure water is a prime concern for day-to-day activities of human life. Since the world population is increasing at an accelerated rate, the usage of water for drinking and personal hygiene purpose is also augmenting and it may cause fresh water scarcity in future. Besides, the rapid industrial development is also a major reason of excess water consumption and arises a possible risk of water pollution due to generating large amount wastewaters containing pollutants of different chemical nature and concentration. Water pollution is considered as one of the topmost global crises in recent times. The elimination of emerging pollutants like heavy metals is a crucial challenge for the scientific community in case of ensuring pure potable water for all. In the new millennium, extensive research works have been conducted to point out the toxic effect of metals and industrial effluents containing heavy metals discharged from textiles, leather, paint and pigments, electroplating and metal finishing industries. For instance, a significant number of research works showed that chromium can pass through the human cell membranes and degrade to reactive intermediates in presence of human antibody that are capable of decaying DNA structure, some essential biomolecules like proteins and lipids, and can harm the cellular growth and functional characteristics. The Cr^{+3} is 1000 times less toxic, immobilized and corrosive than Cr^{+6} for its less affinity towards hydroxyl ion (-OH). The Cr^{+3} is an indispensable micronutrient for plants growth and human body metabolism. However, accumulation of chromium in edible plants may potentially hazardous for animals and humans. Moreover, the other heavy metals are also toxic for environment and human health. Therefore, in relation to the environmental conservation perspective, heavy metals removal from tannery effluents is very essential in this era.

1.4. Aim and objectives

This research focuses on preparation of graphene-based adsorbent such as GO and calcium alginate-GO hydrogel beads and find out the application and effectiveness of removing chromium, copper and cadmium from tannery effluent. The specific objectives included-

a) Synthesis and characterization of GO and calcium alginate-GO hydrogel beads in terms of various spectrophotometric and physicochemical analyses.
b) Evaluation of the metal adsorption efficiency of GO and calcium alginate-GO hydrogel beads.
c) Study the sorption kinetics, mechanism and thermodynamic effect on adsorption.
d) Examination of compatibility of the prepared adsorbent on metal removal and its regeneration and reuse capability.
e) Application of adsorbent in real tannery effluent sample to remove heavy metals.

1.5. Conceptual framework

Framework of the study is categorized into three main sections. The first one is to synthesis of GO from available commercial graphite flakes.

Secondly, the preparation of Calcium alginate-GO beads adsorbent from GO and standard sodium alginate solution polymerization technique and reacting with $CaCl_2$ solution and characterize the synthesized adsorbent.

Thirdly, the assessment of different adsorption parameters to determine the highest metal removal condition, evaluation of adsorption equilibrium by isothermal study, adsorption kinetics from standard reaction models, adsorption mechanism, and sorption randomness by thermodynamic study, and the compatibility of the adsorbent in terms of metal removal and economic perspective as compared to other adsorbents. The conceptual framework of this research work is shown in Fig. 1.1.

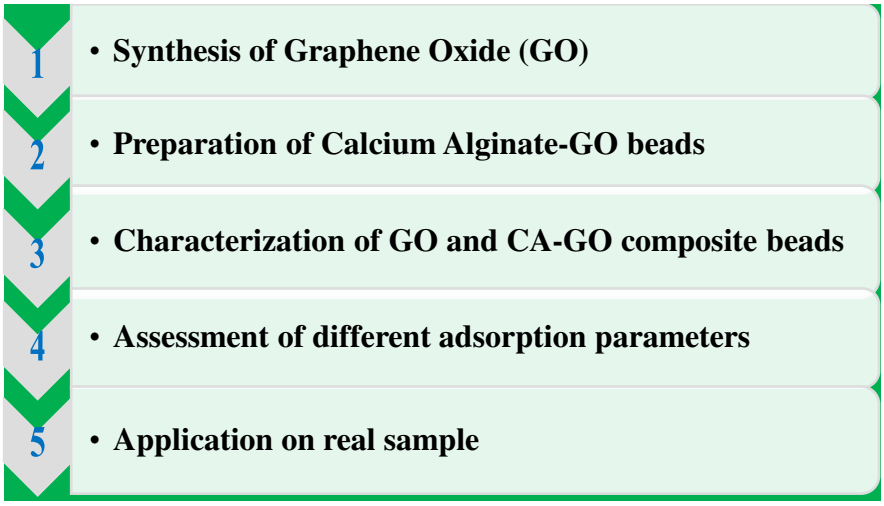

Fig. 1.1: Conceptual framework of the research

1.6. Outline of thesis

This thesis is contained five chapters that facilitate to evident information on the major contributions of this research. Each chapter is demonstrated in such organized format that they contain a general description including own bibliography list.

// **Chapter One** highlights the major environmental problems of tannery effluents including possible public health risks. It also elucidates the problem statement, the rationale, significance, research objectives, and plausible outcomes.

// **Chapter Two** demonstrates the consequences of water pollution in recent times, translocation routes of heavy metals, such as chromium, copper and cadmium into environmental elements, metal contamination in different natural elements, toxicity of heavy metals in different living species, the pros and cons of conventional wastewater treatment methods, implementation of nanotechnology in metal-loaded wastewater treatment, recent advances in graphene-based adsorbents to remove chromium, copper and cadmium from water media including their pros and cons and future prospects based on recently published scholarly articles and related thesis.

// **Chapter Three** briefs about the experimental procedures of this research. It describes the synthesis of calcium alginate-graphene oxide hydrogel bead as adsorbent, characterization of the prepared adsorbents through different spectral and morphological analyses and their instrumentation to narrate its physical, chemical and surface nature. It also ascertains the standardized models and methods to present the adsorption behavior of

calcium alginate-graphene oxide hydrogel bead to remove Cr(III), Cu(II) and Cd(II) from tannery effluents including information on optimized adsorption condition, adsorption kinetics, mechanism and thermodynamic effect at an equilibrium condition.

// **Chapter Four** intends to illustrate the mechanism of bead formation, the physicochemical and morphological characteristics of the prepared adsorbent, the optimization of different influential variables on metal adsorption, the obtained results of the adsorption equilibrium, kinetics, mechanistic, thermodynamic, and feasibility studies.

// **Chapter Five** concludes the summary with major findings of the work. It also demonstrates the limitations, recommendations and future scope of progress in research.

1.7. Expected outcome

It is expected that the GO and CA-GO beads adsorbent will bring about satisfactory result in chromium, copper and cadmium ions adsorption from harmful tannery effluents. If the results of this research would be implemented industrially, the following outcomes could be noticeable-

a) Introduction of prominent and efficient adsorbent for tannery effluent treatment.
b) Reduction of the toxic and hazardous impact of heavy metals like chromium, copper and cadmium on both the environment and human health.
c) Fulfillment of the demand of cost-effective adsorbent material for wastewater treatment.

As a result, tannery will be compliant to buyers and become eco-friendlier that will increase export earnings and accelerate economic development. Additionally, the research will be helpful to achieve the United Nations Organization's (UNO's) sustainable development Goal-6 (Clean water and sanitization), Goal-9 (Industry, innovation and infrastructure) and partially beneficial to attain Goal-14 (Life below water) and Goal-15 (Life on land) for Bangladesh.

Chapter Two

Literature Review

2.1. Water pollution and pollutants

According to World Economic Forum, shortage of pure potable water ranks on top of all global risks which have significant influences on the world's socio-economic context, and ranked eighth on the global risk index (based on sustainability prospects)within the last decades [38]. The United Nations Organizations (UNO) has already announced that the world water supply system will become even scarcer than to date by the year 2050, as in its consequences it will be difficult to provide drinkable water for approximately 9 billion locales (40% of the total world population) in near future which can be a notable barrier to achieve the UNO's Sustainable Development Goal-6 (Clean Water and Sanitation) in many countries [39].

A pollutant is a substance which occurs in the environment due to human activities, and has detrimental effects on the environment. The term pollutant refers to a wide variety of substances that may be carcinogenic, mutagenic, or teratogenic. The two main categories of pollutants are those that have an impact on the physical environment and those that are directly hazardous to organisms, including human beings. Global climate change, desertification, changes in the courses of river basins, reduction in river navigability, seawater invasion, the occurrence of various natural disasters have already taken away a large portion of available water resources [40]. Heavy metals move into food chain by multiple ways allowing them to progressively accumulate over the course of an organism's lifespan and have cumulative harmful effects. Therefore, reliable treatment technologies should be developed for removal of heavy metals like Cr(III), Cu(II) and Cd(II) ion from aqueous media to keep its permissible concentration.

Extensive efforts have been devoted to obtain maximum removal of metal ion from aqueous media. The most common wastewater treatment methods are used for de-contamination of metal-loaded water samples include precipitation, floatation, coagulation, flocculation, ion exchange, membrane filtration, adsorption and so on.

2.2. Tannery effluents

Tannery is the place where animal hides and skins, byproducts of meat industry are processed into leather through a number of mechanical and chemical process, including pre-tanning, tanning and post-tanning (retanning, dyeing, fatliquoring, drying, finishing, etc.) the raw hides and skins with various chemicals, such as sodium hydroxide, calcium

hydroxide, sodium hypochlorite, sodium meta-bi-sulfite, ammonium salts, enzymes, sodium chloride, mineral acid, organic acid, various metallic salts, etc. [41]. In the leather production, wet processing is the most water-intensive and waste generating process [42–44]. In the post-tanning and finishing processes, various organometallic salts, including chromium, cadmium, copper, lead, etc., are widely employed as colorants and mordants to prepare the leather appropriate for their intended use in a variety of products manufacturing [2][45]. Tannery effluent contain a significant quantity of various heavy metals, e.g. Cr, Cu, Cd, Ni, Pb, Ba, As, Fe, etc. [46]. Effluent produced by tanneries causes substantial pollution with high salinity, organic and inorganic materials, soluble and suspended particles, ammonia, organic nitrogen and contaminants including sulfide, chromium, and other harmful metal salt residues [47].

2.3. Physicochemical parameters of tannery effluents

The physicochemical parameters of tannery effluent such as color, odor, pH, Electrical conductivity (EC), Total suspended solid (TSS), Total dissolved solids (TDS), Biological Oxygen Demand (BOD5), Chemical oxygen demand (COD), sulfates and chlorides were determined.

2.3.1. Color

Color was assessed by visual comparison of the sample.

2.3.2. Odor

Half of a wide-mouthed bottle with a stopper was filled with the sample before it was sealed, shaken forcefully for five seconds, and the smell was rapidly assessed. The genuine scent of the sample at the bottle's mouth was noted as either pleasant or objectionable.

2.3.3. pH

The instrument was verified in accordance with the directions after calibration using a buffer solution with a pH that was close to that of the sample. The standard pH value of industrial effluent is 6-9 and 6.5-8.5 according to DoE’97 [48] and ECR’97 [49], respectively. Aquatic ecosystems (fish and plant life) may be at risk of becoming unsustainable if the pH of the surface water deviates too far from the recommended pH range.

2.3.4. Total suspended solid (TSS)

Suspended solids are the amount of insoluble material found in wastewater. When released from the tannery, the insoluble materials generate a variety of issues. Typically, they are composed of solids with two different qualities, such as settleable solids and semi-colloidal solids. Fine protein particles, residues from various chemicals, and reagents that are being released from different effluents are among the settleable solids that are produced at all stages of the beam house process. Additionally, semi-colloidal solids are extremely tiny solids that take a long time to settle out of an effluent. These are typically protein byproducts of operations like liming, vegetable tanning, and retanning that don't directly contribute to sludge problems. Bacterial digestion may take some time to break them down, but they finally settle

2.3.5. Total dissolved solids (TDS)

TDS are all dissolved materials in water other than pure water and suspended solids. It is the total amount of mineral and organic materials dissolved in waste water. Sulfate and chlorides are the two most important pertinent elements in the case of tannery waste water.

2.3.6. Electrical conductivity (EC)

EC is a measurement of a liquid's ability to convey an electric current. The amount of EC rises when water is exposed to pollution because of metal ion contamination.

2.3.7. Biochemical oxygen demand (BOD_5)

The quantity of oxygen in milligram necessary to stabilize 1 liter of effluent biologically at 20°C in five days span is BOD_5. It measures the quantity of soluble oxygen consumed by bacteria in biochemical oxidation of organic matter in the wastewater. Many tannery effluents take longer to degrade; typically, vegetable tanning wastewater has a protracted degradative period that can last up to 20 days. The variety of chemicals used in the production of leather, including as retanning agents, synthetic fat liquors, colors, and leftover keratin-containing proteins, necessitate a longer digestion time. The fact that the waste water components must travel a lengthier distance before breaking down suggests that the environmental impact is dispersed over a longer period of time.

2.3.8. Chemical Oxygen Demand (COD)

The COD indicates the oxygen required in milligram to oxidize or stabilize the chemicals present in 1 liter of effluent under a definite condition. It is a water quality indicator that

calculates how much oxygen is needed to completely oxidize all of the organic and inorganic molecules in a given water body. It represents a value for the chemicals that are not affected by bacterial action, the longer-term biodegradable products, and the effluents that are typically digested in the BOD analysis. Practically, the biodegradability of chemicals used in leather manufacturing processes have an impact on COD value.

2.3.9. Nitrogen (N)

Numerous substances found in tannery effluents have nitrogen as part of their chemical structure. Ammonia produced by deliming agents and nitrogen found in proteinaceous materials from unhairing processes are the most common compounds.

2.3.10. Sulfides (S^{2-})

The main causes of the sulfide concentration in tannery effluent is the unhairing process, where sodium sulfide or hydrosulfide is used.

2.3.11. Neutral salts (chlorides, Cl^-, and sulfates, SO_4^{2-})

In order to preserve raw hides and skins or during the pickling process, which introduces sodium chloride into the body, large quantities of ordinary salt are typically utilized. Since they are highly soluble, persistent, and unaffected by effluent treatment or nature, they continue to be a burden on the environment. Additionally, sulfates are produced when sulfuric acid is used or when compounds with a high sulfate content are used. For instance, several artificial tanning treatments and chrome tanning powder both contain high levels of sulfate. These sulfates can be precipitated by calcium-containing substances by producing the poorly soluble calcium sulfate.

2.3.12. Natural oil and grease

Natural oil and grease are released from the hide or skin during beam house processes. However, some fatty compounds may mix with wastewater as a result of synthetic fat liquor's low absorption during the fat liquoring process. These fats, oils, and greases congregate to form floating layers, which bind other substances and cause blockages, especially in effluent treatment plants.

2.4. Heavy metals occurrence in environment

Heavy metals belongs to the cluster of trace elements with a high specific gravity (higher than 5) and atomic weights between 63.5 and 200.6 [50, 51]. The term “heavy metals” is now referred to hazardous metallic elements and metalloids those are detrimental to the human beings and environment. Some metalloids as well as lighter metals including selenium, arsenic, and aluminum, are poisonous. While some heavy metals, such as gold, are not harmful, they are referred to be heavy metals [52]. By any authoritative organization like the IUPAC (International Union of Pure and Applied Chemistry), has not defined “heavy metal” yet. Its interpretations have been varied so widely by many authors that it is essentially meaningless. To further describe the possible toxicity of metallic elements and their derivatives, the word "bioavailability" can be used. The physicochemical characteristics of metallic elements, their ions, and their compounds affect bioavailability, as do biological factors. These in turn depend on how the metallic elements are arranged atomically [53]. Based on their function in biological systems, heavy metals are divided into two categories: essential and non-essential. For their growth, development and physiological processes living organisms need essential heavy metals such as Fe, Mn, Ni and Zn, however they don’t need non-essential heavy metals such as Cd, Pb, Hg and As [54]. Chromium, copper, cadmium, zinc, arsenic, mercury and other heavy metals are the major pollutants of water which can come from both sources of anthropogenic and natural. As they are non-biodegradable, and tend contamination of living things, endangering human health by impeding growth and development, harming the nervous system, destroying various organs, causing cancer and even death at low concentrations [55–57]. Despite their substantial contribution to economic growth and employment, tanneries have been identified as a potential source of heavy metal burden to the environment [20].

2.5. Metal pollutants

Metal pollutant is one of the most harmful and persistent pollutant in aquatic environment. Metal ions can be concentrated in aquatic species to a point where it impacts their physiological status and can be assimilated into food chains. Due to their non-biodegradability, toxicity, and ability to cause cancer in living organisms, several metal ions are classified as priority pollutants [58–60]. When treating industrial wastewaters, it

is especially important to pay attention to toxic elements like mercury, lead, iron, cadmium, nickel, copper, chromium, and zinc.

The description of few harmful metals is mentioned below.

2.5.1. Chromium

Chromium is naturally occurring element with multiple valence states out of which trivalent form is most stable and can be found naturally in ores like ferrochromite. The second most stable state is the hexavalent form, and Cr(0) is not naturally occurring element. The chromium compounds are brightly colored. It is a brittle, hard, glossy metal having 1907ºC melting point, 2672ºC boiling point and density of 7.19 g/cm^3 at 20ºC that takes a high polish and resists tarnishing [61]. Chromium is the 21st supreme prevalent metal in the earth's mantle, ranging from 100 to 140 mg/kg [62, 63]. A variety of anthropogenic and natural sources, with industrial operations being the primary source of emission. Metal processing, leather processing, chromate manufacturing, stainless steel welding, and ferrochrome and chrome pigments producing industries contribute most to release chromium. Chromium emission into the air and wastewater, primarily from the metallurgical, refractory, and chemical sectors, has been connected to a rise in the amounts of the metal in the environment. The toxicity of chromium varies depending on its oxidation state, ranging from the low toxicity metal form to high toxicity hexavalent form. As atmospheric oxygen passivates pure chromium, it has a strong propensity to combine with it, generating a thin coating of protective oxide on its surface that shields the underlying metal from oxidation [63, 64]. The characteristics of chromium, which define its toxicity and environmental impact, are influenced by its valence state and that of its compounds. Only hexavalent chromium compounds are biologically active and create skin irritation, mutagenesis, and cancer, However, trivalent compounds and metallic chromium do not have these risky characteristics [65–67]. Due to its greater water solubility and mobility, hexavalent chromium is 1,000 times more hazardous than trivalent chromium [20, 68]. However, high concentration of chromium(III) ions can affect significantly on the ecosystem [69, 70].

Chromium is widely used in many industrial processes, and thus many environmental systems are contaminated by it [71]. Commercial uses for chromium compounds include welding, chrome plating, colourants, tanning, etc. Chromium is also utilized as an

anticorrosive in boilers and cooking apparatus [72]. A plenty of trivalent chromium discharged from chrome tanning and retanning process into the tannery effluent.

2.5.2. Copper

The ductile metal copper has a melting point at 1083ºC, outstanding electrical conductivity (59.6 x 10^6 S/m), and a density of 8.93 gm/cc at 20ºC. Orange-red coloured pure copper is turned to reddish tan colour when it exposed to air. Copper with oxidation states of +1 and +2 can create a huge variety of compounds, either binary or coordination compounds with ligands [73]. Copper is extensively used in industrial processes (copper/brass plating, leather and textile dyeing, petroleum, paper, rayon manufacturing, etc.) and in agriculture as fungicides [74, 75]. As a result, waste water contains a significant quantity of copper, mostly in the form of Cu(II), which is soluble can bio-accumulate and enter the food web [76]. Copper is a micronutrient for metabolism of human body, however excess dosage can cause of serious toxicological concerns, even death due to anemia, intestinal disorder, stomach disorder, damage of kidney and liver [77].

2.5.3. Cadmium

Cadmium is a divalent metal which is soft, malleable, ductile, bluish-white in colour, glossy and tarnishable. It has a melting point of 321ºC and a density of 8.65 gm/cc at 20ºC. The principal oxidation state of cadmium is +2, which is a minor component of the majority of zinc ores. In the creation of plastic, batteries, pigments, and corrosion-resistant plating, cadmium is widely employed. Excessive of cadmium is kidney dysfunction, carcinogenic and even causes of death [51, 78].

2.5.4. Nickel

Silvery-white coloured hard, ductile and malleable nickel has a melting point at 1453ºC and a density of 8.91 gm/cc at 20ºC. Nickel's most prevalent oxidation state is +2, which may combine with nearly all anions to generate compounds including hydroxide, carboxylates, carbonate, sulfide, sulfate and halides. The major applications of nickel is in alloy formation, metal finishing, battery production, welding, as a catalyst and in the glass and ceramics industries [79]. Nickel exposure can occur through the air to breath, water to drink, food to eat and cigarettes smoking. Excess intake of nickel can lead to serious problems in lungs, kidneys, gastrointestinal distress, pulmonary fibrosis and skin dermatitis though a small quantity is essential [80].

2.5.5. Lead

Lead is a volatile, soft, ductile and malleable metal with a melting point of 327ºC and density of 11.34 gm/cc at 20ºC. Among all of the stable elements, it is the heaviest non-radioactive element. Lead is found naturally in mineral deposits. Out of three (0, +2 and +4), Pb^{+2} is the most reactive and prevalent in nature. It is generally used as pigments, ceramics glazers, organ pipes, building materials, ammunition, paints, gasoline additives, acid storage batteries, cosmetics (lipsticks, face powder, mascara, etc.). Due to widespread use of lead, people are frequently exposed to it through their food, water and respiration [81].

2.6. Technologies of heavy metal removal

There are a number of treatment approaches that were developed to safeguard environmental safety, and this field of study has become crucial. Methods for removing heavy metals that are more demanding and dependable include ion exchange, precipitation, filtration, electrodialysis, microbiological systems, electrochemical process, advanced oxidation, membrane bioreactors, adsorption, etc. All these methods are broadly categorized as physical, chemical, and biological [82]. However, on the basis of type of heavy metals the procedures of treatment are selected. Every technique has some merits and demerits. Sometime heavy metal removal requires the sequential application of a number of procedures for effective treatment.

A few common methodologies for wastewater treatment are mentioned briefly-

2.6.1. Sedimentation

Sedimentation is the method of allowing particles in suspension media to settle out of the suspension under the effect of gravity. As a primary treatment, sedimentation is used to separate suspended particles from municipal and industrial wastewater [83]. Chemical flocculants, sedimentation basins and clarifiers are used to improve gravity settling of suspended particles.

2.6.2. Filtration

Filtration is a physical process to trap the solid and allows the fluid to pass through using a filter medium for separating solids from liquids or gases. Some popular filtering techniques such as membrane filtration, microfiltration, ultrafiltration, nanofiltration,

reverse osmosis, etc. are used in water treatment. Ultrafiltration and nanofiltration are more effective over microfiltration due to its pore size [83]. Reverse osmosis is an effective filtration technique which is impermeable to most of the contaminants. The RO membrane has pores that are between 0.1 and 1.0 nm in size. Reverse osmosis is being used today for removal of heavy metals from wastewater.

2.6.3. Coagulation and flocculation

The heavy metal precipitation into low solubility molecules such as carbonates, sulfides, and hydroxides is currently treated in this way as an alternative [84]. A colloid cannot be settled down due to the low-density equivalent to that of water. Coagulation treatment techniques are used to either raise the density or remove such colloidal particles. The type of coagulant, the dosage, pH, temperature, alkalinity, and mixing conditions all affect how well a substance clots. Inorganic flocculants such as poly ferric chloride and poly aluminum chloride, as well as $Al_2(SO_4)_3$, $Fe_2(SO_4)_3$, and $FeCl_3$ [85] and their derivatives were used in this process as chemical agents. The addition of flocculants causes the destabilized particles to clump together into bigger particles through mixing or stirring. To separate these larger particles, flotation, filtering, or stretching are used. A novel class of macromolecule flocculants called mercaptoacetyl that can be able to eliminate heavy metals along with turbidity [86]. Heavy metal complexes can be removed using polyelectrolyte flocculation following centrifugation and filtering [51]. Additional treatment methods including precipitation and spontaneous reduction must be used in addition to the coagulation or flocculation process. A combination procedure (e.g. spontaneous reduction-coagulation) is used to minimize copper and zinc ions effectively for different concentrations [87]. Nanoparticles have the capacity to precipitate colloids that are already present in the surface water, in accordance with the Smoluchowski coagulation theory [88]. As a type of nano-coagulant, silver nanoparticles, can deposit heavy metals and reduce TOC in wastewater [88]. Sludge forms during the coagulation process due to the large amounts of sediment flocks and the use of coagulants such alum, iron, etc. Heavy metals like cadmium, chromium, nickel, lead, and zinc are present in the sludge created by the coagulation process and for managing sludge different methods such as recovery, recycling, and reuse are exploited [89]. Though flocculation and coagulation are effective at removing heavy metals from wastewater, they can also produce secondary pollutants including flocks and low-reusable chemical solvents that are toxic to both people and the environment. The main disadvantages of the process is the large quantity

concentrated sludge [90]. Moreover, the control of coagulant dosage is very important and the process is very pH dependent [91].

2.6.4. Ion exchange

Ion exchange is a method of separation that successfully eliminates metal from wastewater by replacing one type of ion with another. In a chemical reaction that may be stopped, an ion from a solution is exchanged for an equivalently charged ion attached to an immobile solid particle. This method produces less sludge than coagulation procedure [92]. Metals can be recovered or eliminated using ion exchange resin. Ion exchange and adsorption have many similarities when it comes to their use in batch and fixed bed processes to produce high-quality water. A variety of heavy metals can be removed from wastewater using this procedure quite well. Regeneration operations make it simple to recover and reuse the used resin. The ions exchanged are not chemically altered as it is a physical separation process [93].

Ion exchange has several drawbacks in treating heavy metals containing wastewater. Appropriate pretreatment systems are required before ion exchange, e.g., removal of suspended solid from waste water. Additionally, not all heavy metals can currently be treated with effective ion exchange resins [94].

2.6.5. Chemical precipitation

Heavy metals can be removed from effluents cheaply and effectively via chemical precipitation, which transferred the component in solution into insoluble form. The solution pH is changed by addition of chemicals for precipitation of metals and preventing the precipitate from dissolving in the solution [95]. This approach can be used with wastewater that contains a lot of heavy metals. The theoretical mechanism for removal of heavy metal by chemical precipitation is shown in the following equation [55].

$$M^{2+} + 2(OH)^{-} = M(OH)^{-}$$

To remove the precipitates from treated water, additional procedures like sedimentation and filtration is required. To attain acceptable amounts of metals in discharged effluents, a significant amount of chemicals needed. Due of their simplicity and affordability, they are typically used in industrial scale. The substantial amount of precipitant containing sludge needs further treatment to prevent long-term environmental effects of sludge disposal. Generally, hydroxide precipitation and sulfide precipitation are used as chemical precipitation process. Although sulfide precipitation is a more effective method for the

treatment of industrial waste containing highly hazardous heavy metals, lime and calcium carbonate are still used as precipitant agents. Some metals can be effectively precipitated even at very low pH values, and a high degree of metal removal can be achieved throughout a wide pH range with a quick reaction [96].

However, there are significant drawbacks to chemical precipitation, such as the sizeable sludge disposal and chemical requirements to bring metals down to a safe level for discharge. The presence of these compounds must also be considered while performing the posttreatment of sludge since they precipitate metals as well as raise the cost of process [94].

2.6.6. Electrochemical process

Electrochemical process can be used together with other techniques to remove heavy metals from aqueous media. Electrochemical separation technique is categorized in three types, namely electro-sorption, electrocoagulation and electrodialysis [97]. In electrocoagulation process electricity is used instead of chemical coagulants. The anode becomes oxidized and releases metal ions into the system when electricity is exposed to electrodes. Several studies opined that the electrocoagulation method is effective for complete elimination of metal like arsenic [98–100]. Electrodialysis is the process of removing ions by the utilization of selective ion or semipermeable membranes while being influenced by an electric field [101, 102].

2.6.7. Ultrafiltration

Based on their molecular size of pollutant, this method employs a membrane to filter out heavy metal ions, dissolved molecules, and other contaminants. Some of the membranes prevent the passage of larger molecules and heavy metals, thus they must be sorted out. Only low molecular solutes are permitted to pass through these membranes. Additionally, it has been broken down into subcategories such complexation-ultrafiltration [103], micellar enhanced ultrafiltration [104], and chelating enhanced ultrafiltration [105].

2.6.8. Nanofiltration

Pressure-driven approach, employed in a variety of chemical and biotech sectors, is extremely reliable. It is an intermediate technique utilized between reverse osmosis and ultrafiltration [82]. Nanofiltration has several advantages over reverse osmosis, including low energy consumption, effectiveness in removing heavy metals, simplicity of usage, and lower pressure requirements [88]. Numerous variables, such as pH, pressure, temperature,

membrane propensity, membrane structure, and feed concentration, have an impact on nanofiltration effectiveness [107]. Surface charges on synthetic polymers used to make membranes for the nanofiltration process are frequently positive or negative due to the membrane's electrostatic interaction with metal ions, this feature aids in the dissociation of heavy metals or enhances membrane functionality. The separation mechanisms employed in nanofiltration are size exclusion and charge exclusion [106].

2.6.9. Reverse osmosis

The principles of size exclusion and charge exclusion determine how reverse osmosis (RO) works. A semi-permeable membrane is used which only allows water to go through to remove dissolved species [92]. A RO membrane has pores that are between 0.1 to 1.0 nm and frequently used in the desalination procedure. Reverse osmosis is increasingly being used in wastewater applications to remove heavy metals. This procedure' primary flaw is that it uses a lot of energy to run. Several RO membrane experiments were conducted to recycle or treat the wastewater from electroplating. The material of the membrane, the pH, the temperature, the pressure, and the membrane's propensity for clogging all affect the capacity of the RO membrane [107].

2.6.10. Biological treatment

The most common and widely used method for removing metal ions and discolouring wastewater is biological treatment [108] as it is both affordable and results in benign byproducts. The process could be aerobic (with oxygen present), anaerobic (without oxygen present), or a combination of the two. In order to remediate wastewater, microorganisms like bacteria, fungus, and yeast are frequently used. Bacillus cereus [109], Pseudomonas aeruginosa [110], and Escherichia coli [111] are examples of metal-bearing bacteria that exhibit very impressive biosorption abilities to metal ions.

2.6.11. Adsorption process

Adsorption is the most popular method for treating heavy metal contaminated wastewater [112]. It is a cost effective and efficient treatment approach with flexibility in design and operation. After a sufficient desorption procedure, the utilized adsorbents can be regenerate and reused because most adsorption is reversible. Adsorption is the process of transferring significant amounts of chemicals from a liquid or gaseous state to a solid surface, where they subsequently bind and/or interact chemically [95]. It is a method where molecules leave the solution and then connect physically and chemically to the

surface of the adsorbent. After a sufficient desorption procedure, the utilized adsorbents can be regenerate and reused because most adsorption is reversible. Adsorption is the process of transferring significant amounts of chemicals from a liquid or gaseous state to a solid surface, where they subsequently bind and/or interact chemically [95]. It is a mechanism where molecules leave the solution and thereby get attached to the surface of adsorbent through physical and chemical bonding [113]. Adsorption and absorption are different process because adsorption is based on surface area whereas, absorption is based on volume.

Adsorption is the process by which particles from a gas, liquid, or dissolved solid attach to a surface as atoms, ions, or molecules. The adsorbate forms a coating on the adsorbent's surface as a result of this activity. Adsorption efficiency is determined by the adsorbent's surface area, surface shape, pore size distribution, polarity, and functional groups attached to the adsorbent surface. For an adsorbent to be economically viable, it must possess a number of characteristics, including high selectivity to enable quick separations, excellent transport and kinetic properties, thermal and chemical stability, mechanical strength, resistance to fouling, regeneration capacity, and low solubility in the contact liquid. Compared to traditional techniques of heavy metal removal, the adsorption process has a number of benefits. Adsorption process is economical, regenerative, metal selective, and effective that does not produce hazardous sludge and can recovers of metal. Due to its ease of application and low cost, adsorption is currently regarded as being particularly suited for wastewater treatment [114–116]. Since occasionally adsorption is reversed, adsorbents can be regenerated by appropriate desorption [51]. There are two categories adsorption:

1. Physiosorption: Physical adsorption or physiosorption is used to define an adsorption in which the attraction between the molecules adsorbed and the solid surface is of a physical nature. Physical adsorption is widely used to describe the weak attractive interactions known as van der Waals forces, which cause reversible adsorption between the molecules and the solid surface.
2. Chemisorption: The adsorption process is known as chemisorption if the attraction force is brought about by chemical bonding. It is difficult to remove species that have been chemisorbed from solid surfaces because of their increased propensity for chemisorption.

2.6.11.1. Influencing factors of adsorption

The quantity of solution is adsorbed on a solid surface depends on the nature of the adsorbent and adsorbate, their interface, the temperature of the framework, the concentration, the pH of the arrangement, the porosity of the adsorbent, the time period allowed, and the method used for the frameworks.

Adsorbent's nature:

The chemical makeup, the presence of pores, edges, corners, creaks, and pretreatment are the main determinants of an adsorbent's nature. In general, adsorption capacity increased as the surface area of the adsorbent increased. As a result, an adsorbent's surface that is more uneven or rough has a higher adsorption capacity.

Adsorbate's (solvent's) nature:

Solubility has played a vital role within the study of surface adsorption. Solvent with slightly soluble adsorbate is more adsorbable than the highly soluble ones.

Adsorbent particle size:

Smaller molecules have less internal resistance to mass transfer and diffusion, allowing the adsorbate to almost completely fill the adsorbent's capacity for adsorption. Higher adsorption rates are provided by the smaller molecular size of the adsorbent [118].

Solute affinity for the adsorbent:

The surface of a slightly polar adsorbent can now absorb non-polar molecules more readily than polar ones [118].

Effect of dosage:

In order to bind metal ions more active sites are available at higher adsorbent concentrations since more exchangeable sites for the ions are offered [117].

Influence of temperature:

Generally, a lower temperature facilitates better adsorption rate, i.e., the general exothermic process. Increasing temperature promotes adsorption in some particular cases. The temperature of the adsorption system boosts the intermolecular interactions between the water molecules adsorbed at the interlayer portion, resulting in greater adsorption in some cases. However, in some circumstances, adsorption decreases with as the temperature increases [117].

2.6.11.2. Activated carbon

Activated carbon (AC) is a popular adsorbent worldwide for heavy metals removal from aqueous media. Typically, it is made from materials like coal, wood, lignite, coconut shells, etc. that have a particularly porous structure and a huge surface area between 500 and 2000 m^2/g [118]. AC is rich in micropores (<2 nm) and mesopores (2-50 nm) with high surface area and surface activity which remove hazardous materials for wastewater [119]. AC can be used both in chemical and physical adsorption.

Numerous scientists were used activated carbon to remove heavy metals from aqueous solutions, a few are mentioned below-

Table 2.1: Heavy metal adsorption capacities of activated carbon from various sources

Name of adsorbent	Metal ions	Parameters studied	Capacity of adsorption (mg/g)	References
Activated carbon fabric cloth (ACF)	Cr^{+3}	Temperature, particle size, pH, adsorbent dosage	40.29	[120]
Activated carbon from date seeds	Cr^{+6}	pH, time, dosage, temperature, and concentration	44.05	[120]
Commercial activated carbon (CAC)	Pb^{2+}	pH, contact time, and temperature	42.50	[121]
	Cu^{2+}		15.00	
	Zn^{2+}		14.00	
Tire-derived activated carbon (TAC)	Pb^{2+}		322.50	
	Cu^{2+}		185.20	
	Zn^{2+}		71.90	
Activated carbon from poly sulfide rubber	Cr^{+6}	pH, dosage, contact time	8.92	[122]

Activated charcoal of neem leaf powder (AC-NLP)	Pb	Adsorbent dosage, temperature and contact time	205.00	[123]
	Cr		110.90	
	Cu		185.80	
	Cd		157.50	
	Zn		133.30	
	Ni		120.60	
Olive stones activated	Cu^{+2}	pH, contact time, dosage	17.66	[124]
	Cd^{+2}		57.09	
	Pb^{+2}		147.52	
Iron oxide/activated carbon (Fe_3O_4/AC)	Cr^{+2}	-	8.06	[125]
	Cu^{+2}		3.20	
	Cd^{+2}		2.15	
Char of peanut straw	Cr^{+3}	pH, contact time, metal ion concentration	0.48	[126]
Char of soybean straw			0.33	
Char of rice straw			0.27	
Char of canola straw			0.28	
Fruit peel litchi	Cr^{+6}	Temperature, concentration, time, pH	50.00	[127]
Ficus natalensis fruits (FNF)	Cu^{+2}	pH, dosage, contact time, temperature, initial concentration	161.29	[128]
	Pb^{+2}		1250	

2.6.11.3. Low-cost adsorbents (LCAs)

The low cost economical adsorbents use to remove heavy metals is more encouraging as there are numerous readily available materials that are less expensive, re-generable after use, environmentally friendly, and useful over a wide pH range [129–131]. These

materials can be either natural or waste products or by-products of industrial, agricultural, biological, and domestic activities. Many researchers have adopted and reported in the literature a variety of research for the creation, usage, and applications of economical cost-effective adsorbents to remove different contaminants from aqueous and industrial wastes. The following list of LCAs is employed, along with a description of their adsorption capacities.

Table 2.2: Heavy metal adsorption capacity of low-cost materials metals from wastewater

Name of adsorbents	Metals ions	Capacity of adsorption (mg/g)	References
Natural rice husk	Cr^{+3}	22.5	[132]
Natural rice husk	Cu^{+2}	7.1	[133]
Natural rice husk	Cu^{+2}	30.0	[132]
Wheat straw	Cu^{+2}	11.43	[134]
Wheat straw (Urea modified)	Cd^{+2}	39.22	[135]
Barley straw	Cu^{+2}	4.64	[136]
	Pb^{+2}	23.2	
Mango peel	Cd^{+2}	68.92	[137]
	Cu^{+2}	46.09	[138]
Orange peel (nitric acid modified)	Cd^{+2}	13.7	[139]
	Cu^{+2}	15.27	
Banana peel	Cd^{+2}	35.52	[140]
Potato peel	Cr^{+3}	38.46	[141]
Thermally activated potato peel	Cu^{+2}	84.74	[142]
Sulfuric acid modified sugarcane bagasse	Cd^{+2}	38.03	[143]
Corn stalk (copolymerization grafted)	Cd^{+2}	21.37	[144]
Sunflower stalk	Cd^{+2}	69.80	[145]
Cashew nut shell	Cd^{+2}	22.11	[146]

Chemically modified (NaOH treated) cashew nut shell (*Anacardium occidentale*)	Cd^{+2}	47.505	[147]
	Cr^{+3}	42.68	
Oil palm shell	Cu^{+2}	1.75	[148]
Fish scale	Cr^{+3}	18.35	[149]
Lentil	Cu^{+2}	9.59	[150]
Rice		2.95	
Wheat		17.42	
Acacia leucocephala	Cd^{+2}	147.1	[151]
	Cu^{+2}	167.7	
Cauliflower waste	Cd^{+2}	21.32	[152]
Carrot residue (CR)	Cr^{+3}	45.09	[153]
	Cu^{+2}	32.74	
	Zn^{+2}	29.61	
Cassava peelings (mercapto acetic acid modified)	Cd^{+2}	119.6	[154]
	Cu^{+2}	127.3	
Sawdust (modified)	Cr^{+6}	8.84	[155]
Saw dust (sodium hydroxide treated)	Cd^{+2}	73.62	[156]
Wheat bran	Cd^{+2}	15.71	[157]
Eggshell	Cr^{+3}	160	[158]
Eggshell	Cd^{+2}	329	[159]
Illitic clay	Cr^{+3}	46.44	[160]
Eggshell waste	Cu^{+2}	142.86	[161]
	Cd^{+2}	111.1	
Chitosan beads	Cr^{+3}	30.03	[162]
	Cr^{+6}	76.92	
Coal fly ash	Cu^{+2}	20.92	[163]
	Cd^{+2}	18.98	
Treated waste newspaper (TWNP)	Cr^{+6}	59.88	[164]

2.7. Graphene based adsorbents

Graphene is one atom thick sheet of graphite in a 2-dimentional plane of densely packed sp^2 hybridized carbon atoms organized in a hexagonal configuration. Graphene emerged as a 'miracle material' being integrated worldwide in electronics, drug delivery, energy storage, bio-sensing, filtration, etc. due to its extraordinary physico-chemical properties [165]. However, the use of graphene-based adsorbents for heavy metal removal from tannery effluents is quiet an emerging area of application.

Owing to having excellent theoretical surface area (2630 m^2/g) as well as controllable surface functionality with various groups like hydroxyl, epoxy, and carboxylic that facilitate adsorption capacity, graphene is an exciting candidate to be utilized as an adsorbent [166–168]. The surface of graphene needs to be functionalized enabling them to interact with various component in order to formation of graphene-based composites. The most common graphene derivative is graphene oxide (GO), contain an innumerable oxygen functionality including hydroxyl, carbonyl and carboxyl groups that give the carbon surface a negative charge. As a result, GO can be utilized to bind divalent heavy metals including Cu, Pb, Cd and Zn from water forming coordination and electrostatic interactions [169, 170]. Since oxygen-containing functional groups (C-O, C=O, and -OH) induce structural flaws in GO, it is highly hydrophilic and may disperse in a variety of solvents, including water [171–176].

Graphene oxide is a layered structural material where hydrogen and epoxy groups are connected to the surface of it [177]. The swelling, intercalating and ion exchanging features of the dispersion are caused by the associated hydrophilic polar groups, which also increase the dispersibility of graphene oxide in aqueous media [177, 178]. Graphene oxide's huge surface area also offers the ability to achieve high adsorption abilities using both electrostatic and coordinate methods [179]. According to previous studies, graphene oxide is an excellent adsorbent of Pb^{2+}, Hg^{2+}, Co^{2+} and Ni^{2+} [180–183]. To further improve their capacity for adsorption, graphene oxide was decorated with a number of functional groups, including chitosan [184], amino [185], poly(N-vinyl carbazole) [186], 4-aminothiophenol and 3-aminopropyltriethoxysilane [187]. The heavy metals removal capacity of graphene and graphene-based adsorbents had been studied by many researchers. A few of them are discussed below:

Chang and co-workers [188] described how graphene adsorb Co(II) and Fe(II) from water. Adsorption was inspected by batch mode and graphene demonstrated excellent adsorption capacities of 370.00 and 299.30 mg/g for Fe^{+2} and Co^{+2}, respectively.

The ability of graphene oxide (GO) to adsorb Cu^{+2} from aqueous solution was examined by Wu and co-workers [189]. The optimal parameters for Cu(II) adsorption by GO in a batch mode were dosage of 1.0 mg/mL, pH 5.3 and contact duration of 150 min. The adsorption of Cu^{+2} on GO was found 117.50 mg/g and the equilibrium data was completely matched to Freundlich isotherm.

Zhang et al. [190] experimented on adsorption behavior of prepared graphene oxide/polyamidoamine dendrimers (GO/PAMAMs) for divalent metal ions and found the adsorption capacity were 568.18, 253.81, 68.68 and 18.29 mg/g for Pb, Cd, Cu, and Mn, respectively. The equilibrium adsorption was 60 min and the sorption was chemical in nature.

Sitko et al. [169] worked on the usage of GO to remove Cu^{+2}, Cd^{+2}, Zn^{+2}, and Pb^{+2}, those were displayed in the following sequences in one metal arrangement: $Pb^{+2} > Cd^{+2} > Zn^{+2} > Cu^{+2}$ and in two metal arrangements: $Pb^{+2} > Cu^{+2} > Cd^{+2} > Zn^{+2}$. The adsorption kinetic data revealed that monolayer adsorption was carried out and chemisorption process was also defined.

Wang et al. [191] used GO to remove Zn(II) ions in water that varied in dosage, pH, and amount. The data followed pseudo-second-order kinetics and Langmuir isotherms. Adsorption capacity of Zn(II) was 246.0 mg/g at 293 K, which was praiseworthy with quick exothermic adsorption.

A comparison was studied by White and co-worker [192] on GO and functionalized GO (GO-COOH) nanoparticles for Cu(II) adsorption. The adsorption capacity of GO and GO-COOH were found maximum as 277.77 and 357.14 mg/g, respectively and the data were matched well with Langmuir isotherm for both cases. Removal efficiencies was found to be 97 and 99.4%, respectively at pH 6.0, and 60 min duration.

Chang et al. [193] synthesized magnetic core-shell $MnFe_2O_4@TiO_2$ nanoparticles on RGO ($MnFe_2O_4@TiO_2$.rGO) and found the maximum adsorption of Cu^{+2} as 225.99 mg/g. Langmuir isotherm and pseudo-second-order kinetic model were followed. The nature of adsorption was spontaneous, chemisorption and endothermic. The adsorbent can be recycled several times using simple external magnetic field.

GO aerogels were developed by Mi and co-worker [177] for removal of Cu^{+2} from aqueous solution. The GO aerogel had lots of oxygen atoms with certain groups and was thus an excellent adsorbent. A quick adsorption rate was found by GO aerogel ranging from 17.73 mg/g at 283 K to 29.59 mg/g at 313 K, which was dependent on pH and concentrations. Based on pseudo-second-order data the adsorption was occurred through chemisorption.

Ahmed et al. [194] studied on removal Cr(III) from tanning through adsorption on GO. The results were demonstrated that treating chrome tanning effluent with 0.6 mg/L GO at pH 4.0 for 20 min could attain 98.77% chromium removal. The maximum capacity was found 366.3 mg/g and equilibrium was followed both the Langmuir and Freundlich isotherms. Thermodynamically it was exothermic and spontaneous at low temperature and followed well pseudo-second-order kinetics.

Mondal and Chakraborty [20] worked on adsorption of Cr^{+6} on GO and found the adsorption capacity 1.222g/g and was fitted with Langmuir isotherm model. Thermodynamics showed the process was spontaneous, endothermic, and entropy-driven.

Use of GO nano-sheets for Cd^{+2} and Co^{+2} adsorption was described by Zhao et at. [37]. It was followed Langmuir isotherm due to monolayer adsorption with 106.3 and 68.2 mg/g for Cd^{+2} and Co^{+2} at pH 6.0. Thermodynamic parameters denoted the process as spontaneous and endothermic in nature.

Tan et al. [197] studied the maximal adsorption capacities for Cu(II), Cd(II), and Ni(II) onto GO membranes from single metal aqueous solutions were found to be 72.6, 83.8, and 62.3 mg/g, respectively. The Langmuir isotherm model and the pseudo-second-order model was maintained for the adsorption process. Within a short period of time, the adsorption equilibrium was reached. Based on the adsorption/desorption cycles, the GO membranes could be regenerated several times with just a minor reduction in adsorption capacity.

Chapter 3

Materials and Methods

3.1. Materials

Chromium sulfate ($Cr_2(SO_4)_3.6H_2O$), Copper chloride ($CuCl_2.2H_2O$) and cadmium sulfate ($3CdSO_4.8H_2O$) were collected from Merck, India and used to prepare the standard solution of Cr(III), Cu(II) and Cd(II). Graphite powder (99.5%, Merck, India), Sulfuric acid (98%, RCI Labscan, Thailand), Hydrogen peroxide (30%, Merck, India), Nitric acid (65%, RCI Labscan, Thailand), Sodium nitrate (Unichem, China), Potassium permanganate (97%, Merck, India), Hydrochloric acid (37%, RCI Labscan, Thailand), Sodium alginate (Merck, India) and Calcium chloride (Unichem, China) were procured and used for preparation of graphene oxide (GO) and calcium alginate-graphene oxide (CA-GO) composite.

The structure of GO and sodium alginate molecule are shown in the Fig. 3.1 and 3.2, respectively.

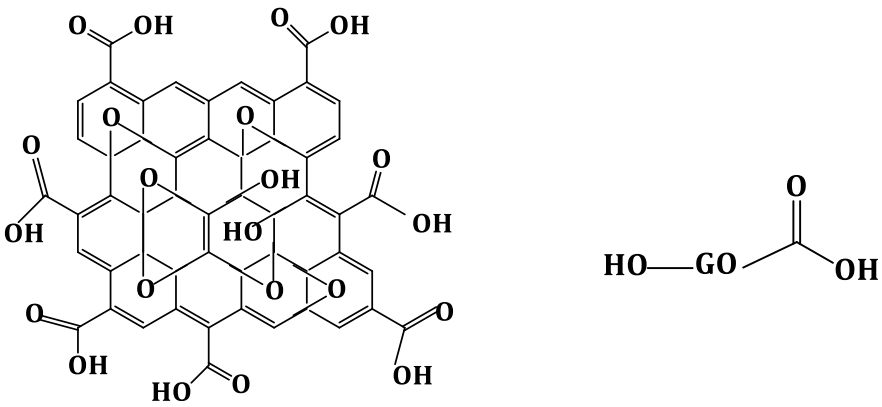

Fig. 3.1: Structure of GO

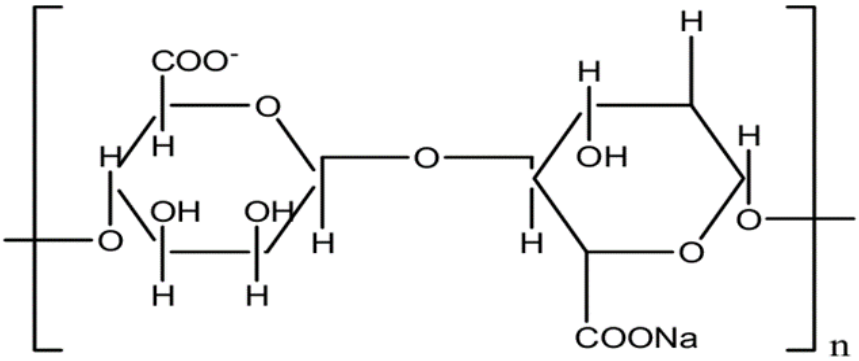

Fig. 3.2: Structure of sodium alginate molecule [195]

3.2. Collection of tannery effluent

In this study adequate tannery effluent samples were collected from Tannery Industrial Estate, Dhaka (TIED), Savar, Dhaka at several times from a big tannery discharge point following a standard method. The collected effluents were filtered with Whatman filter paper no. 41 for removal of suspended particles. The filtrate was then stored for experiment at 4ºC to prevent hydrolysis.

3.3. Physicochemical parameters of tannery effluents

In this study, HANNA Instrument (HI-98107) was used to judge the pH and mercury digital thermometer was used to measure the temperature. TDS, EC and % NaCl of effluent were investigated with HANNA instrument (HI-2300) and BOD5 was determined by HANNA instrument (HI-98193). COD was determined by following official standard method (DIN 38409).

3.4. Heavy metal analysis of tannery effluents

The heavy metals (such as Cr, Cu, Cd, and Pb) in tannery effluent, were analyzed using inductively coupled plasma-mass spectrometry (Agilent 7900 ICP-MS, Model no. G8403A, Agilent Technologies International Japan Ltd.) after acid digestion.

3.5. Synthesis of adsorbents

3.5.1. Preparation of graphene oxide (GO)

Modified Hummers' method was followed to prepare graphene oxide [196]. Graphite powder was oxidized by using conc. H_2SO_4, conc. HNO_3, $KMnO_4$ and $NaNO_3$.

3.5.2. Preparation of calcium alginate beads

Sodium alginate solution and calcium chloride solution were used to prepare calcium alginate beads.

3.5.3. Preparation of calcium alginate-graphene oxide (CA-GO) composite beads

Graphite was oxidized to graphene oxide using Hummers' method. Then sodium alginate and graphene oxide homogeneous suspension were prepared and dropped into calcium chloride solution to prepare calcium alginate-graphene oxide beads.

3.6. Characterization of GO and CA-GO composite beads

In order to characterize the produced graphene oxide (GO) and calcium alginate graphene oxide (CA-GO) composite, Fourier Transform Infrared Spectroscopy (FTIR) (8400S Shimadzu, Japan), Scanning Electron Microscopy (SEM) (JEOL, USA), X-Ray Diffraction (XRD) analysis, and Raman spectroscopy were used. Malvern Zetasizer (Nano-ZS ZEN 3600) was used to measure the zeta potential for produced adsorbent as a function of pH. X-ray photoelectron spectrometer (Model: K-ALPHA, Thermo Fisher Scientific, Czech Republic) was used for elemental analysis of GO. The Brunauer-Emmett-Teller (BET) surface area, pore volume, and pore size distribution of GO were analyzed with BET sorptometer (Model: BET-201-A, PMI, USA). Particle size analyzer (Model: Litesizer 500, Anton Paar) was used for particle size determination.

3.7. Adsorption study

A number of batch studies were run at a range of pH values, adsorbent dosages, initial metal salt concentrations, and contact times. Amounts of metals in the untreated and treated water samples were determined using atomic adsorption spectroscopy (AAS). To determine the adsorbents' capacity for metal adsorption, a fixed quantity of adsorbent was introduced to metal solutions of a specific concentration and pH. After filtering the mixtures and stirring them for a fixed span of time, the AAS was utilized to measure the concentration change. Equations (3.1) and (3.2) were used to determine the adsorption capacity at time t, q_t (mg/g), and the percentage of metal removal, respectively. Equation (3.3) provided the adsorption capacity at equilibrium, q_e (mg/g).

Adsorption capacity at time t, $q_{t=}\frac{(C_0-C_t)\times V}{W}$ (3.1)

$\%$ of removal $= \frac{(C_0-C_e)}{C_0}\times 100$ (3.2)

Adsorption capacity at equilibrium, $q_e=\frac{(C_0-C_e)\times V}{W}$ (3.3)

where, V= volume of metal ions containing solution (L), C_0 = initial concentration of metal ions (mg/L), C_t = concentration of metal ions at time t (mg/L), C_e = concentration of metal ions at equilibrium (mg/L), and W = mass of the GO employed for adsorption (g).

Plotting adsorption capacity against pH allowed researchers to identify the impact of pH on adsorption capacity in this study. At pH values above pHzpc, the greatest metal adsorption capacity was discovered. The optimum dosage was determined through plotting of adsorption capacity and percentage (%) of metal removal against dosage of adsorbents. The point at which the adsorption capacity and percentage (%) of removal intersect with each other, were considered as optimum dosage of adsorbent.

The theoretical maximum adsorption capacity, q_m (mg/g), was calculated using Langmuir isotherm model. The adsorption capabilities at various concentrations and time intervals were plotted to calculate the equilibrium adsorption capacity (q_e). When the concentration is at a specific level, the adsorption capacity rises with time, and after a while, it becomes nearly constant, which is considered as equilibrium adsorption capacity (q_e). The concentration at which the adsorption capacity became constant was considered as equilibrium concentration (C_e).

At a constant temperature, the relationship between adsorption capacity and the amount of residual adsorbate is described by adsorption isotherms [197]. Experimental results was analyzed by Langmuir and Frueundlich isotherms to determine the distribution of adsorbate molecules on adsorbent surface [198]. By creating equilibrium between adsorbate in solution and adsorbate on adsorbent, equilibrium isotherm studies concentrate on adsorption mechanism. It also determines an adsorbent's maximum adsorption capacity when adsorbing a specific material as an adsorbate. The equilibrium adsorption condition was explained using the Langmuir [eq. (3.4) and (3.5)] and Freundlich [eq. (3.6)] isotherms (in their linearized version).

$$\frac{C_e}{q_e} = \frac{1}{q_m \mathrm{b}} + \frac{1}{q_m} C_e \qquad (3.4)$$

$$R_L = \frac{1}{1 + C_m b} \qquad (3.5)$$

$$lnq_e = lnk_F + \frac{1}{n} lnC_e \qquad (3.6)$$

Where C_e = equilibrium metal ion concentration in grams per liter, C_m = maximum metal ion concentration in grams per liter, b = Langmuir constant in grams per liter, R_L = separation factor, and q_e and q_m are the equilibrium and theoretical maximum adsorption capacities in grams per liter, respectively. Plotting the value of C_e/q_e vs. C_e yielded the theoretical maximum adsorption capacity, or q_m, according to the Langmuir model. The separation factor R_L value was determined using the equation (3.5) to ascertain the advantageous nature of the adsorption process. The R_L number provides a qualitative assessment of the process' favorability; $R_L>1$ denotes unfavorable monolayer adsorption, whereas $0<R_L<1$ denotes favorable monolayer adsorption [199].

Freundlich isotherm [eq. (3.6)] shows non-uniform multilayer distribution of adsorbate molecules when n is the Freundlich constant and k_F is the theoretical maximal adsorption capacity (mg/g). Based on the value of n, a favorable assumption regarding adsorption is established. Adsorption becomes more difficult when n decreases, (n=2–10 indicates excellent adsorption, n=1-2 indicates hard adsorption and n<1 indicates poor adsorption) [199].

Adsorption kinetics is vital for evaluating an adsorbent's performance and gaining insight into the underlying mechanisms. In this study, pseudo-first-order and pseudo-second-order kinetic models were used to characterize the adsorption processes. In 1998, Ho and McKay proposed a pseudo-second order rate equation, and Lagergren presented a pseudo-first order rate equation to characterize kinetic process [203].

Using eq. (3.7), a plot of $\log(q_e-q_t)$ vs. t was made to analyze the pseudo-first-order model. Researchers could analyze the pseudo-second-order model by plotting t/q_t vs. t following the eq. (3.8), where k_2 is the rate constant (g/mg min).

$$\log(q_e - q_t) = logq_e - \left(\frac{k_1}{2.303}\right)t \qquad (3.7)$$

$$\frac{t}{q_t} = \left(\frac{1}{k_2 {q_e}^2}\right) + \left(\frac{1}{q_e}\right)\ t \qquad (3.8)$$

where, q_e and q_t represent the adsorption capacity at equilibrium (mg/g) and the adsorption capacity at time t (mg/g) respectively, and k_1 and k_2 represent the constant of pseudo-first-order reaction (1/min) and pseudo-second-order reaction (g/mg min), respectively.

The change of Gibb's free energy (ΔG) provides a hypothesis regarding the adsorption process. Physical adsorption is indicated if ΔG values increase with increased temperature and the process favorable at low temperatures. A thermodynamic assessment of an adsorption determines its randomness, spontaneity, and feasibility [200]. The thermodynamic parameters were assessed at various temperatures (293-338K). The van't Hoff equations were used to calculate the changes of standard free energy, enthalpy and entropy [201]. A calculation of Gibbs free energy change (ΔG) was made using eq. (3.9) and (3.10).

$$\Delta G = -RTlnk_d \qquad (3.9)$$

where, k_d, T and R denote the equilibrium sorption distribution constant, the absolute temperature (K) and the universal gas constant (8.314 J mole^{-1} K^{-1}), respectively.

$$k_d = \frac{q_e}{C_e} \qquad (3.10)$$

The enthalpy change (ΔH) and entropy change (ΔS) are calculated using the linearized van't Hoff isotherm eq. (3.11). A straight line was produced when lnK_d was plotted against 1/T. The ΔH and ΔS values were found by measuring the slope and intercept of the plot's straight line.

$$lnk_d = \frac{-\Delta H}{RT} + \frac{\Delta S}{R} \qquad (3.11)$$

Adsorbent's regeneration ability provides important information about the adsorption mechanism and commercial uses of an adsorbent. Therefore, in this study regeneration of all the used adsorbents were carried out.

The effectiveness of produced adsorbents was tested using diluted real samples of tannery effluent.

3.8. Safety precautions

While conducting this research sufficient precautionary measures were taken as it was dealt with heavy metals, tannery effluents and some other chemicals. Proper personal protective equipment and lab aid were utilized while handling the samples. All activities and processes were carried out in a hygienic and safe manner.

Chapter 4

Results and Discussion

4.1. Part 1. Synthesis, characterization and application of graphene oxide (GO) for the removal of Cr(III), Cu(II) and Cd(II) ions from aqueous solutions.

4.1.1. Preparation of graphene oxide (GO)

Graphene oxide (GO) is prepared by following modified Hummer's method. To prepare graphene oxide, in a round bottom flask graphite powder (3.0 g) was taken to a blend of concentrated H_2SO_4 and HNO_3 (3:1, 75 mL) with vigorous stirring in a water bath to form homogenous suspension. Then addition of $KMnO_4$ (9.0 g) followed by HNO_3 (1.5 g) to the flask was carried out slowly and stirred for 2 h. The mixture was stirred further for overnight to make a thick paste. A deep brown reaction mixture was formed after addition deionized water (120 mL) in the paste and stirred in an oil bath at 35 ℃ for 4 h. Then, additional DI water (420 mL) was added, followed by 30% H_2O_2 (20 mL) addition with continuous stirring to wash and produce mixture that was bright yellow. Finally, 5% HCl (200 mL) added to remove Mn^{2+} ions from produced graphene oxide. The synthesized GO was washed several times to reach the pH at neutral (7.0). Centrifugation was employed to expedite the process of neutralization.

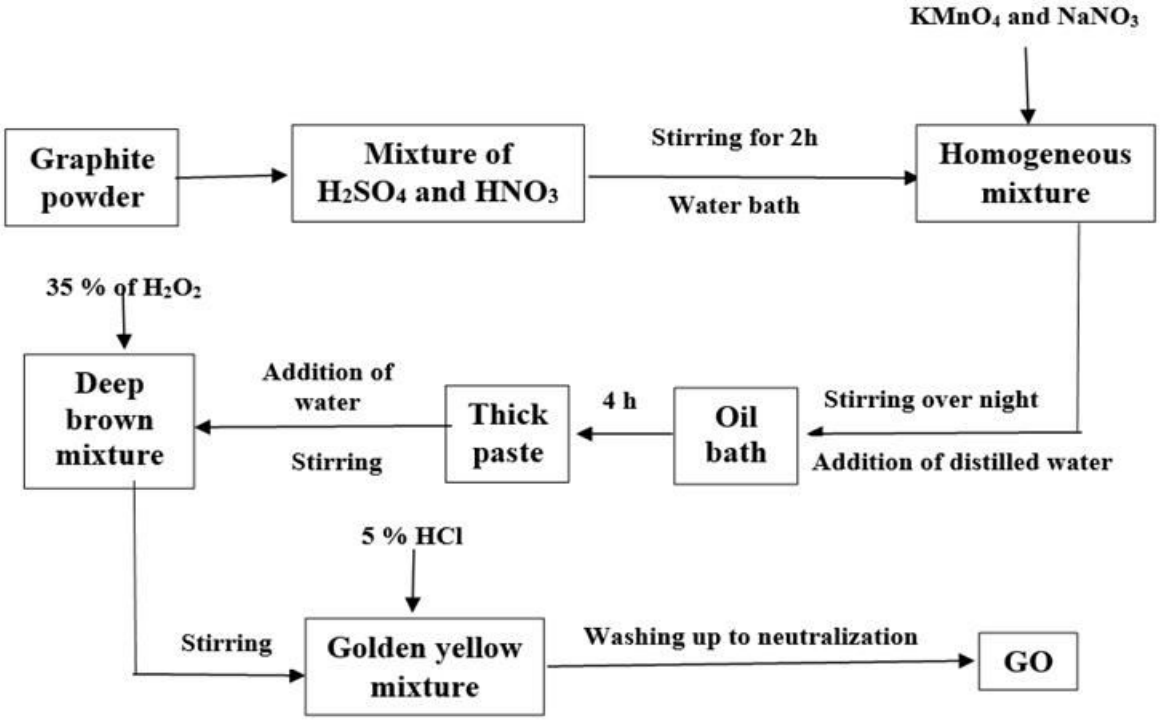

Fig. 4.1: Flow diagram of graphene oxide (GO) synthesis

4.1.2. Characterization of GO

4.1.2.1. Elemental Analysis

Elemental analysis was carried out to find the composition of GO and it was found to contain C (41.23 %), H (3.07 %), N (4.13 %) and S (0.40 %). A significant amount of oxygen (51.17 %) was found to contain which was determined indirectly, it was well-aligned with the literature [202].

4.1.2.2. FTIR Analysis

The FTIR spectroscopy study was performed to investigate the functional groups present in GO. In the Fig. 4, the multiple absorption peaks at different wavenumbers in the infrared area indicated the presence of diverse functional groups on GO surface. A strong and wide O-H stretching vibration was observed at wavelength 3414 cm^{-1}, C-H stretching vibration band was observed at wavelength of 2989 cm^{-1} and 2870 cm^{-1}, a carboxylic group C=O stretching vibration band was observed at wavelength of 1732 cm^{-1}, an aromatic C=C stretching vibration band was observed at a wavelength of 1519 cm^{-1}, a symmetric C-O stretching in the C-O-C group was observed at a wavelength of 1209 cm^{-1}, and a C-O (epoxy) band was observed at a wavelength of 964 cm^{-1} due to extensive oxidation. The FT-IR spectra of GO were consistent with the results of the earlier research [203], [204].

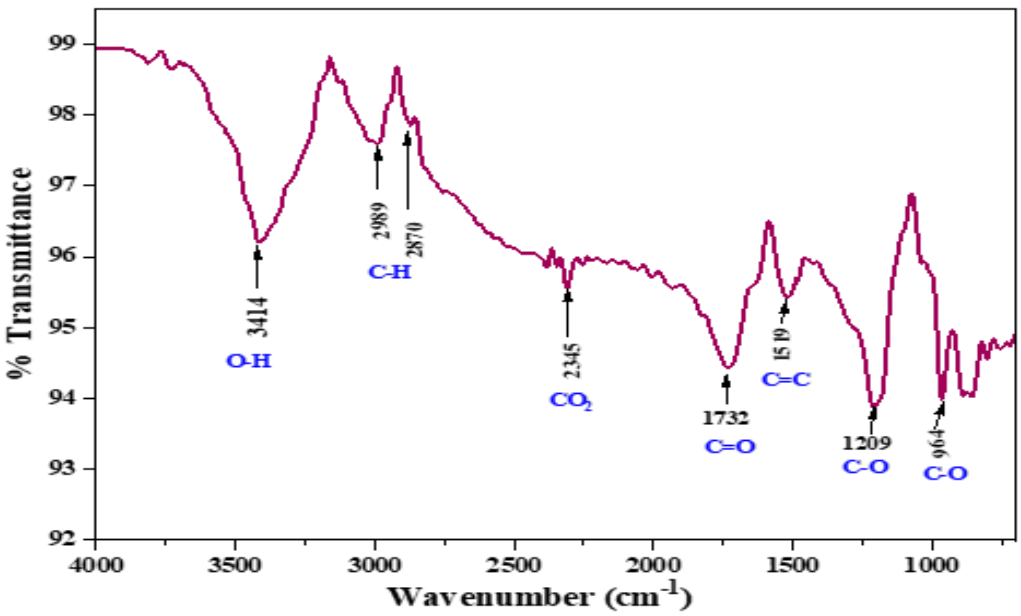

Fig. 4.2: FTIR of GO

4.1.2.3. Scanning Electron Microscopy (SEM)

The scanning electron microscopy was exploited to investigate the microstructure and morphology of GO. The image of GO (Fig. 4.3) was captured in high vacuum mode with 5.0 kV at 20,000X magnification and approximately 6.6 mm working distance. The photographs depicted randomly arranged, fluffy, crumpled sheets with an orientation of variety of pores, which are vital for absorbing metal ions [205]. The fluffiness and wrinkles were the result of layer separation and oxidation of GO. The membrane was employed to absorb some particular heavy metal ions from water showed the similar outcome in the SEM structure [206].

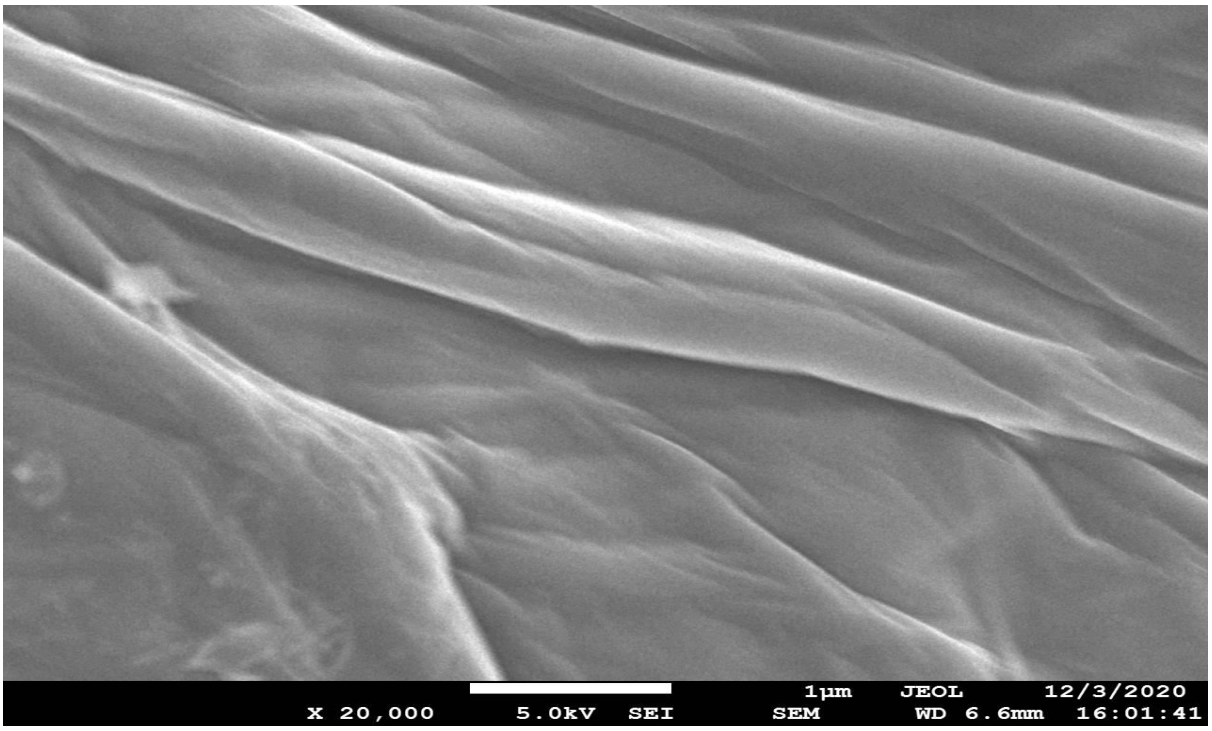

Fig. 4.3: SEM image of prepared GO

4.1.2.4. X-Ray Diffraction (XRD) analysis of GO

The XRD pattern of prepared GO is displayed in Fig. 4.4. It revealed a broad peak at 2θ=10.399º, which corresponded to an interlayer spacing of 8.5Å and was in good agreement with the value of literature as 2θ of 11.4º and d-spacing of 7.8 Å [199]. This is due to introduction of oxygen and formation of amorphous structure of GO.

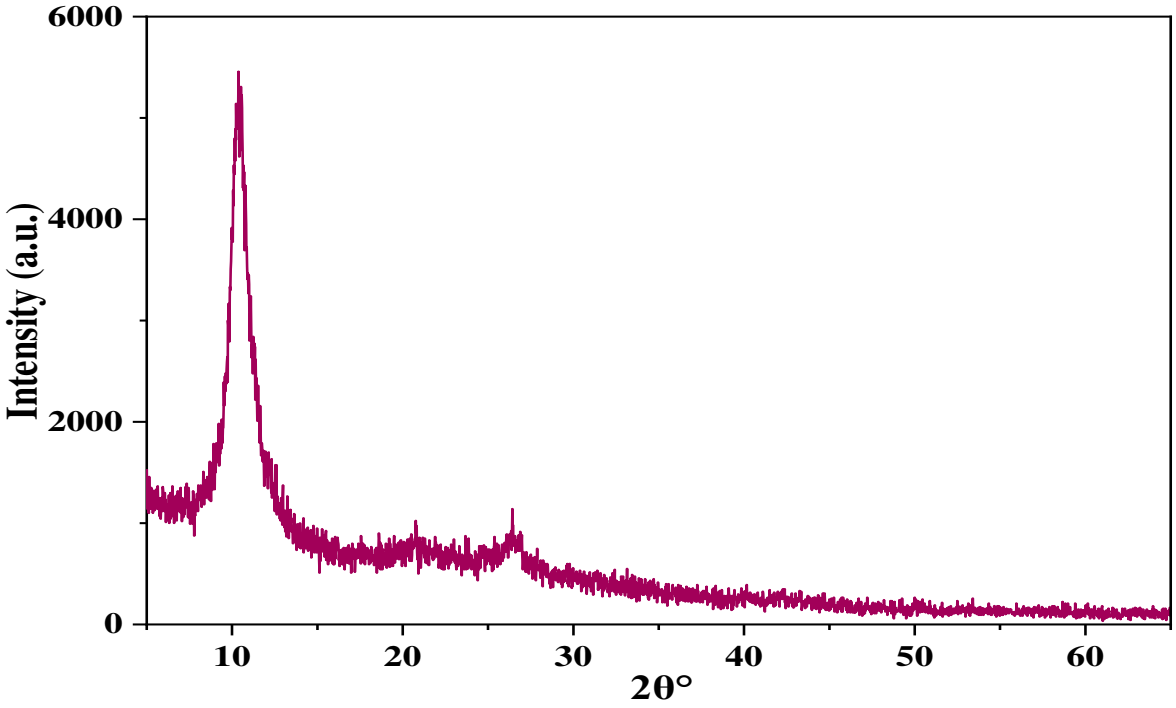

Fig. 4.4: XRD patterns of GO

4.1.2.5. Spectrum analysis of GO

The existence both the D-band and G-band was confirmed by Raman spectrum of GO, which was displayed in Fig. 4.5.

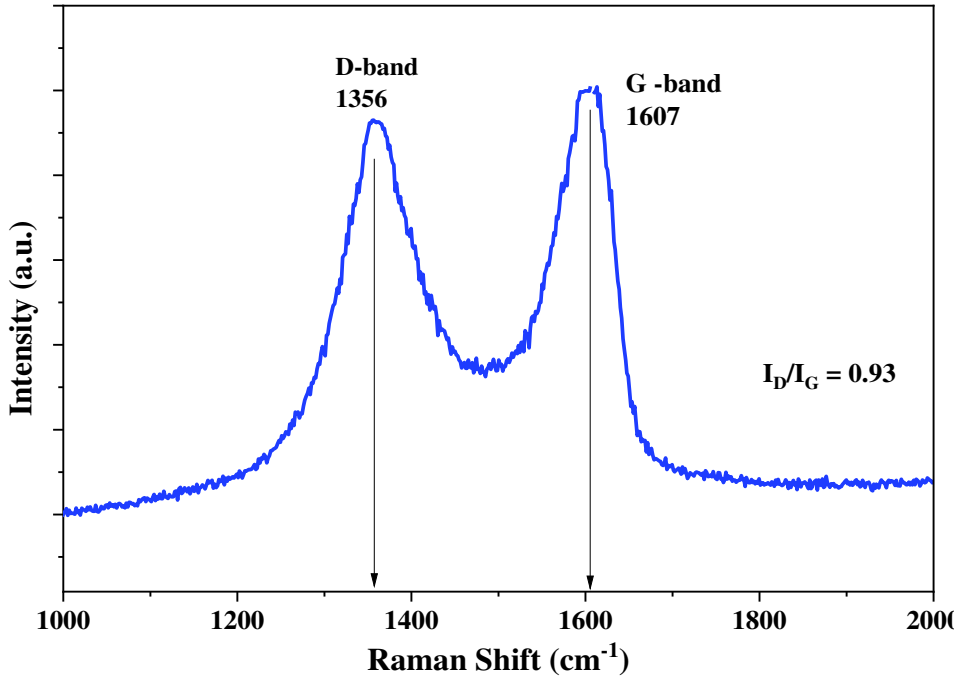

Fig. 4.5: Raman Spectrum of GO

The values of D-band and G-bands are 1356 cm^{-1} and 1607 cm^{-1}, respectively and are well in line with other published material somewhere else. The presence of D-band made it possible to determine the size the size of in-plane sp^2 domain and the existence of defective sites in GO sheets [207]. The D-band and G-band intensity ratio (I_D/I_G) was 0.93, which indicated the amount of structural disorder of graphene oxide [208].

4.1.2.6. XPS Analysis of GO

The XPS spectra of GO (Fig. 4.6) showed the significant strong signals of C and O with corresponding binding energy.

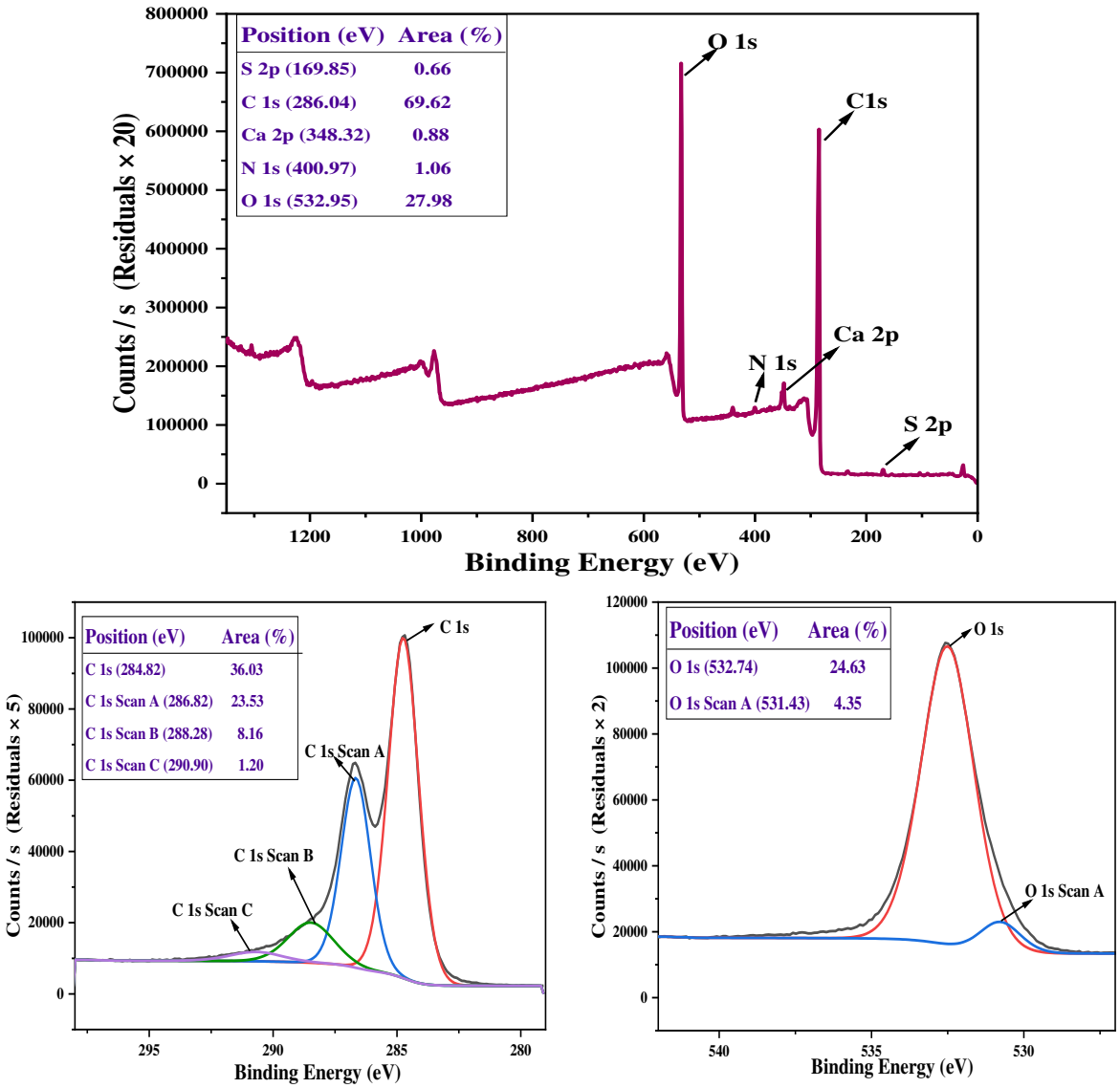

Fig. 4.6: XPS Spectrum of GO

The peaks at 284.82, 286.82, 288.28, and 290.90 eV were assignable to C-C/C-H, C-O, C=O, and O-C=O, respectively (Fig. 4.6b). The C=O and C-O types of oxygen were responsible for the peaks at 532.74 and 531.43 eV, respectively (Fig. 4.6c). Similar XPS spectrum of GO were observed in earlier research [209].

4.1.2.7 Brunaur-Emmett-Teller (BET) analysis of GO

Surface area, pore volume and pore size/diameter of GO were analyzed through nitrogen sorption system are showed in Table 4.1 and Fig. 4.7. The BET analysis recommends that GO has a specific surface area of 127.32 m^2/g which is much lower than the theoretical specific surface area for completely exfoliated and isolated graphene sheets (~2620 m^2/g) [210], which could be due to the agglomeration and overlapping of the GO sheets [211], [212]. Pore sizes are categorized by the International Union of Pure and Applied Chemistry (IUPAC) as micropores (diameter, (d)<20Å), mesopores (20Å<d<500Å) macropores (d>500Å) [213]. Barrett-Joiner-Halenda (BJH) method was followed and the average pore size/diameter was found to be 27.47Å, which indicated that prepared GO was mesoporous and had a total pore volume of 0.0875 cc/g. These characteristics showed the affinity towards the metals like chromium, copper and cadmium.

Table 4.1: Parameters of BET analysis for GO

BET Parameter	Results
BET specific surface area	127.32 m^2/g
Total pore volume	0.0875 cc/g
Average pore diameter	27.47 Å

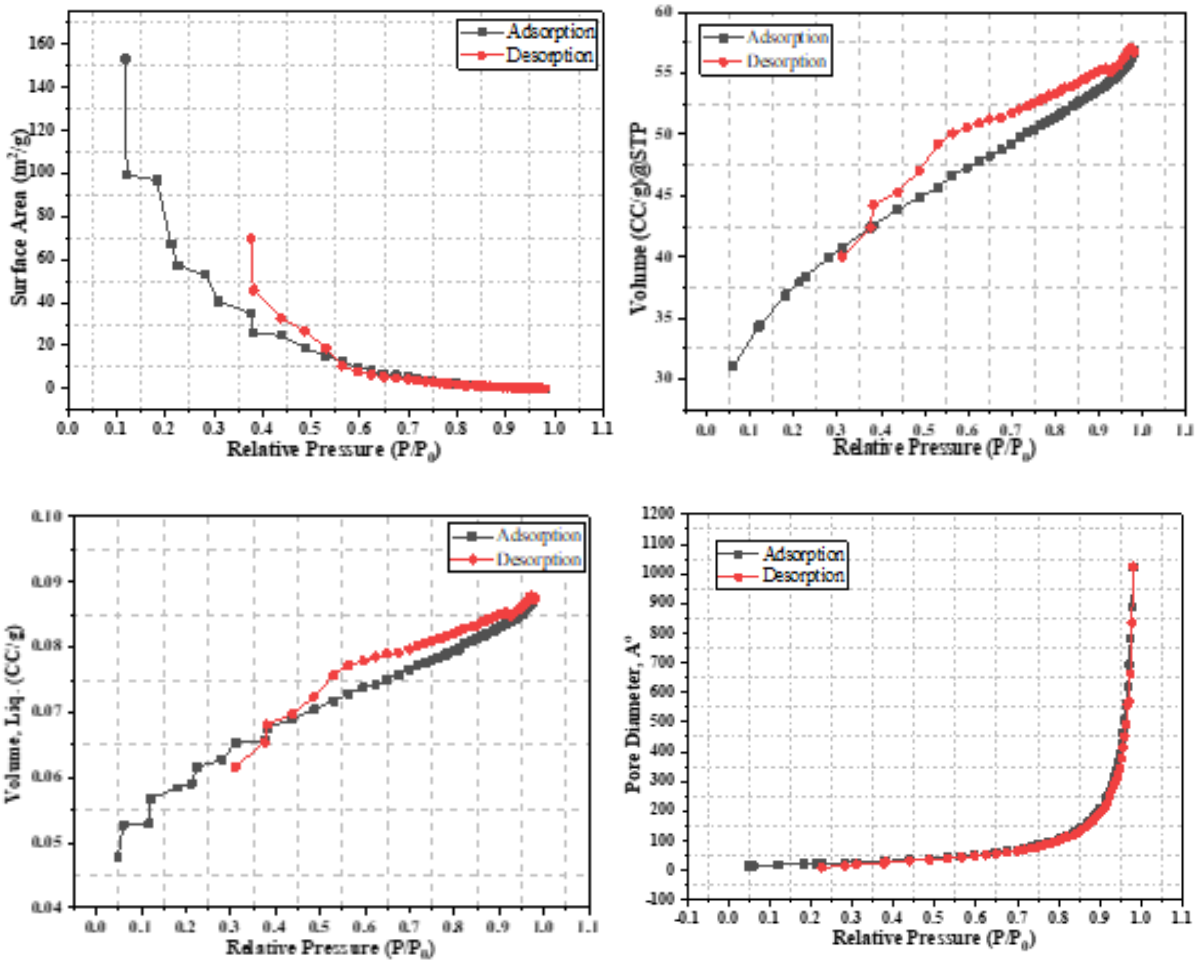

Fig. 4.7: BET analysis of GO

4.1.2.8 Particle size analysis

The size of GO particles in DI water was measured by diffraction light scattering (DLS) using Particle Size Analyzer. The particle size and poly dispersity index were found to be 665.3 nm and 23.9 %, respectively (Table 4.2, Fig. 4.8), which showed good agreement with previous report [214]. The particle size of adsorbents affected their buffering capacity and the buffering capacity increased with decreasing the particle size due to increased surface area [215].

Table 4.2: Parameter of particle size analysis for GO

Parameters	Values
Particle size	665.3 nm
Polydispersity index	23.9 %
Diffusion coefficient	0.7 $\mu m^2/s$
Transmittance	75.7 %

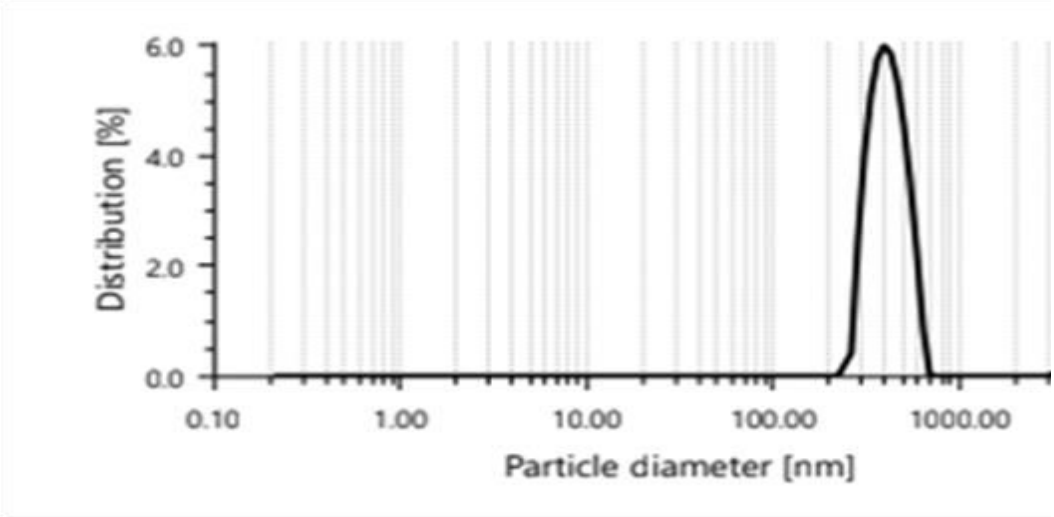

Fig. 4.8: Particle size distribution of GO

4.1.2.9. Zeta potential value of GO

The value of zeta potential for GO was investigated as a function pH. To produce the sample, GO was dispersed in DI water and pH adjusted at 2.0-10.0 with dilute acid and alkali. The results depicted (Table 4.3, Fig. 4.9) that the zeta potential value of GO was positive (0.1710 mV) at pH 2.0, whereas the values was negative (-0.0444 to -0.4400 mV) with an increase of pH from 4.0 to 10.0. It was revealed from the figure that the ZPC of GO was pH 3.5. At pH higher than the ZPC, the carboxyl group of GO deprotonates and becomes negatively charged. Therefore, metal adsorption capacity of GO is boosted at pH higher than ZPC.

Table 4.3: pH and Zeta potential data of GO

pH	2.0	4.0	6.0	8.0	10.0
Zeta potential value (mV)	0.1710	-0.0444	-0.0800	-0.2330	-0.4400

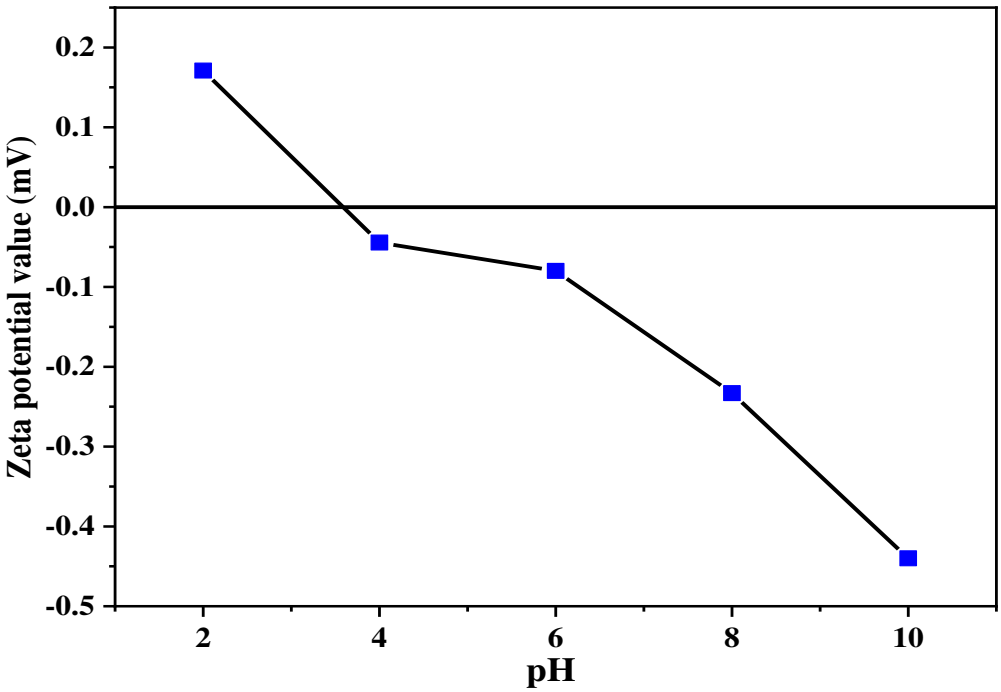

Fig. 4.9: Zeta potential value of GO at diverse pH

4.1.2.10. Ionic behaviour of GO at different pH

The ionic behavior of GO at lower and higher pH is explained through the Fig 4.10. The adsorption process dealt with the attraction between oppositely charged particles through formation of various bonds, including hydrogen bonding, electrostatic attraction or π-π interactions, van der Waals forces, and dipole-dipole induction. Adsorption of solute on an adsorbent was significantly influenced by the chemistry of surface complexation and pore density or pore volume.

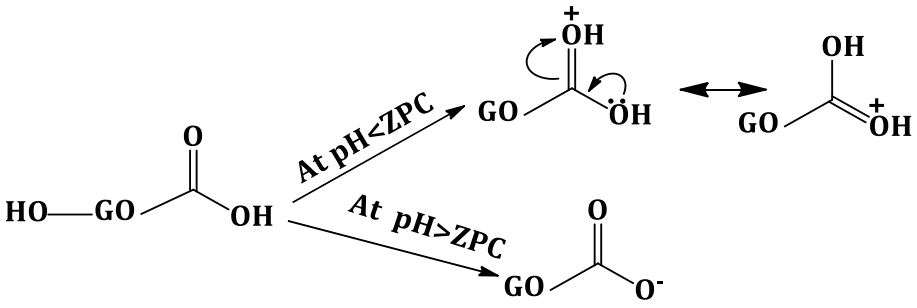

Fig. 4.10: Ionic behaviour of GO at low and high pH

Adsorbents surface became negatively charged when pH of the solution exceeded pH_{zpc}. Graphene oxide exhibited electrostatic interaction with cationic metal ions at pH>pH_{zpc}

due to its negatively charged surface. The net charge on the surface of the particles was zero at pH_{zpc}. The possible mechanism of heavy metals adsorption on GO is shown Fig. 4.11.

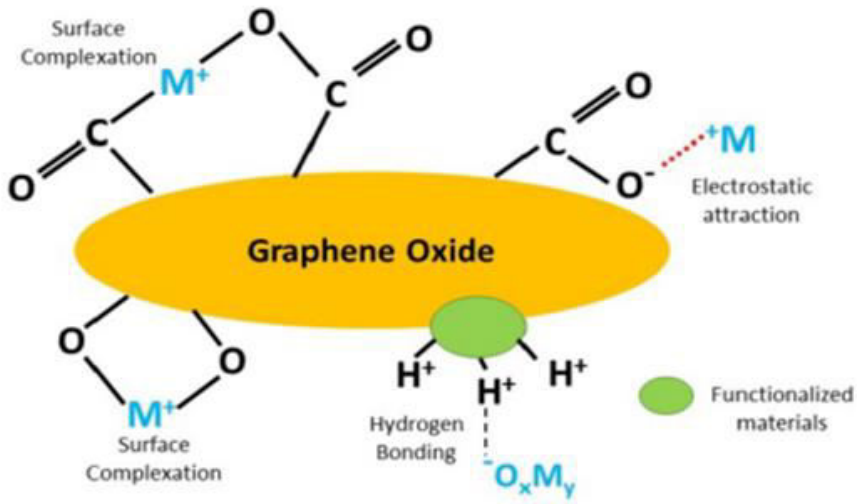

Fig. 4.11: Possible heavy metal (M) removals mechanism on GO adsorbents [216]

4.1.3. Adsorption studies

The efficacy of adsorbent for heavy metal removal is impacted by pH, adsorbent dosages, contact time and initial metal concentration, temperature and other parameters.

4.1.3.1. Adsorption of Cr(III) on GO

4.1.3.1.1. Effect of pH

pH is an important parameter as it influences both the property the adsorbent surface and the nature of the adsorbate [217]. The surface charge of adsorbent and adsorbate can be altered by changing pH. The effects of pH on adsorption of chromium was studied with chromium(III) salt solution (245.5 ppm, 10 mL) was placed in a number of conical flasks and the pH was adjusted to 2.0, 3.0, 4.0, and 5.0. Then GO (0.039 g) was added to each solution and the mixture was shaken for 2 h at room temperature at 150 rpm in an orbital shaker. The mixtures were then filtered and the changes of concentrations were determined by AAS. The percentage of removal and optimum adsorption capacity of GO was found as 99.68% and 125.49 mg/g, respectively at pH 4.0 (Table 4.4, Fig. 4.12). Studies on pH revealed that GO surface had zero charge at pH 3.5 (pH_{zpc}) and below this

pH adsorbent surface was positively charged due to protonation of carboxylic group, which resulted electrostatic repulsion with metal ions. Moreover, at lower pH there was a high competition between the H^+ and metal ions, where adsorbent surface was mostly occupied by proton because of its smaller size and both these phenomena led to lower adsorption of metal ions [218, 219]. On the other hand, at pH above the ZPC, GO surface became negatively charged due to deprotonation of carboxylic group (Fig. 4.10) and resulted electrostatic attraction between the GO surface and metal ions [220]. In addition to that at higher pH, the proton concentration was reduced leading to less competition of protons with cations and resulted higher adsorption of metal ions [221].

Table 4.4: pH, adsorption capacity and % removal data for adsorption of Cr(III) on GO

pH	2.0	3.0	4.0	5.0
Adsorption capacity (mg/g)	76.67	110.08	125.49	125.74
% removal	60.90	87.44	99.68	99.89

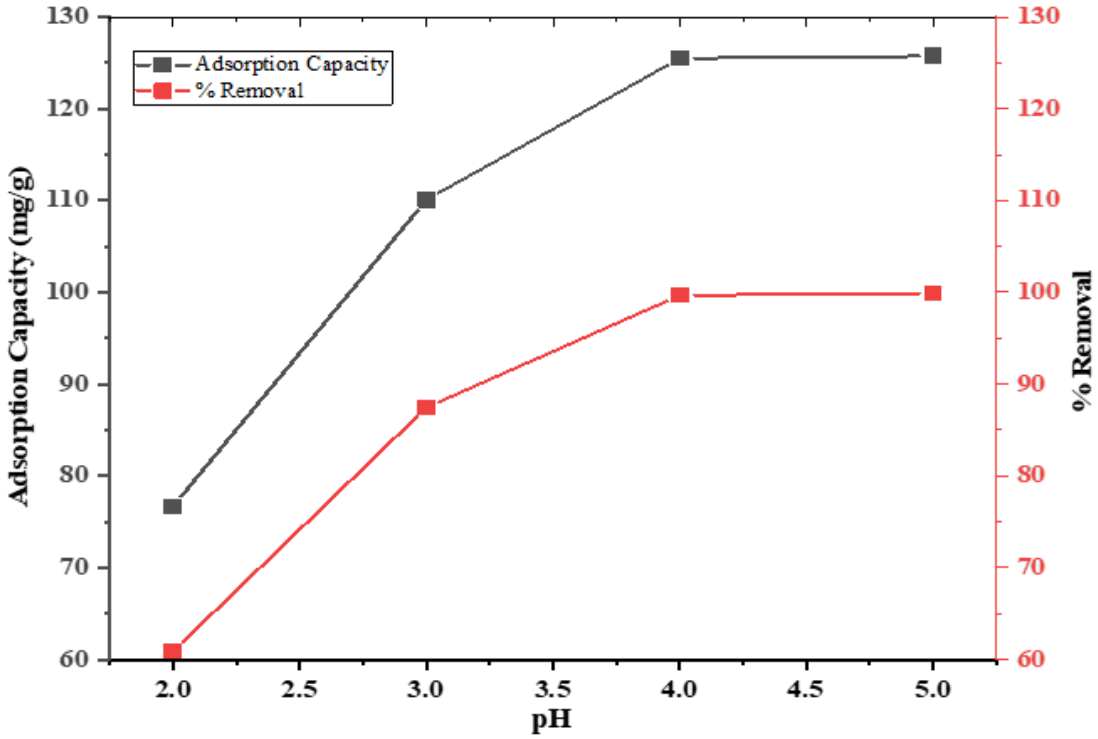

Fig. 4.12: Effect of pH on adsorption capacity and % removal of Cr(III) on to GO

4.1.3.1.2. Effect of dosage

The effects of adsorbent dosage on adsorption of chromium were studied. In order to optimize the dosage of adsorbent, standard chromium salt solution (10 mL, 245.5 ppm) was treated with various dosages (0.25, 0.50, 1.00, 1.50 and 2.0 g/L) at optimum pH (4.0) in an orbital shaker at 150 rpm for 2 h. Adsorption capacity and percentage of removal were measured using the equations (eq. 3.1 and 3.2). It was observed that with the increase of adsorbent dosage the percentage of metal removal increased and adsorption capacity decreased (Table 4.5, Fig. 4.13). Typically, when adsorbent dosages increased, the number of active sites and surface area increased, allowing maximum metal ions to interact with the active sites [206, 222]. At the higher dosage of adsorbent, many of active sites were still unsaturated and remained unreacted. According to the findings of the experiments, the optimum dosage was 0.6 g/L and that was maintained throughout the study.

Table 4.5: Dosage, adsorption capacity and % removal data of GO for Cr(III) adsorption

Dosage (g/L)	0.25	0.50	1.00	1.50	2.00
Adsorption capacity (mg/g)	716.00	410.60	215.30	157.60	120.70
% removal	72.91	83.63	87.70	96.29	98.40

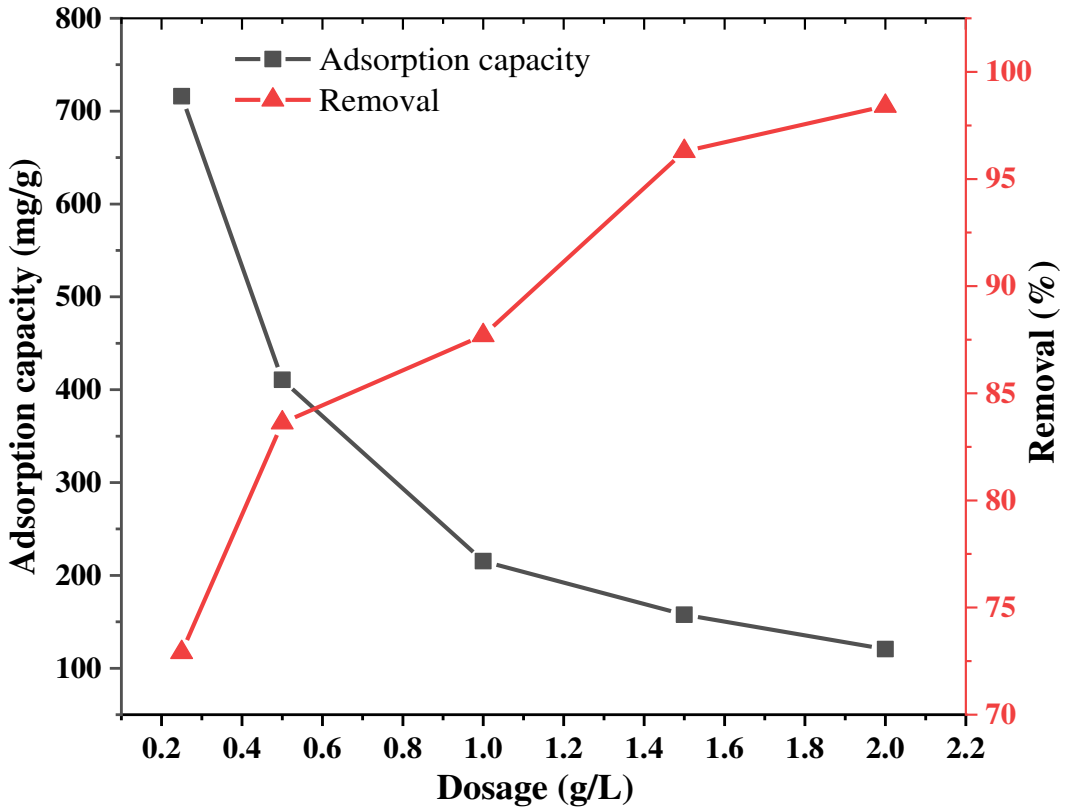

Fig. 4.13: Effect of dosage on adsorption capacity of GO and % of removal

4.1.3.1.3. Effect of contact time and metal concentrations

The impact of contact time and initial chromium concentration were studied using batch method. In the experiments, standard chromium salt solution (10 mL) of several concentrations (104.22, 125.40, 174.00, and 198.57 ppm) were treated with adsorbent at optimum pH (4.0) and dosage (0.6 g/L) for a predefined interval of time (2-120 min). The result depicted that adsorption capacity increased as the span of time passes till reached at equilibrium (Table 4.6, Fig. 4.14). At 20 minutes, the increase in adsorption achieved equilibrium and prolonging the contact duration did not result in any appreciable changes. After reaching equilibrium time, the adsorbate progressively fills the open active sites of adsorbent surface and increase adsorption capacity without any discernable impact [222]. This is because, at initially there were plenty of active sites available, however those sites become saturated with passes time.

Initial metal ions concentration is one of the most significant driving forces for adsorption. It explains the relationship between mass transfer and mass balance for solutes in liquid (adsorbate) and solid (adsorbent) phase [223]. The % removal was high at lower concentration as the amount of adsorbent is high compare to metal adsorbate in the

solution (Table 4.7, Fig. 4.15). The adsorption capacity of GO was increased when the initial chromium concentration increased. Over the time, adsorbate occupied adsorbent's active sites on the surface as long as it had unoccupied active sites, thus the adsorption capacity increased until equilibrium was reached [224] and then the ratio of active sites on the adsorbent was almost equal [225].

Table 4.6: Adsorption capacity of GO at different concentration of Cr(III) at different time intervals

Time (min)	104.22 ppm	125.40 ppm	174.00 ppm	198.57 ppm
2	131.37	145.25	211.58	200.28
5	135.07	153.08	210.75	208.28
10	144.36	160.17	218.67	243.95
15	146.38	169.33	223.50	247.28
20	149.28	174.63	228.67	251.70
30	147.28	175.32	228.13	250.28
60	147.70	173.80	229.62	251.93
120	149.98	174.30	229.35	252.53

Table 4.7: Percentage of Cr(III) removal with GO at different concentration and time intervals

Time (min)	104.22 ppm	125.40 ppm	174.00 ppm	198.57 ppm
2	75.63	69.50	72.96	60.52
5	77.76	73.25	7267	62.92
10	83.11	76.64	75.40	73.71
15	84.27	81.02	77.07	74.72
20	85.94	83.56	78.85	76.05
30	84.79	83.88	78.67	75.63
60	85.03	83.16	79.18	76.12
120	86.35	83.40	79.09	76.30

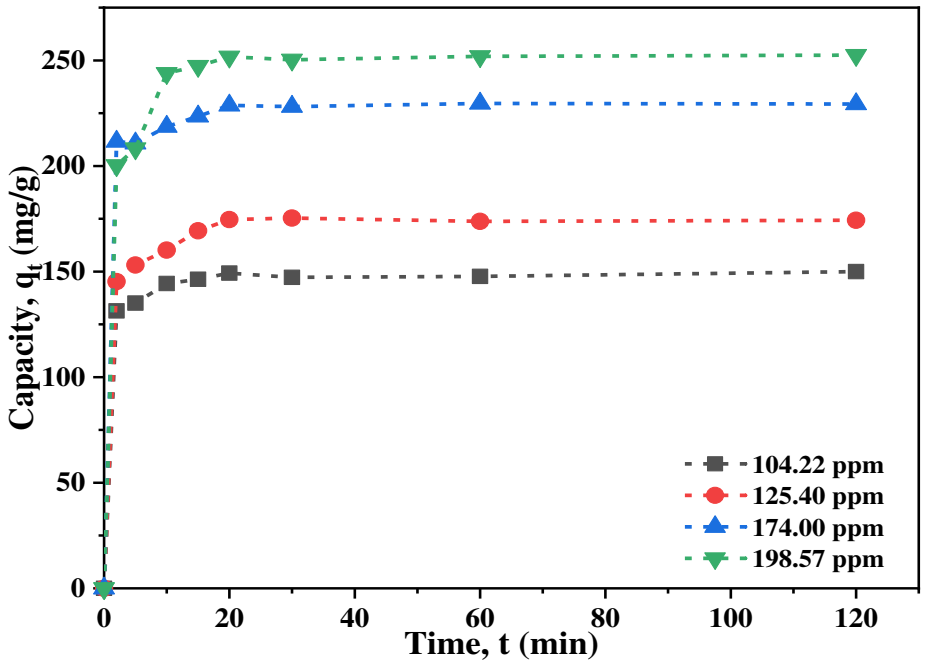

Fig. 4.14: Effect of time and concentration on adsorption of Cr(III) on GO

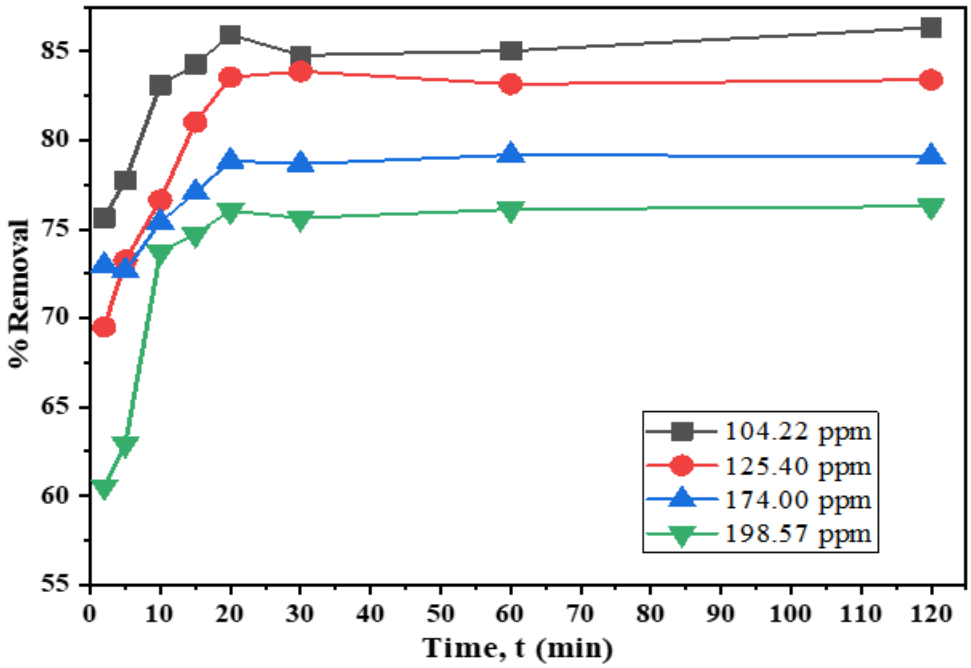

Fig. 4.15: Effect of time and % removal of Cr(III) on GO at different concentration

4.1.3.1.4. Adsorption isotherms for adsorption of Cr(III) on GO

Isothermal studies establish a relation between the adsorbent and the adsorbate at equilibrium state to explain the adsorption mechanism. It also determines an adsorbent's maximum adsorption capacity when adsorbing a specific material as an adsorbate. After the experimental findings were analyzed using Langmuir and Freundlich isotherms, the distribution of adsorbate molecules on the adsorbent surface was examined. Adsorbate is considered to be adsorbed in a monolayer form on unique, equal sites in the Langmuir isotherm without any interaction among adsorbate molecules. On the contrary, adsorbate is considered to be adsorbed in multilayer with non-uniform distribution in the Freundlich isotherm.

4.1.3.1.4.1. Langmuir isotherm

Langmuir isotherm was applied by graphing the values of C_e/q_e against C_e following the eq. (3.4) (Table 4.8, Fig. 4.16). It was observed a linear relationship between C_e/q_e with an acceptable regression co-efficient (R^2=0.998). The slope was used to calculate the theoretical maximum adsorption capacity, q_m, which was 366.3 mg/g for chromium. The separation factor R_L was used to determine the favorability of the adsorption process. A process is considered positive and favorable when the value of R_L stands between 0 and 1 and unfavorable if R_L is greater than 1. R_L value was determined by eq. (3.5) in this study and was found 0.098, which indicated a favorable monolayer adsorption.

Table 4.8: C_e and C_e/q_e data of GO at different concentrations for Cr(III) adsorption

Initial concentration (ppm)	104.22	125.40	174.00	198.57
Equilibrium concentration (C_e)	14.65	20.62	36.8	47.55
C_e/q_e	0.0981	0.118	0.161	0.189

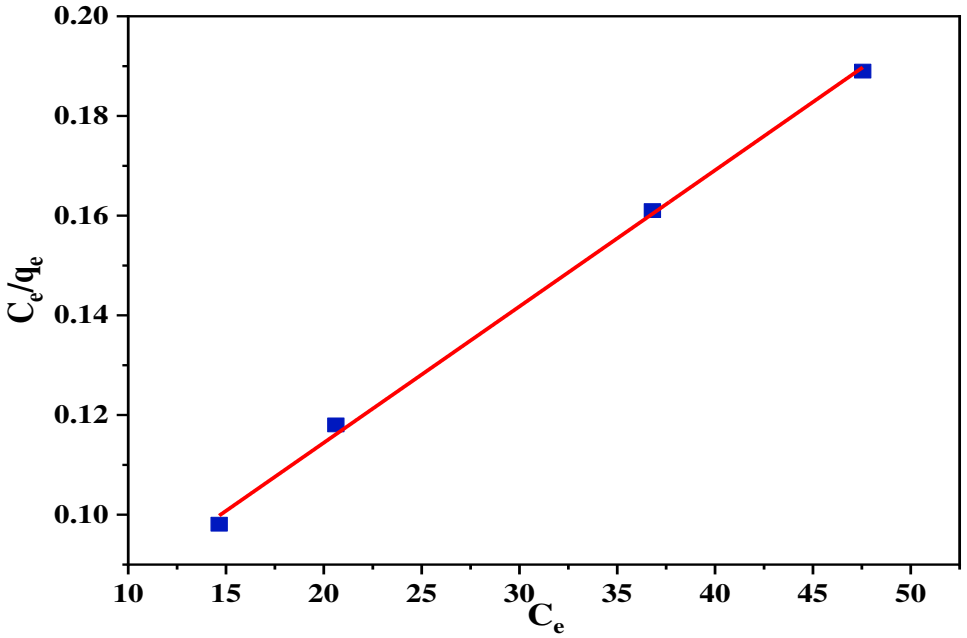

Fig. 4.16: Langmuir adsorption isotherm for adsorption of Cr(III) on GO

4.1.3.1.4.2. Freundlich isotherm

Freundlich adsorption isotherm using eq. (3.6) was also applied by plotting $\ln C_e$ versus $\ln q_e$ (Table 4.9, Fig. 4.17) for verifying multilayer adsorption mechanism. A linear relation was found with excellent regression coefficient (R^2= 0.998) which indicated favorable multilayer adsorption. The value of n was computed as 2.232 by eq. (3.6) that indicated moderate adsorption. As the n value decreases the adsorption becomes more difficult.

Table 4.9: $\ln C_e$ and $\ln q_e$ data of GO at different concentrations for Cr(III) adsorption

Initial concentration (ppm)	104.22	125.40	174.00	198.57
$\ln C_e$	2.684	3.026	3.605	3.862
$\ln q_e$	5.006	5.163	5.432	5.528

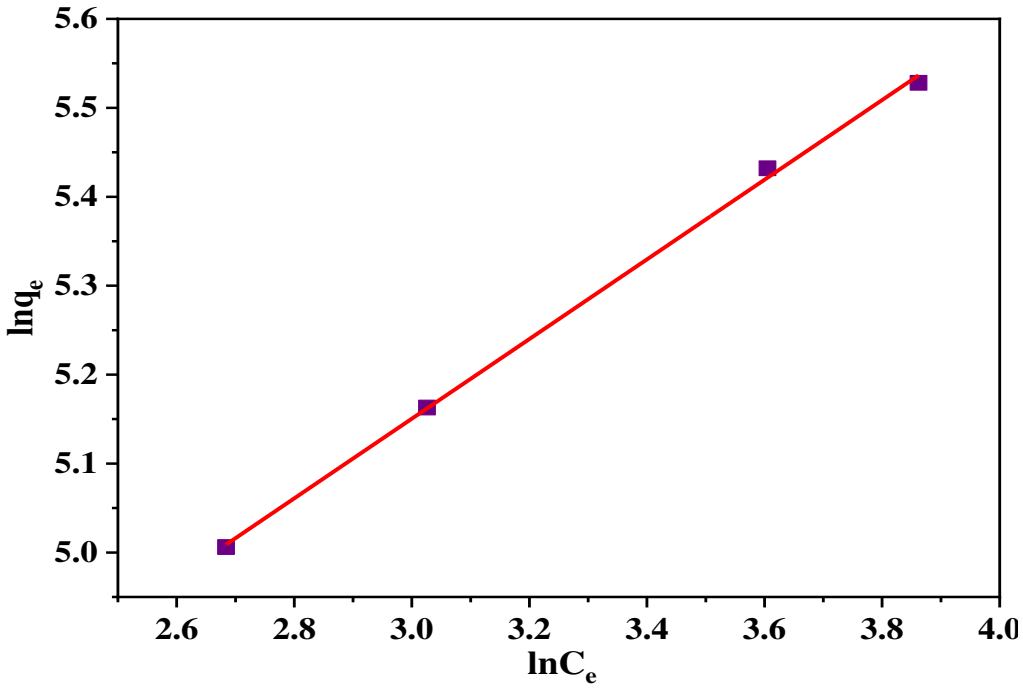

Fig. 4.17: Freundlich adsorption isotherm for adsorption of Cr(III) on GO

Chromium(III) adsorption on GO was followed both the isotherm, showing monolayer and multilayer adsorption with the maximum adsorption capacity, q_m 366.3 mg/g. The equilibrium adsorption model parameters and the correlation coefficient (R^2) values were calculated using OriginPro 2019B software and the results of both the isotherms were reported in a table (Table 4.10).

Table 4.10: Theoretical values of q_m, b, R_L, n, k_F and R^2 of adsorbent GO for Cr(III) adsorption

Parameters	q_m (mg/g)	b, Lmg^{-1}	R^2	R_L	n	k_F
Langmuir isotherm	366.3	0.046	0.998	0.098	-	-
Freundlich isotherm	-	-	0.998	-	2.232	45.02

4.1.3.1.5. Adsorption kinetics for Cr(III) on GO

Adsorption kinetics was used to assess the type of adsorption and adsorbent's effectiveness. The most widely used kinetics, pseudo-first-order and pseudo-second-order reaction models were used in this study to analyze the adsorption processes.

4.1.3.1.5.1. Pseudo-first-order reaction kinetics

Kinetic process pseudo-first-order model is employed through plotting $\log(q_e-q_t)$ versus t, where a linear relation between $\log(q_e-q_t)$ and t was observed (Table 4.11, Fig. 4.18).

Table 4.11: Time, t and $\log(q_e-q_t)$ data of GO at different concentration for Cr(III) adsorption

Time, t (min)	$\log(q_e-q_t)$ at 104.22 ppm	$\log(q_e-q_t)$ at 125.40 ppm	$\log(q_e-q_t)$ at 174.00 ppm	$\log(q_e-q_t)$ at 198.57 ppm
2	1.253	1.468	1.235	1.711
5	1.153	1.333	1.252	1.638
10	0.69	1.16	0.998	0.888
15	0.462	0.724	0.71	0.645

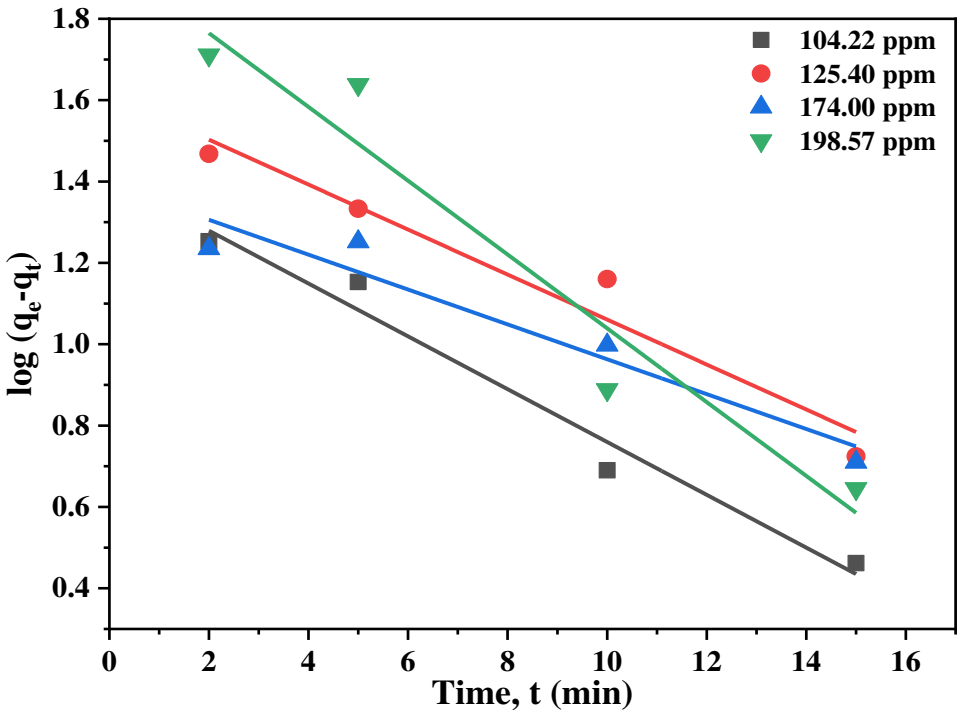

Fig. 4.18: Pseudo-first-order kinetics for adsorption of Cr(III) on GO

4.1.3.1.5.2. Pseudo-second-order reaction kinetics

Pseudo-second-order reaction model was also practiced to evaluate kinetic process where t/q_t versus t was plotted following the eq. (3.8). The time (t) and t/q_t data are represented with the Table 4.12 and Fig. 4.19.

Table 4.12: Time, t and t/q_t data of GO at different concentration for Cr(III) adsorption

Time, t (min)	t/q_t at 104.22 ppm	t/q_t at 125.40 ppm	t/q_t at 174.00 ppm	t/q_t at 198.57 ppm
2	0.0152	0.0138	0.0095	0.00998
5	0.037	0.0327	0.0237	0.024
10	0.0693	0.0624	0.0457	0.04099
15	0.1025	0.0886	0.067	0.0606
20	0.1339	0.1145	0.0875	0.0795

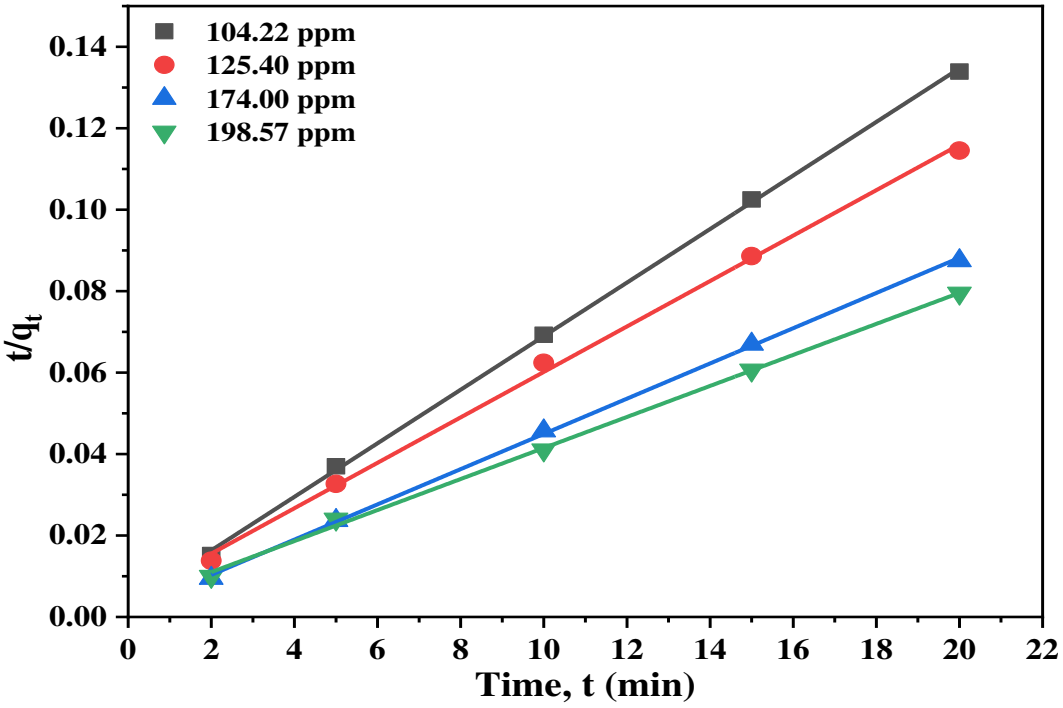

Fig. 4.19: Pseudo-second-order kinetics for adsorption of Cr(III) on GO

Kinetic parameter of experimental work is represented in the Table 4.13. The values of correlation coefficient of pseudo-second-order kinetic model were far better than pseudo-

first-order kinetics. This information also demonstrated that the adsorption process is chemisorption-based. As a result, covalent bonds were formed between metal ion and anionic functional groups of GO (hydroxyl, carboxylates, carbonyl, etc.).

Table 4.13: Kinetics parameters of Cr(III) adsorption on GO

Types of kinetics model	Parameters	Initial concentration of chromium(III)			
		104.22 ppm	**125.40 ppm**	**174.00 ppm**	**198.57 ppm**
Pseudo-first-order	q_e^* (mg/g)	149.28	174.63	228.67	251.70
	k_1 (1/min)	0.149	0.127	0.0986	0.2089
	R^2	0.974	0.953	0.931	0.941
	q_e^{**} (mg/g)	25.64	41.11	24.66	88.31
Pseudo-second-order	k_2 (g/mg min)	0.0135	0.0071	0.011	0.0042
	R^2	0.999	0.998	0.999	0.998
	q_e^{**} (mg/g)	152.21	179.21	230.95	262.47

* Experimental, **Theoretical

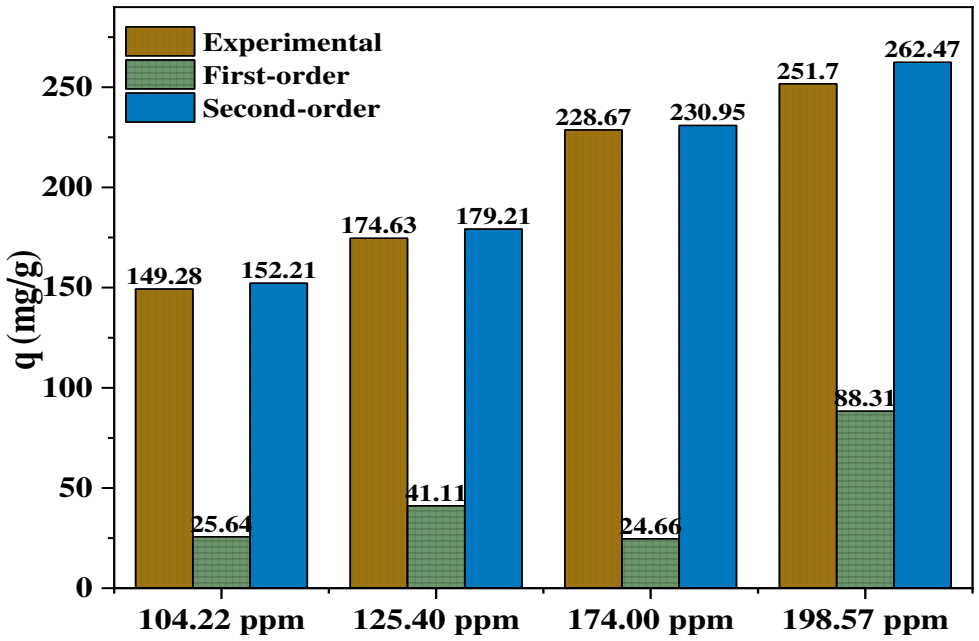

Fig. 4.20: Comparison of Cr(III) adsorption capacities on GO

The experimental values also matched better with the adsorption capacities of pseudo-second-order kinetics (Fig. 4.20).

4.1.3.1.6. Thermodynamic analysis

A thermodynamic analysis of adsorption determined its viability and randomness on the basis of temperature. Using the linearized van't Hoff equation, the thermodynamic parameters, such as Gibb's free energy (ΔG) and standard enthalpy (ΔS), were examined throughout a range of temperatures (293-338 K). The computed results showed that when the temperature rose, the GO's adsorption capabilities decreased. The kinetic energy increases at elevated temperature that helps to release the adsorbate from GO. The studied enthalpy value (-0.0981) specified that the adsorption was entropy-driven and exothermic.

Table 4.14: lnk_d and 1/T data of GO for Cr(III) adsorption

1/T	0.0033	0.0032	0.0031	0.0030
lnk_d	2.905	2.554	2.055	1.582

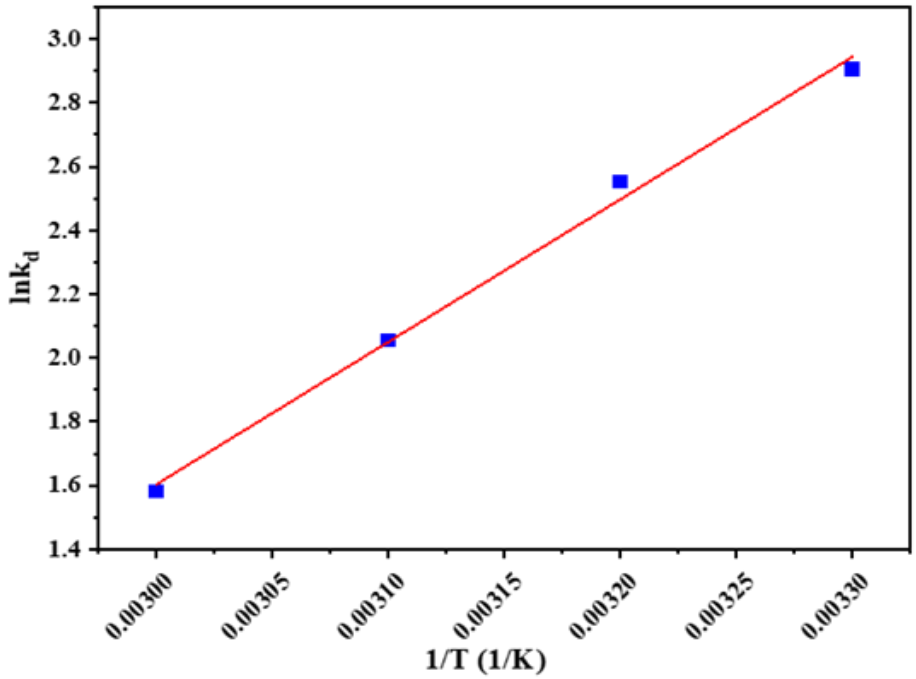

Fig. 4.21: van't Hoff equation data of Cr(III) adsorption on GO

It was obtained a straight line by plotting lnk_d versus 1/T (Table 4.14, Fig. 4.21). Entropy change ΔS from the intercept was -37.147 kJ mol^{-1}, and enthalpy change ΔH from the slope was -0.0981 kJ K^{-1} mol^{-1}. The value of ΔG increased from -7.197 to -4.314 kJ mol^{-1}

when the temperature increased from 298 K to 328 K. (Table 4.15). As a result, at lower temperatures, the Cr(III) adsorption on GO was spontaneous and of a physical nature.

Table 4.15: Thermodynamic parameters for adsorption of Cr(III) on GO

T(K)	ΔG (kJ mol^{-1})	ΔH (kJ mol^{-1})	ΔS (kJ K^{-1} mol^{-1})
298	-7.197	-37.147	-0.0981
308	-6.54		
318	-5.433		
328	-4.314		

4.1.3.1.7. Plausible mechanism for Cr(III) adsorption on GO

Adsorption process deals with interaction between oppositely charged particles forming various bonds, including hydrogen bond, electrostatic bond, van der Waals forces, dipole-dipole interaction, ion exchange, etc. Pore density or pore volume and surface chemistry are the two main variables that significantly affect the adsorption process. GO exhibits electrostatic interaction with the cationic metal ion at pH levels greater than ZPC (3.5) due to its negative surface charge. At pH>ZPC the carboxylate groups of GO create hexa-coordinate complexes by arresting Cr(III) ions (Fig. 4.22)

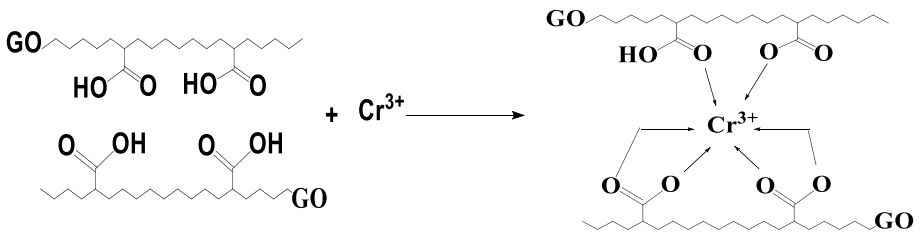

Fig. 4.22: Possible mechanism of adsorption for Cr(III) onto GO

4.1.3.1.8. Regeneration of used GO for Cr(III) adsorption

Using 2% dilute HCl, chromium loaded GO was regenerated and used again for Cr(III) adsorption at optimum pH, dosage and duration to evaluate the feasibility (Fig. 4.23). The results of the regeneration investigations showed that with further development, the regenerate may be utilized to remove Cr(III) from the aqueous solution once more. The

adsorption capacity steadily decreased from 150.85 to 142.87, 118.23 and 68.92 mg/g after recycle-1, recycle-2 and recycle-3, respectively (Fig. 4.24).

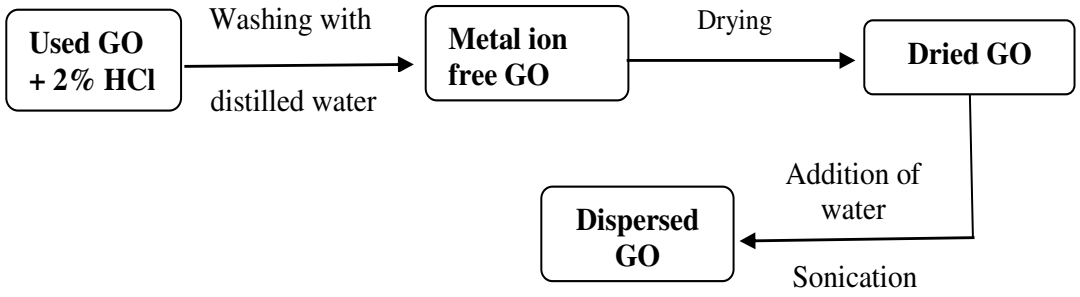

Fig. 4.23: Flow diagram of used GO of regeneration

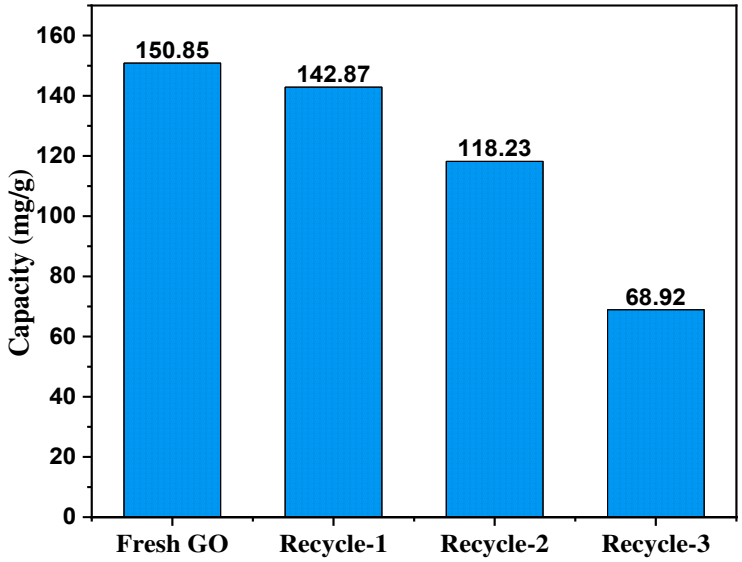

Fig. 4.24: Regeneration of used GO for Cr(III) adsorption

4.1.3.2. Adsorption of Cu(II) on GO

The efficiency of GO for Cu(II) removal is influenced by pH, adsorbent dosage, contact time, metal concentration, temperature and other parameters.

4.1.3.2.1. Effect of pH

pH is a vital parameter to assess the adsorption capacity of prepared GO due to its significant impact on the surface charge of both adsorbent and metal molecules. In order to

investigate the effect of pH on adsorption process, copper(II) solution (166.5 ppm, 20 mL) was taken in five conical flasks and the pH was adjusted to 3.0, 4.0, 5.0, 6.0 and 7.0. Then GO (0.039 g) was added to each solution and agitated at 150 rpm for 2 h at room temperature. The adsorption capacity of Cu(II) on GO surface was calculated and found maximum (84.95 mg/g) at pH 7.0 (Table 4.16, Fig. 4.25). However, it was observed that copper was precipitated at pH>6.0. Therefore pH 6.0 had been chosen as optimum for the adsorption study. The % removal and the optimum adsorption capacity of GO was 87.09% and 74.36 mg/g at pH 6.0 for copper(II) adsorption. The carboxylic groups of GO were deprotonated as pH increased, providing a negatively charged surface that cause the enhancement of Cu(II) adsorption. According to studies on ZPC, the GO had zero charge at pH 3.5 and beyond this pH surface become negatively charged and contributed to the adsorption process because of electrostatic attraction between the GO surface and Cu(II). Furthermore, pH below the ZPC, adsorbent surface was positively charged due to protonation of carboxylic group, which resulted electrostatic repulsion with metal ions. Moreover, at lower pH there was a high competition between the H^+ and metal ions, where adsorbent surface was mostly occupied by proton because of its smaller size and both these phenomena also led to lower adsorption of metal ions [218, 219]. With increasing pH, protonation and competition of H+ decreases, the amount of the negatively charged surfaces increases gradually until the solution pH approaches neutrality and towards the pHpzc. At pH higher than ZPC, GO surface became negatively charged due to deprotonation of carboxylic group (Fig. 4.10) and resulted electrostatic attraction between the GO surface and metal ions [226]. In addition to that at higher pH the proton concentration was reduced leading to less competition of protons with cations and resulted higher adsorption of metal ions [221]. This may result in increased electrostatic interaction and higher adsorption of copper(II) ion.

Table 4.16: pH, adsorption capacity and % removal data of GO for Cu(II) adsorption

pH	3.0	4.0	5.0	6.0	7.0
Adsorption capacity (mg/g)	31.1	48.97	51.03	74.36	84.94
% removal	40.00	57.36	59.76	87.09	99.48

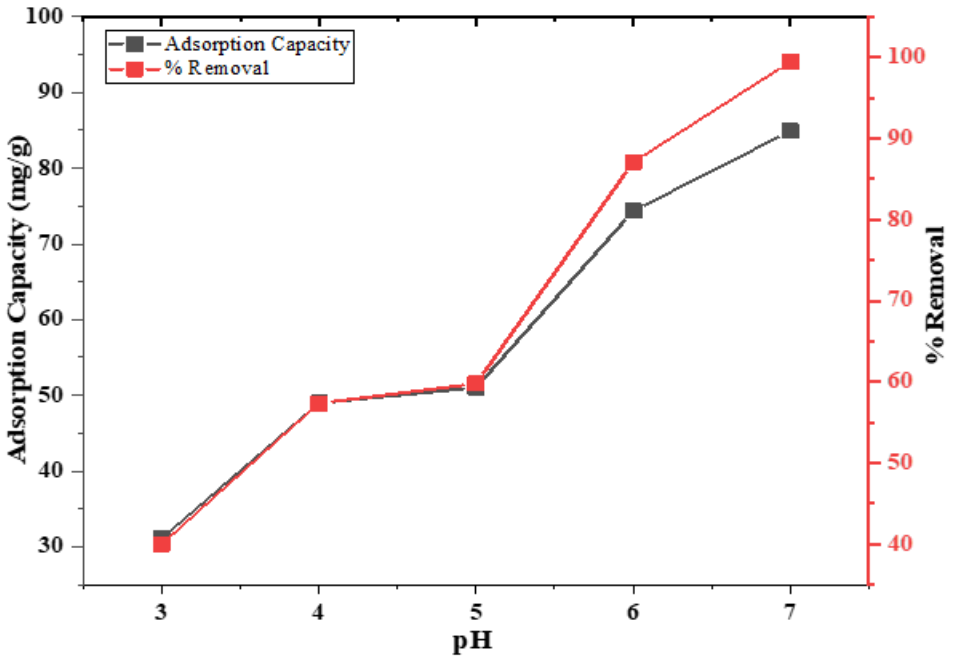

Fig. 4.25: Effect of pH on capacity and % removal of Cu(II) adsorption on GO

4.1.3.2.2. Effect of dosage

Experiment on adsorbent dosage optimization was carried out using standard copper salt (166.5 ppm, 10 mL) solution at optimum pH (6.0) with different dosages (0.25, 0.5, 1.0, 1.5, 2.0 and 2.5 g/L). The mixture was shaken in an orbital shaker at 150 rpm for 2 h. Adsorption capacity and percentage of removal were measured using equation (3.1 and 3.2). It was observed that the adsorption capacity was decreased, and the percentage of copper removal was increased with the increase of adsorbent dosage. In this study, 1.0 g/L dosage demonstrated optimum result as it was meet both the percentage of removal and adsorption capacity (Table 4.17, Fig. 4.26). Therefore, this dosage was taken as optimum for copper(II) adsorption.

Table 4.17: Dosage, adsorption capacity and % removal data of GO for Cu(II) adsorption

Dosage (g/L)	0.25	0.50	1.00	1.50	2.00	2.50
Adsorption capacity (mg/g)	204.80	146.20	134.00	98.33	79.20	69.24
% removal	30.75	43.90	80.48	88.59	95.14	96.46

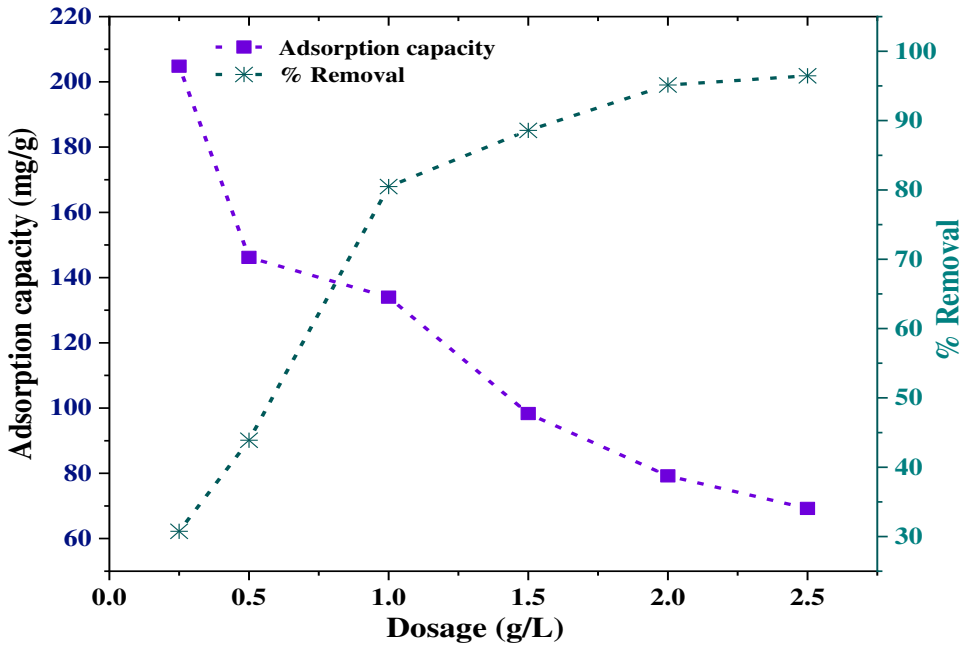

Fig. 4.26: Effect of dosage on capacity of Cu(II) adsorption on GO

4.1.3.2.3. Effect of Cu(II) ion concentration and contact duration

Batch experiments were used to investigate the impact of the initial Cu(II) concentration and contact time on adsorption capacity of GO (Table 4.18, Fig. 4.27). In the experiment, copper salt solution (10 mL) of different concentrations (99.3, 151.23, 203.6 and 240.3 ppm) were used at optimum pH (6.0) and dosage (1.0 g/L) for a certain time (2-120 min). The adsorption process was reached at equilibrium just after 20 min. The adsorbent surface's active sites gradually engaged by adsorbate as long as it had unoccupied active sites and increased adsorbent capacity until equilibrium was reached [224]. However, at lower concentration, the % removal was high since the quantity of metal was less as compared to the amount of adsorbents (Table 4.19, Fig. 4.28).

Table 4.18: Time and adsorption capacity data for Cu(II) adsorption on GO at different concentration

Time (min)	99.30 ppm	151.23 ppm	203.60 ppm	240.30 ppm
2	81.02	111.66	117.9	91.62
5	83.13	115.75	122.29	105.66
10	85.71	120.04	127.4	116.76
15	88.86	123.98	133.66	122.13
20	92.85	131.97	152.48	156.75
30	92.92	132.47	159.36	174.36
60	92.88	132.06	159.41	174.39
120	93.02	131.78	158.87	174.03

Table 4.19: Time and % removal data for Cu(II) adsorption on GO at different concentration

Time (min)	99.30 ppm	151.23 ppm	203.60 ppm	240.30 ppm
2	87.85	73.17	57.91	38.13
5	89.22	76.54	60.06	43.97
10	90.94	79.38	62.57	48.60
15	93.04	81.98	65.65	50.82
20	95.70	87.26	74.89	65.36
30	95.75	87.60	78.27	72.56
60	95.72	87.32	78.30	72.57
120	95.81	87.14	78.03	72.42

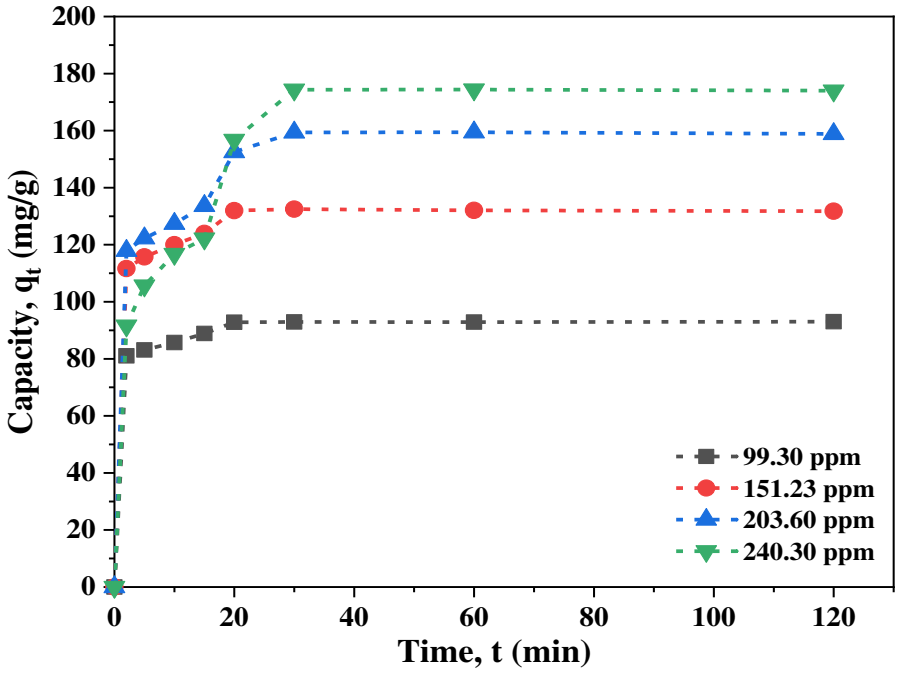

Fig. 4.27: Effect of time and concentration of Cr(III) on adsorption capacity of GO

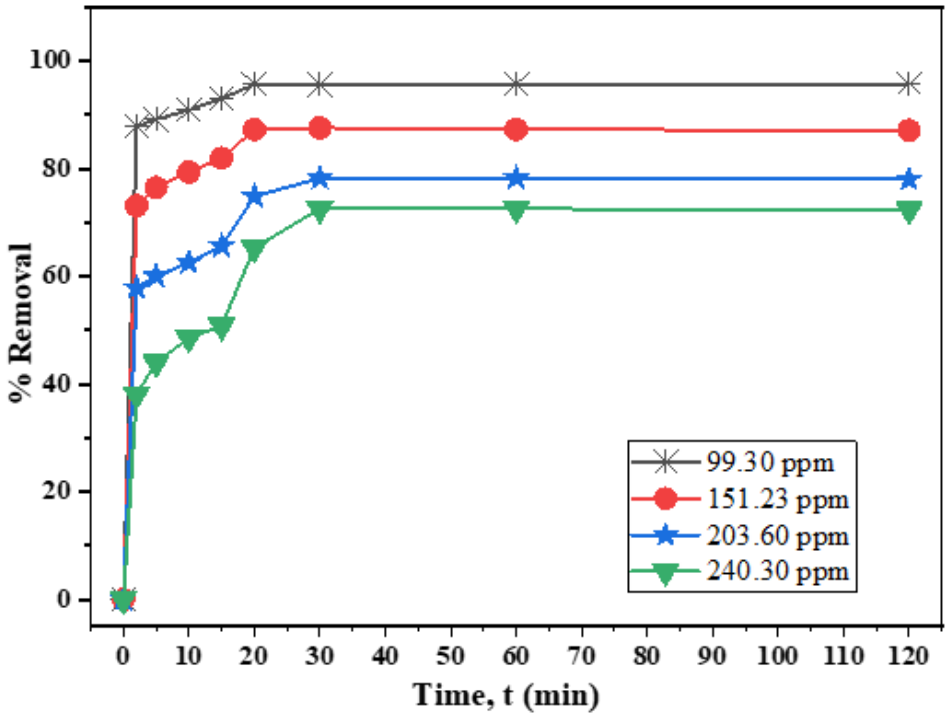

Fig. 4.28: Time and % removal of Cu(II) on GO at different concentration

4.1.3.2.4. Adsorption isotherms for Cu(II) adsorption on GO

Equilibrium isotherm studies have focused on the adsorption mechanism by generating equilibrium between adsorbate in solution and adsorbate on the surface of adsorbent.

Additionally, it establishes an adsorbent's maximum adsorption capacity when using a specific substance as an adsorbent. Copper(II) ion distribution on the GO surface was studied using both the Langmuir and Freundlich isotherm. The equilibrium adsorption model parameters and the correlation coefficient (R^2) values were calculated using OriginPro 2019B software and the results of both the isotherms were reported in a table (Table 4.22).

4.1.3.2.4.1. Langmuir isotherms

The theoretical maximum adsorption capacity, q_m from Langmuir model was calculated by plotting C_e/q_e versus C_e following the eq. (3.4) eq. (3.4) (Table 4.20, Fig. 4.29). Adsorption revealed a linear relationship between C_e/q_e and C_e with an acceptable regression coefficient (R^2=0.997). The slope was used calculate the theoretical maximum adsorption capacity, q_m which was 193.05 mg/g. The separation factor R_L was determined 0.032, which indicated favorable monolayer adsorption mechanism.

Table 4.20: C_e/q_e and C_e data for Cu(II) adsorption on GO at different concentration

Initial concentration (ppm)	99.30	151.23	203.60	240.30
Equilibrium concentration (C_e)	6.45	19.26	44.24	65.94
C_e/q_e	0.0694	0.1459	0.2776	0.3782

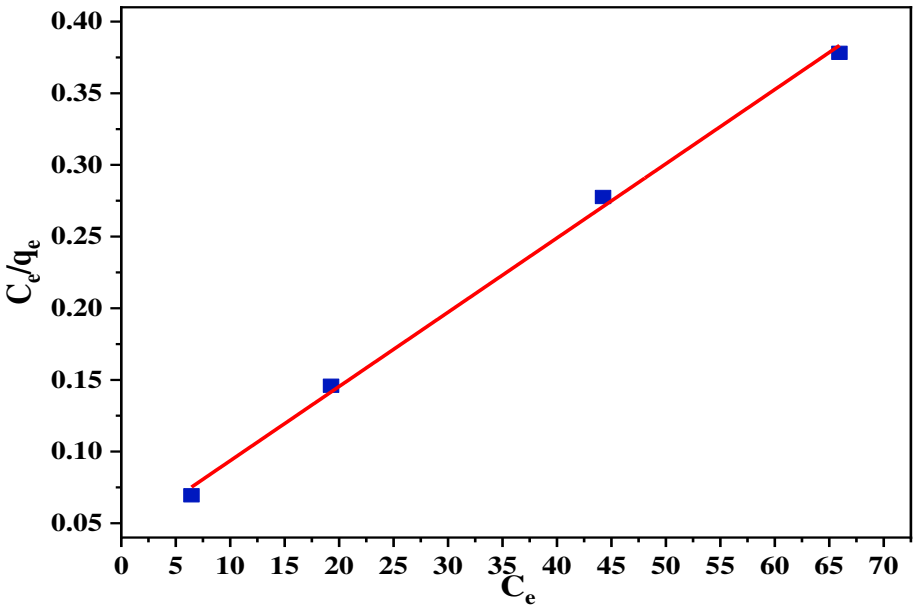

Fig. 4.29: Langmuir adsorption isotherm for Cu(II) adsorption on GO

4.1.3.2.4.2. Freundlich Isotherms

Plotting $\ln C_e$ versus $\ln q_e$ following eq. (3.6) was done to test the experimental data for the multilayer adsorption mechanism (Table 4.21, Fig. 4.30). An excellent regression coefficient (R^2=0.991) was observed along with a linear relationship. The n value was found to be 3.7, indicating that the adsorption was good (Table 4.20).

Table 4.21: $\ln C_e$ and $\ln q_e$ data of GO at different concentration for Cu(II) adsorption

Initial concentration (ppm)	99.30	151.23	203.60	240.30
$\ln C_e$	1.864	2.958	3.789	4.189
$\ln q_e$	4.531	4.883	5.071	5.161

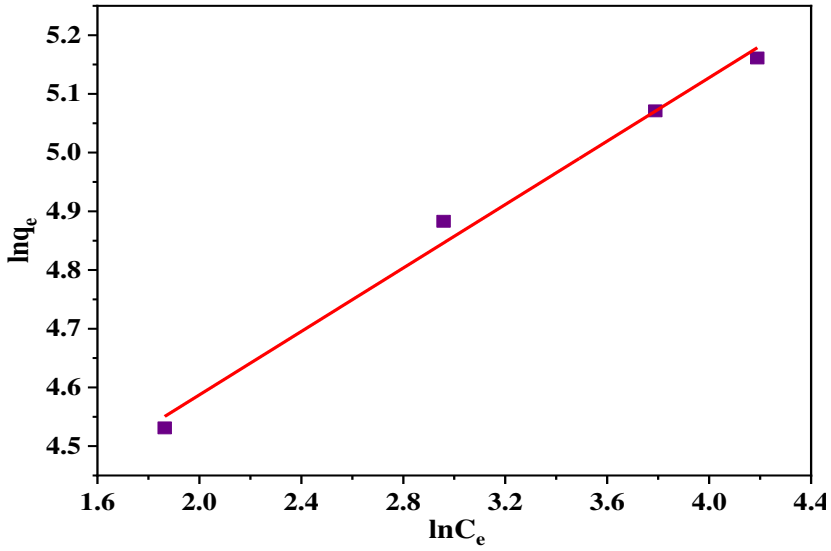

Fig. 4.30: Freundlich adsorption isotherm for Cu(II) adsorption on GO

The several parameters of both the isotherms are furnished in Table 4.22. The results show that the adsorption of Cu(II) on GO is consistent with the models.

Table 4.22: Theoretical values of q_m, b, R_L, n, k_F and R^2 of adsorbent GO for Cu(II) adsorption

Parameters	q_m, (mg/g)	b, Lmg^{-1}	R^2	R_L	n	k_F
Langmuir isotherm	193.05	0.1239	0.997	0.032	-	-
Freundlich isotherm	-	-	0.991	-	3.70	57.23

Considering the parameters and the value of R^2, Cu(II) adsorption on GO surfaces followed both the Langmuir and Freundlich isotherm model (Table 2.22, Fig. 4.29, 4.30) that represented monolayer and multilayer adsorption with maximum adsorption capacity (q_{max}) of 193.05 mg/g. The R_L value of Cu(II) was 0.032, which supported the monolayer adsorption mechanism [227], the overlapping patterns of several Langmuir-type sorption phenomena occurring at different sites on adsorbents could result Freundlich type isotherms [228]. Therefore, both the Langmuir and Freundlich isotherms were followed, which was regarded as the composite type isotherm. The composite isotherm was linear since the component Langmuir isotherms were linear.

4.1.3.2.5. Adsorption kinetics for Cu(II) on GO

Pseudo-first-order and pseudo-second-order kinetic models were used to describe the adsorption process of Cu(II) on GO.

4.1.3.2.5.1. Pseudo-first-order kinetics

Pseudo-first-order model was achieved by plotting $\log(q_e-q_t)$ versus t following the eq. (7), where a linear relation between them was found (Table 4.23, Fig. 4.29).

Table 4.23: Time, t (min) and $\log(q_e-q_t)$ data of GO at different concentration for Cu(II) adsorption

Time, t (min)	$\log(q_e-q_t)$ at 99.30 ppm	$\log(q_e-q_t)$ at 151.23 ppm	$\log(q_e-q_t)$ at 203.60 ppm	$\log(q_e-q_t)$ at 240.30 ppm
2	1.073	1.307	1.618	1.918
5	0.988	1.21	1.569	1.837
10	0.854	1.076	1.504	1.76
15	0.601	0.903	1.409	1.717
20	-	-	0.837	1.245

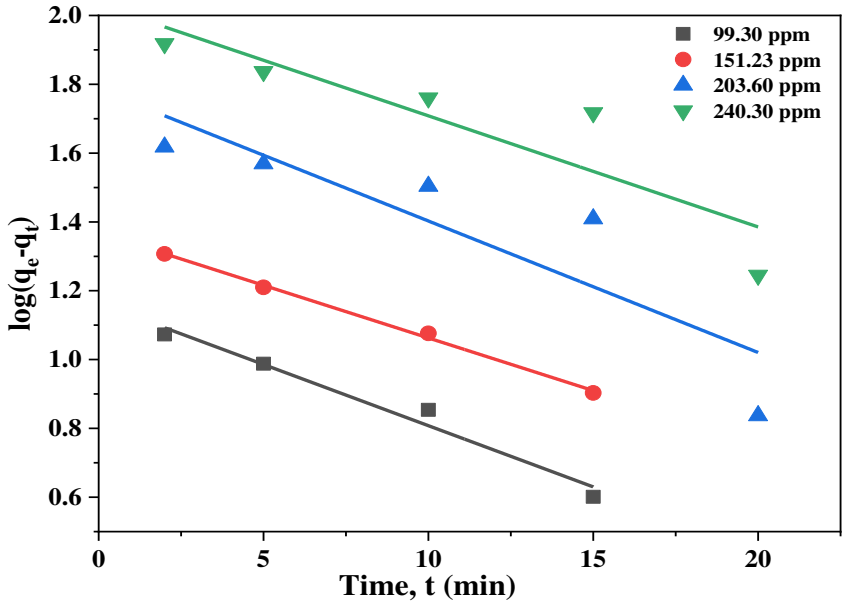

Fig: 4.31: Pseudo-first-order kinetics for adsorption of Cu(II) on GO

4.1.3.2.5.2. Pseudo-second-order kinetics

Pseudo-second-order model were gained by plotting the value of t/q_t versus t (Table 4.24, Fig. 4.32), following the eq. (3.8).

Table 4.24: Time, t (min) and t/q_t data of GO at different concentration for Cu(II) adsorption

Time, t (min)	t/q_t at 99.30 ppm	t/q_t at 151.23 ppm	t/q_t at 203.60 ppm	t/q_t at 240.30 ppm
2	0.025	0.018	0.017	0.021
5	0.06	0.043	0.041	0.047
10	0.117	0.083	0.078	0.086
15	0.168	0.121	0.112	0.123
20	0.215	0.152	0.131	0.128
30	-	-	0.188	0.172

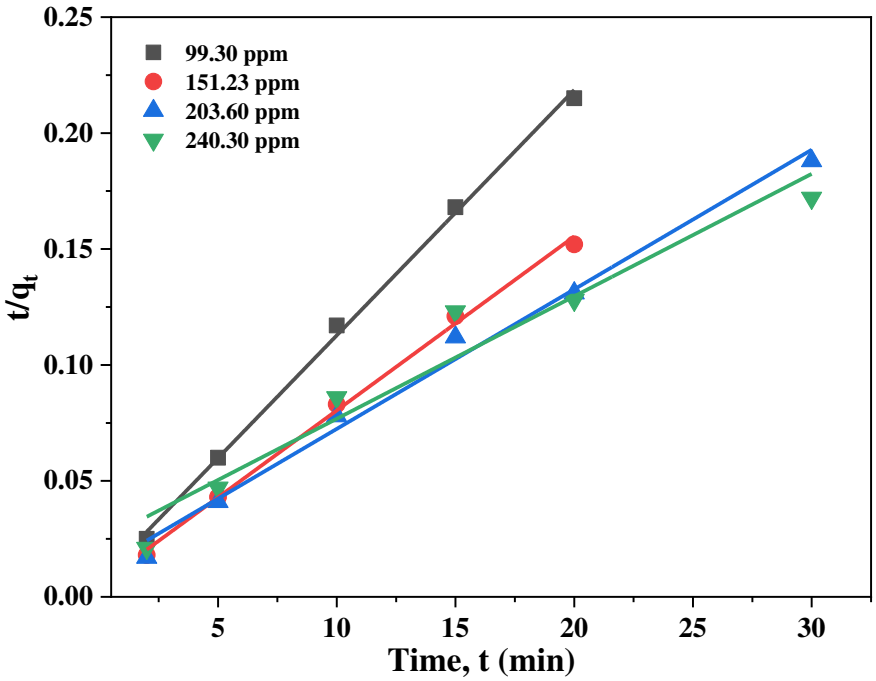

Fig: 4.32: Pseudo-second-order kinetics for adsorption of Cu(II) on GO

Considering the values of various parameters (Table 4.25), the results best fitted with pseudo-second-order model as the experimental values of q_e matched better and the regression coefficient value (R^2) of copper (0.998, 0.997, 0.989 and 0.949) also supportive

of pseudo-second-order model. The evidence suggests that the adsorption process is chemisorption. Hence, a strong attraction force develops between metal ions and the anionic functional groups present in the GO, resulting in the formation of electrostatic bonds during the adsorption process. The comparison of adsorption capacities for adsorption of Cu(II) on GO is shown in the Fig. 4.33.

Table 4.25: Kinetics parameter for Cu(II) adsorption on GO

Types of kinetics model	Parameters	Initial concentrations of Cu(II)			
		99.30 ppm	**151.23 ppm**	**203.60 ppm**	**240.30 ppm**
Pseudo-first-order	q_e^* (mg/g)	92.85	131.97	159.36	174.36
	k_1 (1/min)	0.0817	0.07	0.087	0.074
	R^2	0.973	0.997	0.772	0.802
	q_e^{**} (mg/g)	14.57	23.38	55.98	107.64
Pseudo-second-order	k_2 (g/mg min)	0.016	0.01	0.0029	0.0012
	R^2	0.998	0.997	0.989	0.949
	q_e^{**} (mg/g)	94.52	133.33	166.11	189.39

* Experimental, ** Theoretical

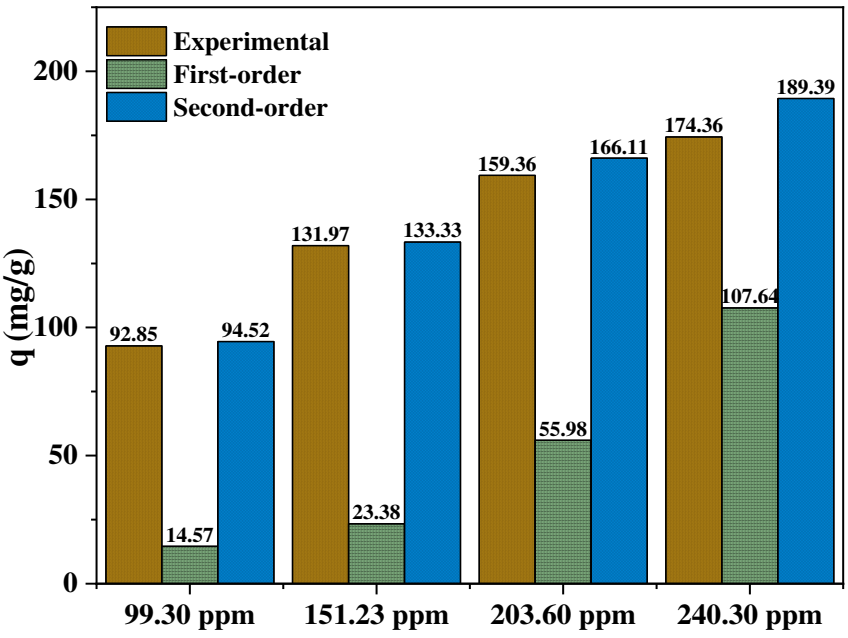

Fig. 4.33: Comparison of Cu(II) adsorption capacities for adsorption on GO

4.1.3.2.6. Thermodynamic analysis for Cu(II) adsorption on GO

At different temperatures (298-328 K), the Gibb's free energy changes (ΔG) for Cu(II) adsorption on GO were investigated. The parameters were evaluated using eq. (3.9) and (3.10), by calculating the changes of standard free energy, enthalpy and entropy. A straight line was found through plotting $\ln k_d$ versus 1/T (Table 4.26, Fig. 4.34). The process was demonstrated exothermic and spontaneous nature by values of changes in free energy (ΔG) and enthalpy (ΔH) (Table 4.27).

Table 4.26: $\ln k_d$ and 1/T data of GO for Cu(II) adsorption

1/T	0.0033	0.0032	0.0031	0.003
$\ln k_d$	1.925	1.498	1.066	0.728

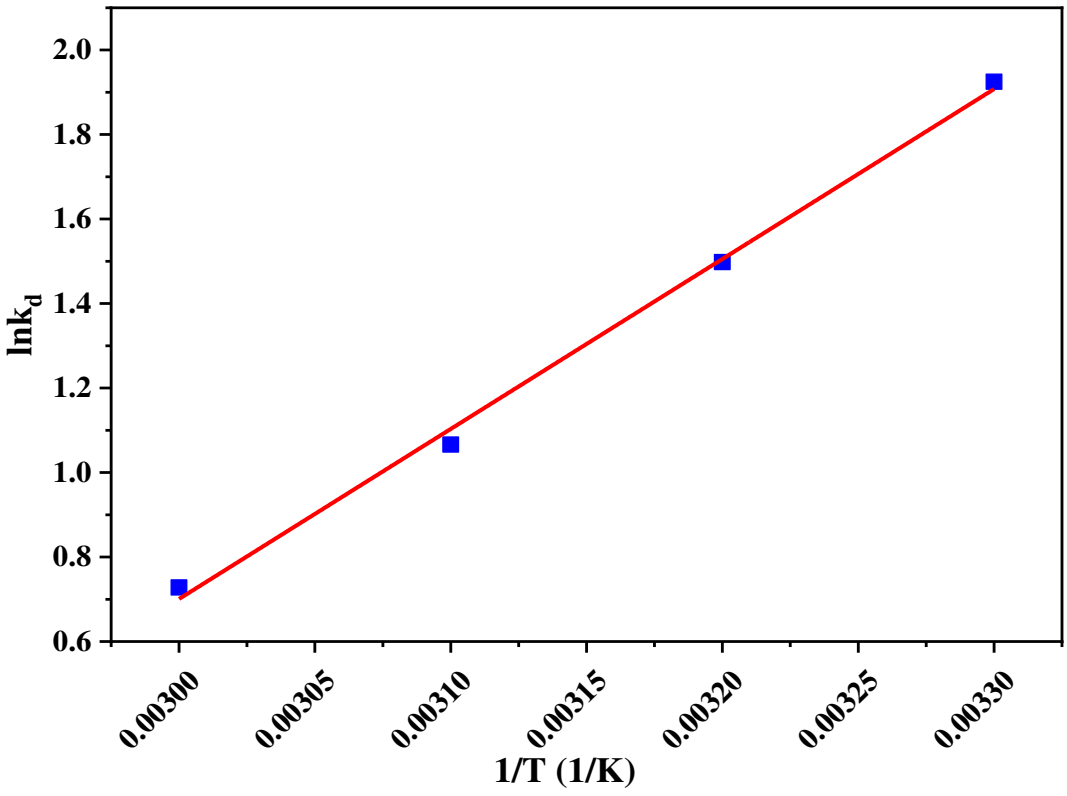

Fig. 4.34: van't Hoff equation data for Cu(II) adsorption on GO

Table 4.27: Thermodynamic parameters of GO for Cu(II) adsorption

T(K)	ΔG (kJ mol^{-1})	ΔH (kJ)	ΔS (kJ K^{-1} mol^{-1})
298	-4.769	-33.447	-0.0945
308	-3.836		
318	-2.818		
328	-1.985		

4.1.3.2.7. Plausible mechanism for Cu(II) adsorption on GO

Generally, hydrogen bonds, electrostatic interactions, dipole-dipole interaction, Vander Waals forces, etc. are the reasons of metal adsorption. Graphene oxide possesses negative surface charge at pH higher than its ZPC (>3.5), which interacts with positively charged copper ion through electrostatic bond (Fig. 4.35).

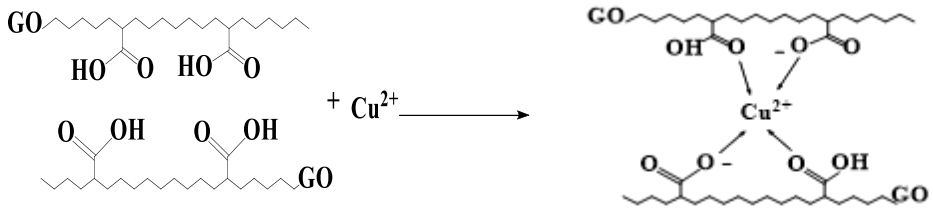

Fig. 4.35: Adsorption mechanism Cu(II) onto GO

Electrostatic attraction, external ion exchange and complexation were mostly responsible for Cu(II) adsorption onto GO as per the equations below:

$$GO - COOH + Cu^{2+} \rightarrow GO - COO^{-} - Cu^{2+} + H^{+} \quad \text{(i)}$$

$$(GO - COOH)_2 + Cu^{2+} \rightarrow (GO - COO^{-})_2 - Cu^{2+} + 2H \quad \text{(ii)}$$

$$GO - OH + Cu^{2+} \rightarrow GO - O^{-} - Cu^{2+} + 2H^{+} \quad \text{(iii)}$$

$$(GO - OH)_2 + Cu^{2+} \rightarrow (GO - O^{-})_2 - Cu^{2+} + 2H^{+} \quad \text{(iv)}$$

The projected adsorption mechanism was also supported by the fact that the equilibrium pH was lower than the initial pH that was mainly caused by the discharge of protons from

the -COOH and –OH groups of GO [229]. The possible chelation of copper ions may be represented as the Fig. 4.35.

4.1.3.2.8. Regeneration of used GO for Cu(II) adsorption

Regeneration studies of exhausted adsorbents provide valuable information about mechanism of adsorption. The regeneration was conducted with 2% HCl and reused for Cu(II) adsorption. The experiments revealed that adsorption capacity gradually reduced with multiple recycling. The Cu(II) adsorption capacity of fresh GO was 105.61 mg/g whereas after recycle-1, recycle-2, and recycle-3, it was reduced to 91.72, 81.21 and 77.49 mg/g, respectively (Fig. 4.36).

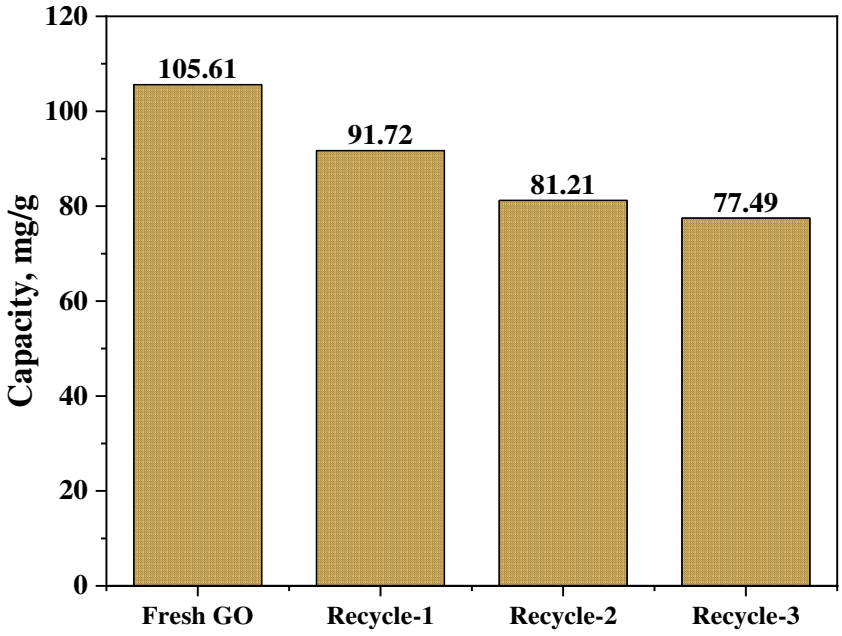

Fig. 4.36: Regeneration of used GO for Cu(II) adsorption

4.1.3.3. Adsorption of Cd(II) on GO

4.1.3.3.1. Effect of pH

pH of solution is a vital indicator as it can alter the surface charge of adsorbent and adsorbate. Effect of pH were studied at the range of pH 3-8. In these studies, cadmium(II) solutions (201.50 ppm, 20 mL) were taken in each of five conical flasks and the pH was adjusted to 3.0, 4.0, 5.0, 6.0, 7.0 and 8.0. Then GO (0.039 g) was added to each solution and stirred for 2 h at room temperature at 150 rpm in an orbital shaker. It was observed

that precipitation of Cd(II) was occurred at pH>7.0. Therefore, the pH 7.0 was considered as optimum at which the adsorption capacity and % removal were 87.45 mg/g and 84.62%, respectively (Table 4.28, Fig. 4.37). Studies on pH revealed that GO surface had zero charge at pH 3.5 (pH_{zpc}) and below this pH adsorbent surface was positively charged due to protonation of carboxylic group, which resulted electrostatic repulsion with metal ions. Moreover, at lower pH there was a high competition between the H^+ and metal ions, where adsorbent surface was mostly occupied by proton due to its smaller size. As a result, lower adsorption of cadmium(II) ions onto GO. On the contrary, at pH higher than ZPC, GO surface became negatively charged because of deprotonation of carboxylic group and resulted electrostatic attraction between the GO surface and cadmium ions. Moreover, at higher pH the proton concentration was reduced leading to less competition of protons with cadmium ions and resulted higher adsorption of Cd(II) ions.

Table 4.28: pH vs adsorption capacity and % removal data of GO for Cd(II) adsorption

pH	3.0	4.0	5.0	6.0	7.0	8.0
Adsorption capacity (mg/g)	65.9	81.54	85.4	85.64	87.45	103.09
% removal	63.77	78.91	82.63	82.88	84.62	99.77

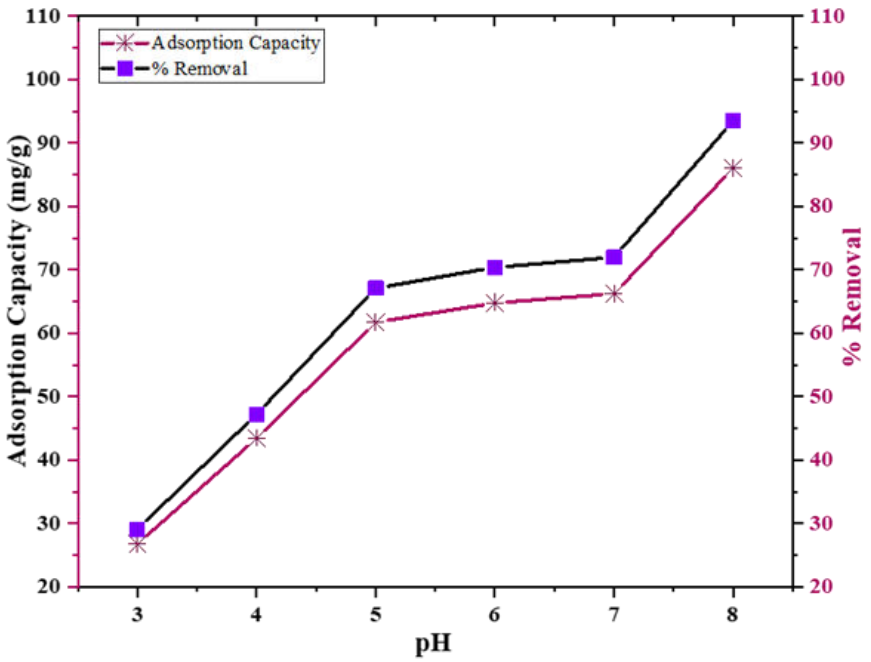

Fig. 4.37: Effect of pH on adsorption capacity and % removal of Cd(II) on GO

4.1.3.3.2. Effect of adsorbent dosage

Effects of dosage on adsorption of cadmium(II) were investigated using cadmium(II) salt solution at different dosages (0.25-2.5 g/L) at optimum pH 7.0. Adsorbent capacities and percentage of removals were measured and found that % of Cd(II) removals were increased with the increase of dosages, however adsorption capacity of GO decreased (Table 4.29, Fig. 4.38). The optimum dosage of GO for was observed 1.5 g/L for cadmium removal.

Table 4.29: Dosage, adsorption capacity and % removal data of GO for Cd(II) adsorption

Dosage (g/L)	0.50	1.00	1.50	2.00	2.50
Adsorption capacity (mg/g)	147	131.9	102.6	90.4	75.68
% removal	36.48	65.46	76.38	89.73	93.89

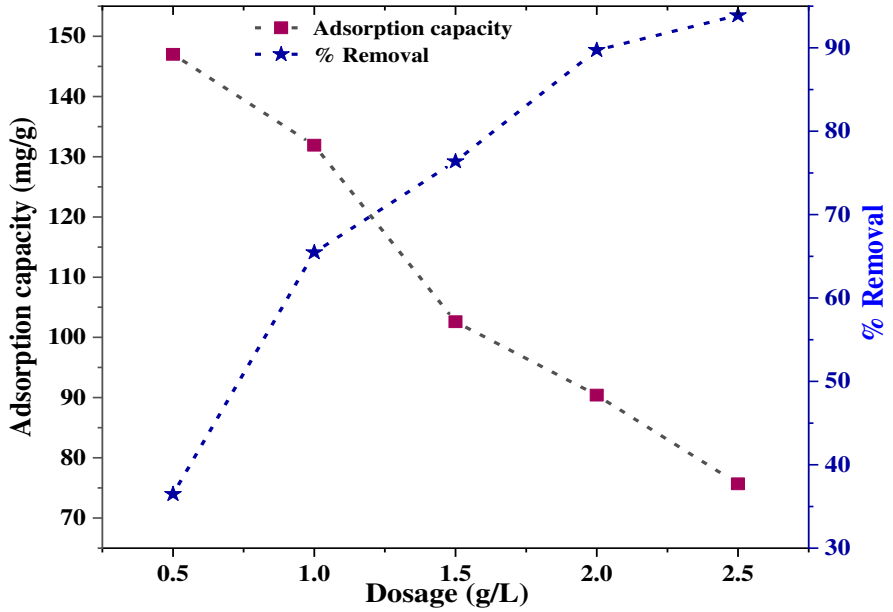

Fig. 4.38: Effect of dosage for adsorption of Cd(II) on GO

4.1.3.3.3. Effect of Cd(II) ion concentrations and contact duration

Batch experiments were conducted using cadmium salt solution (10 mL) of different concentration (103.82, 152.15, 201.40 and 250.65 ppm) at pH (7.0) and dosage (1.5 g/L) for a certain time (2-120 min) to study the effect of metal concentration and contact

duration (Table 4.30, Fig. 4.39). The cadmium adsorption process reached at equilibrium at 20 min. Enormous active sites of adsorbent were available initially, however as the time passed on those sites became saturated. Therefore, the adsorption capacity of GO increased over time until it stabilized at equilibrium. If initial cadmium concentration increased, equilibrium adsorption capacity also increased due to higher concentration gradient.

Table 4.30: Adsorption capacity of GO at different concentration of Cd(II) at different time intervals

Time (min)	103.82 ppm	152.15 ppm	201.40 ppm	250.65 ppm
2	49.32	70.57	97.17	117.18
5	52.59	76.59	99.46	118.71
10	55.03	78.58	102.55	122.69
15	57.11	81.31	105.41	126.13
20	59.31	84.56	108.37	130.08
30	60.03	84.69	108.85	130.45
60	59.69	84.47	108.24	130.02
120	59.38	83.93	108.54	130.55

Table 4.31: Time and % removal data for Cu(II) adsorption on GO at different concentration

Time (min)	103.82 ppm	152.15 ppm	201.40 ppm	250.65 ppm
2	71.26	69.58	72.38	70.13
5	75.91	74.78	74.09	71.04
10	79.51	77.48	76.39	73.42
15	82.50	80.17	78.52	75.48
20	85.68	83.37	80.71	77.85
30	86.74	83.51	81.08	78.07
60	86.25	83.29	80.62	77.67
120	85.79	82.75	80.84	77.93

As a result, mass transfer occurred between the cadmium solution and adsorbent GO [230]. However, the % removal was higher at lower cadmium concentration since the amount of Cd was less as compared to the amount of adsorbent, GO (Table 4.31, Fig. 4.40).

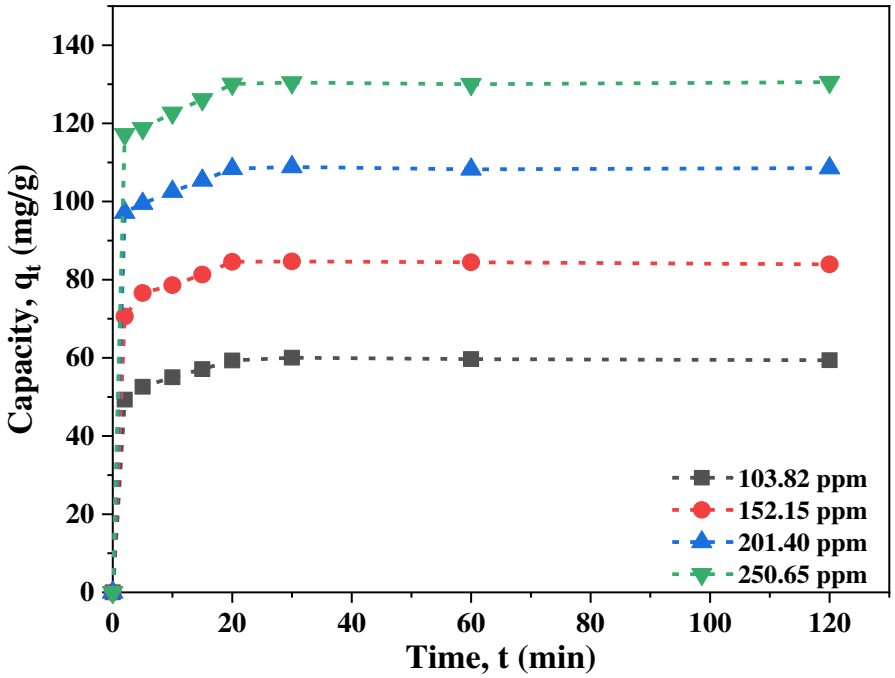

Fig. 4.39: Effect of Cd(II) ion concentration and contact duration on adsorption capacity of GO

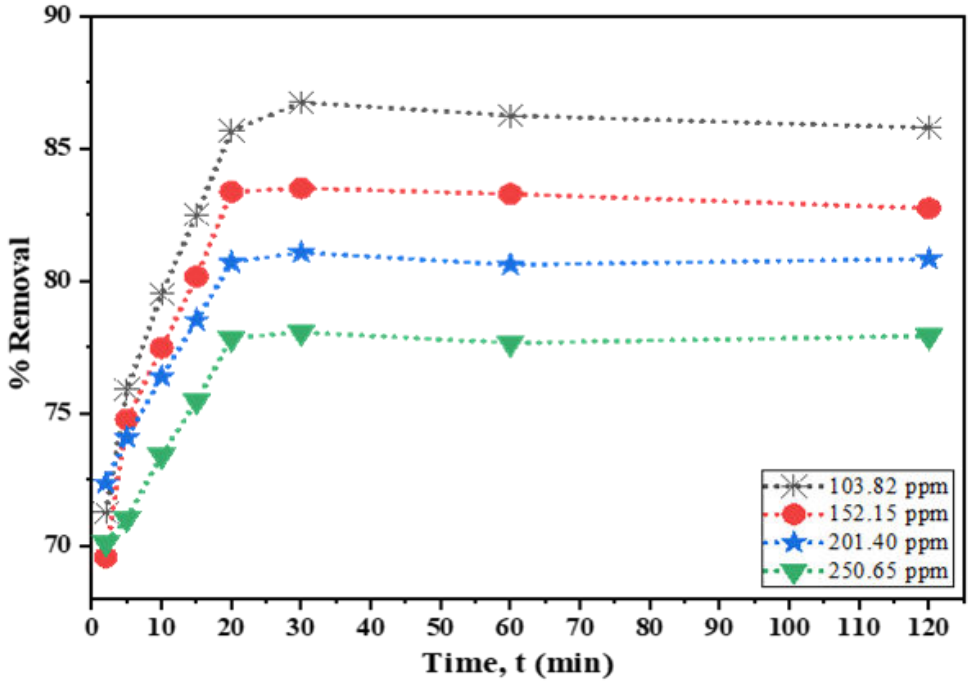

Fig. 4.40: Effect of time and % removal at different concentration of Cu(II)

4.1.3.3.4. Adsorption isotherms for Cd(II) adsorption on GO

Langmuir and Freundlich isotherm were used to investigate the distribution of cadmium on GO. Monolayer adsorption followed by Langmuir isotherm and multilayer adsorption followed by Freundlich adsorption.

4.1.3.3.4.1. Langmuir isotherm

Langmuir model was applied by plotting C_e/q_e versus C_e following the eq. (3.4) and (3.5) for cadmium(II) adsorption on GO. A linear relationship between C_e/q_e and C_e was found (Table 4.32, Fig. 4.41) with an acceptable regression coefficient (R^2=0.999). The calculated theoretical maximum adsorption capacity, q_m was observed to be 231.48 mg/g and separation factor, R_L was 0.148, which indicated a favorable monolayer adsorption process.

Table 4.32: C_e and C_e/q_e data of GO at different concentration for Cd(II) adsorption

Initial concentration (ppm)	103.82	152.15	201.40	250.65
Equilibrium concentration (C_e)	14.86	25.31	38.84	55.53
C_e/q_e	0.251	0.299	0.358	0.427

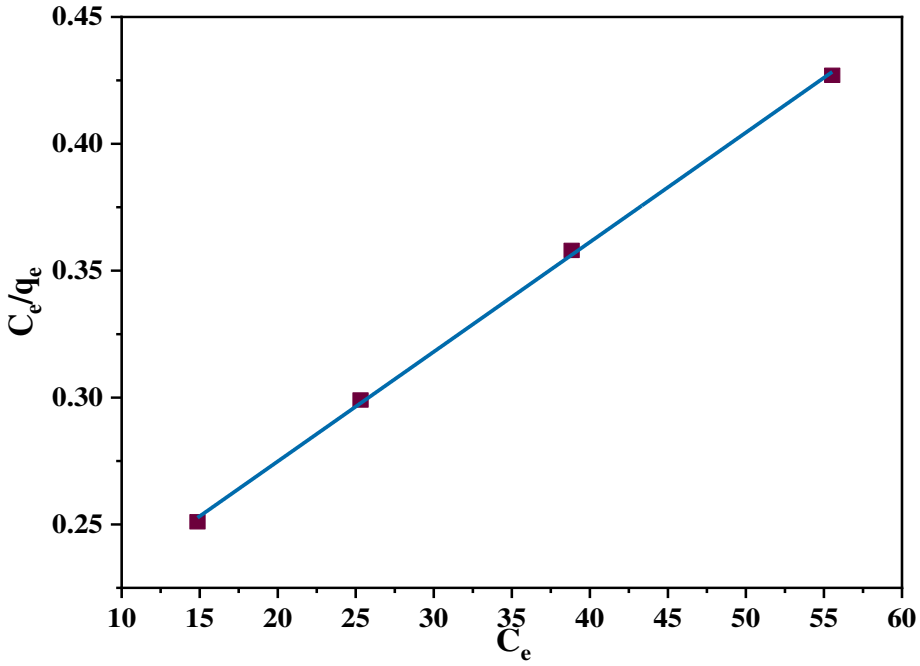

Fig. 4.41: Langmuir adsorption isotherm for adsorption of Cd(II) on GO

4.1.3.3.4.2. Freundlich isotherm

Freundlich isotherm was carried out by plotting $\ln C_e$ versus $\ln q_e$ following eq. (3.6). A linear relation was observed (Table 4.33, Fig. 4.42) with an excellent regression coefficient (R^2=0.996). The n value was calculated and found to be 1.675 which indicated the adsorption was difficult.

Table 4.33: $\ln C_e$ and $\ln q_e$ data of GO at different concentration for Cd(II) adsorption

Initial concentration (ppm)	103.82	152.15	201.40	250.65
$\ln C_e$	2.699	3.231	3.659	4.017
$\ln q_e$	4.083	4.437	4.686	4.868

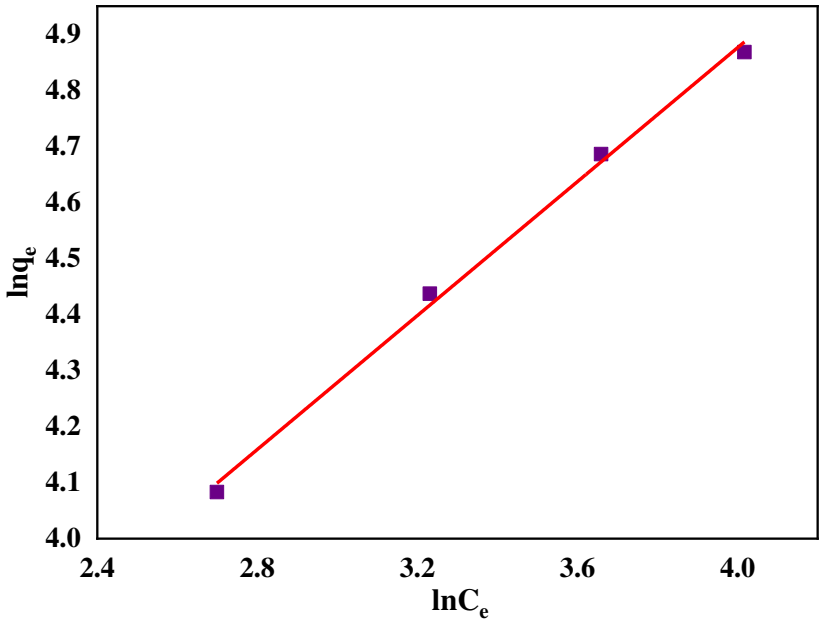

Fig. 4.42: Freundlich adsorption isotherm for Cd(II) adsorption on GO

The several Langmuir and Freundlich isotherm parameters and the correlation coefficient (R^2) values were calculated using OriginPro 2019B software and were furnished in the Table 4.34 which evidenced that the cadmium ion was adsorbed on GO following both the models.

Table 4.34: Theoretical values of q_m, b, R_L, n, k_F and R^2 of adsorbent GO for Cu(II) adsorption

Parameters	q_m, (mg/g)	b, Lmg^{-1}	R^2	R_L	n	k_F
Langmuir isotherm	231.48	0.023	0.999	0.148	-	-
Freundlich isotherm	-	-	0.996	-	1.675	12.019

Considering the parameters and the value of R^2, cadmium(II) adsorption on GO surfaces followed both the Langmuir and Freundlich isotherm model (Table 4.34, Fig. 4.41, 4.42), which represented monolayer and multilayer adsorption of Cd(II) ion with maximum adsorption capacity (q_{max}) of 231.48 mg/g. The R_L value 0.148 supported the advantageous monolayer adsorption mechanism [227]. The overlapping patterns of several Langmuir-type sorption phenomena occurring at different sites on adsorbents could result Freundlich type isotherms [228]. Therefore, both the Langmuir and Freundlich isotherms were

followed, which was regarded as the composite type isotherm. The composite isotherm was linear since the component Langmuir isotherms were linear.

4.1.3.3.5. Adsorption kinetics for Cd(II) adsorption on GO

Adsorption kinetics is very significant for evaluating the performance of an adsorbent. Pseudo-first-order and pseudo-second-order kinetic models were used to explain the adsorption of cadmium on GO.

4.1.3.3.5.1. Pseudo-first-order kinetics

Pseudo–first-order model was attained by plotting $\log(q_e-q_t)$ versus t at several initial concentrations of cadmium following the eq. (3.7) where a linear relationship between $\log(q_e-q_t)$ and t was found. The time (t) and $\log(q_e-q_t)$ data at different concentrations for Cd(II) adsorption is shown in Table 4.35 and pseudo-first-order kinetics for adsorption of Cd(II) on GO is shown in Fig. 4.43.

Table 4.35: Time, t and $\log(q_e-q_t)$ data of GO at different concentration for Cd(II) adsorption

Time, t (min)	$\log(q_e-q_t)$ at 103.82 ppm	$\log(q_e-q_t)$ at 152.15 ppm	$\log(q_e-q_t)$ at 201.40 ppm	$\log(q_e-q_t)$ at 250.65 ppm
2	0.999	1.146	1.049	1.111
5	0.827	0.901	0.949	1.055
10	0.631	0.776	0.764	0.868
15	0.342	0.512	0.471	0.596

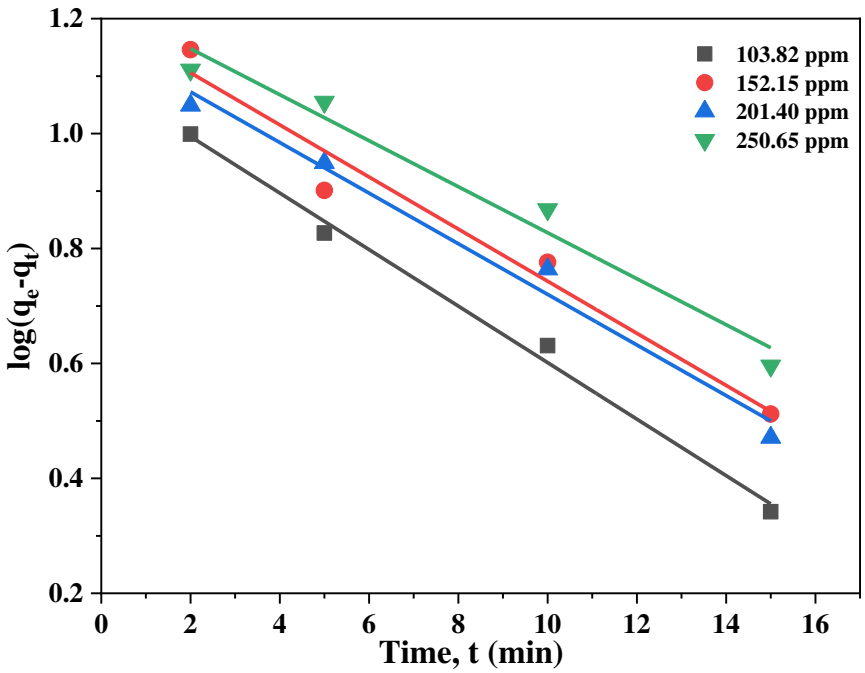

Fig. 4.43: Pseudo-first-order kinetics for adsorption of Cd(II) on GO

4.1.3.3.5.2. Pseudo-second-order kinetics

Pseudo-second-order model was obtained by plotting t/q_t versus t following the eq. (3.8). A linear relation was found between t/q_t and t (Table 4.36, Fig. 4.44). Taking into account the kinetic parameters listed in the Table 4.37, it was found that second-order kinetics consistently performed notably better than first-order kinetics in terms of correlation coefficient values.

Table 4.36: Time, t and t/q_t data of GO at different concentration for Cd(II) adsorption

Time, t (min)	t/q_t at 103.82 ppm	t/q_t at 152.15 ppm	t/q_t at 201.40 ppm	t/q_t at 250.65 ppm
2	0.041	0.028	0.021	0.017
5	0.0951	0.065	0.05	0.042
10	0.182	0.127	0.098	0.082
15	0.263	0.184	0.142	0.119
20	0.337	0.236	0.185	0.154

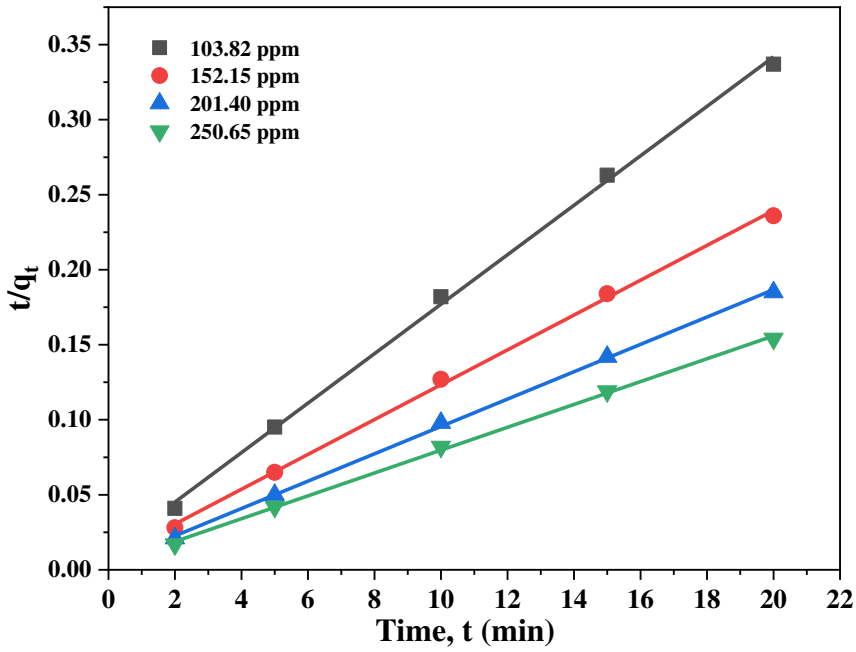

Fig. 4.44: Pseudo-second-order model for adsorption of Cd(II) on GO

Table 4.37: Kinetic parameters for adsorption of Cd(II) on GO

Kinetics model	Parameters	103.82 ppm	152.15 ppm	201.40 ppm	250.65 ppm
Pseudo-first-order	q_e^* (mg/g)	59.31	84.56	108.37	130.08
	k_1(1/min)	0.1131	0.1043	0.101	0.092
	R^2	0.993	0.964	0.982	0.971
	q_e^{**} (mg/g)	12.39	15.72	14.47	16.89
Pseudo-second-order	k_2 (g/mg min)	0.022	0.018	0.0189	0.016
	R^2	0.998	0.998	0.999	0.998
	q_e^{**} (mg/g)	60.68	86.13	109.65	131.41

* Experimental, **Theoretical

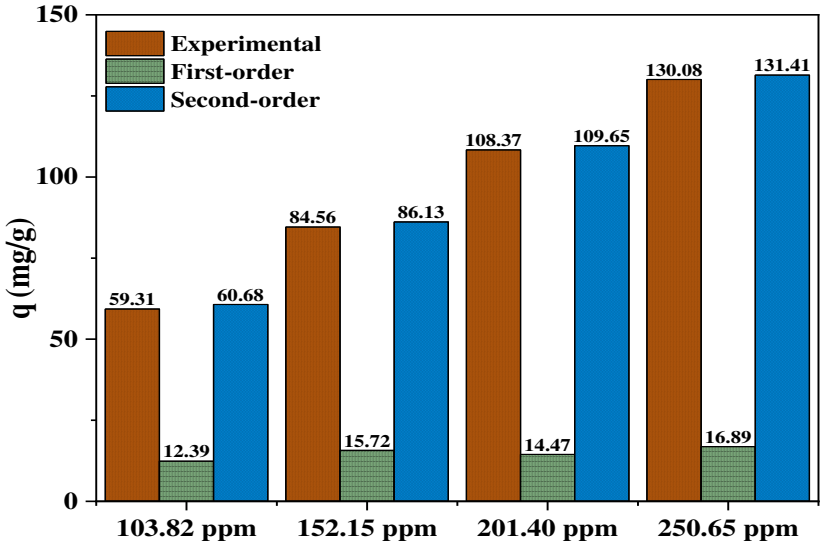

Fig. 4.45: Comparison of Cd(II) adsorption capacities on GO

The regression coefficient value (R^2) of cadmium (0.998, 0.998, 0.999, 0.998) are supportive of pseudo-second-order model (Table 4.37). The evidence suggests that the adsorption process is chemisorption, where a strong attraction force develops between metal ions and the anionic functional groups present in the GO resulting in the formation of electrostatic bonds during the adsorption process. It was also evidenced that the estimated values of adsorption capacities for pseudo-second-order kinetics fitted better with the observed experimental values (Fig. 4.45).

4.1.3.3.6. Thermodynamic analysis for adsorption of Cd(II) on GO

Thermodynamic parameters were evaluated using van't Hoff equations for removal of cadmium(II) with GO at different temperatures (298-328 K) by calculating change of Gibb's free energy, enthalpy and entropy. It was obvious from the findings (Table 4.38, Fig. 4.46, Table 4.39) as well as free energy change (ΔG) and enthalpy change (ΔH), that the process was exothermic, spontaneous and the Cd(II) adsorption on GO was a physical adsorption.

Table 4.38: 1/T and $\ln k_d$ data of GO for Cd(II) adsorption

1/T	0.0033	0.0032	0.0031	0.003
$\ln k_d$	1.206	0.951	0.639	0.289

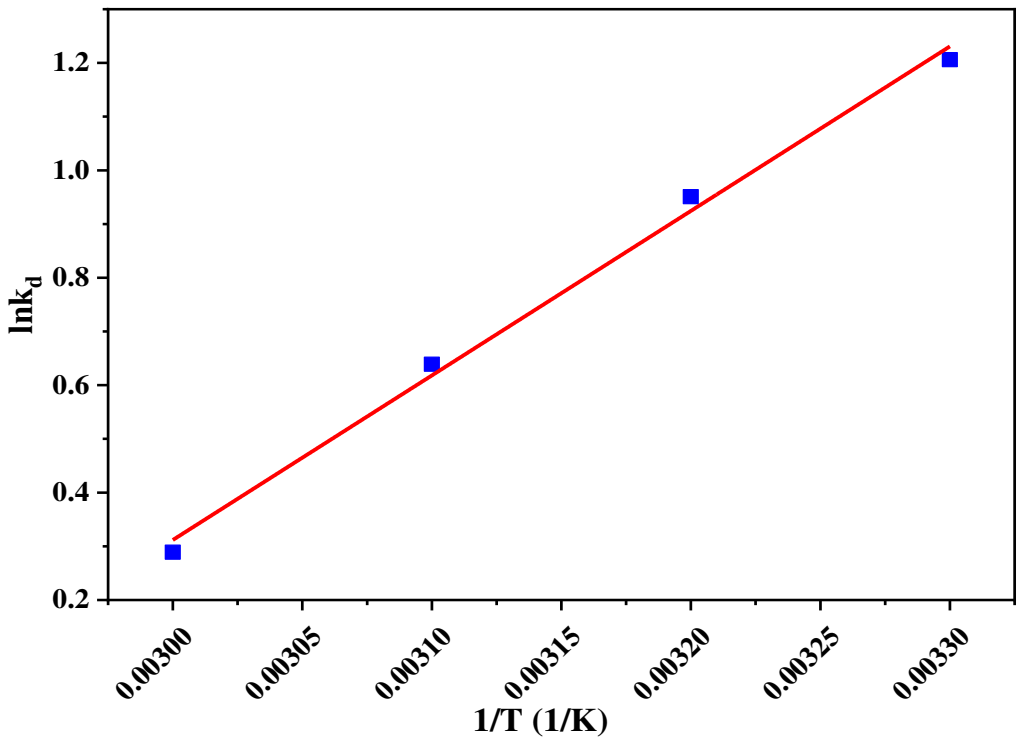

Fig. 4.46: van't Hoff equation data for adsorption of Cd(II) on GO

Table 4.39: Parameters of thermodynamic study for adsorption of Cd(II) on GO

T (K)	ΔG (kJ mol^{-1})	ΔH (kJ)	ΔS (kJ K^{-1} mol^{-1})
298	-2.987	-25.465	-0.0738
308	- 2.434		
318	- 1.689		
328	- 0.788		

4.1.3.3.7. Plausible mechanism for Cd(II) adsorption on GO

Adsorption occurs when oppositely charged particles come into contact through a variety of binding mechanisms, including electrostatic interactions, hydrogen bonds, dipole-dipole interactions, van der Waals forces, ion exchange, etc. Graphene oxide has a negative surface charge at pH higher than ZPC (>3.5), positively charged cadmium ions can interact electrostatically with it. The GO surface contained negatively charged carboxylate groups at pH >ZPC and resulted electrostatic attraction between the GO surface and cadmium ions. In addition to that at higher pH the proton concentration was reduced

leading to less competition of protons with cations and resulted higher adsorption of cadmium ions on to GO. The Fig. 4.47 may be used to illustrate the potential chelation of cadmium(II) ions.

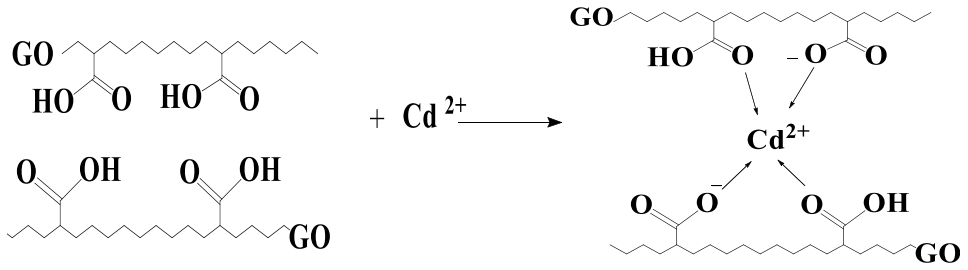

Fig. 4.47: Possible adsorption mechanism of Cd(II) onto GO

4.1.3.3.8. Regeneration of used GO for Cd(II) adsorption

The regeneration was done with 2% HCl and reused for Cd(II) adsorption to investigate the potential re-use. It is revealed that adsorption capacity gradually decreased with multiple recycling (Fig. 4.48). Adsorption capacity of fresh GO was 63.13 mg/g, however, it was 61.54, 54.23 and 45.24 mg/g after first, second and third recycling, respectively.

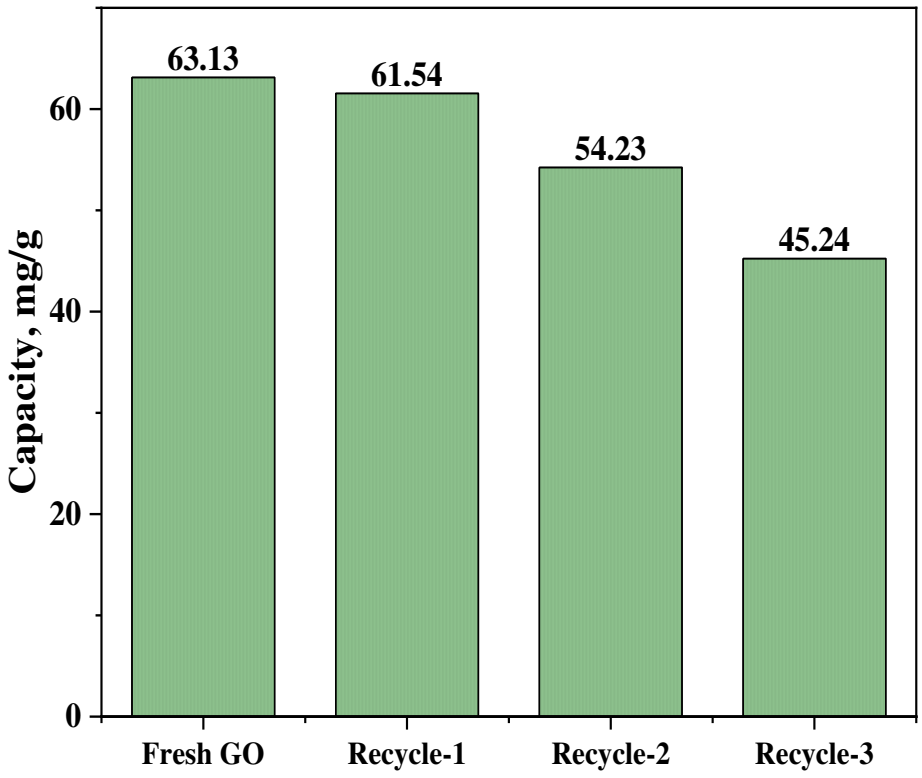

Fig. 4.48: Regeneration of GO for Cd(II) adsorption

4.1.3.3.9. Application of GO on tanning effluents

After assessing the capacity of GO in removing Cr(III), Cu(II) and Cd(II) form prepared standard solution by various batch adsorption methods, the performance to remove chromium, copper and cadmium ions from real sample of chrome tanning effluent was verified. In order to observe the adsorption of Cr(III), Cu(II) and Cd(II) from concentrated effluent, 5 g of GO was added to 500 mL of chrome tanning effluent and shaken for 4 h at pH 4.8 at room temperature. After filtration, the concentrations of chromium, copper and cadmium were analyzed by ICP-MS and other water quality parameters such as pH, TDS, EC, % of NaCl, BOD_5, and COD were also evaluated and the results were shown in the Table 4.40.

Table 4.40: Physicochemical characteristics of chrome tanning effluent before and after adsorption with GO

Parameters	Before adsorption	After adsorption	% of removal	DoE Standard
Cr(III) (ppm)	3276.64	1278.41	60.98	2.00
Adsorption capacity (mg/g)	-	199.82	-	-
Cu(II) (ppm)	1.29	0.57	55.81	0.50
Cd(II) (ppm)	0.94	0.10	52.38	0.50
pH	4.60	5.40	-	6-9
TDS (ppm)	6,014	2,307	61.64	2,100
EC (µS/cm)	9,875	3,124	68.36	1200
NaCl (%)	14.97	7.84	47.63	-
BOD_5 (ppm)	3,678	1,126	69.39	100
COD (ppm)	10,516	3,115	71.33	200

4.1.3.3.10. Application of GO on tannery effluents

To examine the performance of prepared GO for removal of chromium, copper and cadmium ions from real sample of tannery effluents, 1.25 g of GO was added to 500 mL of tannery effluents and agitated at 150 rpm at room temperature for 4 h at pH 5.8. The concentration of chromium, copper and cadmium before and after adsorption was determined by ICPMS. The other quality parameters like pH, TDS, EC, NaCl %, BOD_5 and COD were also determined. The evaluated data are shown in Table 4.41.

Table 4.41: Physicochemical characteristics of tannery effluents before and after adsorption with GO

Parameters	**Before adsorption**	**After adsorption**	**% of removal**	**DoE Standard**
Cr(III) (ppm)	423.28	62.47	85.24	2.00
Adsorption Capacity (mg/g)	-	144.32	-	
Cu(II) (ppm)	2.05	0.64	68.78	0.50
Cd(II) (ppm)	1.17	0.35	74.36	0.50
pH	5.8	6.1	-	6-9
TDS (ppm)	7,842	2,792	66.42	2100
EC (µS/cm)	5,426	1,656	69.48	1200
NaCl (%)	12.57	7.32	58.24	-
BOD_5 (ppm)	2,149	1,248	58.08	100
COD (ppm)	6,332	2,480	60.83	200

4.2 Part 2. Synthesis, characterization and application of calcium alginate graphene oxide (CA-GO) for Cr(III), Cu(II) and Cd(II) ions removal from aqueous solutions

4.2.1 Synthesis of calcium alginate (CA) and CA-GO composite beads

4.2.1.1 Preparation of CA beads

Calcium-alginate beads were synthesized using a calcium chloride solution and a sodium alginate solution. In order to achieve homogeneous dispersion in the solution media, 2 g of sodium alginate were first dissolved in 50 mL deionized (DI) water under magnetic stirring at 150 rpm for three h at room temperature and then ultrasonicated for 30 min to produce uniform dispersion. This dispersion was then carefully dropped into an aqueous coagulation bath containing 6% $CaCl_2$ (w/v). The bath was continuously agitated with a magnetic stirrer to prevent agglomeration of beads. The beads were left for 24 h without agitation to complete cross-linking and formation of calcium alginate beads. The simplified flow chart for the calcium alginate beads formation is shown in Fig. 4.49.

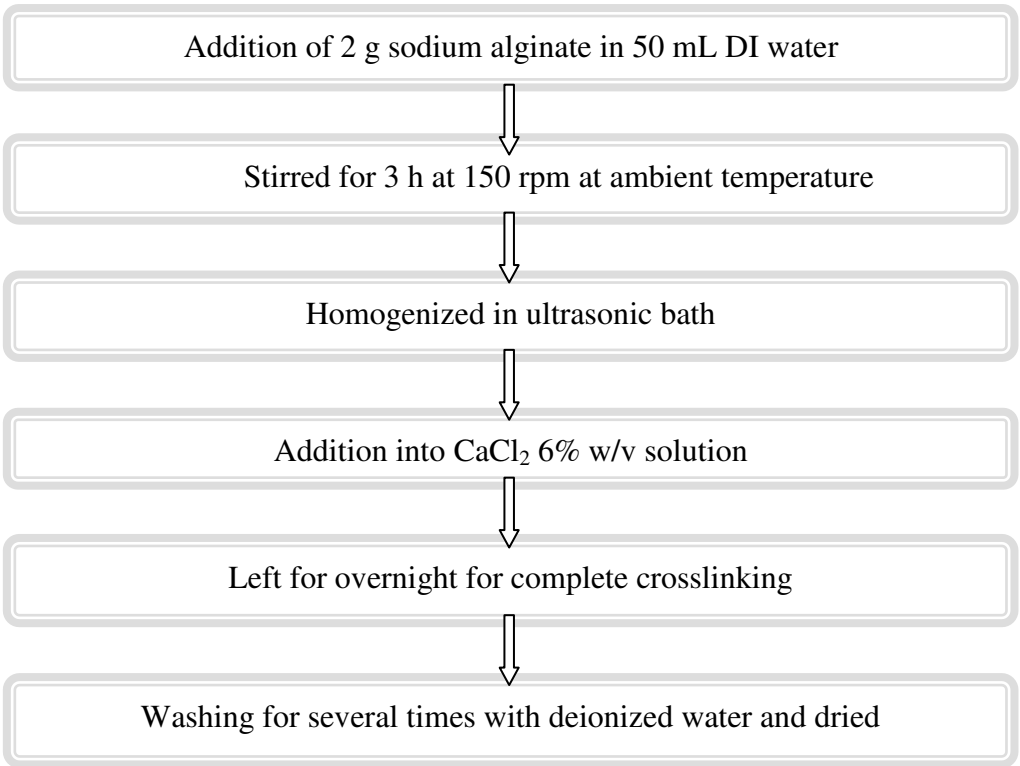

Fig. 4.49: Flow diagram of CA beads fabrication

4.2.1.2 Preparation of CA-GO beads

To prepare CA-GO beads, first graphite was oxidized to graphene oxide using Hummers' method. In 50 mL of DI water, 2 g of sodium alginate was dissolved under magnetic stirring at 150 rpm for 3 h at room temperature. Then the addition of 20 mg GO was followed by homogenization using an ultra-sonic device. This mixture was then carefully dropped into an aqueous coagulation bath containing 6% $CaCl_2$ w/v solution. The bath was continuously agitated with a magnetic stirrer to prevent agglomeration of CA-GO beads. The beads were left for 24 h without agitation to complete cross-linking. Fig. 4.50 is a simplified flow sheet for the preparation of CA-GO.

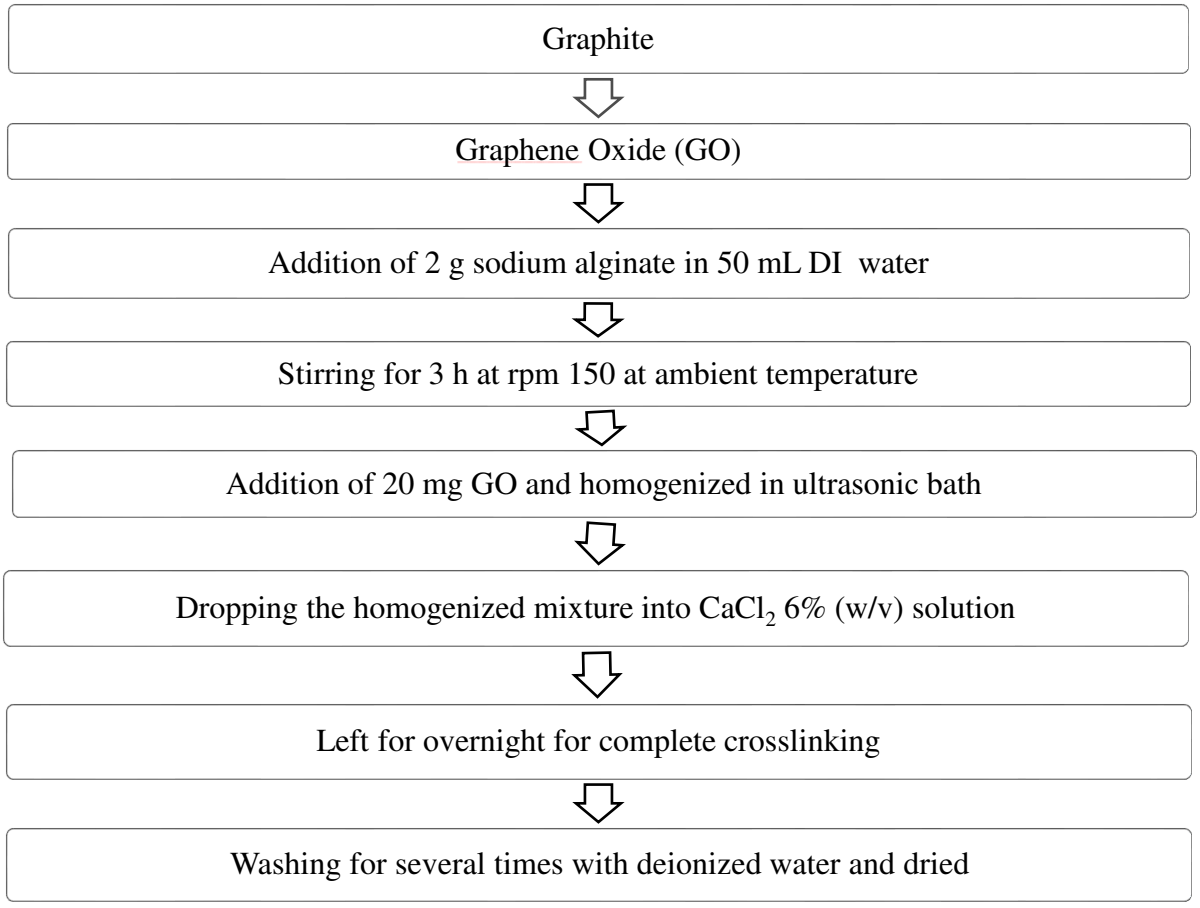

Fig. 4.50: Preparation of CA-GO beads

The Fig. 4.51 show the picture of prepared CA beads and CA-GO beads.

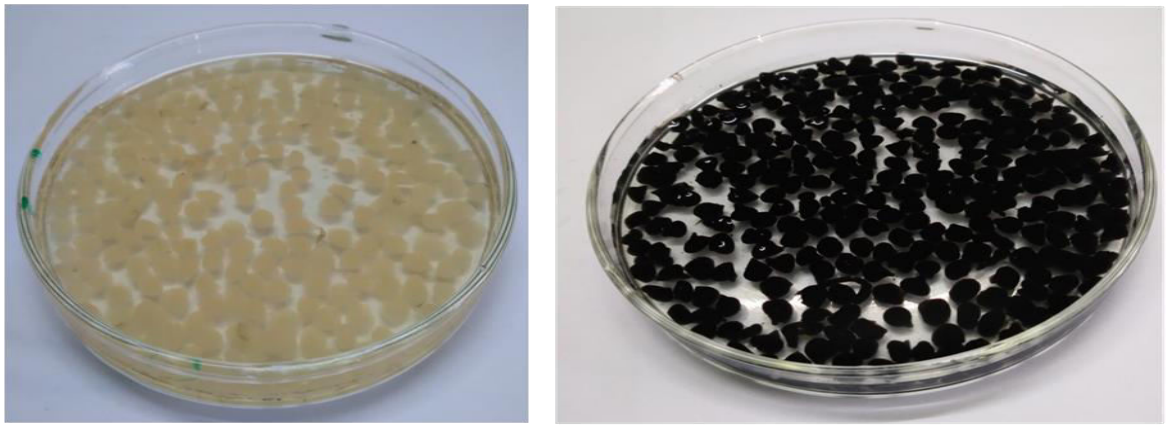

Fig. 4.51: Image of prepared CA and CA-GO composite beads

4.2.2 Characterization of CA-GO beads

4.2.2.1 Structure of CA-GO beads

The Fig. 4.52 shows the structure of CA-GO composite beads where graphene sheet is mentioned separately.

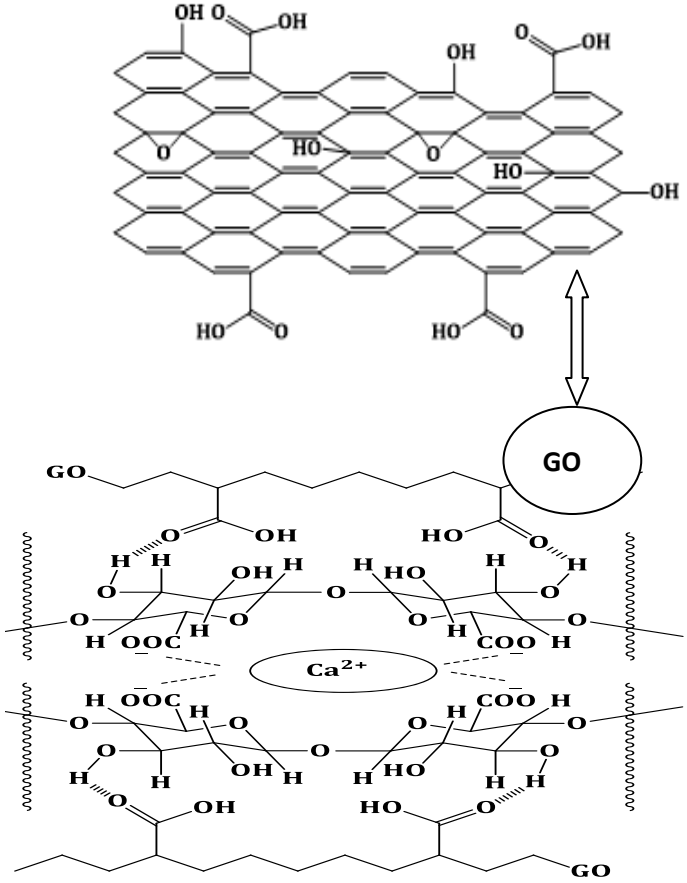

Fig. 4.52: Structure of CA-GO composite beads

The sodium cations in the alginate are driven away from the -COONa on the mannuronic and guluronic acid residues in the presence of the $CaCl_2$ solution resulting in crosslinking of the carboxylate ions with the Ca^{2+} cations, forming calcium alginate $(C_{12}H_{14}CaO_{12})n$.

4.2.2.2 FTIR Analysis

In the infrared region, quite significant adsorptive peaks were observed in the GO, SA and CA-GO spectrum at various wavenumbers (Fig. 4.53). For GO, the peaks found at 3414 cm^{-1}, 2989 cm^{-1}, 1732 cm^{-1} and 1209 cm^{-1} corresponded to O-H stretching vibration, C-H stretching vibration, C=O stretching vibration of carboxylic group and C-O stretching vibration of C-O-C group. In the CA-GO spectrum, peaks were found at 3367 cm^{-1}, 2870 cm^{-1}, 1726 cm^{-1}, and 1099 cm^{-1} corresponding to O-H stretching vibration, C-H stretching vibration, C=O stretching vibration of carboxylic group, C-O stretching vibration in the C-O-C group. During formation of CA-GO beads, the stretching vibration peaks of O-H for GO shifted from 3414 cm^{-1} to 3367 cm^{-1}, C=O stretching vibration shifted from 1732 cm^{-1} to 1726 cm^{-1} and C-O stretching vibration shifted from 1209 cm^{-1} to 1099 cm^{-1}. Some other peaks also little changed due to forming composition of CA-GO beads.

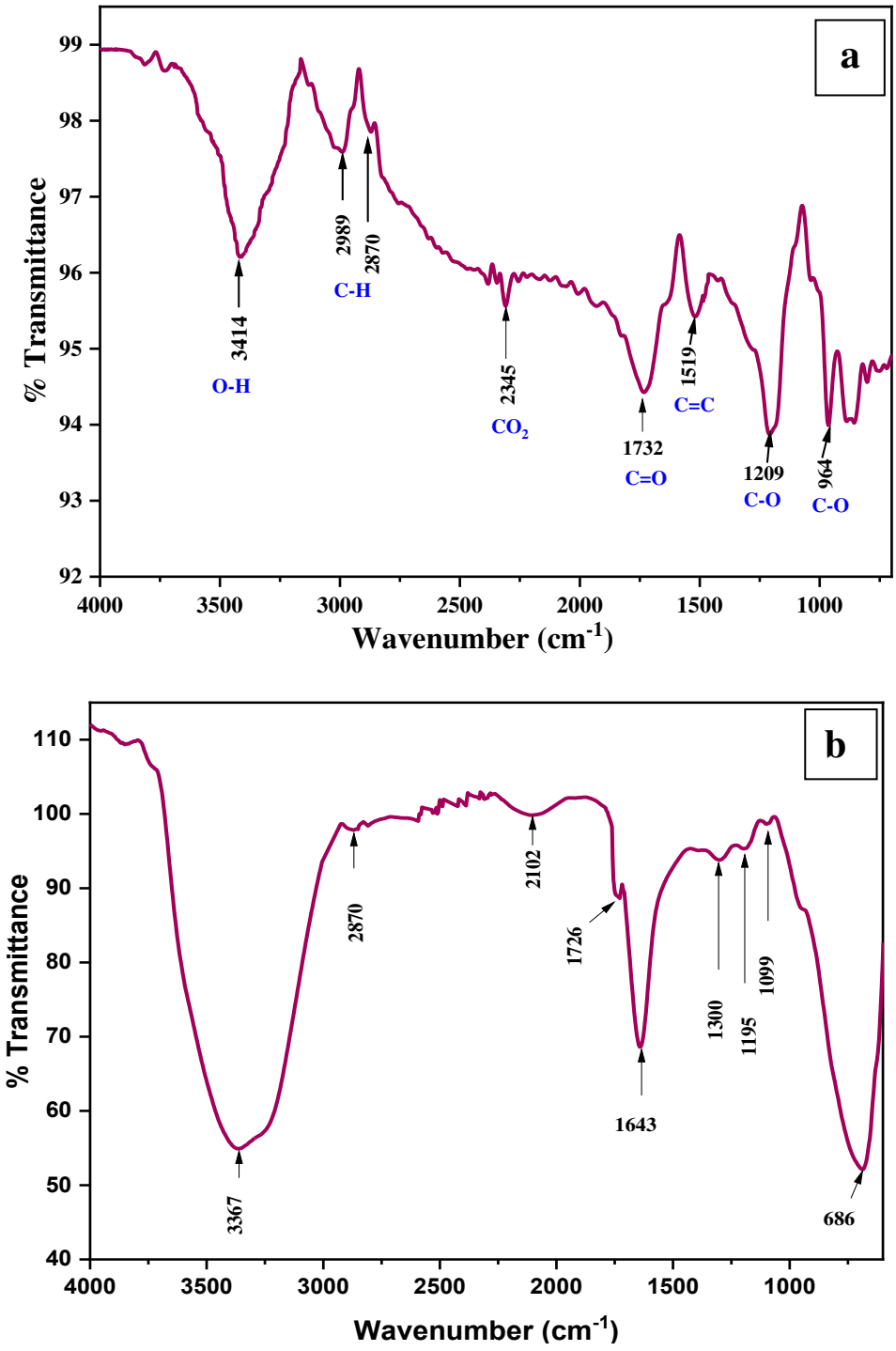

Fig. 4.53: FTIR of (a) GO, (b) CA-GO

4.2.2.3. Scanning Electron Microscopy (SEM)

CA-GO micrograph was studied with SEM. The SEM image of CA-GO was captured at 3000X magnification and approximately 14.3 mm working distance at high vacuum mode

with 15.00 kV. A layered structure was observed because of incorporation of GO in sodium alginate and finally reacted with $CaCl_2$ (Fig. 4.54).

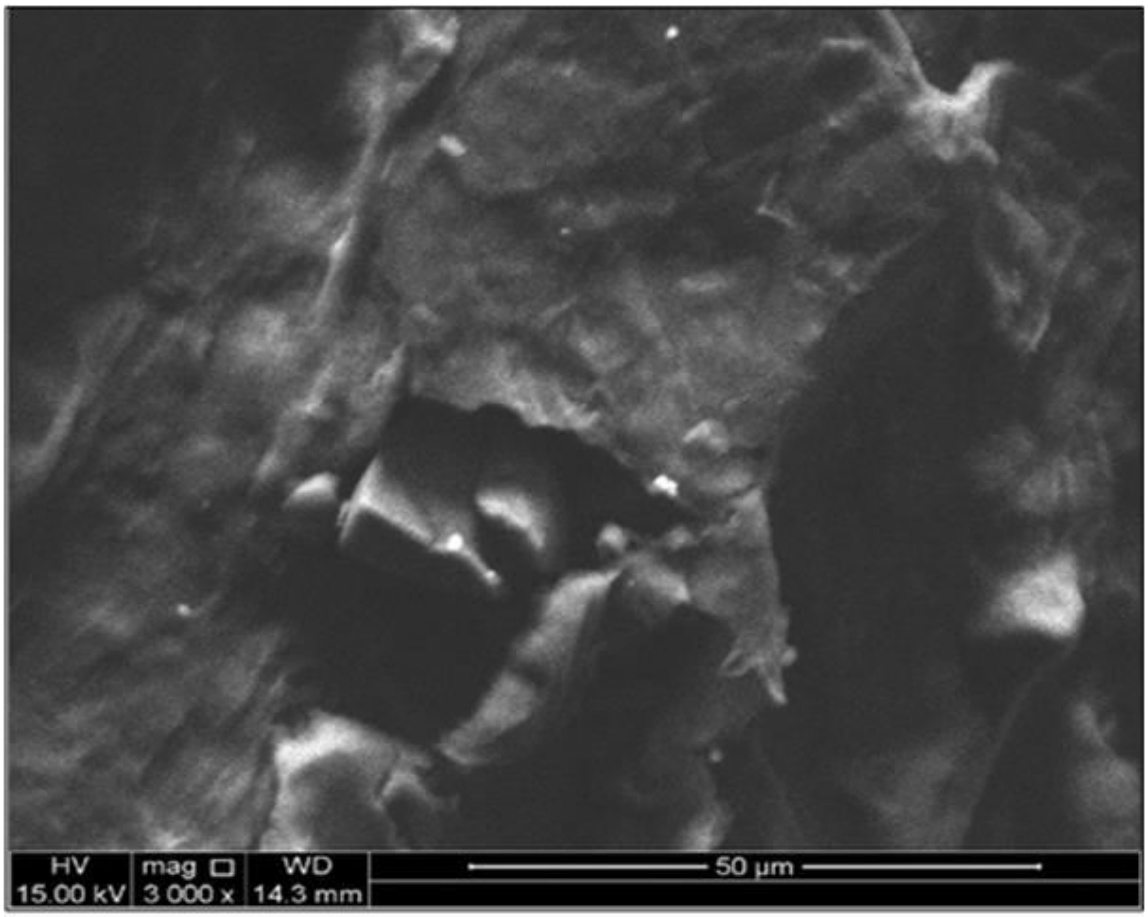

Fig. 4.54: SEM image of CA-GO composite beads

4.2.2.4. XRD Analysis of CA-GO beads

The XRD patterns of GO, CA and CA-GO composite is represented in Fig. 4.55. The XRD pattern of CA presented peaks at 2θ=17.76º corresponding to interlayer spacing 3.341Å indicating an amorphous structure. The XRD pattern was observed at 2θ=17.5º and interlayer spacing of 3.023Å for CA-GO. For GO, the value of 2θ was 10.399º corresponding to an interlayer spacing of 8.58Å. These results revealed that the diffraction as well as interlayer spacing of CA-GO becomes close to calcium alginate.

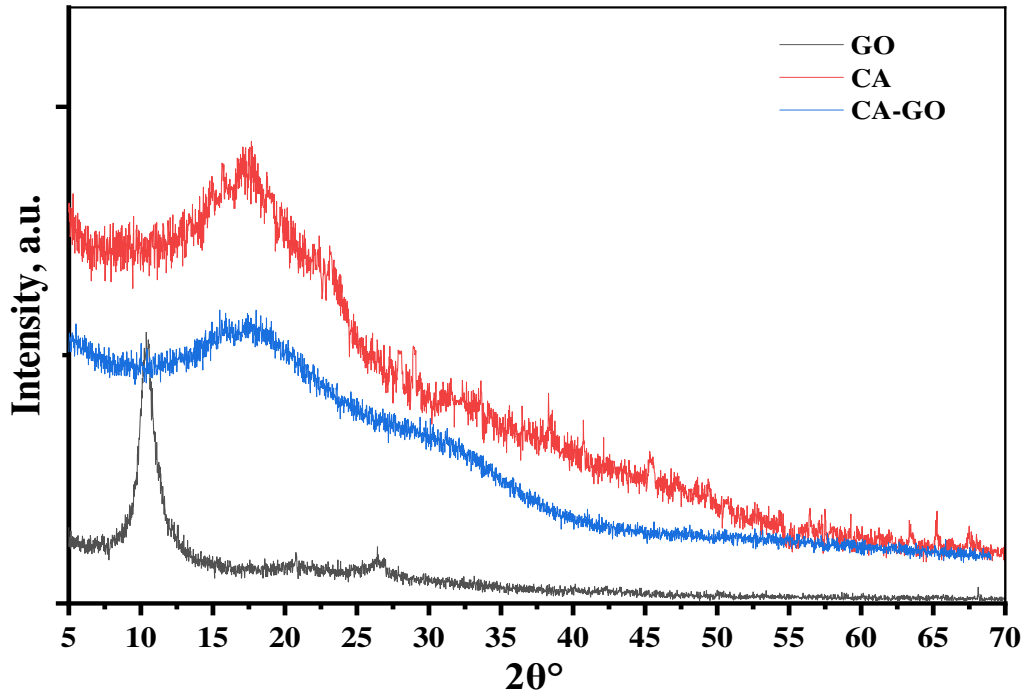

Fig. 4.55: XRD patterns of CA-GO composite beads

4.2.2.5. Spectrum Analysis of CA-GO beads

The existence of the D-band and G-band was confirmed by the Raman spectrum of GO and CA-GO (Fig. 4.56). The D-band indicate the existence defect sites on the adsorbents. The values of D-band and G-band for GO are 1356 cm^{-1} and 1607 cm^{-1} whereas these values for CA-GO were 1359 cm^{-1} and 1670 cm^{-1}. The structural disorder is measured by integrated intensity of D-band and G-band (I_D/I_G) ratio which were 0.93 for GO and 0.86 for CA-GO, thus CA-GO has fewer defective sites as compared to GO.

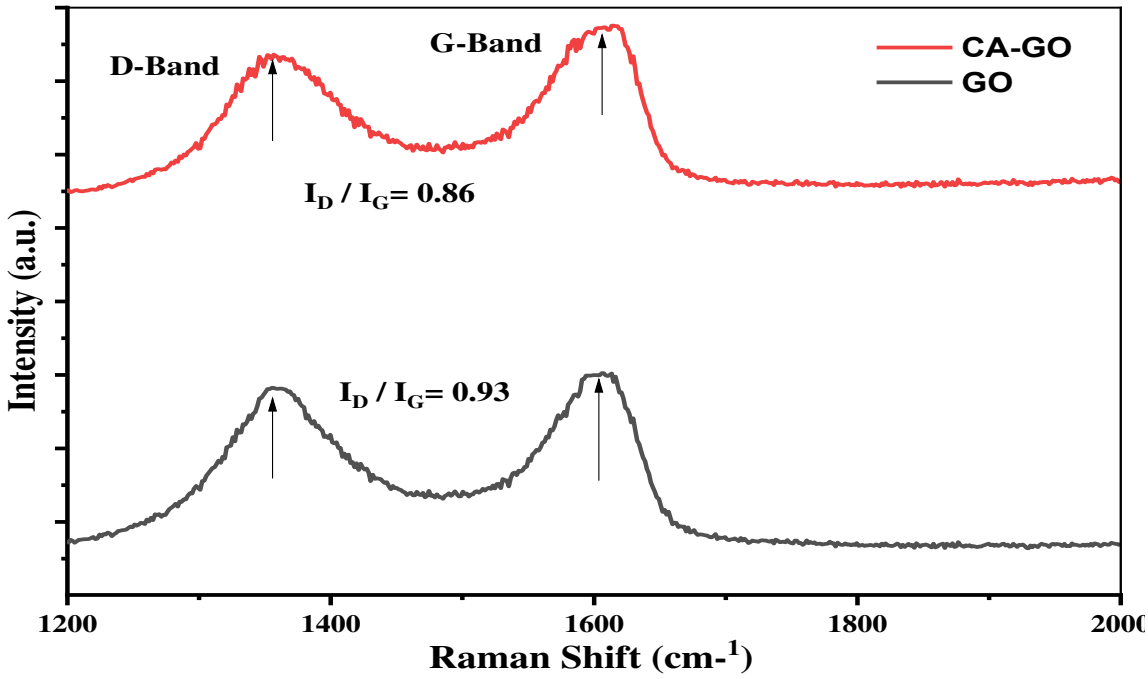

Fig. 4.56: Raman Spectrum of GO and CA-GO composite beads

4.2.2.6. Brunaur-Emmett-Teller (BET) analysis of CA-GO

Nitrogen sorption system was used to analyze the surface area, pore diameter of CA-GO (Table 4.42, Fig. 4.57). It was found that the CA-GO has a specific surface area of 188.27 m^2/g, which is higher than the GO since is a bit spongy than the GO. The average pore diameter was determined by Barrett-Joiner-Halenda (BJH) method and found to be 47.18 Å, which indicate that CA-GO consists of mesopores [213]. It was found the total pore volume of CA-GO was 0.2221 cc/g.

Table 4.42: Parameters of BET analysis for CA-GO composite beads

BET Parameter	Results
BET specific surface area	188.27 m^2/g
Total pore volume	0.2221 cc/g
Average pore diameter	47.18 Å

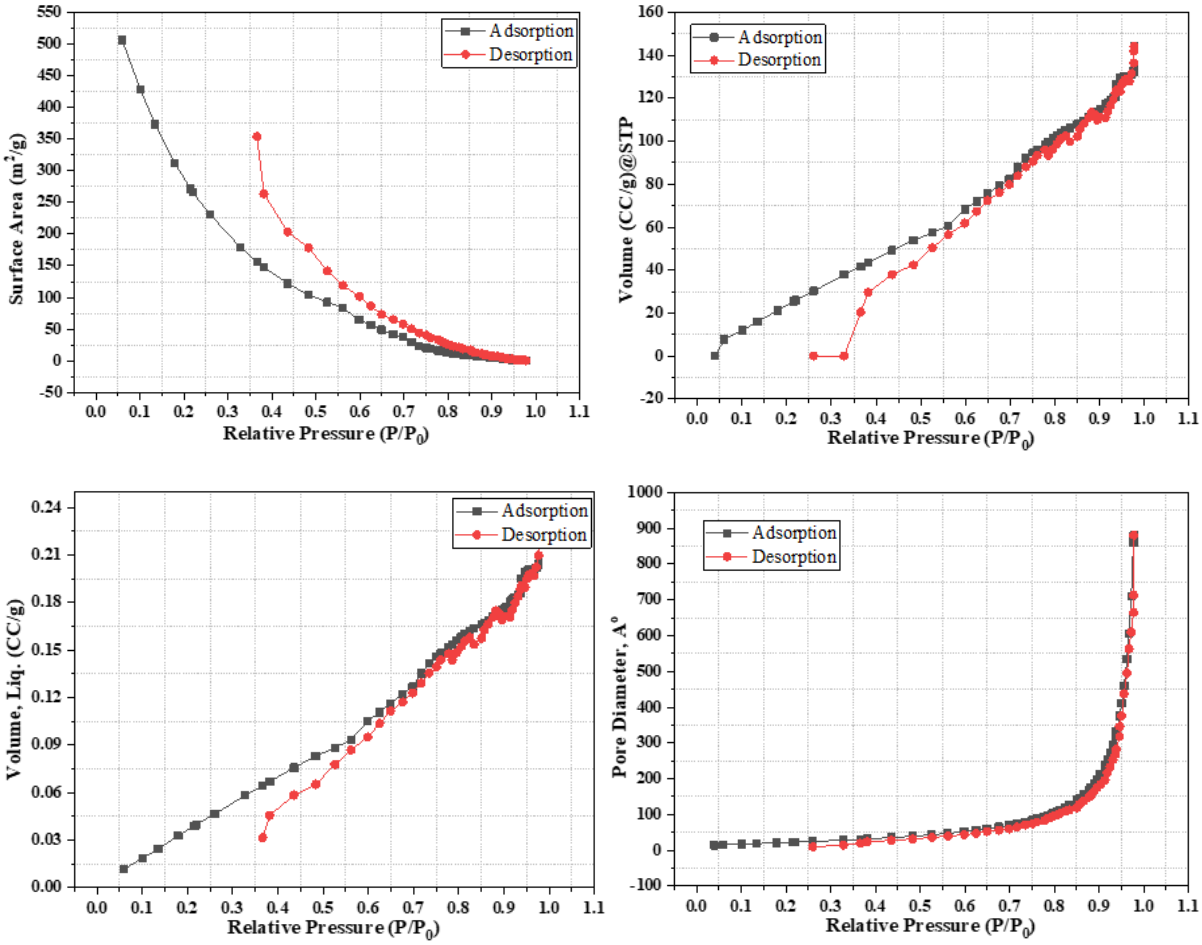

Fig. 4.57: BET analysis of CA-GO composite beads

4.2.2.7. Zeta potential charge of CA-GO beads

The CA-GO composite was dispersed in DI water and the pH were adjusted using dilute HCl and NaOH solution to 2.0, 4.0, 6.0, 8.0, and 10.0. A zeta potential analyzer (Nano-ZS ZEN 3600) was used to measure the zeta potential charge (ZPC). The result showed that the zeta potential value of CA-GO was positive (0.0908 mV) at pH 2.0 which became negative (-0.160 to -0.419 mV) as the pH increased from 4.0 to 10.0. The ZPC of CA-GO was zero at pH nearly 3.0 (Table 4.43, Fig. 4.58).

Table 4.43: pH and Zeta potential data of CA-GO beads

pH	2.0	4.0	6.0	8.0	10.0
Zeta potential value (mV)	0.0908	-0.160	-0.265	-0.387	-0.419

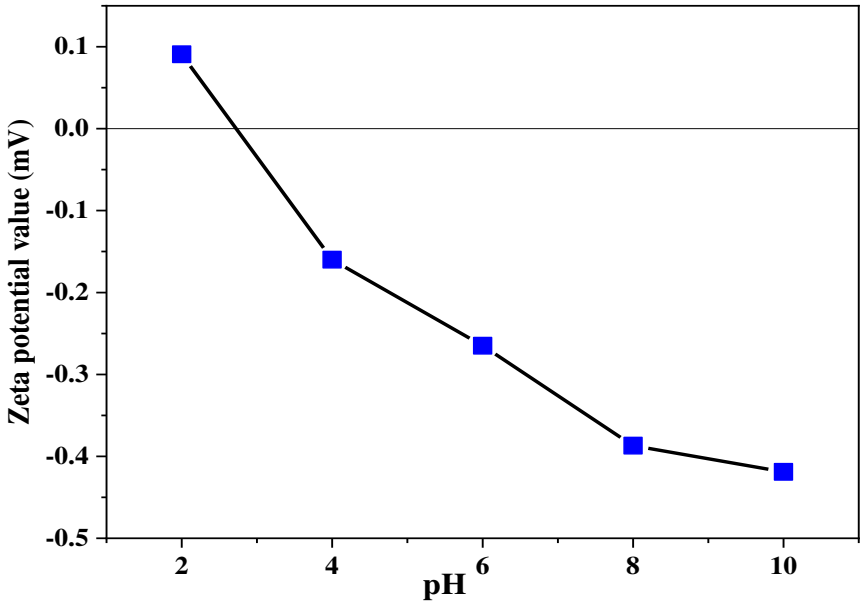

Fig. 4.58: Zeta potential value of CA-GO at different pH

4.2.2.8. Ionic behaviour of CA-GO

The carboxyl group of CA-GO was deprotonated at pH higher than the ZPC and became negatively charged. The positively charged sites of CA-GO increased at pH lower than the ZPC (Fig. 4.56). Therefore, the metal adsorption capacity was favoured at higher pH since cationic metal ion and negative surface charge of CA-GO interacted electrostatically.

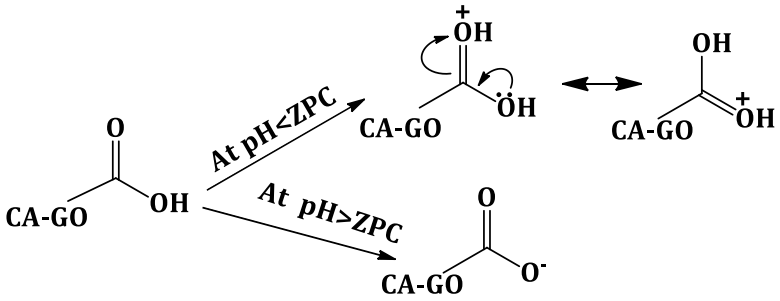

Fig. 4.59: pH effect on ionic behavior of CA-GO beads

4.2.3. Adsorption studies

The efficiency of adsorbent for heavy metal removal is impacted by pH, adsorbent dosages, contact time and initial metal concentration, temperature and other parameters.

4.2.3.1. Adsorption of Cr(III) on CA-GO

4.2.3.1.1. Effect of pH

pH has a substantial effect on the surface charges of CA-GO and metal, which in turn affects the ability of adsorption. The impact of pH on metal adsorption capacity of CA-GO was investigated with chromium(III) salt solution (20 mL, 146.7 ppm) and treated with CA-GO beads (1.116 g/L, 22.0 mg) at the pH range (2.0-6.0). The mixture was agitated for 2 h at room temperature at rpm 150 in an orbital shaker. The concentration changes were determined by AAS after filtering the mixtures. The result revealed that adsorption capacity increased with increasing pH (Table 4.44, Fig. 4.60). However, after pH 5.0 the removal rate drastically increased (51.88 mg/g to 99.82 mg/g) which was due to precipitation of chromium. Therefore, optimum pH was selected as pH 4.5, at which the adsorption capacity and % removal were 45.96% and 34.97 mg/g.

Table 4.44: pH, adsorption capacity and % removal data of CA-GO for Cr(III) adsorption

pH	2.0	3.0	3.5	4.0	4.5	5.0	5.5	6.0
Adsorption Capacity (mg/g)	11.60	16.39	26.16	34.40	45.96	51.88	99.82	117.29
% removal	8.83	12.47	19.90	26.18	34.97	39.95	75.94	89.23

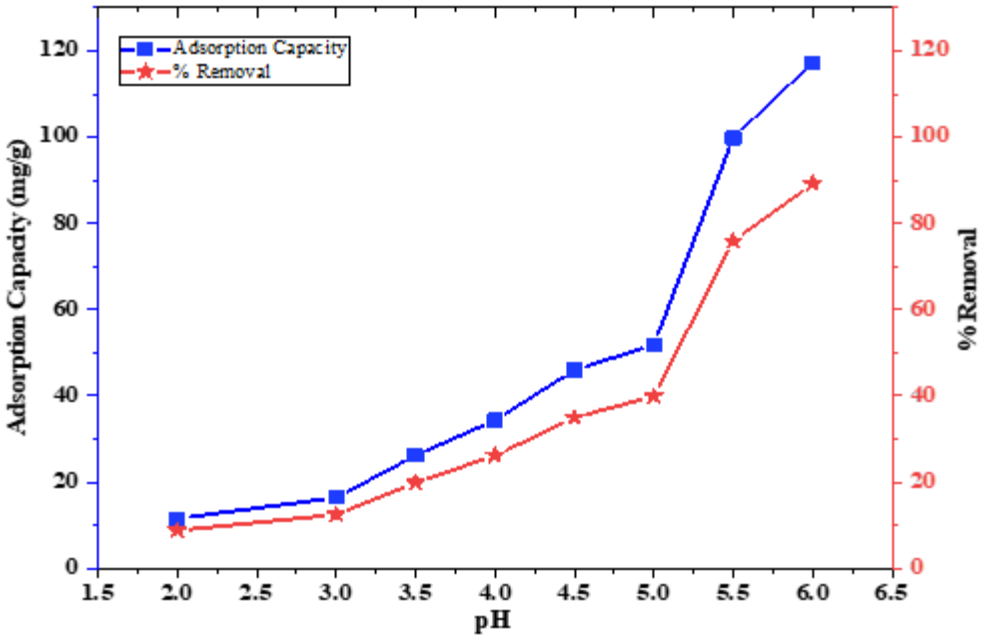

Fig. 4.60: Effect of pH on capacity and % removal of Cr(III) adsorption on CA-GO

4.2.3.1.2. Effect of dosage

The effect of CA-GO dosage on adsorption of chromium(III) was investigated using 89.23 ppm Cr(III) solution at pH 4.5. The process was conducted for 2 h at 150 rpm with the different dosages (0.248-1.612 g/L). It was found that with increasing of dosage, the percentage of Cr(III) removal increased, however the adsorption capacity was decreased (Table 4.45, Fig. 4.61). The optimum dosage selected 0.62 g/L by the experimental results, which was maintained throughout the study.

Table 4.45: Dosage, adsorption capacity and % removal data of CA-GO for Cr(III) adsorption

Dosage (g/L)	0.248	0.372	0.620	0.868	1.116	1.364	1.612
Adsorption capacity (mg/g)	84.79	78.92	63.44	55.03	51.12	50.66	50.33
% removal	23.56	32.9	44.07	53.53	63.93	77.45	90.93

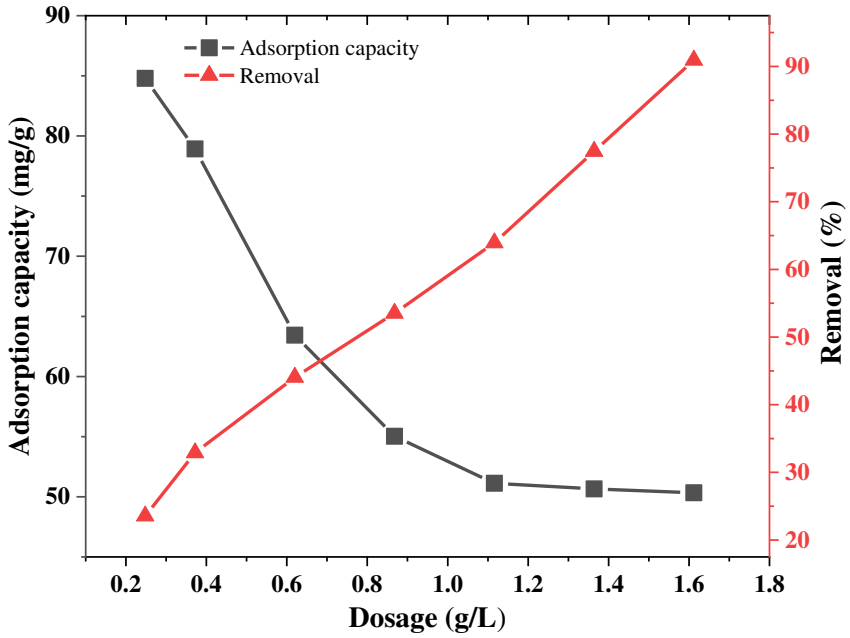

Fig. 4.61: Effect of dosage on Cr(III) adsorption capacity and % of removal

4.2.3.1.3. Effect of Cr(III) concentration and contact duration

Chromium salt solutions (20 mL) of different concentrations at pH 4.5 were prepared and 0.62 g/L dosage of CA-GO were added to each solution to observe the effect of Cr(III) concentration and contact duration on adsorption capacity of CA-GO. The mixture was agitated for 5 to 120 mins. Initially, more adsorbent active sites were available, however as time passed, those sites got saturated. Therefore, the adsorption capacity of CA-GO enhanced with increasing time until reached at equilibrium and became constant at 40 min (Table 4.46, Fig. 4.62). Equilibrium metal ion adsorption capacity increased with increasing initial metal ion concentration due to increase in concentration gradient between metal ions in the bulk solution, which favoured mass transfer of chromium ions onto the CA-GO surface [230]. However, the % removal was higher at lower initial concentration of chromium since the amount of Cr was less as compared to the amount of adsorbent, CA-GO composite (Table 4.47, Fig. 4.63).

Table 4.46: Adsorption capacity of CA-GO at different concentration of Cr(III) at different time intervals

Time (min)	45.80 ppm	65.29 ppm	83.57 ppm	98.86 ppm
5	13.58	21.32	18.35	21.26
10	23.48	33.35	30.59	34.33
20	32.53	43.77	49.52	49.59
30	40.26	54.67	61.64	59.88
40	56.02	66.08	73.24	79.74
60	56.79	66.35	72.82	80.81
120	55.93	67.45	73.59	79.96

Table 4.47: Time and % removal data of Cr(III) adsorption on CA-GO at different concentration

Time (min)	45.80 ppm	65.29 ppm	83.57 ppm	98.86 ppm
5	18.38	20.25	13.62	13.33
10	31.79	31.67	22.70	21.54
20	44.04	41.57	36.74	31.10
30	54.50	51.92	45.73	37.56
40	75.83	62.75	54.34	50.01
60	76.88	63.01	54.03	50.68
120	75.72	64.05	54.60	50.15

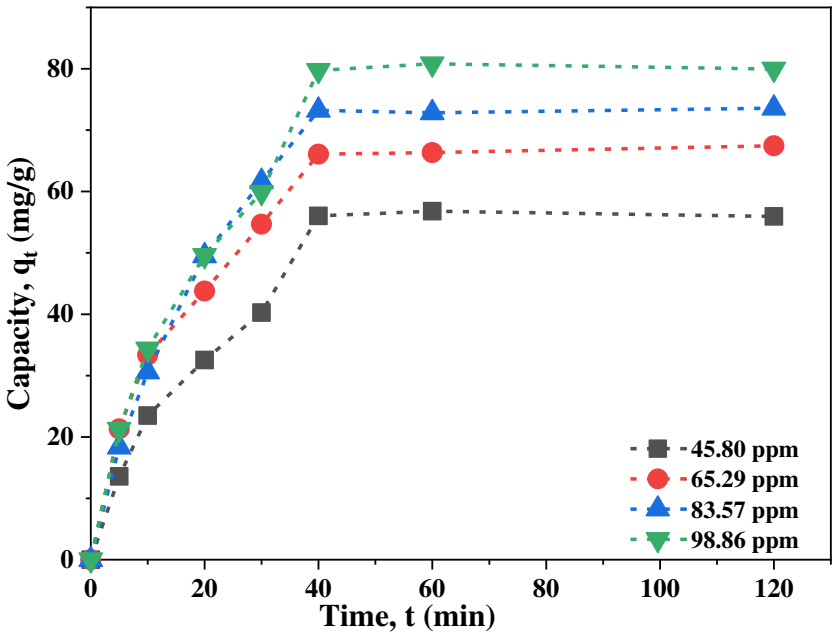

Fig. 4.62: Effect of time and concentration on adsorption of Cr(III) on CA-GO

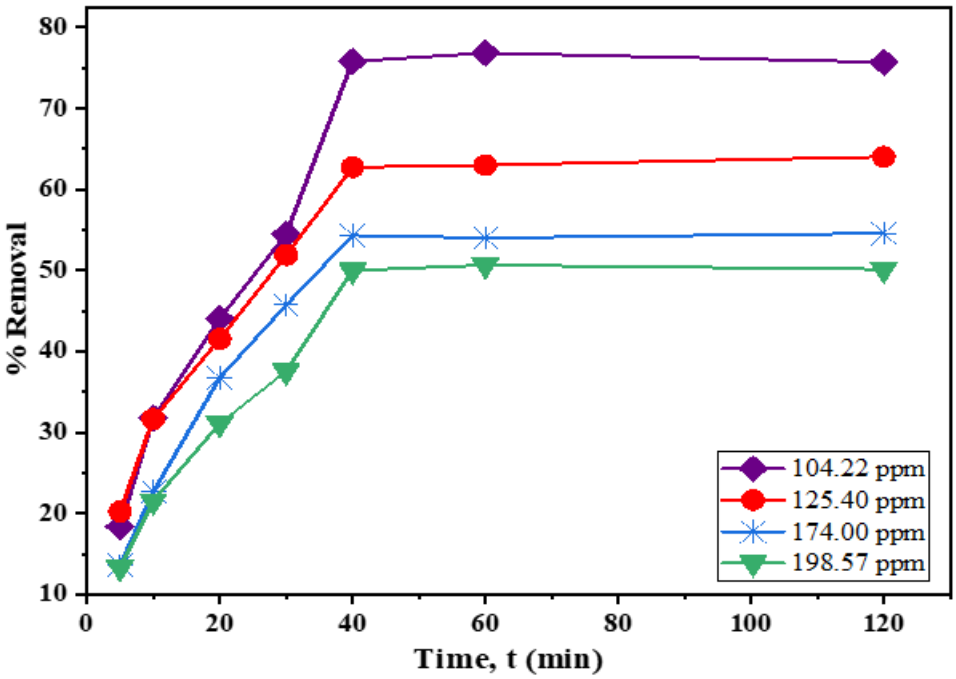

Fig. 4.63: Time and adsorption capacity for Cr(III) adsorption on CA-GO at different concentrations

4.2.3.1.4. Adsorption isotherms for adsorption of Cr(III) on CA-GO

Langmuir and Freundlich models were applied to understand how chromium ions were distributed on the CA-GO surface.

4.2.3.1.4.1. Langmuir isotherm

Langmuir model was verified by plotting C_e/q_e versus Ce value following the eq. (3.4). A linear relationship between C_e/q_e and Ce was found (Table-4.48, Fig. 4.64) with regression coefficient (R^2=0.993) (Table-4.50). The slope was used to calculate the maximum theoretical adsorption capacity, q_m which was found to be 90.58 mg/g. Using eq. (3.5), the separation factor R_L was calculated and the resultant value of 0.126 indicated that monolayer adsorption was favorable.

Table 4.48: C_e, C_e/q_e data of CA-GO at different concentration for Cr(III) adsorption

Initial concentration (ppm)	45.80	65.29	83.57	98.86
Equilibrium concentration (C_e)	11.07	24.32	38.16	49.42
C_e/q_e	0.1976	0.368	0.521	0.6197

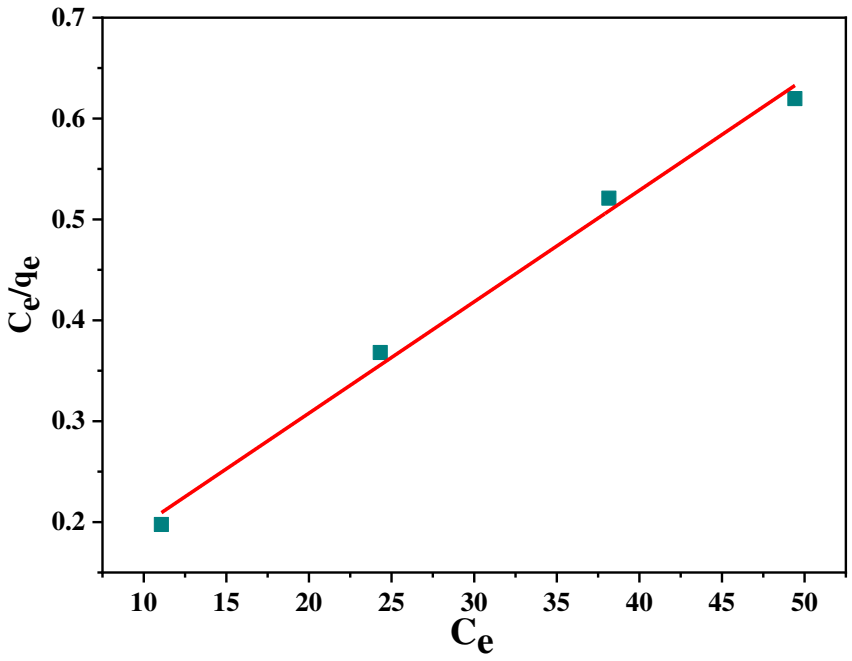

Fig. 4.64: Langmuir adsorption isotherm for Cr(III) on CA-GO

4.2.3.1.4.2. Freundlich isotherm

The experimental data were examined for multilayer adsorption mechanism applying Freundlich isotherm by plotting $\ln C_e$ versus $\ln q_e$ using the eq. (3.6). A linear connection

was found (Table 4.49, Fig. 4.65) with an excellent regression coefficient (R^2=0.992) (Table 4.50). The n value was calculated using the eq. (3.6) and the result was 2.58, indicating that the adsorption was of a moderate to good quality.

Table 4.49: lnC_e and lnq_e data of CA-GO at different concentration for Cr(III) adsorption

Initial concentration (ppm)	45.80	65.29	83.57	98.86
lnC_e	2.404	3.191	3.642	3.9
lnq_e	4.026	4.19	4.293	4.378

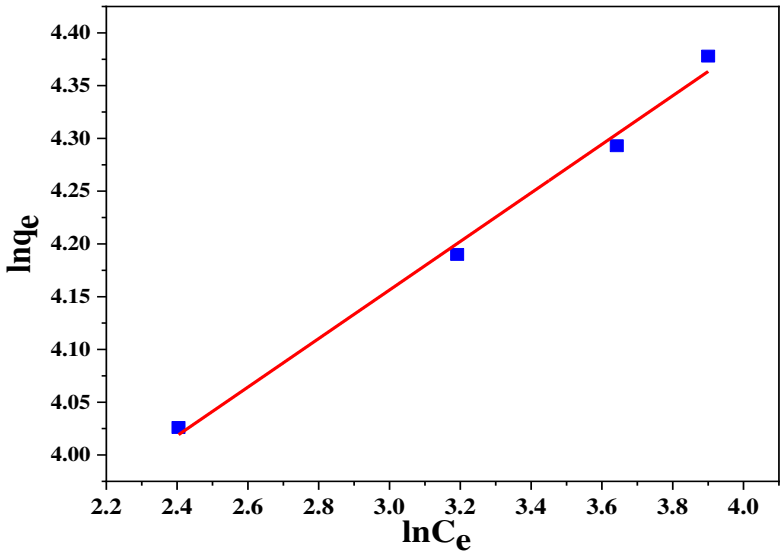

Fig. 4.65: Freundlich adsorption isotherm for Cr(III) on CA-GO

The various parameters of both the models are shown in the Table 4.46. It was marked that both models, preferably the Langmuir isotherm model were followed in the chromium(III) adsorption of CA-GO beads.

Table 4.50: Theoretical values of q_m, b, R_L, n, k_F and R^2 of adsorbent CA-GO for Cr(III) adsorption

Parameters	**q_m, (mg/g)**	**b (Lmg^{-1})**	**R^2**	**R_L**	**n**	**k_F**
Langmuir isotherm	90.58	0.126	0.993	0.074	-	-
Freundlich isotherm	-	-	0.992	-	4.346	32.01

4.2.3.1.5. Adsorption kinetics for adsorption of Cr(III) on CA-GO

Adsorption kinetics was investigated to evaluate the efficacy of an adsorbent and learn more about underlying causes. Two kinetic models were applied to explain the adsorption processes, in this study.

4.2.3.1.5.1. Pseudo-first-order kinetics

Pseudo-first-order model is produced by plotting $\log(q_e-q_t)$ versus t using the eq. (3.7). In the graph, a linear relation between $\log(q_e-q_t)$ and t was observed (Table 4.51, Fig. 4.66).

Table 4.51: Time, t (min) and $\log(q_e-q_t)$ data of CA-GO at different concentration for Cr(III) adsorption

Time, t (min)	$\log(q_e-q_t)$ at 45.80 ppm	$\log(q_e-q_t)$ at 65.29 ppm	$\log(q_e-q_t)$ at 83.57 ppm	$\log(q_e-q_t)$ at 98.86 ppm
5	1.627	1.651	1.739	1.767
10	1.512	1.514	1.629	1.657
20	1.371	1.348	1.375	1.479
30	1.197	1.057	1.064	1.297

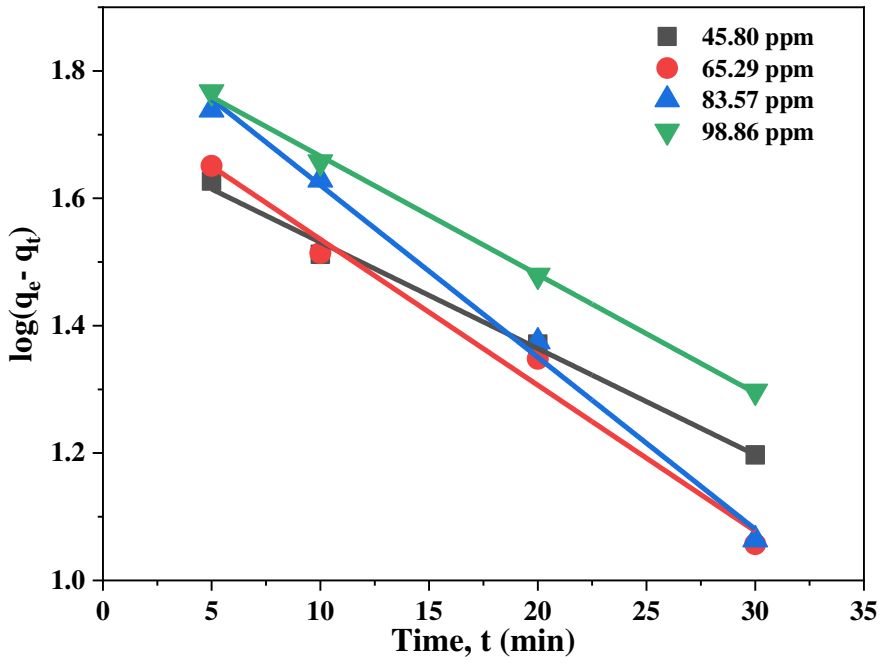

Fig. 4.66: Pseudo-first-order kinetics for Cr(III) adsorption on CA-GO

4.2.3.1.5.2. Pseudo-second-order kinetics

Pseudo-second-order model was achieved by potting t/q_t against t using eq. (3.8) and a linear relationship between t/q_t and t was observed (Table 4.52, Fig. 4.67).

Table 4.52: Time, t (min) and t/q_t data of CA-GO at different concentration for Cr(III) adsorption

Time, t (min)	t/q_t at 45.80 ppm	t/q_t at 65.29 ppm	t/q_t at 83.57 ppm	t/q_t at 98.86 ppm
5	0.368	0.235	0.272	0.235
10	0.426	0.299	0.327	0.291
20	0.615	0.457	0.403	0.403
30	0.745	0.549	0.487	0.501
40	0.714	0.605	0.546	0.502

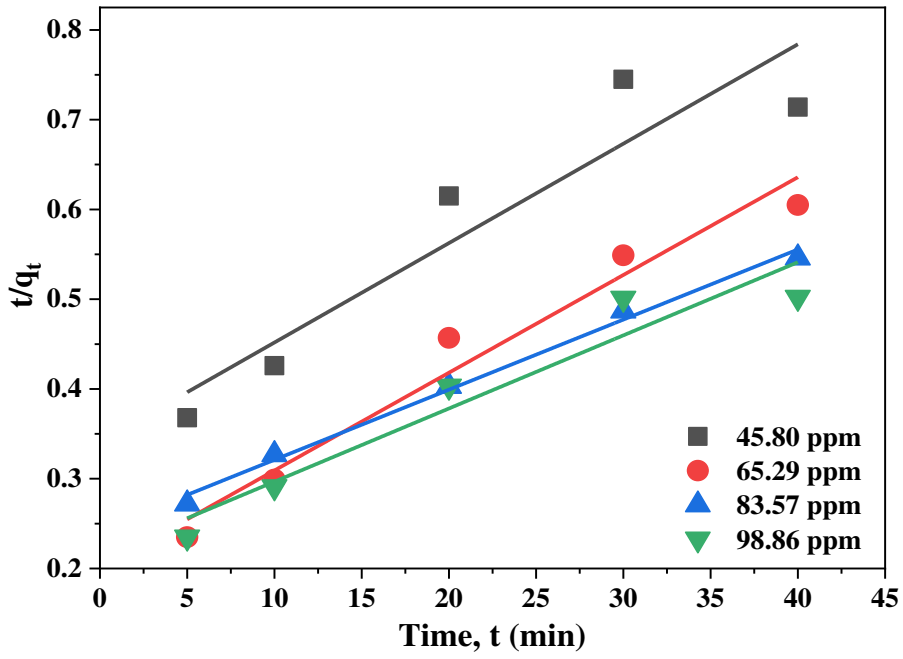

Fig. 4.67 Pseudo-second-order kinetics for Cr(III) adsorption on CA-GO

Kinetic parameters are recorded in the Table 4.53 and it was found that the correlation coefficient (R^2) values for pseudo-first-order kinetics were significantly higher than those of pseudo-second-order kinetics.

Table 4.53: Kinetics parameters for adsorption of Cr(III) on CA-GO

Kinetics model	Parameters	Initial concentration of chromium(III)			
		45.80 ppm	**65.29 ppm**	**83.57 ppm**	**98.86 ppm**
Pseudo-first-order	q_e^* (mg g^{-1})	56.02	66.08	73.24	79.74
	k_1(1/min)	0.038	0.051	0.0621	0.0426
	R^2	0.994	0.986	0.995	0.998
	q_e^{**} (mg g^{-1})	49.79	58.07	77.62	71.12
Pseudo-second-order	k_2 (g/mg min)	3.548 X 10^{-4}	5.823 X 10^{-4}	3.048 X 10^{-4}	2.511 X 10^{-4}
	R^2	0.875	0.965	0.926	0.993
	q_e^{**} (mg g^{-1})	90.91	92.59	123.45	128.04

* Experimental, ** Theoretical

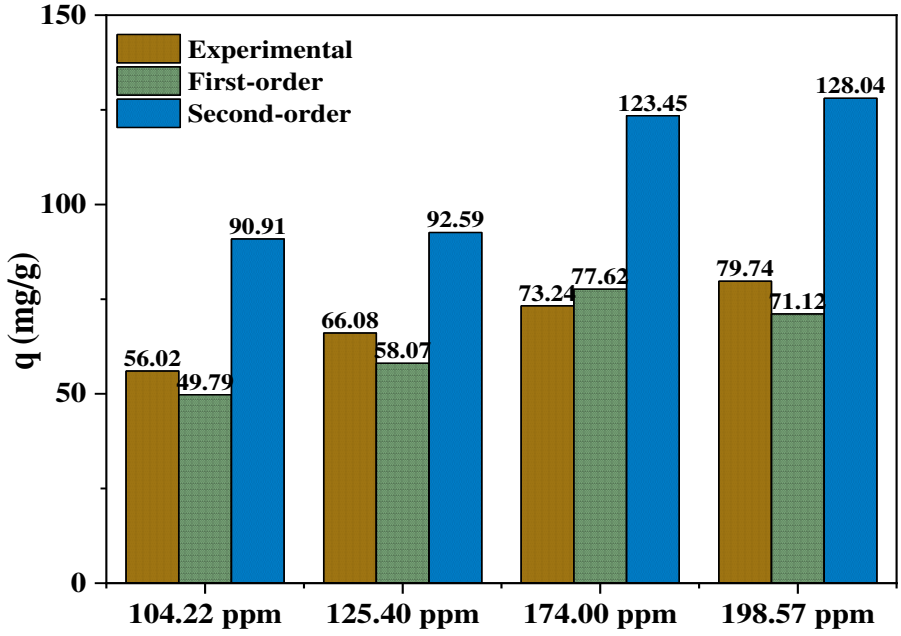

Fig. 4.68: Comparison of Cr(III) adsorption capacities on CA-GO

It is observed from the Fig. 4.68 that pseudo-first-order kinetics adsorption capacity closely matched with the experimental results. In contrast to pseudo-second-order model,

pseudo-first-order kinetic model showed better correlation for chromium(III) adsorption on CA-GO.

4.2.3.1.6. Thermodynamic analysis for Cr(III) adsorption on CA-GO

The Gibb's free energy change for adsorption of chromium onto CA-GO at various temperatures was investigated using CA-GO dosage of 0.62 g/L employing 55.33 ppm Cr(III) solution at a pH 4.5 for each experiment. The solutions (20 mL each) were shaken for optimum time of 40 mins at 298 K, 308 K, 318 K, and 328 K. A straight line was produced after plotting the values of $\ln k_d$ against 1/T (Table 4.54, Fig. 4.69). The van't Hoff equation [eq. (10)] was used to calculate the Gibb's free energy change (ΔG), enthalpy change (ΔH) and entropy change (ΔS) during adsorption. The calculated Gibb's free energy was obtained -3.580 kJ mol^{-1}, -2.461 kJ mol^{-1}, -1.374 kJ mol^{-1}, and 0.592 kJ mol^{-1} at 298 K, 308 K, 318 K, and 328 K, respectively.

Table 4.54: $\ln k_d$ vs 1/T data for Cr(III) adsorption on CA-GO

1/T	0.0033	0.0032	0.0031	0.0030
$\ln k_d$	1.445	0.961	0.520	0.217

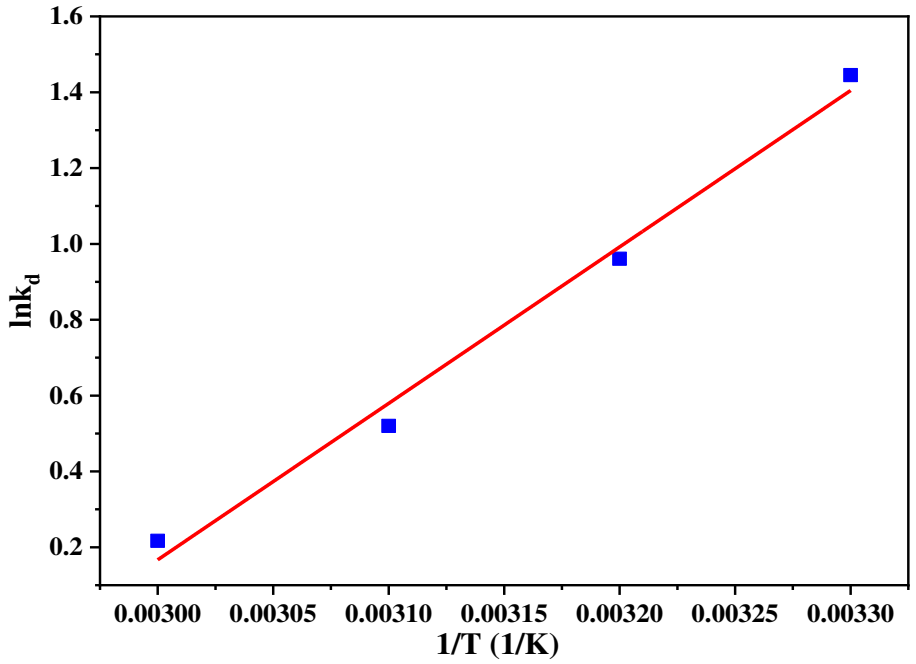

Fig. 4.69: Plot for van't Hoff equation for Cr(III) adsorption on CA-GO

The enthalpy change (ΔH) and entropy change (ΔS) were estimated from the slope and intercept, respectively and their values were -34.295 kJ mol^{-1} and -0.1014 kJ K^{-1} mol^{-1} (Table 4.55). The value of ΔG increased from -3.580 to -0.592 kJ mol^{-1} with increasing the temperature from 298 to 328 K. Therefore, the chromium(III) adsorption on CA-GO was physical and spontaneous at lower temperatures.

Table 4.55: Thermodynamic parameters of Cr(III) adsorption on CA-GO

T(K)	ΔG (kJ mol^{-1})	ΔH (kJ mol^{-1})	ΔS (kJ K^{-1} mol^{-1})
298	-3.580	-34.295	-0.1014
308	-2.461		
318	-1.374		
328	-0.592		

4.2.3.1.7. Plausible mechanism for Cr(III) adsorption on CA-GO

Adsorption involves interactions between particles having opposite charges that produces a variety of bondings, including hydrogen bonds, electrostatic bonds, van der Waals forces, dipole-dipole interactions, ion exchange, etc. CA-GO exhibits electrostatic interaction with the cationic chromium ion due to its negative surface charge at pH 4.5. The CA-GO's carboxylate groups bind Cr(III) ions from the solution to create coordinate complexes (Fig. 4.70).

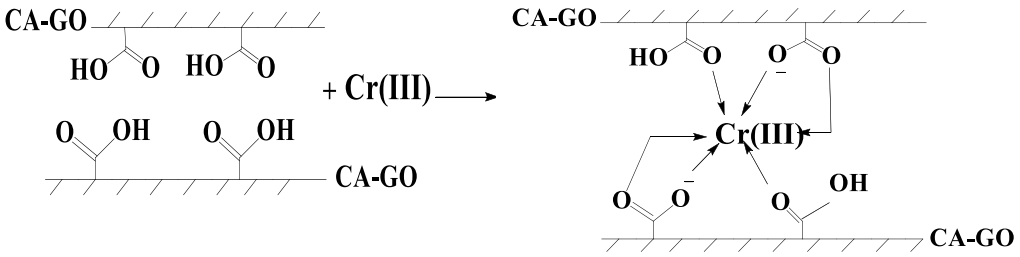

Fig. 4.70: **Possible mechanism Cr(III) adsorption onto SA-GO**

4.2.3.1.8. Regeneration of used CA-GO for Cr(III) adsorption

Regeneration studies of used adsorbents provide valuable information about commercial application of an adsorbent. 2% HCl was used to regenerate CA-GO, which was then

neutralized by repeatedly washing with distilled. The feasibility of reuse was investigated by drying the regenerated CA-GO and using it for further adsorption at optimum pH, duration and adsorption dosage. The experiments results showed that the adsorption capacity of regenerated CA-GO gradually decreased from 59.74 mg/g to 47.29, 35.02 and 21.20 mg/g after first, second and third recycle, accordingly (Fig. 4.71).

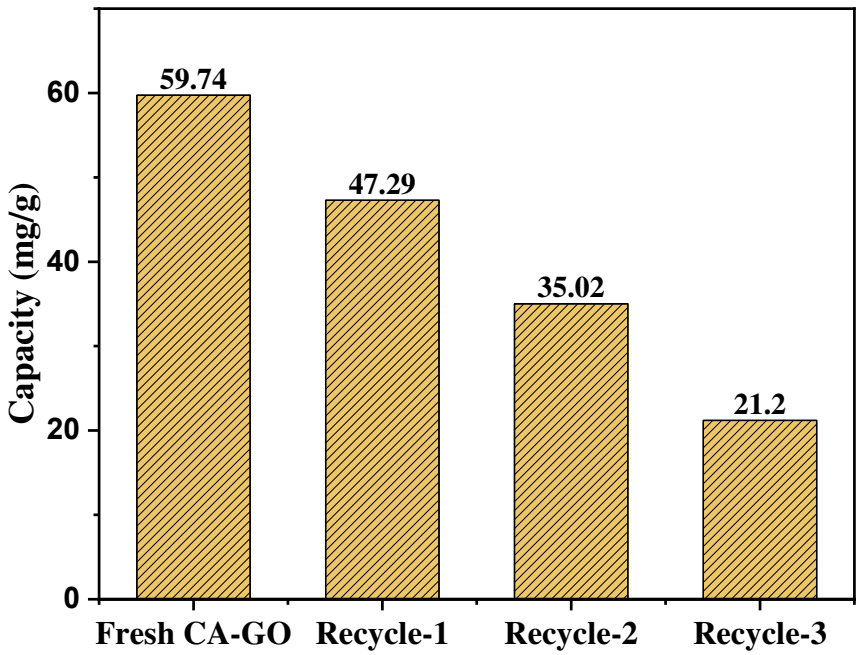

Fig. 4.71: Regeneration of used CA-GO for Cr (III) adsorption

4.2.3.2. Adsorption of Copper(II) on CA-GO

Copper(II) adsorption on CA-GO is influenced by a number of factors, including pH, adsorbent dosage, contact time, metal concentration, temperature and others parameters.

4.2.3.2.1. Effect of pH

The surface charge of CA-GO and copper as well as the adsorption capacity are significantly influenced by pH. The effect pH on copper adsorption on CA-GO was investigated at pH ranging from 3.0 to 7.0. In this study, copper(II) salt solution (20 mL, 124.3 ppm) was collected, the pH was adjusted to 3.0, 4.0, 5.0, 6.0 and 7.0 and then treated with CA-GO (22.32 mg, 1.116 g/L). The mixture was agitated for 2 h at room temperature at 150 rpm in an orbital shaker. The concentration changes were determined by AAS after filtering the mixtures. The results revealed that as pH increased, adsorption

capacity increased steadily and suddenly it increased higher and reached maximum (108.37 mg/g) at pH 7.0 due to precipitation occurred (Table 4.56, Fig. 4.72). However, it was observed that copper was precipitated at pH>6.0. Hence, pH 6.0 had been selected as optimized for the study. At pH 6.0 the adsorption capacity of CA-GO was 76.95 mg/g and % removal of Cu(II) was 85.58%. The pH_{zpc} of CA-GO is nearly 3.0 and beyond this the CA-GO surface become negatively charged and contributed to cationic copper ion adsorption process through the electrostatic attraction.

Table 4.56: pH, adsorption capacity and % removal data of CA-GO for Cu(II) adsorption

pH	3.0	4.0	5.0	6.0	7.0
Adsorption Capacity (mg/g)	38.98	47.49	69.53	76.95	108.37
% removal	35.00	42.64	62.43	85.58	97.30

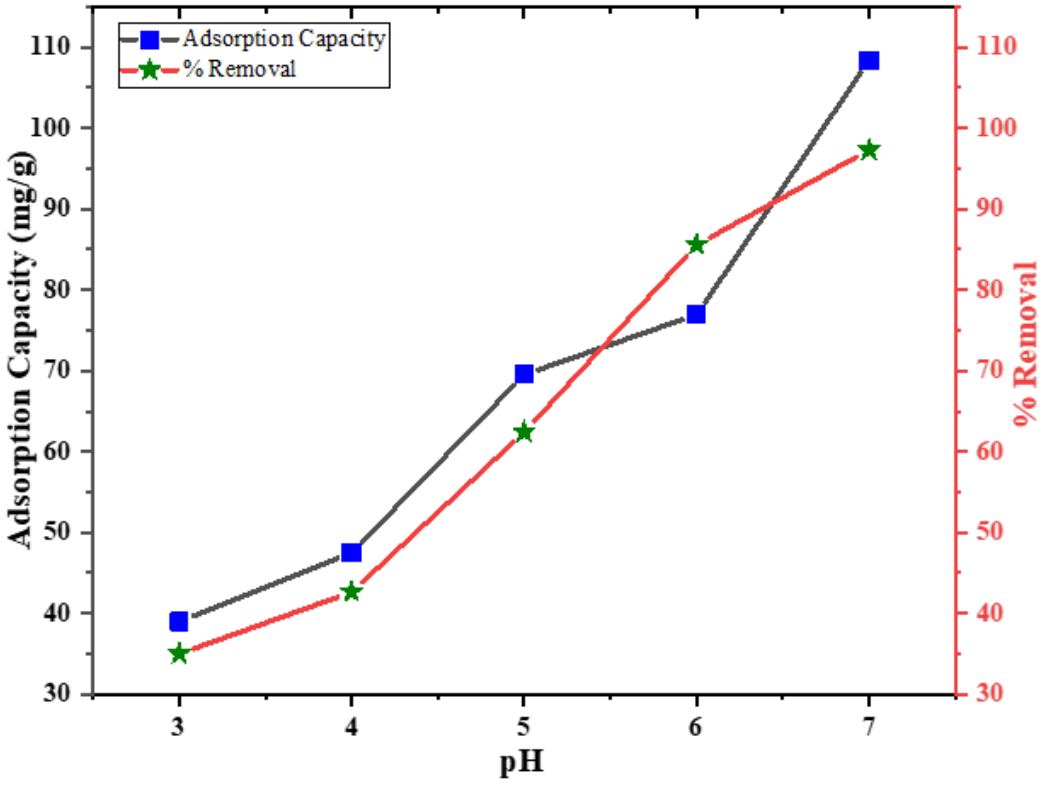

Fig. 4.72: Effect of pH on capacity and % removal of Cu(II) adsorption on CA-GO beads

4.2.3.2.2. Effect of dosage

Using a standard solution of copper salt (102.8 ppm, 20 mL) at optimum pH (6.0) with different dosages (0.248, 0.372, 0.620, 0.868, 1.116 and 1.364 g/L), the effect of CA-GO dosage on Cu(II) adsorption was studied. It was found that with increasing dosages, the percentage of Cu(II) removal was increased and the adsorption capacity of CA-GO was decreased due to a decrease the amount of adsorbate per unit mass of adsorbent (Table 4.57, Fig. 4.73). Here, the dosage (0.6 g/L) demonstrated the optimum result since it was meet the balance of the adsorption capacity and percentage of removal.

Table 4.57: Dosage, adsorption capacity and % removal data for Cu(II) adsorption on CA-GO

Dosage (g/L)	0.248	0.372	0.620	0.868	1.116	1.364
Adsorption capacity (mg/g)	150	146.77	108.38	82.02	65.77	55.43
% of removal	36.19	53.11	65.36	69.26	71.4	73.54

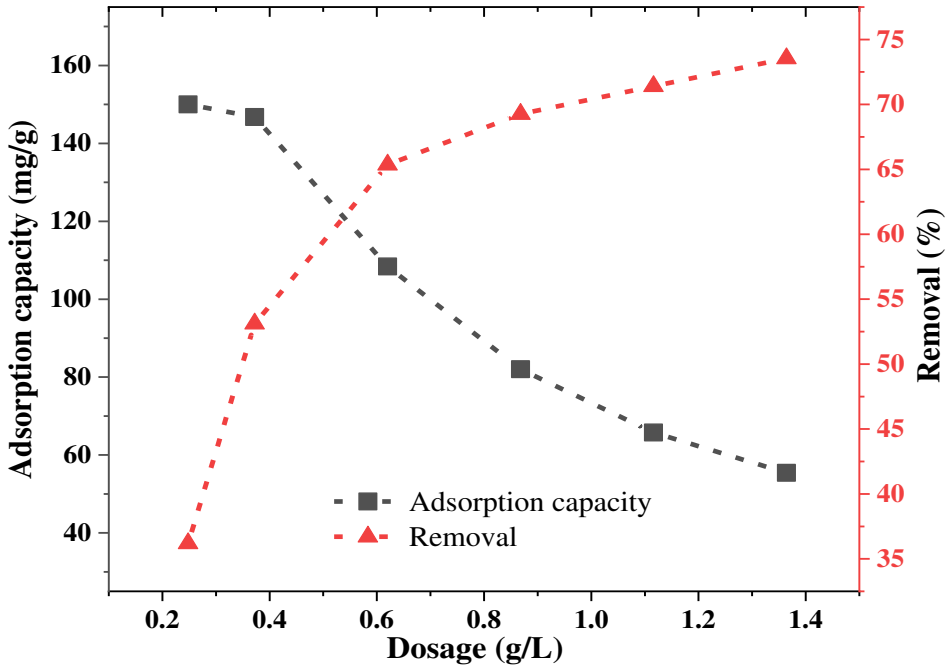

Fig. 4.73: Effect of adsorbent dosage for Cu(II) adsorption on CA-GO

4.2.3.2.3. Effect of Cu(II) ion concentrations and contact duration

To investigate the effect of initial Cu(II) ion concentration and contact duration on adsorption capacity of CA-GO, batch experiments were conducted (Table 4.58, Fig. 4.74).

In the experiments, copper salt solution (20 mL) of different concentrations (49.90, 57.45, 76.60, and 90.75 ppm) were used at optimum pH (6.0) and dosage (0.6 g/L) for a certain period (5-120 min). After 40 min, the adsorption process was reached at equilibrium. The adsorption capacity increased with time due to the presence of additional active sites until equilibrium was attained and these sites became saturated [230]. At lower initial Cu(II) concentration, the % removal was higher since the amount of chromium was less as compared to the amount of adsorbent, CA-GO composite (Table 4.59, Fig. 4.75).

Table 4.58: Adsorption capacity of CA-GO at different concentration of Cu(II) at different time intervals

Time (min)	49.90 ppm	57.45 ppm	76.60 ppm	90.75 ppm
5	22.25	26.85	38.54	48.5
10	27.58	41.37	54.95	53.24
20	47.26	52.63	63.06	66.03
30	52.74	57.66	71.04	77.79
40	61.27	66.69	78.71	86.8
60	62.29	66.25	79.76	88.59
120	61.4	64.91	80.08	89

Table 4.59: Time and % removal data of Cu(II) on CA-GO at different concentration

Time (min)	49.90 ppm	57.45 ppm	76.60 ppm	90.75 ppm
5	27.66	29.50	31.20	33.14
10	43.69	44.64	44.48	36.37
20	58.72	56.48	51.04	45.11
30	65.53	62.23	57.51	53.15
40	76.13	71.98	63.71	59.31
60	77.39	71.47	64.56	60.53
120	76.29	70.06	64.82	60.80

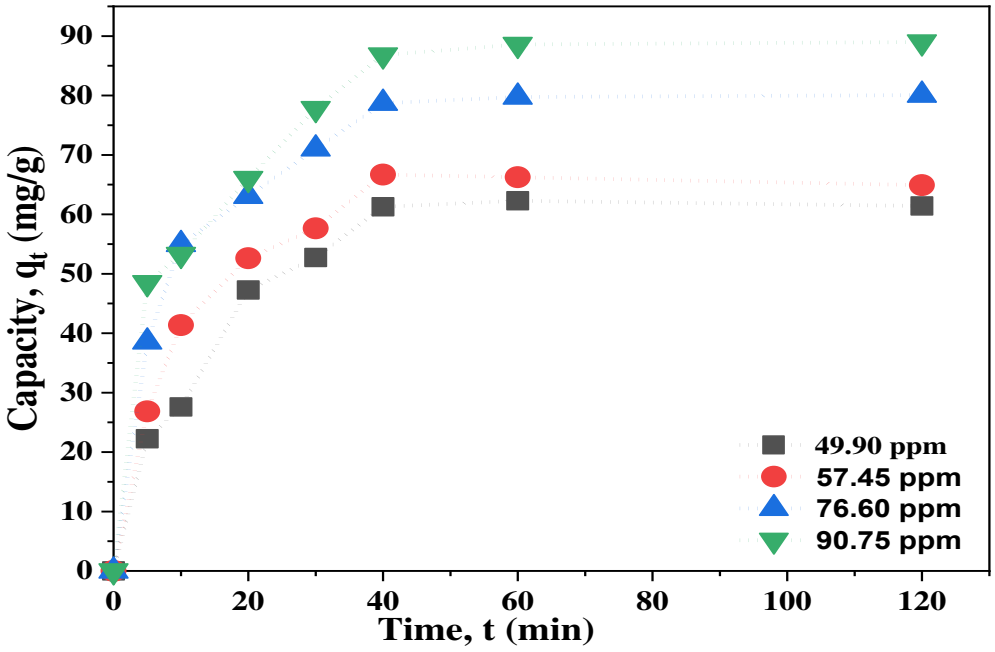

Fig. 4.74: Effect of Cu(II) ion concentration and contact time on adsorption capacity of CA-GO

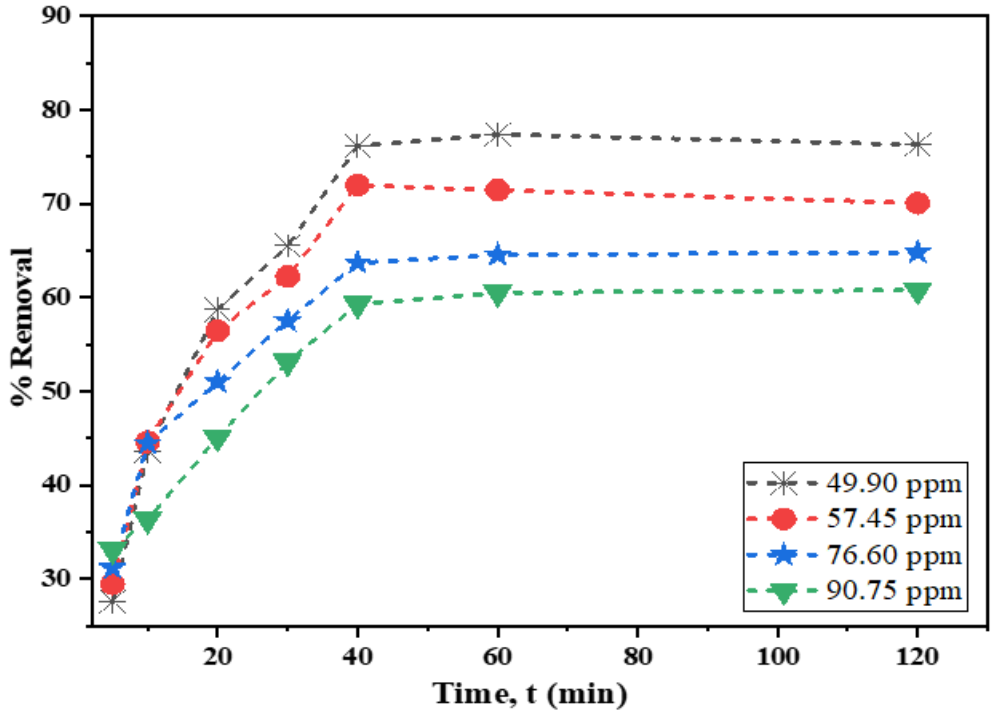

Fig. 4.75: Effect of time and % removal of Cu(II) on CA-GO at different concentration

4.2.3.2.4. Adsorption isotherms for Cu(II) adsorption on CA-GO

To study the distribution of Cu(II) on CA-GO, the Langmuir and Freundlich isotherm models were employed. Langmuir isotherms provide assumption about monolayer adsorption and Freundlich isotherm gives assumption about multilayer adsorption.

4.2.3.2.4.1. Langmuir isotherm

The Langmuir isotherm model was verified by plotting C_e/q_e versus C_e values following the eq. (3.4) and theoretical maximum adsorption capacity, q_m was estimated. A linear connection between C_e/q_e and C_e was observed for adsorption with acceptable regression coefficient (R^2=0.996). The q_m was determined 108.57 mg/g from the slope and the separation factor, R_L was 0.097, which indicated a favorable monolayer adsorption process of CA-GO (Table 4.60, Fig. 4.76).

Table 4.60: C_e vs C_e/q_e data of CA-GO at different concentration for Cu(II) adsorption

Initial concentration (ppm)	49.90	57.45	76.60	90.75
Equilibrium concentration (C_e)	11.91	16.1	27.8	36.93
C_e/q_e	0.1943	0.2421	0.353	0.425

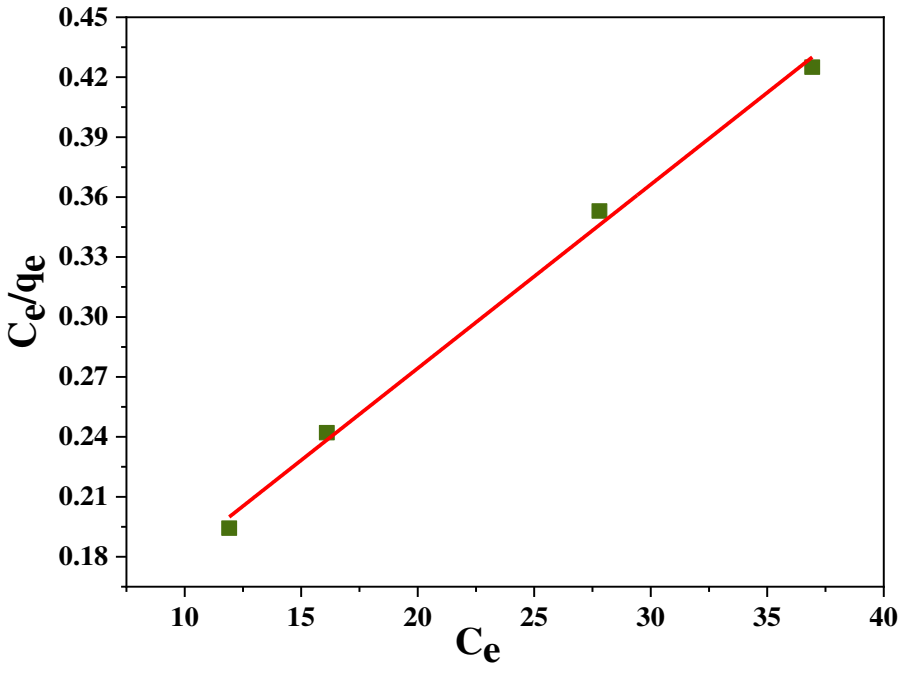

Fig. 4.76: Langmuir adsorption isotherm of Cu(II) adsorption on CA-GO

4.2.3.2.4.2. Freundlich Isotherm

Freundlich isotherm was studied by plotting lnC_e versus lnq_e following the eq. (3.6) to test the experimental data for multilayer adsorption mechanism. A linear relationship was observed (Table 4.61, Fig. 4.77) with an excellent regression coefficient (R^2=0.998). The value of n was found 3.254 that identified the adsorption was moderate to good (Table 4.62).

Table 4.61: lnC_e and lnq_e data of CA-GO at different concentration for Cu(II) adsorption

Initial concentration (ppm)	49.90	57.45	76.60	90.75
lnC_e	2.477	2.778	3.325	3.609
lnq_e	4.115	4.200	4.366	4.464

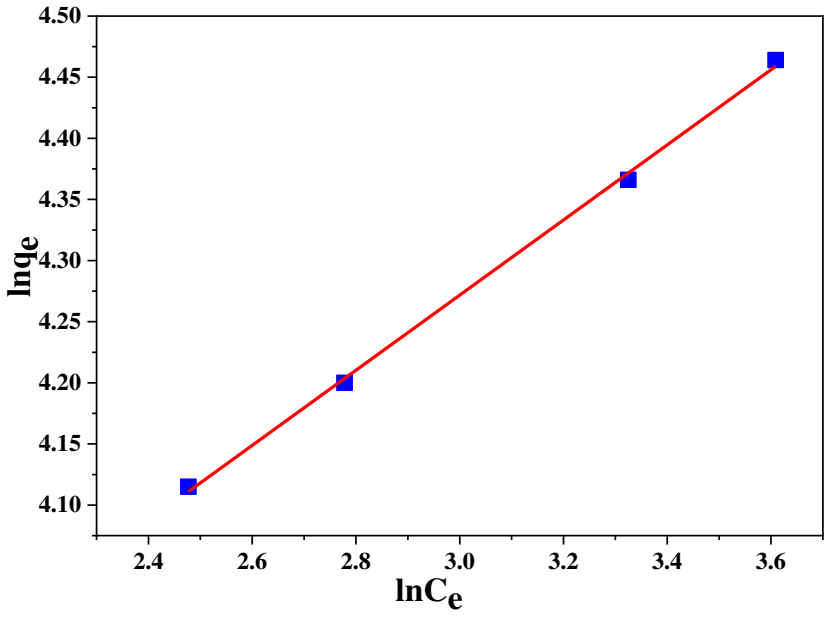

Fig. 4.77: Freundlich adsorption isotherm of Cu(II) adsorption on CA-GO

The different parameters of both isotherms were enlisted in the Table 4.62, which evidenced that the adsorption Cu(II) on CA-GO was followed both the models.

Table 4.62: Theoretical values of q_m, b, R_L, n, k_F and R^2 of adsorbent CA-GO for Cu(II) adsorption

Parameters	q_m, (mg/g)	b, Lmg^{-1}	R^2	R_L	n	k_F
Langmuir isotherm	108.57	0.102	0.996	0.097	-	-
Freundlich isotherm	-	-	0.998	-	3.254	28.49

4.2.3.2.5. Adsorption kinetics for Cu(II) adsorption on CA-GO

Adsorption kinetics is of great importance for evaluating the performance of adsorbent. Both pseudo-first –order and second-order models were used to relate the adsorption process of Cu(II) on CA-GO.

4.2.3.2.5.1. Pseudo-first-order kinetics

By plotting $\log(q_e-q_t)$ versus t following the eq. (3.7) pseudo-first-order model was yield, where a linear relationship between $\log(q_e-q_t)$ and t was observed (Table 4.63, Fig. 4.78).

Table 4.63: Time, t and $\log(q_e-q_t)$ data of CA-GO at different concentration for Cu(II) adsorption

Time, t (min)	$\log(q_e-q_t)$ at 49.90 ppm	$\log(q_e-q_t)$ at 57.45 ppm	$\log(q_e-q_t)$ at 76.60 ppm	$\log(q_e-q_t)$ at 90.75 ppm
5	1.591	1.6	1.604	1.583
10	1.417	1.403	1.376	1.526
20	1.146	1.156	1.195	1.317
30	0.931	0.956	0.883	0.956

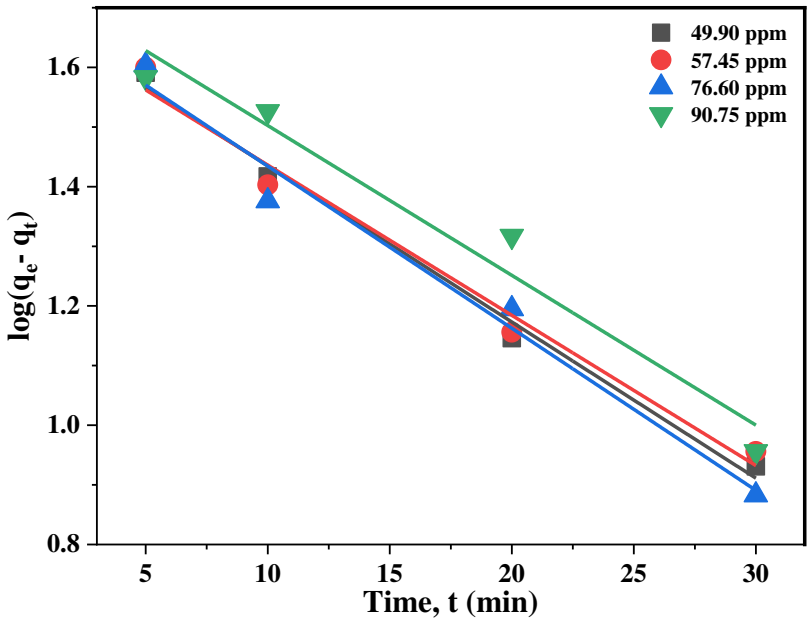

Fig. 4.78: Pseudo-first-order kinetics for Cu(II) adsorption on CA-GO

4.2.3.2.5.2. Pseudo-second-order kinetics

Pseudo-second-order kinetic model was achieved by plotting t/q_t versus t values following the eq. (3.8). A linear relationship between them was observed (Table 4.64, Fig. 4.79).

Table 4.64: Time, t and t/q_t data of CA-GO at different concentration for Cu(II) adsorption

Time, t (min)	t/q_t at 49.90 ppm	t/q_t at 57.45 ppm	t/q_t at 76.60 ppm	t/q_t at 90.75 ppm
5	0.224	0.186	0.129	0.103
10	0.284	0.242	0.182	0.187
20	0.423	0.382	0.317	0.303
30	0.569	0.52	0.422	0.386
40	0.653	0.599	0.508	0.461

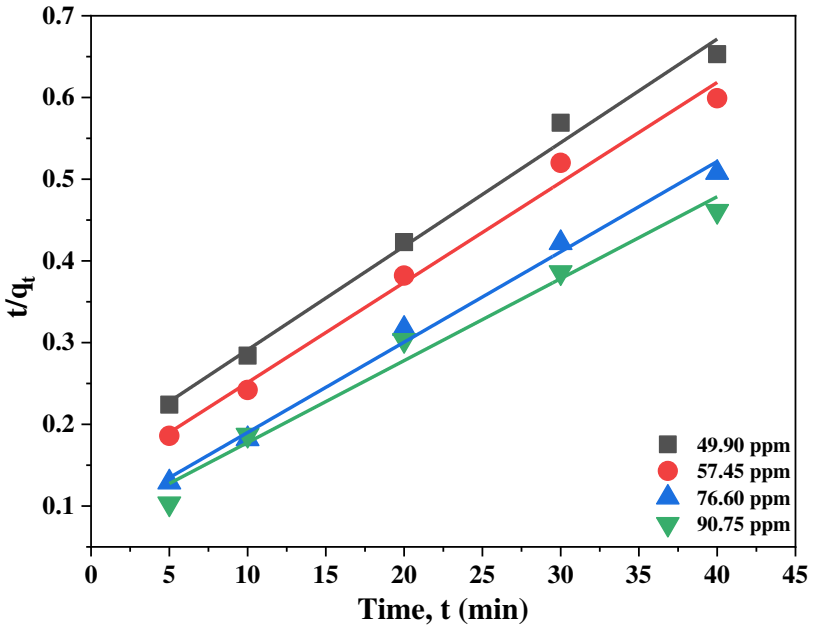

Fig. 4.79: Pseudo-second-order kinetics for Cu(II) adsorption on CA-GO

The values of various kinetics parameters are listed in Table 4.65 and Fig. 4.80. Regression coefficient (R^2) values and experimental values of q_e for pseudo-second-order kinetics were found to be significantly better than pseudo-first-order model.

Table 4.65: Kinetic parameter for Cu(II) adsorption on CA-GO

Kinetics model	Parameters	Initial concentration of copper(II)			
		49.90 ppm	57.45 ppm	76.60 ppm	90.75 ppm
Pseudo-first-order	q_e^* (mg g^{-1})	61.27	66.69	78.71	86.80
	k_1 (1/min)	0.0645	0.0575	0.0621	0.0575
	R^2	0.991	0.983	0.979	0.963
	q_e^{**} (mg g^{-1})	49.65	48.75	50.82	56.70
Pseudo-second-order	k_2 (g/mg min)	5.99 X 10^{-4}	1.12 X 10^{-3}	1.52 X 10^{-3}	1.29 X 10^{-3}
	R^2	0.992	0.990	0.993	0.980
	q_e^{**} (mg g^{-1})	79.36	83.33	90.91	100.00

* Experimental, **Theoretical

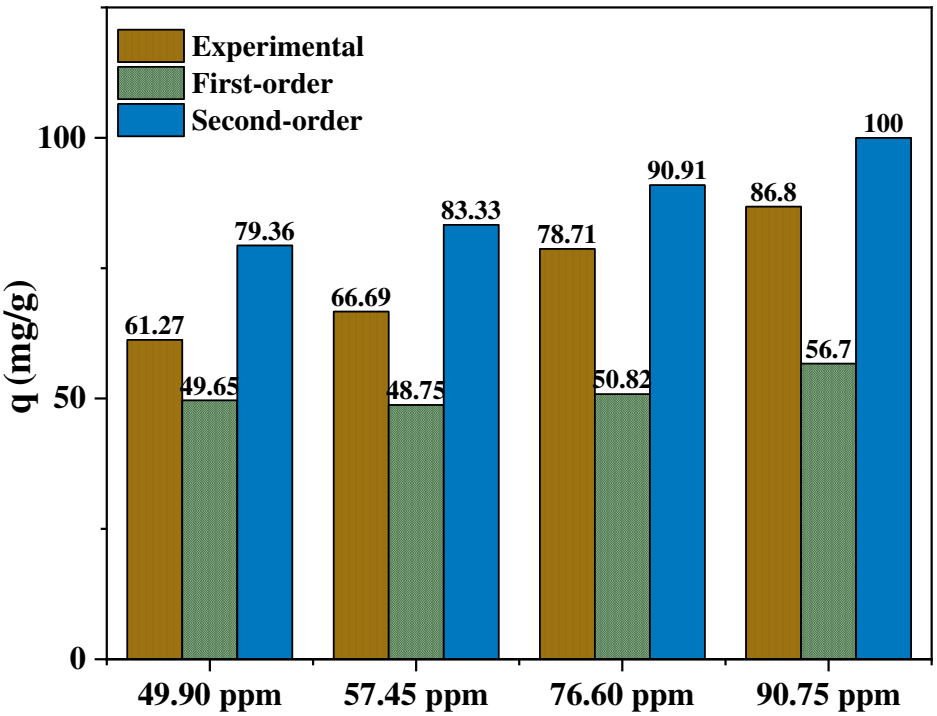

Fig. 4.80: Comparison of Cu(II) adsorption capacities of CA-GO

4.2.3.2.6. Thermodynamic analysis for Cu(II) adsorption on CA-GO

The Gibb's free energy, enthalpy and entropy change for Cu(II) adsorption on CA-GO at various temperatures (298-328 K) were evaluated using van't Hoff equation [eq. (3.10)]. A linear relationship was found while plotting $\ln k_d$ versus 1/T values (Table 4.66, Fig. 4.81).

Table 4.66: 1/T vs $\ln k_d$ data of CA-GO for Cu(II) adsorption

1/T	0.0033	0.0032	0.0031	0.003
$\ln k_d$	1.134	0.626	0.318	0.071

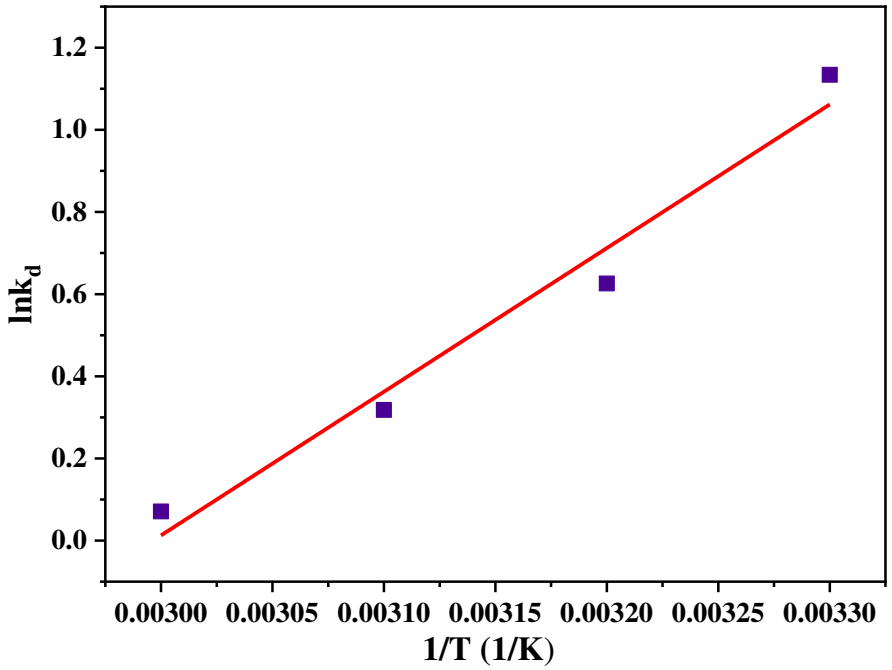

Fig. 4.81: van't Hoff equation data of Cu(II) adsorption on CA-GO

Enthalpy change (ΔH) and entropy change (ΔS) were calculated from the slope and intercept, respectively which were of -29.07 kJ mol^{-1} and -0.0871 kJ K^{-1} mol^{-1}, respectively. As temperature increase from 298 to 328 K, ΔG changed from -2.809 to -0.193 $kJmol^{-1}$ (Table 4.67). Cu(II) was thus spontaneously adsorbed on CA-GO at lower temperatures and the adsorption was physical in nature.

Table 4.67: Thermodynamic parameters of CA-GO for Cu(II) adsorption

T (K)	ΔG (kJ mol^{-1})	ΔH (kJ mol^{-1})	ΔS (kJ K^{-1} mol^{-1})
298	-2.809	-29.07	-0.0871
308	-1.603		
318	-0.841		
328	-0.193		

4.2.3.2.7. Plausible mechanism for Cu(II) adsorption on CA-GO

The two most important factors have a key impact on adsorption of a solute on an adsorbent are the surface chemistry and pore density. The interaction between oppositely

charged particles formed various bonds. Calcium alginate-graphene oxide surface possesses negative surface charge at pH higher than ZPC (pH 3.0) and unveils electrostatic interaction with cationic copper ion (Fig. 4.82). Electrostatic attraction, external ion exchange and complexation were mostly responsible for adsorption of Cu(II) on CA-GO.

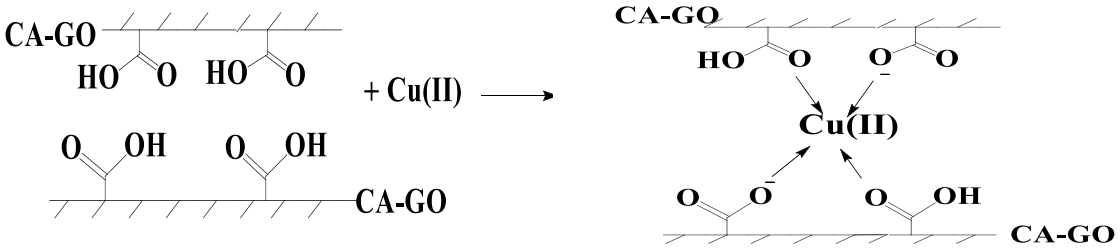

Fig. 4.82: Possible mechanism for Cu(II) adsorption onto CA-GO

4.2.3.2.8. Regeneration of used CA-GO for Cu(II) adsorption

To regenerate CA-GO, 2% dilute HCl was added with used adsorbent to take out copper and then neutralized by washing with distilled water. This neutralized CA-GO was then dried and used for further adsorption at optimum pH, time and adsorption dosage to examine the suitability of reuse. Fresh CA-GO had a Cu(II) adsorption capacity of 52.27 mg/g for 63.62 ppm salt solution, whereas it was reduced to 40.29, 33.79 and 18.45 mg/g after first, second and third recycle1st, 2nd and 3rd recycle, respectively (Fig. 4.83).

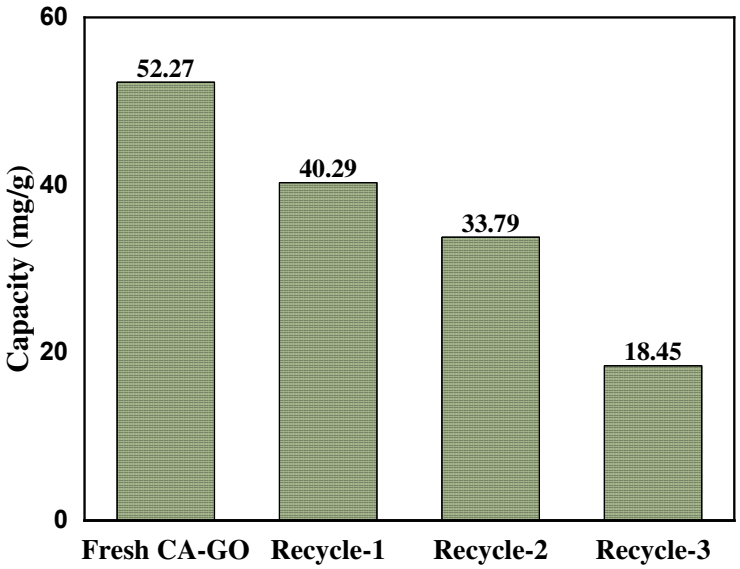

Fig. 4.83: Regeneration of used CA-GO beads for Cu(II) adsorption

4.2.3.3. Adsorption of Cd(II) on CA-GO

4.2.3.3.1. Effect of pH

Effects of pH on Cd(II) adsorption on CA-GO were investigated at a range of pH 3 to 8. In the experiments, the pH of cadmium(II) salt solutions (102.69 ppm, 20 mL) were adjusted 3.0, 4.0, 5.0, 6.0, 7.0 and 8.0. The CA-GO beads (22.32 mg, 1.116 g/L) was added to each solution and stirred at room temperature for 2 h at 150 rpm. The changes of concentration were measured by AAS, after filtering the mixtures. Then the adsorption capacity was determined and found high at higher pH. It was noticed that the capacity increased drastically at pH 8.0 (Table 4.68, Fig. 4.84), which was due to the precipitation of cadmium. It was observed that precipitation of Cd(II) occurred at pH>7.0.

Table 4.68: pH, adsorption capacity and % removal data of CA-GO for Cd(II) adsorption

pH	3.0	4.0	5.0	6.0	7.0	8.0
Adsorption capacity (mg/g)	26.78	43.45	61.73	64.77	66.21	86.01
% removal	29.11	47.22	67.09	70.37	71.95	93.48

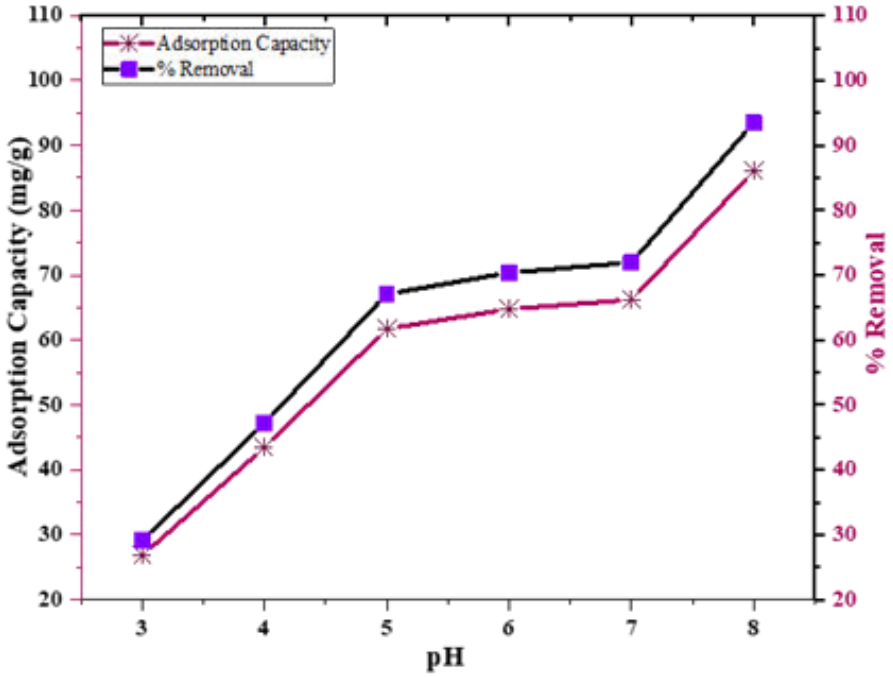

Fig. 4.84: Effect of pH on capacity and % removal of Cd(II) on CA-GO

Therefore, the pH 7.0 was selected as optimum for adsorption study. At this pH the adsorption capacity and % removal was 66.21 mg/g and 71.95%, respectively.

4.2.3.3.2. Effect of adsorbent dosage

The study was performed to evaluate adsorbent dosage effect of cadmium(II) adsorption ions on CA-GO. In view of optimization of adsorbent dosage, standard cadmium salt solution (20 mL, 80.68 ppm) was treated with different dosages (0.248-1.364 g/L) at optimum pH (7.0). Adsorbent capacities and percentage of removals were measured and it was apparent that adsorbent capacity was decreased with increasing adsorbent dosage, however percent of cadmium removal was increased (Table 4.69, Fig. 4.85). It is clear that the quantity of adsorbate per unit mass of adsorbent dropped when adsorbent dosage was increased [231]. The unsaturation of some active sites of adsorbent (CA-GO) and few of them were remained unreacted at the higher dosage of adsorbent. According to the findings of the experiments, the optimum dosage was selected 0.6 g/L, which was maintained throughout the study.

Table 4.69: Dosage, adsorption capacity and % removal data of CA-GO for Cd(II) adsorption

Dosage (g/L)	0.248	0.372	0.620	0.868	1.116	1.364
Adsorption capacity (mg/g)	91.05	80.05	62.77	52.3	42.36	38.76
% removal	27.98	36.91	48.24	56.27	58.6	65.56

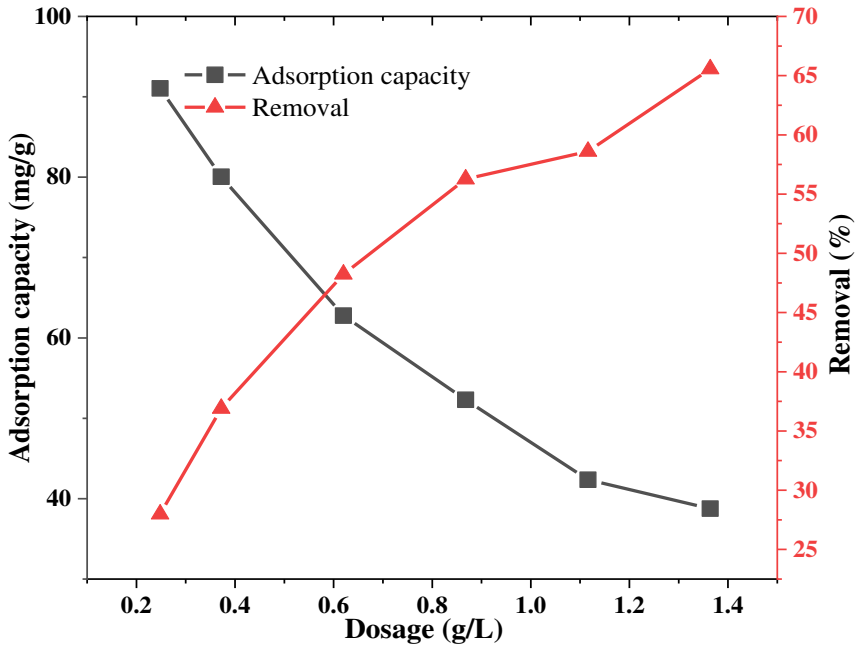

Fig. 4.85: Effect of dosage of Cd(II) adsorption on CA-GO composite beads

4.2.3.3.3. Effect of Cd(II) ion concentration and contact duration

To observe effect of concentration and contact duration on adsorption capacity of CA-GO for Cd(II), standard cadmium salt solution (20 mL) of different concentrations (45.69, 62.92, 76.82, and 90.16 ppm) at pH (7.0) and dosage (0.6 g/L) were treated with batch experiments (Table 4.70, Fig. 4.86) for a certain time (0-120 min). Initially abundant active sites of adsorbent were available, however as time passing those sites were saturated. As a result, the adsorption capacity of CA-GO was increased over time until it approached equilibrium. Owing to an increase in concentration gradient and mass transfer between adsorbate and adsorbent, equilibrium adsorption capacity also improves when adsorbent concentration increases [230]. The adsorption process of cadmium by CA-GO reached at equilibrium at around 40 min. The % removal was high at lower concentration as the amount of adsorbent is high compare to metal adsorbate in the solution (Table 4.71, Fig. 4.87). When the initial concentration of Cd increased, the adsorption capacity of CA-GO was increased and % removal of Cd decreased.

Table 4.70: Time and adsorption capacity data of CA-GO at different concentration for Cd(II) adsorption

Time (min)	45.69 ppm	62.92 ppm	76.82 ppm	90.16 ppm
5	19.66	20.32	23.79	29.49
10	35.08	24.48	34.37	37.53
20	38.41	38.68	51.22	45.48
30	42.00	54.55	61.69	55.40
40	51.53	60.71	72.88	76.08
60	51.87	64.06	75.15	84.56
120	52.08	61.85	73.16	84.34

Table 4.71: Time and % removal data of CA-GO at different concentration for Cd(II) adsorption

Time (min)	45.69 ppm	62.92 ppm	76.82 ppm	90.16 ppm
5	26.68	20.03	19.20	20.26
10	47.60	24.13	27.74	25.81
20	52.13	38.11	41.34	31.28
30	56.99	53.75	49.79	38.10
40	69.93	59.82	56.22	52.32
60	70.39	63.13	60.65	58.15
120	70.67	60.95	59.05	58.00

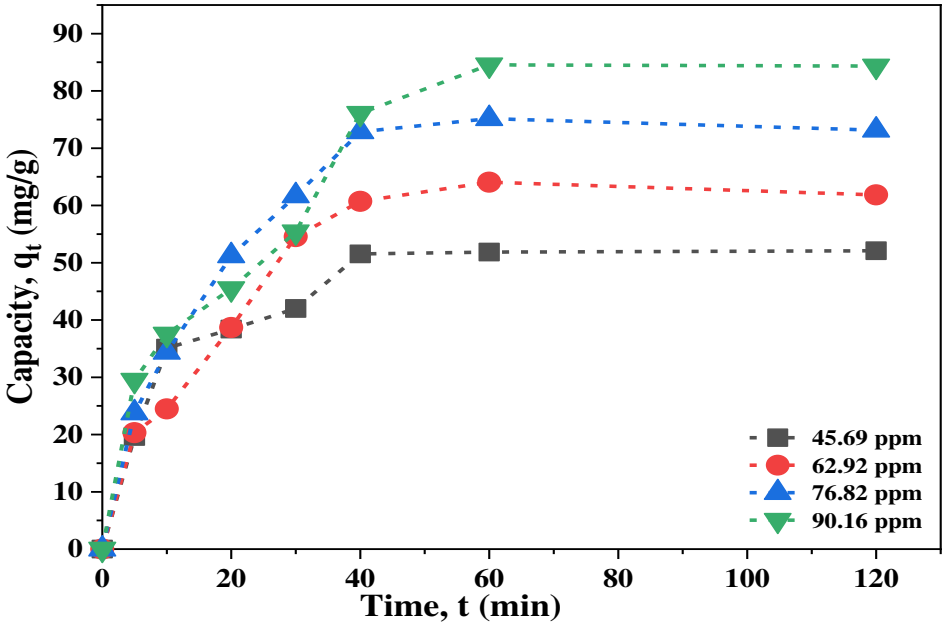

Fig. 4.86: Effect of Cd(II) ion concentration and contact duration on adsorption capacity of CA-GO composite beads

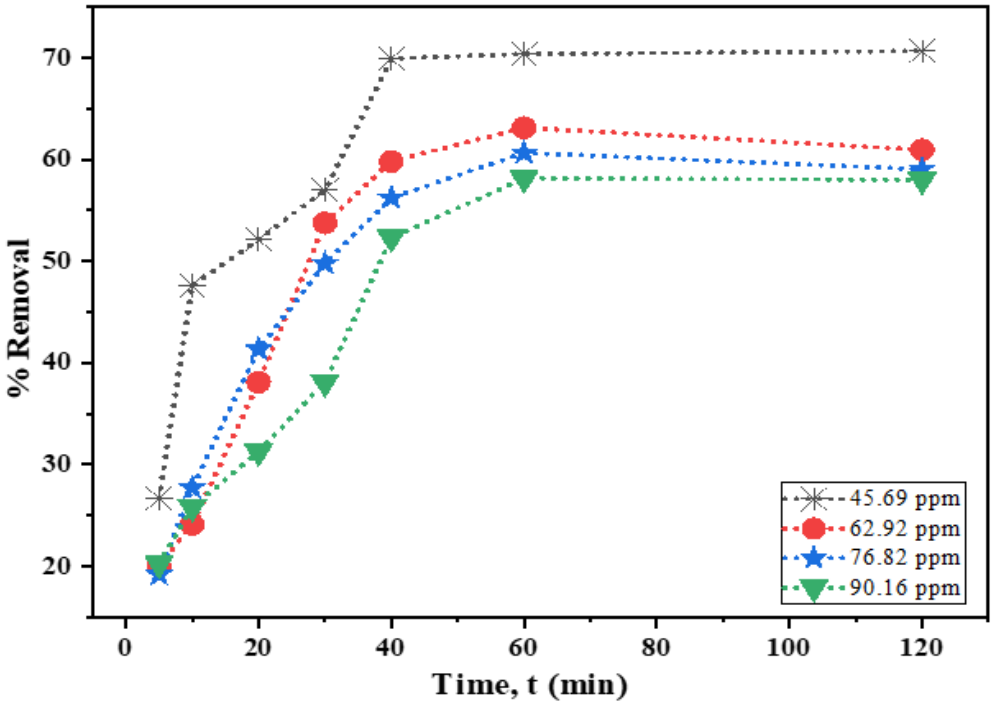

Fig. 4.87: Effect of time and % removal of Cd(II) on CA-GO composite beads at different concentrations

4.2.3.3.4. Adsorption isotherms of Cd(II) adsorption on CA-GO beads

Langmuir and Freundlich isotherm were exploited to investigate distribution of cadmium ion on CA-GO beads. Langmuir isotherm provides the information about monolayer adsorption and Freundlich isotherm provides assumption about multilayer adsorption.

4.2.3.3.4.1. Langmuir isotherm

Langmuir isotherm was verified by plotting Ce/qe against Ce following the eq. (4) and (5). A linear relationship between C_e/q_e and C_e was observed (Table 4.72, Fig. 4.88) with a good regression coefficient (R^2=0.975). The theoretical maximum adsorption capacity, q_m was calculated as 134.77 mg/g and the separation factor, R_L was 0.207 that indicated a favorable monolayer adsorption process.

Table 4.72: C_e and C_e/q_e data of CA-GO at different concentration for Cd(II) adsorption

Initial concentration (ppm)	45.69	62.92	76.82	90.16
Equilibrium concentration (C_e)	13.74	23.2	30.23	37.73
C_e/q_e	0.266	0.362	0.402	0.446

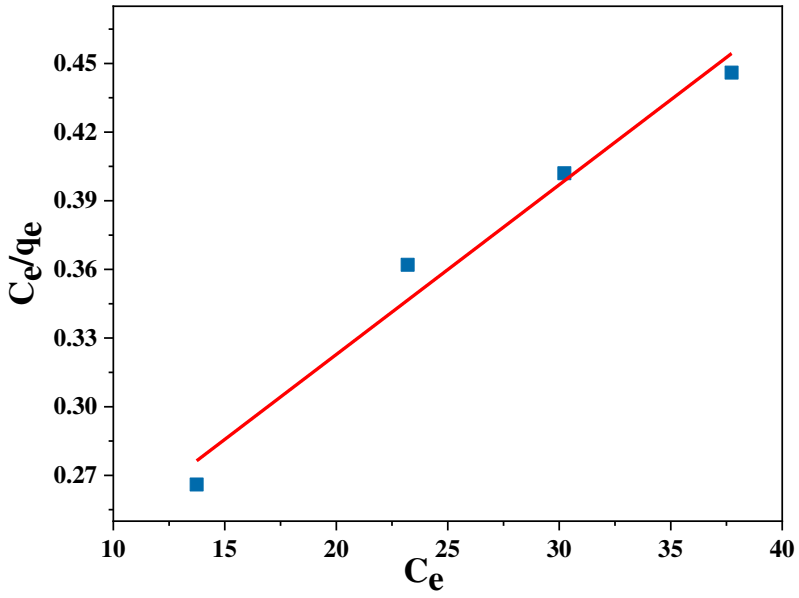

Fig. 4.88: Langmuir adsorption isotherm for Cd(II) adsorption on CA-GO composite beads

4.2.3.3.4.2. Freundlich isotherm

Freundlich adsorption isotherm was verified by plotting lnC_e against lnq_e following the eq, (3.6). An acceptable regression coefficient (R^2= 0.992) and a linear relation between lnC_e and lnq_e was observed (Table 4.73, Fig. 4.89). The calculated n value (2.037) indicated the adsorption was good.

Table 4.73: lnC_e and lnq_e data of CA-GO at different concentration for Cd(II) adsorption

Initial concentration (ppm)	45.69	62.92	76.82	90.16
lnC_e	2.62	3.144	3.408	3.63
lnq_e	3.942	4.159	4.319	4.437

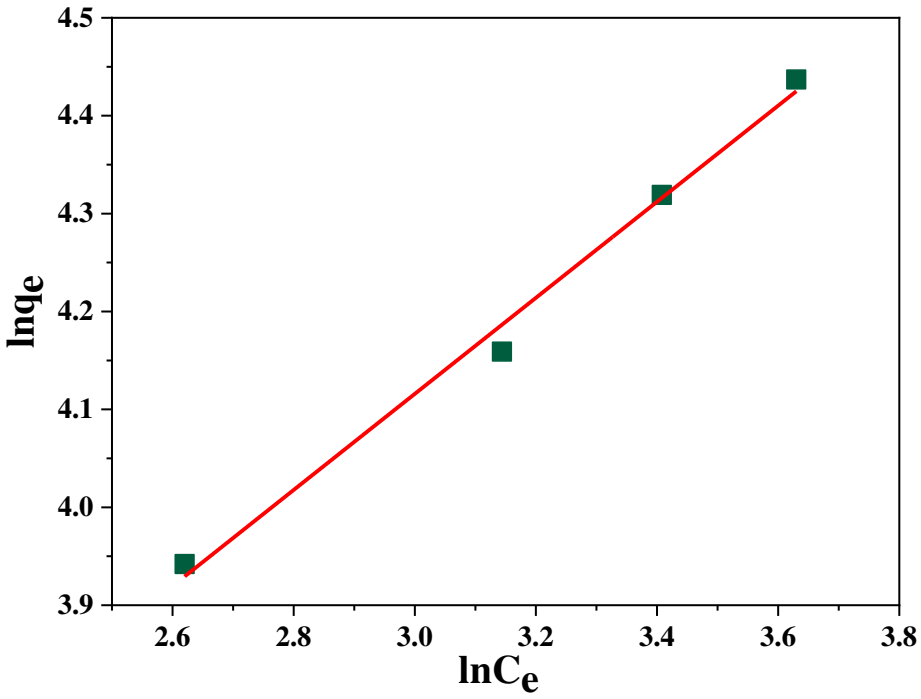

Fig. 4.89: Freundlich adsorption isotherm for Cd(II) adsorption on CA-GO composite

The different parameters of isotherms were listed in the Table 4.74. It was noticeable that the cadmium adsorption on CA-GO followed both the models, preferably the Freundlich isotherm model.

Table 4.74: Theoretical values of q_m, b, R_L, n, k_F and R^2 of adsorbent CA-GO for Cu(II) adsorption

Parameters	q_m, (mg/g)	b (Lmg^{-1})	R^2	R_L	n	k_F
Langmuir isotherm	134.77	0.0425	0.975	0.207	-	-
Freundlich isotherm	-	-	0.992	-	2.037	14.06

4.2.3.3.5. Adsorption kinetics for Cd(II) adsorption on CA-GO

Adsorption kinetics is very significant for assessing adsorbent's performance. Pseudo-first-order and second-order kinetic models were used to explain adsorption process of CA-GO for cadmium(II) ions.

4.2.3.3.5.1. Pseudo-first-order reaction kinetics

Following eq. (3.7), pseudo-first-order model was obtained by plotting $\log(q_e-q_t)$ against t at various initial concentrations of cadmium, where a linear relation between $\log(q_e-q_t)$ and t was observed (Table 4.75, Fig. 4.90).

Table 4.75: Time and $\log(q_e-q_t)$ data of CA-GO at different concentration for Cd(II) adsorption

Time, t (min)	$\log(q_e-q_t)$ at 45.69 ppm	$\log(q_e-q_t)$ at 62.92 ppm	$\log(q_e-q_t)$ at 76.82 ppm	$\log(q_e-q_t)$ at 90.16 ppm
5	1.503	1.641	1.711	1.741
10	1.216	1.597	1.610	1.672
20	1.117	1.404	1.379	1.592
30	0.979	0.979	1.129	1.464
40	-	0.527	0.356	0.928

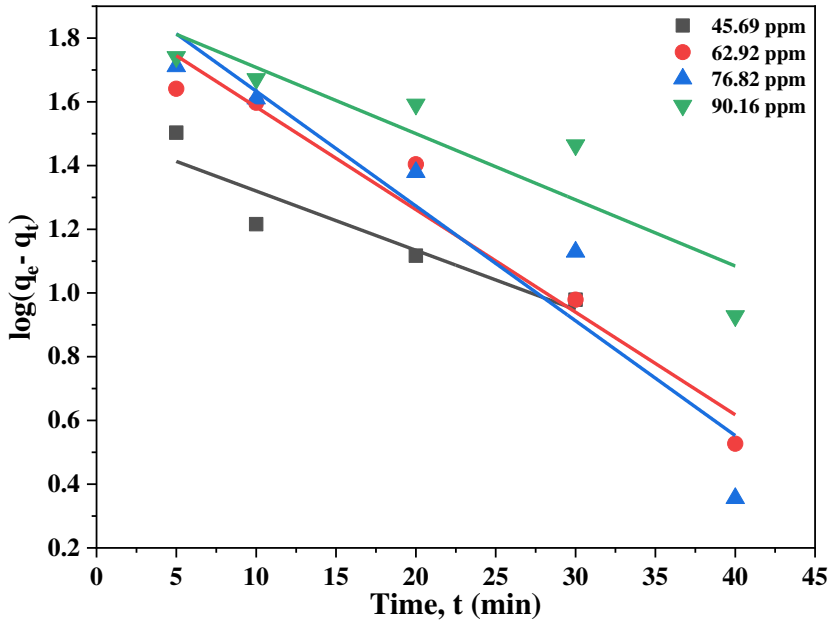

Fig. 4.90: Pseudo-first-order kinetics for Cd(II) adsorption on Ca-GO composite

4.2.3.3.5.2. Pseudo-second-order reaction kinetics

Pseudo-second-order model was attained by plotting the value of t/q_t versus t at different initial concentrations of cadmium solution following the eq. (3.8) (Table 4.76, Fig. 4.91). A linear relation was observed between t/q_t and t.

Table 4.76: Time, t (min) and t/q_t data of CA-GO at different concentration for Cd(II) adsorption

Time, t (min)	t/q_t at 45.69 ppm	t/q_t at 62.92 ppm	t/q_t at 76.82 ppm	t/q_t at 90.16 ppm
5	0.254	0.246	0.21	0.169
10	0.302	0.408	0.291	0.266
20	0.521	0.517	0.39	0.439
30	0.714	0.549	0.486	0.541
40	0.776	0.659	0.548	0.526
60	-	0.936	0.798	0.709

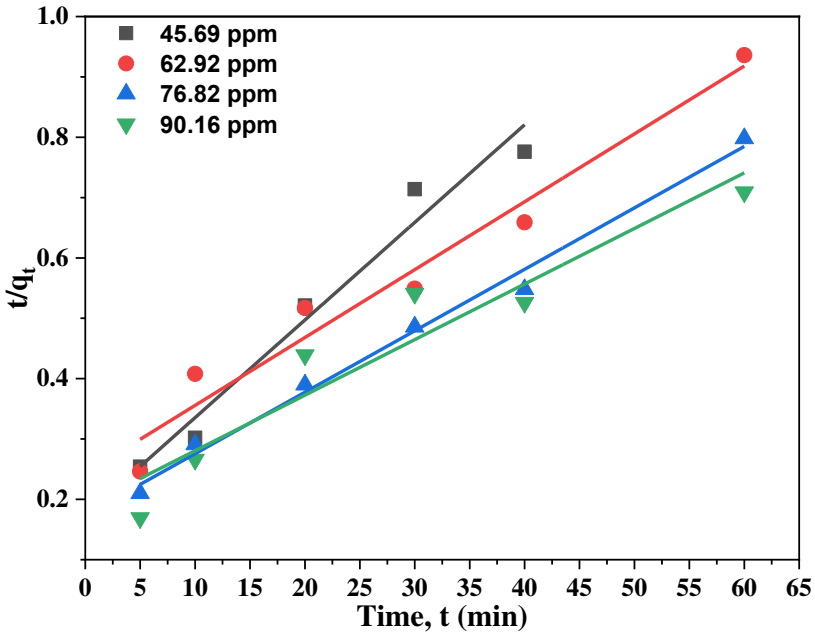

Fig. 4.91: Pseudo-second-order kinetics for adsorption of Cd(II) on CA-GO

It was demonstrated that the correlation coefficient (R^2) values for second-order-kinetics were much greater than that of first-order model (Table 4.77). However, the estimated pseudo-first-order kinetics adsorption capabilities were in good agreement with the experimental values (Fig. 4.92). Therefore, the adsorption of cadmium on CA-GO was physicochemical adsorption.

Table 4.77: Kinetics parameter for adsorption on Cd(II) on CA-GO

Kinetics model	Parameters	45.69 ppm	62.92 ppm	76.82 ppm	90.16 ppm
Pseudo-first-order	q_e^* (mg g^{-1})	51.53	64.08	75.15	84.56
	k_1(1/min)	0.0414	0.0736	0.0829	0.0476
	R^2	0.863	0.954	0.908	0.837
	q_e^{**} (mgg^{-1})	32.06	80.48	98.51	82.32
Pseudo-second-order	k_2 (g/mg min)	1.479X10^{-3}	0.497X10^{-3}	0.575X10^{-3}	0.43X10^{-3}
	R^2	0.969	0.961	0.991	0.913
	q_e^{**} (mg g^{-1})	62.50	90.91	100.00	111.11

* Experimental, **Theoretical

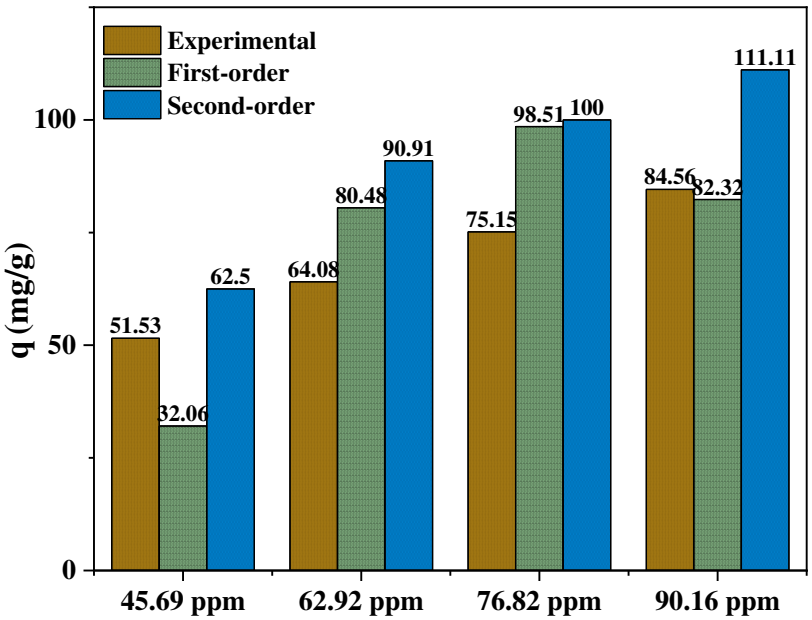

Fig. 4.92: Comparison of adsorption capacities for Cd(II) adsorption on CA-GO beads

4.2.3.3.6. Thermodynamic analysis for adsorption of Cd(II) on CA-GO

The thermodynamic analysis of an adsorption system determined its viability and randomness in terms of temperature. Using linearized van't Hoff isotherm eq. (3.11), changes of thermodynamic parameters, such as Gibb's free energy (ΔG), enthalpy (ΔS) and entropy (ΔH) for cadmium(II) adsorption on CA-GO at different temperatures (298-328 K) were studied. The estimated results revealed that as the temperature were raised, cadmium adsorption capacities of CA-GO were reduced due to release of adsorbate (cadmium) from adsorbent (CA-GO), which was assisted by higher kinetic energy at increased temperature. Following eq. (3.10), Gibb's free energies were calculated and were found to be -3.723, -2.469, -1.328, and -0.408 $kJmol^{-1}$ at 298, 308, 318 and 328 K, respectively. A straight line was achieved by plotting lnk_d values against 1/T (Table 4.78, Fig. 4.93).

Table 4.78: 1/T and lnk_d data of GO for Cd(II) adsorption

1/T	0.0033	0.0032	0.0031	0.003
lnk_d	1.503	0.9645	0.5025	0.1498

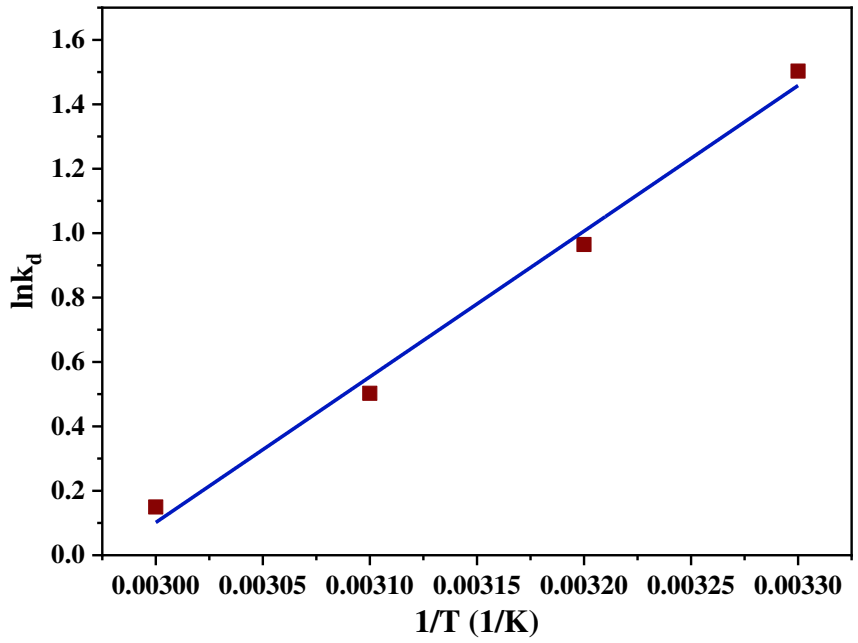

Fig. 4.93: van't Hoff equation data of Cd(II) adsorption on CA-GO

The enthalpy change (ΔH) and entropy change (ΔS) were calculated from the line's slope and intercept, respectively and their values were found to be -37.59 $kJmol^{-1}$ and -0.1119 $kJK^{-1}mol^{-1}$. When temperature was increased from 298 K to 328 K, the value of ΔG was also increased from -3.723 to -0.408 kJ mol-1 (Table 4.79). Hence, the adsorption of cadmium(II) ions on CA-GO beads was physicochemical and spontaneous at lower temperatures.

Table 4.79: Thermodynamic parameters of CA-GO for Cd(II) adsorption

T(K)	ΔG (kJ mol^{-1})	ΔH (kJ mol^{-1})	ΔS (kJ K^{-1} mol^{-1})
298	-3.723	-37.59	-0.1119
308	-2.469		
318	-1.328		
328	-0.408		

4.2.3.3.7. Plausible Mechanism for adsorption of Cd(II) on CA-GO

Surface chemistry of an adsorbent plays a major role on adsorption process. The adsorption mechanism deals with interactions between oppositely charged particles which

forms a variety of bonding like hydrogen bonds, electrostatic bonds, dipole-dipole interaction, van der Waals forces, and ion exchange. Calcium alginate-graphene oxide composite demonstrates electrostatic interaction with cationic cadmium ion because of its negative surface charge at pH higher than its ZPC (3.0). The negatively charged carboxylate group of CA-GO bind cationic Cd(II) ions from the solution electrostatic interaction and forming coordinate complexes (Fig. 4.94).

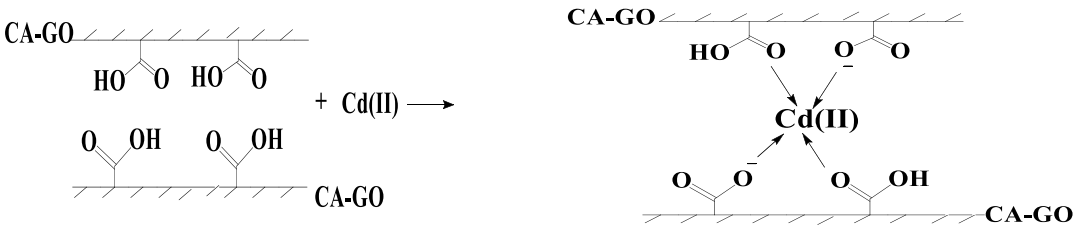

Fig. 4.94: Possible mechanism for Cd(II) adsorption on CA-GO

4.2.3.3.8. Regeneration of used CA-GO for Cd (II) adsorption

Regeneration studies of used adsorbents provide valuable information about commercial application. The regeneration of CA-GO was conducted using 2% dilute HCl to eliminate cadmium and then neutralize by repeated washing with distilled water. This regenerated CA-GO composite was dried properly and used further for adsorption of Cd(II) at optimum condition to examine the possibility of usefulness.

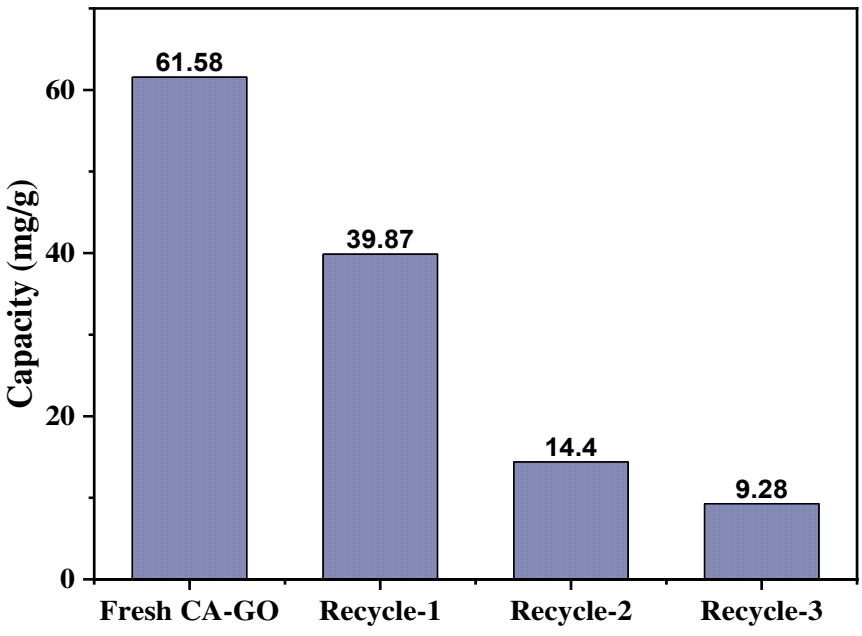

Fig. 4.95: Regeneration of CA-GO for Cd(II) adsorption

Fresh CA-GO composite demonstrated adsorption capacity 61.58 mg/g for 65.64 ppm Cd(II) solution at pH 7.0 while the regenerated CA-GO of recyle-1, recycle-2 and recycle-3 showed the adsorption capacities of 39.87, 14.4 and 9.28 mg/g, respectively (Fig. 4.95).

4.2.3.3.9. Adsorption capacity of GO, CA and CA-GO

The adsorption capacity of GO, CA and CA-GO are compared in the bar chart with the values (Fig. 4.96). The adsorption capacity of GO was found highest in case of all the metals of chromium, copper and cadmium, whereas it was the lowest for CA. The moderate and acceptable adsorption capacity were observed for CA-GO composite for all the metals studied.

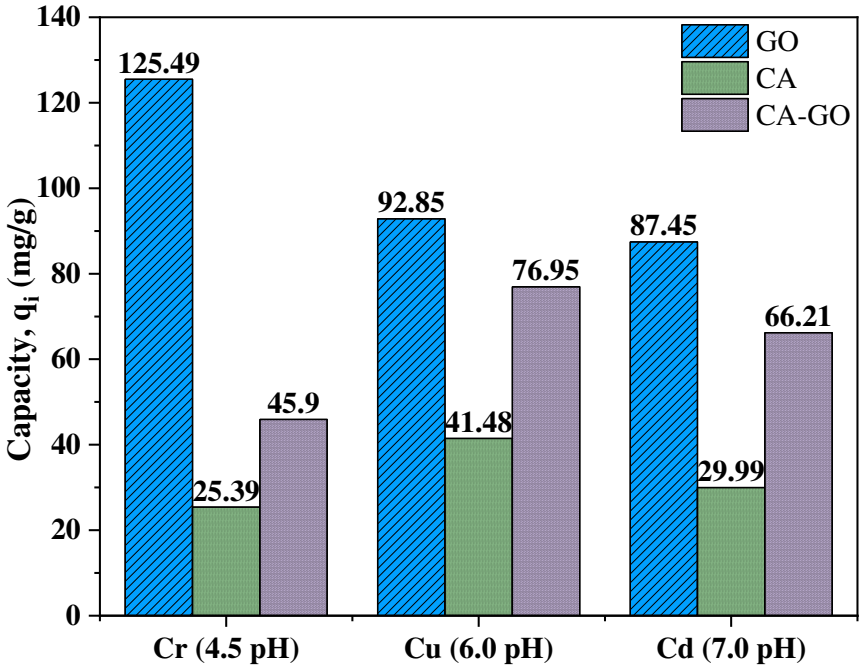

Fig. 4.96: Comparison of adsorption capacity of GO, CA and CA-GO

4.2.3.3.10. Application of CA-GO on chrome tanning effluents

After evaluating the capacity of CA-GO for removal of chromium, copper and cadmium ions from standard salt solutions through a number of batch experiments, the effectiveness in removing selective metal ions from real sample, i.e., chrome tanning effluent was justified. In order to measure the adsorption of Cr, Cu, and Cd ions from real chrome tanning effluent, 15 g of CA-GO composite beads added to 500 mL of chrome tanning effluent and agitated at room temperature for 4 h duration at 150 rpm. The concentration

of Cr, Cu and Cd before and after adsorption was analyzed by ICP-MS. The other water quality parameters, such as pH, TDS, EC, NaCl %, BOD5, and COD were also assessed and presented in the Table 4.80.

Table 4.80: Physicochemical characteristics of chrome tanning effluent before and after adsorption with CA-GO beads

Parameters	Before adsorption	After adsorption	% of removal	DoE Standard
Cr(III) (ppm)	3145.57	1258.84	59.98	2.00
Adsorption Capacity (mg/g)	-	62.89	-	-
Cu(II) (ppm)	1.26	0.62	50.79	0.50
Cd(II) (ppm)	0.98	0.49	50.00	0.50
pH	4.70	5.20	-	6-9
TDS (ppm)	5,980	2,817	52.89	2100
EC (µS/cm)	9,213	3,120	66.13	1200
NaCl (%)	13.42	7.32	45.45	
BOD_5 (ppm)	3,123	1,216	61.06	100
COD (ppm)	8,938	2,870	67.88	200

4.2.3.3.11. Application of CA-GO on tannery effluents

To investigate the adsorption performance of CA-GO on tannery effluent, 5.0 g of CA-GO adsorbent was added to 500 mL of tannery effluent and shaken at ambient temperature for 4 h at 150 rpm. The concentration of chromium, copper and cadmium before and after adsorption was determined by ICP-MS. Moreover, water quality parameter such as pH, TDS, EC, NaCl %, BOD_5, and COD were also determined, and the results are tabulated in the Table 4.81.

Table 4.81: Physicochemical characteristics of tannery effluents before and after adsorption with CA-GO beads

Parameters	Before adsorption	After adsorption	% of removal	DoE Standard
Cr(III) (ppm)	526.12	102.36	80.54	2.0
Adsorption Capacity (mg/g)	-	42.38	-	
Cu(II) (ppm)	2.17	0.63	70.96	0.50
Cd(II) (ppm)	1.28	0.53	58.59	0.50
pH	5.75	6.0		6-9
TDS (ppm)	7,338	2698	63.23	2100
EC (µS/cm)	5,120	1,535	70.02	1200
NaCl (%)	11.46	6.92	39.61	
BOD_5 (ppm)	3,050	982	67.80	≤100
COD (ppm)	7,132	1291	81.90	200

Chapter 5

Conclusions and Scope of Further Study

5.1. Conclusions

The following conclusions may be drawn from the present study-

• Graphene oxide (GO) can be synthesized from inexpensive and available graphite powder that minimizes the production cost and make it usable in the treatment of tannery effluent.

• The prepared GO possesses a negative surface charge and shows excellent adsorption capacity towards cationic metal ions. The adsorption capacity of the prepared graphene oxide was 366.3 mg/g for Cr(III) at pH 4.0, 193.05 mg/g for Cu(II) at pH 6.0 and 231.48 mg/g for Cd(II) at pH 7.0, which is quite significant.

• GO can be used as a cost-effective and efficient adsorbent for heavy metals (Cr, Cu and Cd) removal from aqueous media.

• CA-GO composite beads can be prepared using the ratio sodium alginate and GO (10:1) and 6% $CaCl_2$ w/w solution, which also provide good results for the removal of metals from aqueous solution. The adsorption capacity of CA-GO was 90.58 mg/g for Cr(III) at pH 4.5, 108.57 mg for Cu(II) at pH 6.0 and 134.77 mg/g for Cd(II) at pH 7.0.

• The used GO and CA-GO composite can be regenerated and reused several times.

• The pseudo-second-order kinetic model provided a better correlation for metals (Cr, Cu and Cd) and adsorbents (GO and CA-GO) than the pseudo-first-order model.

• The adsorption isotherm of Cr(III), Cu(II) and Cd(II) followed both the Langmuir and Freundlich models by GO and CA-GO adsorbents.

• The value of Gibb's free energy and enthalpy change for both the GO and CA-GO composite bead adsorbents were negative at different temperatures, which revealed the adsorption processes were spontaneous and physico-chemical.

5.2. Scope of Further Study

• Prepared GO and CA-GO composite can be applied for the removal of other heavy metals also.

• Prepared graphene-based adsorbents can be used for the treatment of any other industrial effluents.

• GO composite can be prepared by mixing various materials, like polymers and adsorption capacity can be studied with different heavy metals and pollutants.

• Further research can be designed for developing high mechanical strength tailored composite adsorbents to separate easily from the liquid phase after wastewater treatment.

• The graphene-based adsorbents used for heavy metal removal are limited to lab scale, at present. Therefore, further research is required to scale up for a large-scale practical application.

References:

[1] M. Appiah-Brempong, H. M. K. Essandoh, N. Y. Asiedu, S. K. Dadzie, and F. W. Y. Momade, "An insight into artisanal leather making in Ghana," *J. Leather Sci. Eng.*, vol. 2, no. 1, 2020, doi: 10.1186/s42825-020-00039-8.

[2] M. M. Mahdi, F. T. Zohra, and S. Ahmed, "Dyeing of Shoe Upper Leather with Extracted Dye from Acacia Nilotica Plant Bark-An Eco-Friendly Initiative," *Prog. Color. Color. Coatings*, vol. 14, no. 4, pp. 241–258, 2021, doi: 10.30509/pccc.2020.166673.1074.

[3] V. J. Sundar, A. Gnanamani, C. Muralidharan, N. K. Chandrababu, and A. B. Mandal, "Recovery and utilization of proteinous wastes of leather making: A review," *Rev. Environ. Sci. Biotechnol.*, vol. 10, no. 2, pp. 151–163, 2011, doi: 10.1007/s11157-010-9223-6.

[4] A. Shahriar, F.-T.- Zohra, A. B. M. W. Murad, and S. Ahmed, "Enhancement of Waterproofing Properties of Finished Upper Leather Produced from Bangladeshi Cow Hides," *Eur. J. Eng. Res. Sci.*, vol. 4, no. 7, pp. 63–71, 2019, doi: 10.24018/ejers.2019.4.7.1426.

[5] Y. Li, R. Guo, W. Lu, and D. Zhu, "Research progress on resource utilization of leather solid waste," *J. Leather Sci. Eng.*, vol. 1, no. 1, pp. 1–17, 2019, doi: 10.1186/s42825-019-0008-6.

[6] R. S. Velusamy Mozhiarasi, Bhavya B Krishna, Velmurugan Nagabalaji, Shanmugham Venkatachalam Srinivasan, Thallada Bhaskar, "Chapter 10 - Leather industry waste based biorefinery," in *Waste Biorefinery, Elsevier*, E. R. R. Thallada Bhaskar, Sunita Varjani, Ashok Pandey, Ed. 2021, pp. 267–304. doi: https://doi.org/10.1016/B978-0-12-821879-2.00010-7.

[7] H. L. Paul, A. P. M. Antunes, A. D. Covington, P. Evans, and P. S. Philips, “Bangladeshi leather industry: An overview of recent sustainable developments,” *J. Soc. Leather Technol. Chem.*, vol. 97, no. 1, pp. 25–32, 2013.

[8] A. S. Hassen and T. B. Woldeamanuale, “Evaluation and Characterization of Tannery Wastewater in each process at batu and modjo tannery, Ethiopia,” *Int. J. Rural Dev. Environ. Heal. Res.*, vol. 1, no. 3, pp. 2456–8678, 2017.

[9] T. H. Meneberu, “Evaluation and Characterization of Wastewater from Tannery industries and their Impact on Water Quality of the Receiving River, Ethiopia,” *Int. J. Sci. Acad. Res.*, vol. 3, no. 2, pp. 13–21, 2021.

[10] P. C. Nagajyoti, K. D. Lee, and T. V. M. Sreekanth, “Heavy metals, occurrence and toxicity for plants: A review,” *Environ. Chem. Lett.*, vol. 8, no. 3, pp. 199–216, 2010, doi: 10.1007/s10311-010-0297-8.

[11] G. Lofrano, M. Carotenuto, R. K. Gautam, and M. C. Chattopadhyaya, “Chapter 12. Heavy Metals in Tannery Wastewater and Sludge: Environmental Concerns and Future Challenges,” *Heavy Met. Water*, pp. 249–260, 2014, doi: 10.1039/9781782620174-00249.

[12] É. Hansen, P. M. de Aquim, and M. Gutterres, “Environmental assessment of water, chemicals and effluents in leather post-tanning process: A review,” *Environ. Impact Assess. Rev.*, vol. 89, no. February, 2021, doi: 10.1016/j.eiar.2021.106597.

[13] P. M. de Aquim, É. Hansen, and M. Gutterres, “Water reuse: An alternative to minimize the environmental impact on the leather industry,” *J. Environ. Manage.*, vol. 230, no. August 2018, pp. 456–463, 2019, doi: 10.1016/j.jenvman.2018.09.077.

[14] S. shan Guo, Y. hui Xu, and J. yan Yang, “Simulating the migration and species distribution of Cr and inorganic ions from tanneries in the vadose zone,” *J. Environ. Manage.*, vol. 288, no. March, p. 112441, 2021, doi: 10.1016/j.jenvman.2021.112441.

[15] M. J. Uddin and Y. K. Jeong, “Urban river pollution in Bangladesh during last 40 years: potential public health and ecological risk, present policy, and future prospects toward smart water management,” *Heliyon*, vol. 7, no. 2, p. e06107, 2021, doi: 10.1016/j.heliyon.2021.e06107.

[16] D. Gao, Y. Cheng, P. Wang, F. Li, Y. Wu, B. Lyu, J. Ma, and J. Qin, “An eco-friendly approach for leather manufacture based on P(POSS-MAA)-aluminum tanning agent combination tannage,” *J. Clean. Prod.*, vol. 257, p. 120546, 2020,

doi: 10.1016/j.jclepro.2020.120546.

[17] S. Ahmed, Fatema-Tuj-Zohra, M. S. H. Khan, and M. A. Hashem, “Chromium from tannery waste in poultry feed: A potential cradle to transport human food chain,” *Cogent Environ. Sci.*, vol. 3, no. 1, 2017, doi: 10.1080/23311843.2017.1312767.

[18] M. A. Hashem, M. Hasan, M. A. Momen, S. Payel, and M. S. Nur-A-Tomal, “Water hyacinth biochar for trivalent chromium adsorption from tannery wastewater,” *Environ. Sustain. Indic.*, vol. 5, p. 100022, 2020, doi: 10.1016/j.indic.2020.100022.

[19] R. Khalid, Z. Aslam, A. Abbas, W. Ahmad, N. Ramzan, and R. Shawabkeh, “Adsorptive potential of Acacia nilotica based adsorbent for chromium(VI) from an aqueous phase,” *Chinese J. Chem. Eng.*, vol. 26, no. 3, pp. 614–622, 2018, doi: 10.1016/j.cjche.2017.08.017.

[20] N. K. Mondal and S. Chakraborty, “Adsorption of Cr(VI) from aqueous solution on graphene oxide (GO) prepared from graphite: equilibrium, kinetic and thermodynamic studies,” *Appl. Water Sci.*, vol. 10, no. 2, pp. 1–10, 2020, doi: 10.1007/s13201-020-1142-2.

[21] M. Das, K. Ahmed, S. Islam, M. Islam, and M. S. Akter, “Heavy Metal in Industrial Effluents (Tannery and Textile) and Adjacent Rivers of Dhaka City , Bangladesh,” *Terr. Aquat. Environ. Toxicol.*, vol. 5, no. 1, pp. 8–13, 2010.

[22] T. Xu, F. Nan, X. Jiang, Y. Tang, Y. Zeng, W. Zhang, and B. Shi, “Effect of soil pH on the transport, fractionation, and oxidation of chromium(III),” *Ecotoxicol. Environ. Saf.*, vol. 195, no. 24, p. 110459, 2020, doi: 10.1016/j.ecoenv.2020.110459.

[23] R. T. Achmad, Budiawan, and E. I. Auerkari, “Effects of chromium on human body,” *Annu. Res. Rev. Biol.*, vol. 13, no. 2, pp. 1–8, 2017, doi: 10.9734/ARRB/2017/33462.

[24] H. Chen, J. M. Arocena, J. Li, R. W. Thring, and J. Zhou, “Assessments of chromium (and other metals) in vegetables and potential bio-accumulations in humans living in areas affected by tannery wastes,” *Chemosphere*, vol. 112, pp. 412–419, 2014, doi: 10.1016/j.chemosphere.2014.04.091.

[25] M. W. Xaba, J. O. Olowoyo, and G. Scott, “Trace metal deposition on soil and accumulation in plants around a coal power station in Pretoria, South Africa,” *J.*

Environ. Sci. Manag., vol. 21, no. 2, pp. 23–29, 2018, doi: 10.47125/jesam/2018_2/04.

[26] M. S. Alam, B. Han, Al-Mizan, and J. Pichtel, "Assessment of soil and groundwater contamination at a former Tannery district in Dhaka, Bangladesh," *Environ. Geochem. Health*, vol. 42, no. 7, pp. 1905–1920, 2019, doi: 10.1007/s10653-019-00457-6.

[27] Al-Mizan, M. A. I. Juel, M. S. Alam, J. Pichtel, and T. Ahmed, "Environmental and health risks of metal-contaminated soil in the former tannery area of Hazaribagh, Dhaka," *SN Appl. Sci.*, vol. 2, no. 11, 2020, doi: 10.1007/s42452-020-03680-4.

[28] S. Ahmed, Fatema-Tuj-Zohra, M. M. Mahdi, M. Nurnabi, M. Z. Alam, and T. R. Choudhury, "Health risk assessment for heavy metal accumulation in leafy vegetables grown on tannery effluent contaminated soil," *Toxicol. Reports*, vol. 9, pp. 346–355, 2022, doi: 10.1016/j.toxrep.2022.03.009.

[29] Al-Mizan, M. A. I. Juel, M. S. Alam, J. Pichtel, and T. Ahmed, "Environmental and health risks of metal-contaminated soil in the former tannery area of Hazaribagh, Dhaka," *SN Appl. Sci.*, vol. 2, no. 11, pp. 1–17, 2020, doi: 10.1007/s42452-020-03680-4.

[30] M. Nur-E-Alam, M. A. S. Mia, F. Ahmad, and M. M. Rahman, "An overview of chromium removal techniques from tannery effluent," *Appl. Water Sci.*, vol. 10, no. 9, 2020, doi: 10.1007/s13201-020-01286-0.

[31] G. Crini and E. Lichtfouse, "Advantages and disadvantages of techniques used for wastewater treatment," *Environ. Chem. Lett.*, vol. 17, no. 1, pp. 145–155, 2019, doi: 10.1007/s10311-018-0785-9.

[32] M. İnce and O. Kaplan İnce, "An Overview of Adsorption Technique for Heavy Metal Removal from Water/Wastewater: A Critical Review," *Int. J. Pure Appl. Sci.*, no. January 2018, pp. 10–19, 2017, doi: 10.29132/ijpas.372335.

[33] B. Silva, M. Martins, M. Rosca, M. Martins, M. Rosca, V. Rocha, L. Ana, I. C. Neves, and T. Tavares, "Waste-based biosorbents as cost-effective alternatives to commercial adsorbents for the retention of fluoxetine from water," *Sep. Purif. Technol.*, vol. 235, no. April 2019, p. 116139, 2020, doi: 10.1016/j.seppur.2019.116139.

[34] T. P. Dasari Shareena, D. McShan, A. K. Dasmahapatra, and P. B. Tchounwou, "A Review on Graphene-Based Nanomaterials in Biomedical Applications and Risks in

Environment and Health," *Nano-Micro Lett.*, vol. 10, no. 3, 2018, doi: 10.1007/s40820-018-0206-4.

[35] S. M. Elgengehi, S. El-Taher, M. A. A. Ibrahim, J. K. Desmarais, and K. E. El-Kelany, "Graphene and graphene oxide as adsorbents for cadmium and lead heavy metals: A theoretical investigation," *Appl. Surf. Sci.*, vol. 507, p. 145038, 2019, doi: 10.1016/j.apsusc.2019.145038.

[36] G. Zhao, X. Ren, X. Gao, X. Tan, J. Li, C. Chen, Y. Huan, and X. Wang, "Removal of Pb(ii) ions from aqueous solutions on few-layered graphene oxide nanosheets," *Dalt. Trans.*, vol. 40, no. 41, pp. 10945–10952, 2011, doi: 10.1039/c1dt11005e.

[37] G. Zhao, J. Li, X. Ren, C. Chen, and X. Wang, "Few-layered graphene oxide nanosheets as superior sorbents for heavy metal ion pollution management," *Environ. Sci. Technol.*, vol. 45, no. 24, pp. 10454–10462, 2011, doi: 10.1021/es203439v.

[38] S. Sharma and S. Soederberg, "Redesigning the business of development: the case of the World Economic Forum and global risk management," *Rev. Int. Polit. Econ.*, vol. 27, no. 4, pp. 828–854, 2020, doi: 10.1080/09692290.2019.1640125.

[39] K. Imasiku and E. Ntagwirumugara, "An impact analysis of population growth on energy-water-food-land nexus for ecological sustainable development in Rwanda," *Food Energy Secur.*, vol. 9, no. 1, 2020, doi: 10.1002/fes3.185.

[40] L. Huber, J. Rüdisser, C. Meisch, R. Stotten, G. Leitinger, and U. Tappeiner, "Agent-based modelling of water balance in a social-ecological system: A multidisciplinary approach for mountain catchments," *Sci. Total Environ.*, vol. 755, p. 142962, 2021, doi: 10.1016/j.scitotenv.2020.142962.

[41] Z. Ali, R. N. Malik, Z. K. Shinwari, and A. Qadir, "Enrichment, risk assessment, and statistical apportionment of heavy metals in tannery-affected areas," *Int. J. Environ. Sci. Technol.*, vol. 12, no. 2, pp. 537–550, 2015, doi: 10.1007/s13762-013-0428-4.

[42] A. L. Tasca and M. Puccini, "Leather tanning: Life cycle assessment of retanning, fatliquoring and dyeing," *J. Clean. Prod.*, vol. 226, pp. 720–729, 2019, doi: 10.1016/j.jclepro.2019.03.335.

[43] M. M. Uddin, M. J. Hasan, Y. Mahmud, F. T. Zohra, and S. Ahmed, "Evaluating suitability of glutaraldehyde tanning in conformity with physical properties of conventional chrome-tanned leather," *Text. Leather Rev.*, vol. 3, no. 3, pp. 135–145,

2020, doi: 10.31881/TLR.2020.09.

[44] J. K. Kanagaraj, R. C. Panda, and M. V. K. Vinodh Kumar, “Trends and advancements in sustainable leather processing: Future directions and challenges-A review,” *J. Environ. Chem. Eng.*, vol. 8, no. 5, p. 104379, 2020, doi: 10.1016/j.jece.2020.104379.

[45] N. M. Sivaram and D. Barik, *Toxic waste from leather industries*. Elsevier Ltd., 2018. doi: 10.1016/B978-0-08-102528-4.00005-5.

[46] H. I. Abdel-Shafy, W. Hegemann, and E. Genschow, “Fate of heavy metals in the leather tanning industrial wastewater using an anaerobic process,” *Environ. Manag. Heal.*, vol. 6, no. 2, pp. 28–33, 1995, doi: 10.1108/09566169510085135.

[47] Z. Song, C. J. Williams, and R. G. J. Edyvean, “Treatment of tannery wastewater by chemical coagulation,” *Desalination*, vol. 164, no. 3, pp. 249–259, 2004, doi: 10.1016/S0011-9164(04)00193-6.

[48] DoE, “The Environment Conservation Rules, 1997,” *Bangladesh Dep. Environ. Minist. Environ. For. Gov. People’s Repub. Bangladesh*, pp. 179–227, 1997.

[49] G. of the P. R. of Bangladesh., *ECR (1997). The Environment Conservation Rules,*.

[50] N. K. Srivastava and C. B. Majumder, “Novel biofiltration methods for the treatment of heavy metals from industrial wastewater,” *J. Hazard. Mater.*, vol. 151, no. 1, pp. 1–8, 2008, doi: 10.1016/j.jhazmat.2007.09.101.

[51] F. Fu and Q. Wang, “Removal of heavy metal ions from wastewaters: A review,” *J. Environ. Manage.*, vol. 92, no. 3, pp. 407–418, 2011, doi: 10.1016/j.jenvman.2010.11.011.

[52] J. Briffa, E. Sinagra, and R. Blundell, “Heavy metal pollution in the environment and their toxicological effects on humans,” *Heliyon*, vol. 6, no. 9, p. e04691, 2020, doi: 10.1016/j.heliyon.2020.e04691.

[53] A. Baysal, N. Ozbek, and S. Akm, “Determination of Trace Metals in Waste Water and Their Removal Processes,” *Waste Water - Treat. Technol. Recent Anal. Dev.*, 2013, doi: 10.5772/52025.

[54] G. Chitrakoot, G. Vishwavidyalaya, N. Kumar, A. Mahatma, J. Tiwari, J. Pathak, R. Singh, and N. Kumar Ahirwar,, “Review on Sources and Effect of Heavy Metal in Soil: Its Bioremediation,” *Int. J. Res. Applied, Nat. Soc. Sci.*, no. August, pp. 1–22, 2018, [Online]. Available: https://www.researchgate.net/publication/327551253

[55] M. A. Barakat, “New trends in removing heavy metals from industrial wastewater,” *Arab. J. Chem.*, vol. 4, no. 4, pp. 361–377, 2011, doi: 10.1016/j.arabjc.2010.07.019.

[56] I. Sherameti and A. Varma, *Soil Biology Series Editor Ajit Varma , Amity Institute of Microbial Sciences ,* vol. 19. 2010.

[57] Y. C. Sharma, V. Srivastava, V. K. Singh, S. N. Kaul, and C. H. Weng, “Nano-adsorbents for the removal of metallic pollutants from water and wastewater,” *Environ. Technol.*, vol. 30, no. 6, pp. 583–609, 2009, doi: 10.1080/09593330902838080.

[58] B. Yasemin and T. Zeki, “Removal of heavy metals from aqueous solution by sawdust adsorption,” *J. Environ. Sci.*, vol. 19, no. 2, pp. 160–166, 2007.

[59] B. Hastuti, Mudasir, D. Siswanta, and Triyono, “The Synthesis of Carboxymethyl Chitosan-Pectin Film as Adsorbent for Lead (II) Metal,” *Int. J. Chem. Eng. Appl.*, vol. 4, no. 6, pp. 349–353, 2013, doi: 10.7763/ijcea.2013.v4.323.

[60] C. P. A. Edited ByJacques Guertin, James A. Jacobs, *Chromium(VI) Handbook*, vol. 1st, no. 1. 2004. doi: 10.1016/S0048-9697(03)00451-0.

[61] J. D. Horn, *“Chromium, Physical and Chemical Properties,” in Encyclopedia of Metalloproteins,*. 2013.

[62] J. Barnhart, “Chromium chemistry and implications for environment,” *J. Soil Contam.*, vol. 6, no. 6, pp. 561–568, 2008.

[63] R. Saha, R. Nandi, and B. Saha, “Sources and toxicity of hexavalent chromium,” *J. Coord. Chem.*, vol. 64, no. 10, pp. 1782–1806, 2011, doi: 10.1080/00958972.2011.583646.

[64] W. E. Motzer, S. M. Testa, J. Guertin, and F. T. Stanin, *Independent Environmental Technical Evaluation Group, Chromium(VI) Hand Book,* 1st ed. New York,: CRC Press, 2005.

[65] A. Demirbaş, “Adsorption of Cr(III) and Cr(VI) ions from aqueous solutions on to modified lignin,” *Energy Sources*, vol. 27, no. 15, pp. 1449–1455, 2005, doi: 10.1080/009083190523352.

[66] A. Bedemo, B. S. Chandravanshi, and F. Zewge, “Removal of trivalent chromium from aqueous solution using aluminum oxide hydroxide,” *Springerplus*, vol. 5, no. 1, 2016, doi: 10.1186/s40064-016-2983-x.

[67] J. L. Gardea-Torresdey, K. Tiemann, V. Armendariz, L. Bess-Oberto, R. R.

Chianelli, J. Rios, J. G. Parsons, and G. Gamez, "Characterization of Cr(VI) binding and reduction to Cr(III) by the agricultural byproducts of Avena monida (Oat) biomass," *J. Hazard. Mater.*, vol. 80, no. 1–3, pp. 175–188, 2000, doi: 10.1016/S0304-3894(00)00301-0.

[68] Y. Shi, R. Shan, L. Lu, H. Yuan, H. Jiang, Y. Zhang, and Y. Chen, "High-efficiency removal of Cr(VI) by modified biochar derived from glue residue," *J. Clean. Prod.*, vol. 254, no. Vi, p. 119935, 2020, doi: 10.1016/j.jclepro.2019.119935.

[69] T. S. Anirudhan and P. G. Radhakrishnan, "Chromium(III) removal from water and wastewater using a carboxylate-functionalized cation exchanger prepared from a lignocellulosic residue," *J. Colloid Interface Sci.*, vol. 316, no. 2, pp. 268–276, 2007, doi: 10.1016/j.jcis.2007.08.051.

[70] S. Yang, L. Li, Z. Pei, C. Li, J. Lv, J. Xie, B. Wen, and S. Zhang, "Adsorption kinetics, isotherms and thermodynamics of Cr(III) on graphene oxide," *Colloids Surfaces A Physicochem. Eng. Asp.*, vol. 457, no. 1, pp. 100–106, 2014, doi: 10.1016/j.colsurfa.2014.05.062.

[71] M. D. Cohen, B. Kargacin, C. B. Klein, and M. Costa, "Mechanisms of chromium carcinogenicity and toxicity," *Crit. Rev. Toxicol.*, vol. 23, no. 3, pp. 255–281, 1993, doi: 10.3109/10408449309105012.

[72] X. F. Wang, M. L. Xing, Y. Shen, X. Zhu, and L. H. Xu, "Oral administration of Cr(VI) induced oxidative stress, DNA damage and apoptotic cell death in mice," *Toxicology*, vol. 228, no. 1, pp. 16–23, 2006, doi: 10.1016/j.tox.2006.08.005.

[73] S. Karamat, R. S. Rawat, T. L. Tan, P. Lee, S. V. Springham, Anis-Ur-Rehman, R. Chen, and H. D. Sun, "Exciting dilute magnetic semiconductor: Copper-doped ZnO," *J. Supercond. Nov. Magn.*, vol. 26, no. 1, pp. 187–195, 2013, doi: 10.1007/s10948-012-1710-2.

[74] L. Trakal, R. Šigut, H. Šillerová, D. Faturíková, and M. Komárek, "Copper removal from aqueous solution using biochar: Effect of chemical activation," *Arab. J. Chem.*, vol. 7, no. 1, pp. 43–52, 2014, doi: 10.1016/j.arabjc.2013.08.001.

[75] R. A. K. Rao and S. Ikram, "Sorption studies of Cu(II) on gooseberry fruit (emblica officinalis) and its removal from electroplating wastewater," *Desalination*, vol. 277, no. 1–3, pp. 390–398, 2011, doi: 10.1016/j.desal.2011.04.065.

[76] M. V. Subbaiah, Y. Vijaya, A. S. Reddy, G. Yuvaraja, and A. Krishnaiah, "Equilibrium, kinetic and thermodynamic studies on the biosorption of Cu(II) onto

Trametes versicolor biomass," *Desalination*, vol. 276, no. 1–3, pp. 310–316, 2011, doi: 10.1016/j.desal.2011.03.067.

[77] A. T. Paulino, F. A. S. Minasse, M. R. Guilherme, A. V. Reis, E. C. Muniz, and J. Nozaki, "Novel adsorbent based on silkworm chrysalides for removal of heavy metals from wastewaters," *J. Colloid Interface Sci.*, vol. 301, no. 2, pp. 479–487, 2006, doi: 10.1016/j.jcis.2006.05.032.

[78] C. A. Dyer, "As Endocrine-Disrupting Chemicals," no. 1, pp. 111–133.

[79] V. M. Nurchi and I. Villaescusa, "Agricultural biomasses as sorbents of some trace metals," *Coord. Chem. Rev.*, vol. 252, no. 10–11, pp. 1178–1188, 2008, doi: 10.1016/j.ccr.2007.09.023.

[80] C. E. Borba, R. Guirardello, E. A. Silva, M. T. Veit, and C. R. G. Tavares, "Removal of nickel(II) ions from aqueous solution by biosorption in a fixed bed column: Experimental and theoretical breakthrough curves," *Biochem. Eng. J.*, vol. 30, no. 2, pp. 184–191, 2006, doi: 10.1016/j.bej.2006.04.001.

[81] A. M. Florea and D. Büsselberg, "Occurrence, use and potential toxic effects of metals and metal compounds," *BioMetals*, vol. 19, no. 4, pp. 419–427, 2006, doi: 10.1007/s10534-005-4451-x.

[82] C. F. Carolin, P. S. Kumar, A. Saravanan, G. J. Joshiba, and M. Naushad, "Efficient techniques for the removal of toxic heavy metals from aquatic environment: A review," *J. Environ. Chem. Eng.*, vol. 5, no. 3, pp. 2782–2799, 2017, doi: 10.1016/j.jece.2017.05.029.

[83] N. P. Cheremisinoff, "Water Sterilization Technologies," *Handb. Water Wastewater Treat. Technol.*, pp. 446–495, 2002, doi: 10.1016/b978-075067498-0/50014-0.

[84] M. Visa, "Synthesis and characterization of new zeolite materials obtained from fly ash for heavy metals removal in advanced wastewater treatment," Powder Technology, vol. 294. Elsevier B.V., 2016. doi: 10.1016/j.powtec.2016.02.019.

[85] F. Renault, B. Sancey, P. M. Badot, and G. Crini, "Chitosan for coagulation/flocculation processes - An eco-friendly approach," *Eur. Polym. J.*, vol. 45, no. 5, pp. 1337–1348, 2009, doi: 10.1016/j.eurpolymj.2008.12.027.

[86] Q. Chang, M. Zhang, and J. Wang, "Removal of Cu^{2+} and turbidity from wastewater by mercaptoacetyl chitosan," *J. Hazard. Mater.*, vol. 169, no. 1–3, pp. 621–625, 2009, doi: 10.1016/j.jhazmat.2009.03.144.

[87] A. L. Bojic, D. Bojic, and T. Andjelkovic, “Removal of Cu^{2+} and Zn^{2+} from model wastewaters by spontaneous reduction-coagulation process in flow conditions,” *J. Hazard. Mater.*, vol. 168, no. 2–3, pp. 813–819, 2009, doi: 10.1016/j.jhazmat.2009.02.096.

[88] W. Tao, G. Chen, G. Zeng, M. Yan, A. Chen, Z. Guo, Z. Huang, K. He, L. Hu, and L. Wang, “Influence of silver nanoparticles on heavy metals of pore water in contaminated river sediments,” *Chemosphere*, vol. 162, pp. 117–124, 2016, doi: 10.1016/j.chemosphere.2016.07.043.

[89] T. Ahmad, K. Ahmad, and M. Alam, “Sustainable management of water treatment sludge through 3’R’ concept,” *J. Clean. Prod.*, vol. 124, pp. 1–13, 2016, doi: 10.1016/j.jclepro.2016.02.073.

[90] P. W. Wong, T. T. Teng, and N. A. R. Nik Norulaini, “Efficiency of the coagulation-flocculation method for the treatment of dye mixtures containing disperse and reactive dye,” *Water Qual. Res. J. Canada*, vol. 42, no. 1, pp. 54–62, 2007, doi: 10.2166/wqrj.2007.008.

[91] J. W. Lee, S. P. Choi, R. Thiruvenkatachari, W. G. Shim, and H. Moon, “Evaluation of the performance of adsorption and coagulation processes for the maximum removal of reactive dyes,” *Dye. Pigment.*, vol. 69, no. 3, pp. 196–203, 2006, doi: 10.1016/j.dyepig.2005.03.008.

[92] M. Bilal, J. Shah, T. Ashfaq, S. M. H. Gardazi, A. A. Tahir, A. Pervez, H. Haroon, and Q. Mahmood, “Waste biomass adsorbents for copper removal from industrial wastewater-A review,” *J. Hazard. Mater.*, vol. 263, pp. 322–333, 2013, doi: 10.1016/j.jhazmat.2013.07.071.

[93] T. M. Zewail and N. S. Yousef, “Kinetic study of heavy metal ions removal by ion exchange in batch conical air spouted bed,” *Alexandria Eng. J.*, vol. 54, no. 1, pp. 83–90, 2015, doi: 10.1016/j.aej.2014.11.008.

[94] T. A. Kurniawan, G. Y. S. Chan, W. H. Lo, and S. Babel, “Physico-chemical treatment techniques for wastewater laden with heavy metals,” *Chem. Eng. J.*, vol. 118, no. 1–2, pp. 83–98, 2006, doi: 10.1016/j.cej.2006.01.015.

[95] M. A. Hashim, S. Mukhopadhyay, J. N. Sahu, and B. Sengupta, “Remediation technologies for heavy metal contaminated groundwater,” *J. Environ. Manage.*, vol. 92, no. 10, pp. 2355–2388, 2011, doi: 10.1016/j.jenvman.2011.06.009.

[96] D. Feng, C. Aldrich, and H. Tan, “Treatment of acid mine water by use of heavy

metal precipitation and ion exchange," *Miner. Eng.*, vol. 13, no. 6, pp. 623–642, 2000, doi: 10.1016/S0892-6875(00)00045-5.

[97] D. Syam Babu and P. V. Nidheesh, "A review on electrochemical treatment of arsenic from aqueous medium," *Chem. Eng. Commun.*, vol. 208, no. 3, pp. 389–410, 2021, doi: 10.1080/00986445.2020.1715956.

[98] M. Kobya, U. Gebologlu, F. Ulu, S. Oncel, and E. Demirbas, "Removal of arsenic from drinking water by the electrocoagulation using Fe and Al electrodes," *Electrochim. Acta*, vol. 56, no. 14, pp. 5060–5070, 2011, doi: 10.1016/j.electacta.2011.03.086.

[99] M. Kobya, F. Ulu, U. Gebologlu, E. Demirbas, and M. S. Oncel, "Treatment of potable water containing low concentration of arsenic with electrocoagulation: Different connection modes and Fe-Al electrodes," *Sep. Purif. Technol.*, vol. 77, no. 3, pp. 283–293, 2011, doi: 10.1016/j.seppur.2010.12.018.

[100] E. Şık, E. Demirbas, A. Y. Goren, M. S. Oncel, and M. Kobya, "Arsenite and arsenate removals from groundwater by electrocoagulation using iron ball anodes: Influence of operating parameters," *J. Water Process Eng.*, vol. 18, no. May, pp. 83–91, 2017, doi: 10.1016/j.jwpe.2017.06.004.

[101] A. B. Ribeiro, E. P. Mateus, L. M. Ottosen, and G. Bech-Nielsen, "Electrodialytic removal of Cu, Cr, and As from chromated copper arsenate-treated timber waste," *Environ. Sci. Technol.*, vol. 34, no. 5, pp. 784–788, 2000, doi: 10.1021/es990442e.

[102] I. Ali, T. A. Khan, and M. Asim, "Removal of arsenic from water by electrocoagulation and electrodialysis techniques," *Sep. Purif. Rev.*, vol. 40, no. 1, pp. 25–42, 2011, doi: 10.1080/15422119.2011.542738.

[103] R. Molinari, T. Poerio, and P. Argurio, "Selective separation of copper(II) and nickel(II) from aqueous media using the complexation-ultrafiltration process," *Chemosphere*, vol. 70, no. 3, pp. 341–348, 2008, doi: 10.1016/j.chemosphere.2007.07.041.

[104] J. Landaburu-Aguirre, V. García, E. Pongrácz, and R. L. Keiski, "The removal of zinc from synthetic wastewaters by micellar-enhanced ultrafiltration: statistical design of experiments," *Desalination*, vol. 240, no. 1–3, pp. 262–269, 2009, doi: 10.1016/j.desal.2007.11.077.

[105] A. Kryvoruchko, L. Yurlova, and B. Kornilovich, "Purification of water containing heavy metals by chelating-enhanced ultrafiltration," *Desalination*, vol. 144, no. 1–3,

pp. 243–248, 2002, doi: 10.1016/S0011-9164(02)00319-3.

[106] A. W. Mohammad, Y. H. Teow, W. L. Ang, Y. T. Chung, D. L. Oatley-Radcliffe, and N. Hilal, "Nanofiltration membranes review: Recent advances and future prospects," *Desalination*, vol. 356, pp. 226–254, 2015, doi: 10.1016/j.desal.2014.10.043.

[107] S. S. Hosseini, E. Bringas, N. R. Tan, I. Ortiz, M. Ghahramani, and M. A. Alaei Shahmirzadi, "Recent progress in development of high performance polymeric membranes and materials for metal plating wastewater treatment: A review," *J. Water Process Eng.*, vol. 9, pp. 78–110, 2016, doi: 10.1016/j.jwpe.2015.11.005.

[108] M. Sultana, M. H. Rownok, M. Sabrin, M. H. Rahaman, and S. M. N. Alam, "A review on experimental chemically modified activated carbon to enhance dye and heavy metals adsorption," *Clean. Eng. Technol.*, vol. 6, no. December, p. 100382, 2022, doi: 10.1016/j.clet.2021.100382.

[109] J. Pan, R. Liu, and H. Tang, "Surface reaction of biomass and its biosorption for lead and copper ions," *J. Environ. Sci.*, vol. 19, no. 4, pp. 403–408, 2007.

[110] M. Tuzen, K. O. Saygi, C. Usta, and M. Soylak, "Pseudomonas aeruginosa immobilized multiwalled carbon nanotubes as biosorbent for heavy metal ions," *Bioresour. Technol.*, vol. 99, no. 6, pp. 1563–1570, 2008, doi: 10.1016/j.biortech.2007.04.013.

[111] C. Quintelas, Z. Rocha, B. Silva, B. Fonseca, H. Figueiredo, and T. Tavares, "Biosorptive performance of an Escherichia coli biofilm supported on zeolite NaY for the removal of Cr(VI), Cd(II), Fe(III) and Ni(II)," *Chem. Eng. J.*, vol. 152, no. 1, pp. 110–115, 2009, doi: 10.1016/j.cej.2009.03.039.

[112] H. A. Hegazi, "Removal of heavy metals from wastewater using agricultural and industrial wastes as adsorbents," *HBRC J.*, vol. 9, no. 3, pp. 276–282, 2013, doi: 10.1016/j.hbrcj.2013.08.004.

[113] E. I. Ugwu, O. Tursunov, D. Kodirov, L. M. Shaker, A. A. Al-Amiery, I. Yangibaeva, and F. Shavkarov, "Adsorption mechanisms for heavy metal removal using low cost adsorbents: A review," *IOP Conf. Ser. Earth Environ. Sci.*, vol. 614, no. 1, 2020, doi: 10.1088/1755-1315/614/1/012166.

[114] J. S. Kwon, S. T. Yun, J. H. Lee, S. O. Kim, and H. Y. Jo, "Removal of divalent heavy metals (Cd, Cu, Pb, and Zn) and arsenic(III) from aqueous solutions using scoria: Kinetics and equilibria of sorption," *J. Hazard. Mater.*, vol. 174, no. 1–3, pp.

307–313, 2010, doi: 10.1016/j.jhazmat.2009.09.052.

[115] S. K. R. Yadanaparthi, D. Graybill, and R. von Wandruszka, “Adsorbents for the removal of arsenic, cadmium, and lead from contaminated waters,” *J. Hazard. Mater.*, vol. 171, no. 1–3, pp. 1–15, 2009, doi: 10.1016/j.jhazmat.2009.05.103.

[116] A. Afkhami, T. Madrakian, Z. Karimi, and A. Amini, “Effect of treatment of carbon cloth with sodium hydroxide solution on its adsorption capacity for the adsorption of some cations,” *Colloids Surfaces A Physicochem. Eng. Asp.*, vol. 304, no. 1–3, pp. 36–40, 2007, doi: 10.1016/j.colsurfa.2007.04.029.

[117] Z. L. He, X. E. Yang, and P. J. Stoffella, “Trace elements in agroecosystems and impacts on the environment,” *J. Trace Elem. Med. Biol.*, vol. 19, no. 2–3, pp. 125–140, 2005, doi: 10.1016/j.jtemb.2005.02.010.

[118] P. J. M. Carrott, M. M. L. Ribeiro Carrott, and J. M. V. Nabais, “Influence of surface ionization on the adsorption of aqueous mercury chlorocomplexes by activated carbons,” *Carbon N. Y.*, vol. 36, no. 1–2, pp. 11–17, 1998, doi: 10.1016/S0008-6223(97)00145-0.

[119] M. Belhachemi and F. Addoun, “Adsorption of congo red onto activated carbons having different surface properties: Studies of kinetics and adsorption equilibrium,” *Desalin. Water Treat.*, vol. 37, no. 1–3, pp. 122–129, 2012, doi: 10.1080/19443994.2012.661263.

[120] D. Mohan, K. P. Singh, and V. K. Singh, “Trivalent chromium removal from wastewater using low cost activated carbon derived from agricultural waste material and activated carbon fabric cloth,” *J. Hazard. Mater.*, vol. 135, no. 1–3, pp. 280–295, 2006, doi: 10.1016/j.jhazmat.2005.11.075.

[121] R. Shahrokhi-Shahraki, C. Benally, M. G. El-Din, and J. Park, “High efficiency removal of heavy metals using tire-derived activated carbon vs commercial activated carbon: Insights into the adsorption mechanisms,” *Chemosphere*, vol. 264, p. 128455, 2021, doi: 10.1016/j.chemosphere.2020.128455.

[122] S. Mortazavian, A. Saber, J. Hong, J. H. Bae, D. Chun, N. Wong, D. Gerrity, J. Batista, K. J. Kim, and J. Moon, “Synthesis, characterization, and kinetic study of activated carbon modified by polysulfide rubber coating for aqueous hexavalent chromium removal,” *J. Ind. Eng. Chem.*, vol. 69, pp. 196–210, 2019, doi: 10.1016/j.jiec.2018.09.028.

[123] H. Patel, “Batch and continuous fixed bed adsorption of heavy metals removal

using activated charcoal from neem (Azadirachta indica) leaf powder," *Sci. Rep.*, vol. 10, no. 1, pp. 1–12, 2020, doi: 10.1038/s41598-020-72583-6.

[124] T. Bohli, A. Ouederni, N. Fiol, and I. Villaescusa, "Evaluation of an activated carbon from olive stones used as an adsorbent for heavy metal removal from aqueous phases," *Comptes Rendus Chim.*, vol. 18, no. 1, pp. 88–99, 2015, doi: 10.1016/j.crci.2014.05.009.

[125] M. Jain, M. Yadav, T. Kohout, M. Lahtinen, V. K. Garg, and M. Sillanpää, "Development of iron oxide/activated carbon nanoparticle composite for the removal of Cr(VI), Cu(II) and Cd(II) ions from aqueous solution," *Water Resour. Ind.*, vol. 20, no. Vi, pp. 54–74, 2018, doi: 10.1016/j.wri.2018.10.001.

[126] J. Pan, J. Jiang, and R. Xu, "Adsorption of Cr(III) from acidic solutions by crop straw derived biochars," *J. Environ. Sci. (China)*, vol. 25, no. 10, pp. 1957–1965, 2013, doi: 10.1016/S1001-0742(12)60305-2.

[127] R. A. K. Rao, F. Rehman, and M. Kashifuddin, "Removal of Cr(VI) from electroplating wastewater using fruit peel of Leechi (Litchi chinensis)," *Desalin. Water Treat.*, vol. 49, no. 1–3, pp. 136–146, 2012, doi: 10.1080/19443994.2012.708211.

[128] G. Musumba, C. Nakiguli, C. Lubanga, P. Mukasa, and E. Ntambi, "Adsorption of Lead (II) and Copper (II) Ions from Mono Synthetic Aqueous Solutions Using Bio-Char from Ficus natalensis Fruits," *J. Encapsulation Adsorpt. Sci.*, vol. 10, no. 04, pp. 71–84, 2020, doi: 10.4236/jeas.2020.104004.

[129] R. V. Hemavathy, P. S. Kumar, K. Kanmani, and N. Jahnavi, "Adsorptive separation of Cu(II) ions from aqueous medium using thermally/chemically treated Cassia fistula based biochar," *J. Clean. Prod.*, vol. 249, no. Ii, p. 119390, 2020, doi: 10.1016/j.jclepro.2019.119390.

[130] C. P. J. Isaac and A. Sivakumar, "Removal of lead and cadmium ions from water using Annona squamosa shell: Kinetic and equilibrium studies," *Desalin. Water Treat.*, vol. 51, no. 40–42, pp. 7700–7709, 2013, doi: 10.1080/19443994.2013.778218.

[131] E. Abu-Danso, S. Peräniemi, T. Leiviskä, T. Y. Kim, K. M. Tripathi, and A. Bhatnagar, "Synthesis of clay-cellulose biocomposite for the removal of toxic metal ions from aqueous medium," *J. Hazard. Mater.*, vol. 381, 2020, doi: 10.1016/j.jhazmat.2019.120871.

[132] S. Sobhanardakani, H. Parvizimosaed, and E. Olyaie, “Heavy metals removal from wastewaters using organic solid waste-rice husk,” *Environ. Sci. Pollut. Res.*, vol. 20, no. 8, pp. 5265–5271, 2013, doi: 10.1007/s11356-013-1516-1.

[133] W. Nakbanpote, P. Thiravetyan, and C. Kalambaheti, “Preconcentration of gold by rice husk ash,” *Miner. Eng.*, vol. 13, no. 4, pp. 391–400, 2000, doi: 10.1016/S0892-6875(00)00021-2.

[134] V. B. H. Dang, H. D. Doan, T. Dang-Vu, and A. Lohi, “Equilibrium and kinetics of biosorption of cadmium(II) and copper(II) ions by wheat straw,” *Bioresour. Technol.*, vol. 100, no. 1, pp. 211–219, 2009, doi: 10.1016/j.biortech.2008.05.031.

[135] U. Farooq Umar, M. A. Khan, M. Athar, and J. A. Kozinski, “Effect of modification of environmentally friendly biosorbent wheat (Triticum aestivum) on the biosorptive removal of cadmium(II) ions from aqueous solution,” *Chem. Eng. J.*, vol. 171, no. 2, pp. 400–410, 2011, doi: 10.1016/j.cej.2011.03.094.

[136] E. Pehlivan, T. Altun, and S. Parlayici, “Utilization of barley straws as biosorbents for Cu2+ and Pb2+ ions,” *J. Hazard. Mater.*, vol. 164, no. 2–3, pp. 982–986, 2009, doi: 10.1016/j.jhazmat.2008.08.115.

[137] M. Iqbal, A. Saeed, and S. I. Zafar, “FTIR spectrophotometry, kinetics and adsorption isotherms modeling, ion exchange, and EDX analysis for understanding the mechanism of Cd^{2+} and Pb^{2+} removal by mango peel waste,” *J. Hazard. Mater.*, vol. 164, no. 1, pp. 161–171, 2009, doi: 10.1016/j.jhazmat.2008.07.141.

[138] M. Iqbal, A. Saeed, and I. Kalim, “Characterization of adsorptive capacity and investigation of mechanism of Cu^{2+}, Ni^{2+} and Zn^{2+} adsorption on mango peel waste from constituted metal solution and genuine electroplating effluent,” *Sep. Sci. Technol.*, vol. 44, no. 15, pp. 3770–3791, 2009, doi: 10.1080/01496390903182305.

[139] M. R. Lasheen, N. S. Ammar, and H. S. Ibrahim, “Adsorption/desorption of Cd(II), Cu(II) and Pb(II) using chemically modified orange peel: Equilibrium and kinetic studies,” *Solid State Sci.*, vol. 14, no. 2, pp. 202–210, 2012, doi: 10.1016/j.solidstatesciences.2011.11.029.

[140] J. R. Memon, S. Q. Memon, M. I. Bhanger, G. Z. Memon, A. El-Turki, and G. C. Allen, “Characterization of banana peel by scanning electron microscopy and FT-IR spectroscopy and its use for cadmium removal,” *Colloids Surfaces B Biointerfaces*, vol. 66, no. 2, pp. 260–265, 2008, doi: 10.1016/j.colsurfb.2008.07.001.

[141] M. Aschale, F. Tsegaye, and M. Amde, “Potato peels as promising low-cost

adsorbent for the removal of lead, cadmium, chromium and copper from wastewater," *Desalin. Water Treat.*, vol. 222, pp. 405–415, 2021, doi: 10.5004/dwt.2021.27108.

[142] E. K. Guechi and O. Hamdaoui, "Evaluation of potato peel as a novel adsorbent for the removal of Cu(II) from aqueous solutions: equilibrium, kinetic, and thermodynamic studies," *Desalin. Water Treat.*, vol. 57, no. 23, pp. 10677–10688, 2016, doi: 10.1080/19443994.2015.1038739.

[143] D. Mohan and K. P. Singh, "Single- and multi-component adsorption of cadmium and zinc using activated carbon derived from bagasse - An agricultural waste," *Water Res.*, vol. 36, no. 9, pp. 2304–2318, 2002, doi: 10.1016/S0043-1354(01)00447-X.

[144] L. Zheng, C. Zhu, Z. Dang, H. Zhang, X. Yi, and C. Liu, "Preparation of cellulose derived from corn stalk and its application for cadmium ion adsorption from aqueous solution," *Carbohydr. Polym.*, vol. 90, no. 2, pp. 1008–1015, 2012, doi: 10.1016/j.carbpol.2012.06.035.

[145] M. Jalali and F. Aboulghazi, "Sunflower stalk, an agricultural waste, as an adsorbent for the removal of lead and cadmium from aqueous solutions," *J. Mater. Cycles Waste Manag.*, vol. 15, no. 4, pp. 548–555, 2013, doi: 10.1007/s10163-012-0096-3.

[146] P. S. Kumar, S. Ramalingam, V. Sathyaselvabala, S. D. Kirupha, A. Murugesan, and S. Sivanesan, "Removal of cadmium(II) from aqueous solution by agricultural waste cashew nut shell," *Korean J. Chem. Eng.*, vol. 29, no. 6, pp. 756–768, 2012, doi: 10.1007/s11814-011-0259-2.

[147] G. F. Coelho *et al.*, "Removal of Cd(II), Pb(II) and Cr(III) from water using modified residues of Anacardium occidentale L.," *Appl. Water Sci.*, vol. 8, no. 3, 2018, doi: 10.100concentrations0724-8.

[148] H. L. H. Chong, P. S. Chia, and M. N. Ahmad, "The adsorption of heavy metal by Bornean oil palm shell and its potential application as constructed wetland media," *Bioresour. Technol.*, vol. 130, pp. 181–186, 2013, doi: 10.1016/j.biortech.2012.11.136.

[149] F. Teshale, R. Karthikeyan, and O. Sahu, "Synthesized bioadsorbent from fish scale for chromium (III) removal," *Micron*, vol. 130, no. Iii, p. 102817, 2020, doi: 10.1016/j.micron.2019.102817.

[150] H. Aydin, Y. Bulut, and Ç. Yerlikaya, “Removal of copper (II) from aqueous solution by adsorption onto low-cost adsorbents,” *J. Environ. Manage.*, vol. 87, no. 1, pp. 37–45, 2008, doi: 10.1016/j.jenvman.2007.01.005.

[151] V. S. Munagapati, V. Yarramuthi, S. K. Nadavala, S. R. Alla, and K. Abburi, “Biosorption of Cu(II), Cd(II) and Pb(II) by Acacia leucocephala bark powder: Kinetics, equilibrium and thermodynamics,” *Chem. Eng. J.*, vol. 157, no. 2–3, pp. 357–365, 2010, doi: 10.1016/j.cej.2009.11.015.

[152] M. A. Hossain, H. H. Ngo, W. S. Guo, T. V. Nguyen, and S. Vigneswaran, “Performance of cabbage and cauliflower wastes for heavy metals removal,” *Desalin. Water Treat.*, vol. 52, no. 4–6, pp. 844–860, 2014, doi: 10.1080/19443994.2013.826322.

[153] B. Nasernejad, T. E. Zadeh, B. B. Pour, M. E. Bygi, and A. Zamani, “Camparison for biosorption modeling of heavy metals (Cr (III), Cu (II), Zn (II)) adsorption from wastewater by carrot residues,” *Process Biochem.*, vol. 40, no. 3–4, pp. 1319–1322, 2005, doi: 10.1016/j.procbio.2004.06.010.

[154] M. Horsfall, A. I. Spiff, and A. A. Abia, “Studies on the influence of mercaptoacetic acid (MAA) modification of cassava (Manihot sculenta Cranz) waste biomass on the adsorption of Cu^{2+} and Cd^{2+} from aqueous solution,” *Bull. Korean Chem. Soc.*, vol. 25, no. 7, pp. 969–976, 2004, doi: 10.5012/bkcs.2004.25.7.969.

[155] R. Chakraborty, R. Verma, A. Asthana, S. S. Vidya, and A. K. Singh, “Adsorption of hazardous chromium (VI) ions from aqueous solutions using modified sawdust: kinetics, isotherm and thermodynamic modelling,” *Int. J. Environ. Anal. Chem.*, vol. 101, no. 7, pp. 911–928, 2021, doi: 10.1080/03067319.2019.1673743.

[156] S. Q. Memon, N. Memon, S. W. Shah, M. Y. Khuhawar, and M. I. Bhanger, “Sawdust-A green and economical sorbent for the removal of cadmium (II) ions,” *J. Hazard. Mater.*, vol. 139, no. 1, pp. 116–121, 2007, doi: 10.1016/j.jhazmat.2006.06.013.

[157] L. Nouri, I. Ghodbane, O. Hamdaoui, and M. Chiha, “Batch sorption dynamics and equilibrium for the removal of cadmium ions from aqueous phase using wheat bran,” *J. Hazard. Mater.*, vol. 149, no. 1, pp. 115–125, 2007, doi: 10.1016/j.jhazmat.2007.03.055.

[158] K. Chojnacka, “Biosorption of Cr(III) ions by eggshells,” *J. Hazard. Mater.*, vol.

121, no. 1–3, pp. 167–173, 2005, doi: 10.1016/j.jhazmat.2005.02.004.

[159] M. Baláž, Z. Bujňáková, P. Baláž, A. Zorkovská, Z. Danková, and J. Briančin, "Adsorption of cadmium(II) on waste biomaterial," *J. Colloid Interface Sci.*, vol. 454, no. Ii, pp. 121–133, 2015, doi: 10.1016/j.jcis.2015.03.046.

[160] I. Ghorbel-Abid, K. Galai, and M. Trabelsi-Ayadi, "Retention of chromium (III) and cadmium (II) from aqueous solution by illitic clay as a low-cost adsorbent," *Desalination*, vol. 256, no. 1–3, pp. 190–195, 2010, doi: 10.1016/j.desal.2009.06.079.

[161] W. Zheng, X. Li, Q. Yang, G. Zeng, X. Shen, Y. Zhang, and J. Liu, "Adsorption of Cd(II) and Cu(II) from aqueous solution by carbonate hydroxylapatite derived from eggshell waste," *J. Hazard. Mater.*, vol. 147, no. 1–2, pp. 534–539, 2007, doi: 10.1016/j.jhazmat.2007.01.048.

[162] W. S. Wan Ngah, A. Kamari, S. Fatinathan, and P. W. Ng, "Adsorption of chromium from aqueous solution using chitosan beads," *Adsorption*, vol. 12, no. 4, pp. 249–257, 2006, doi: 10.1007/s10450-006-0501-0.

[163] A. Papandreou, C. J. Stournaras, and D. Panias, "Copper and cadmium adsorption on pellets made from fired coal fly ash," *J. Hazard. Mater.*, vol. 148, no. 3, pp. 538–547, 2007, doi: 10.1016/j.jhazmat.2007.03.020.

[164] M. H. Dehghani, D. Sanaei, I. Ali, and A. Bhatnagar, "Removal of chromium(VI) from aqueous solution using treated waste newspaper as a low-cost adsorbent: Kinetic modeling and isotherm studies," *J. Mol. Liq.*, vol. 215, pp. 671–679, 2016, doi: 10.1016/j.molliq.2015.12.057.

[165] K. S. Novoselov, V. I. Fal'Ko, L. Colombo, P. R. Gellert, M. G. Schwab, and K. Kim, "A roadmap for graphene," *Nature*, vol. 490, no. 7419, pp. 192–200, 2012, doi: 10.1038/nature11458.

[166] Z. Niu, L. Liu, L. Zhang, and X. Chen, "Porous graphene materials for water remediation," *Small*, vol. 10, no. 17, pp. 3434–3441, 2014, doi: 10.1002/smll.201400128.

[167] R. Wijaya, G. Andersan, S. Permatasari Santoso, and W. Irawaty, "Green Reduction of Graphene Oxide using Kaffir Lime Peel Extract (Citrus hystrix) and Its Application as Adsorbent for Methylene Blue," *Sci. Rep.*, vol. 10, no. 1, pp. 1–9, 2020, doi: 10.1038/s41598-020-57433-9.

[168] X. Yang, T. Zhou, B. Ren, A. Hursthouse, and Y. Zhang, "Removal of Mn (II) by

Sodium Alginate/Graphene Oxide Composite Double-Network Hydrogel Beads from Aqueous Solutions," *Sci. Rep.*, vol. 8, no. 1, pp. 1–16, 2018, doi: 10.1038/s41598-018-29133-y.

[169] R. Sitko, E. Turek, B. Zawisza, E. Malicka, E. Talik, J. Heimann, A. Gagor, B. Feist, and R. Wrzalik, "Adsorption of divalent metal ions from aqueous solutions using graphene oxide," *Dalt. Trans.*, vol. 42, no. 16, pp. 5682–5689, 2013, doi: 10.1039/c3dt33097d.

[170] S. Wang, H. Sun, H. M. Ang, and M. O. Tadé, "Adsorptive remediation of environmental pollutants using novel graphene-based nanomaterials," *Chem. Eng. J.*, vol. 226, pp. 336–347, 2013, doi: 10.1016/j.cej.2013.04.070.

[171] S. Pei and H. M. Cheng, "The reduction of graphene oxide," *Carbon N. Y.*, vol. 50, no. 9, pp. 3210–3228, 2012, doi: 10.1016/j.carbon.2011.11.010.

[172] L. Stobinski, B. Lesiak, A. Malolepszy, M. Mazurkiewicz, B. Mierzwa, J. Zemek, , P. Jiricek, and I. Bieloshapka, "Graphene oxide and reduced graphene oxide studied by the XRD, TEM and electron spectroscopy methods," *J. Electron Spectros. Relat. Phenomena*, vol. 195, pp. 145–154, 2014, doi: 10.1016/j.elspec.2014.07.003.

[173] D. C. Marcano, D. Kosynkin, J. M. Berlin, A. Sinitskii, Z. Sun, A. Slesarev, L. B. Alemany, W. Lu, and J. M. Tour, "Improved Synthesis of Graphene Oxide," *ACS Nano*, vol. 4, no. 8, pp. 4806–4814, 2010, doi:10.1021/nn1006368.

[174] C. Fu, G. Zhao, H. Zhang, and S. Li, "Evaluation and characterization of reduced graphene oxide nanosheets as anode materials for lithium-ion batteries," *Int. J. Electrochem. Sci.*, vol. 8, no. 5, pp. 6269–6280, 2013.

[175] S. Stankovich, D. Dikin, R. Piner, K. A. Kohlhaas, A. Kleinhammes, Y. Jia, Y. Wu, S. B. T. Nguyen, and R. Ruoff, "Synthesis of graphene-based nanosheets via chemical reduction of exfoliated graphite oxide," *Carbon N. Y.*, vol. 45, no. 7, pp. 1558–1565, 2007, doi: 10.1016/j.carbon.2007.02.034.

[176] W. Guoxiu, Y. Juan, P. Jinsoo, G. Xinglong, W. Bei, L.Hao, and Y. Jane, "Facile synthesis and characterization of graphene nanosheets," *J. Phys. Chem. C*, vol. 112, no. 22, pp. 8192–8195, 2008, doi: 10.1021/jp710931h.

[177] X. Mi, G. Huang, W. Xie, W. Wang, Y. Liu, and J. Gao, "Preparation of graphene oxide aerogel and its adsorption for Cu^{2+} ions," *Carbon N. Y.*, vol. 50, no. 13, pp. 4856–4864, 2012, doi: 10.1016/j.carbon.2012.06.013.

[178] K. S. Kim, Y. Zhao, H. Jang, S. Y. Lee, J. M. Kim, K. S. Kim, J. H. Ahn, P. Kim, J.

Y. Choi, and B. H. Hong, “Large-scale pattern growth of graphene films for stretchable transparent electrodes,” *Nature*, vol. 457, no. 7230, pp. 706–710, 2009, doi: 10.1038/nature07719.

[179] S. Wang, H. Sun, H. M. Ang, and M. O. Tadé, “Adsorptive remediation of environmental pollutants using novel graphene-based nanomaterials,” *Chem. Eng. J.*, vol. 226, no. June, pp. 336–347, 2013, doi: 10.1016/j.cej.2013.04.070.

[180] Z. Han, Z. Tang, S. Shen, B. Zhao, G. Zheng, and J. Yang, “Strengthening of Graphene Aerogels with Tunable Density and High,” pp. 1–6, 2014, doi: 10.1038/srep05025.

[181] W. Gao, M. Majumder, L. B. Alemany, T. N. Narayanan, M. A. Ibarra, B. K. Pradhan, and P. M. Ajayan, “Engineered Graphite Oxide Materials for Application in Water Purification,” *ACS Appl. Mater. Interfaces*, vol. 3, pp. 1821–1826, 2011. doi: 10.1021/am200300u

[182] K. Zhang, X. Wang, B. Sun, J. Zhen, and J. Wang, "Removal of cobalt ions from aqueous solution by an amination graphene oxide nanocomposite," *Journal of Hazardous Materials*, Elsevier B.V., 2014. doi: 10.1016/j.jhazmat.2014.01.031.

[183] Y. Lei, F. Chen, Y. Luo, and L. Zhang, “Synthesis of three-dimensional graphene oxide foam for the removal of heavy metal ions,” *Chem. Phys. Lett.*, vol. 593, pp. 122–127, 2014, doi: 10.1016/j.cplett.2013.12.066.

[184] B. Yu, J. Xu, J. Liu, S. Yang, J. Luo, and Q. Zhou, “Journal of Environmental Chemical Engineering Adsorption behavior of copper ions on graphene oxide – chitosan aerogel,” *Biochem. Pharmacol.*, pp. 1–7, 2013, doi: 10.1016/j.jece.2013.08.017.

[185] L. Chen, D. Zhao, S. Chen, X. Wang, and C. Chen, “One-step fabrication of amino functionalized magnetic graphene oxide composite for uranium (VI) removal” *J. Colloid Interface Sci.*, vol. 562, p. 618, 2020, doi: 10.1016/j.jcis.2019.11.020.

[186] D. F. Rodrigues, “polymer-based graphene oxide nanocomposite,” pp. 3789–3796, 2013, doi: 10.1039/c3ta01616a.

[187] D. Chen, H. Zhang, K. Yang, and H. Wang, “Functionalization of 4-aminothiophenol and 3-aminopropyltriethoxysilane with graphene oxide for potential dye and copper removal,” *J. Hazard. Mater.*, vol. 310, pp. 179–187, 2016, doi: 10.1016/j.jhazmat.2016.02.040.

[188] C. F. Chang, Q. D. Truong, and J. R. Chen, “Graphene sheets synthesized by ionic-

liquid-assisted electrolysis for application in water purification," *Appl. Surf. Sci.*, vol. 264, pp. 329–334, 2013, doi: 10.1016/j.apsusc.2012.10.022.

[189] W. Wu, Y. Yang, H. Zhou, T. Ye, Z. Huang, R. Liu, and Y. Kuang, "Highly efficient removal of Cu(II) from aqueous solution by using graphene oxide," *Water. Air. Soil Pollut.*, vol. 224, no. 1, 2013, doi: 10.1007/s11270-012-1372-5.

[190] F. Zhang, B. Wang, S. He, and R. Man, "Preparation of Graphene-Oxide/Polyamidoamine Dendrimers and Their Adsorption Properties toward Some Heavy Metal Ions," *J. Chem. Eng. Data*, vol. 59, no. 5, pp. 1719–1726, 2014, doi: 10.1021/je500219e.

[191] H. Wang, X. Yuan, Y. Wu, H. Huang, G. Zeng, Y. Liu, X. Wang, N. Lin, and Y. Qi, "Adsorption characteristics and behaviors of graphene oxide for Zn(II) removal from aqueous solution," *Appl. Surf. Sci.*, vol. 279, no. Ii, pp. 432–440, 2013, doi: 10.1016/j.apsusc.2013.04.133.

[192] R. L. White, C. M. White, H. Turgut, A. Massoud, and Z. R. Tian, "Comparative studies on copper adsorption by graphene oxide and functionalized graphene oxide nanoparticles," *J. Taiwan Inst. Chem. Eng.*, vol. 85, pp. 18–28, 2018, doi: 10.1016/j.jtice.2018.01.036.

[193] L. Chang, Y. Pu, P. Jing, Y. Cui, G. Zhang, S. Xu, B. Cao, J. Guo, F. Chen, and C. Qiao, "Magnetic core-shell MnFe2O4@TiO2 nanoparticles decorated on reduced graphene oxide as a novel adsorbent for the removal of ciprofloxacin and Cu(II) from water," *Appl. Surf. Sci.*, vol. 541, no. September, p. 148400, 2021, doi: 10.1016/j.apsusc.2020.148400.

[194] S. Ahmed, Fatema-Tuj-Zohra, M. M. Mahdi, D. M. Mahmudunnabi, T. R. Choudhury, M. Z. Alam, and M. Nurnabi, "Synthesis and characterization of graphene oxide for removal of Cr(III) from tannery effluent," *Desalin. Water Treat.*, vol. 244, pp. 201–211, 2021, doi: 10.5004/dwt.2021.27895.

[195] A. Homayouni, M. R. Ehsani, A. Azizi, M. S. Yarmand, and S. H. Razavi, "Effect of lecithin and calcium chloride solution on the microencapsulation process yield of calcium alginate beads," *Iran. Polym. J. (English Ed.*, vol. 16, no. 9, pp. 597–606, 2007.

[196] Y. Zhu, S. Murali, W. Cai, X. Li, J, Suk, J. R. Potts, and R. S. Ruoff, "Graphene and graphene oxide: Synthesis, properties, and applications," *Adv. Mater.*, vol. 22, no. 35, pp. 3906–3924, 2010, doi: 10.1002/adma.201001068.

[197] Y. Li, Q. Du, T. Liu, X. Peng, J. Wang, J. Sun, Y. Wang, S. Wu, Z. Wang, Y. Xia, and L. Xia, "Comparative study of methylene blue dye adsorption onto activated carbon, graphene oxide, and carbon nanotubes," *Chem. Eng. Res. Des.*, vol. 91, no. 2, pp. 361–368, 2013, doi: 10.1016/j.cherd.2012.07.007.

[198] G. Uslu and M. Tanyol, "Equilibrium and thermodynamic parameters of single and binary mixture biosorption of lead (II) and copper (II) ions onto Pseudomonas putida: Effect of temperature," *J. Hazard. Mater.*, vol. 135, no. 1–3, pp. 87–93, 2006, doi: 10.1016/j.jhazmat.2005.11.029.

[199] M. Z. Iqbal and A. A. Abdala, "Thermally reduced graphene: Synthesis, characterization and dye removal applications," *RSC Adv.*, vol. 3, no. 46, pp. 24455–24464, 2013, doi: 10.1039/c3ra43914c.

[200] S. Kebede, "Groundwater in Ethiopia: Features, numbers and opportunities," *Groundw. Ethiop. Featur. Numbers Oppor.*, pp. 1–285, 2013, doi: 10.1007/978-3-642-30391-3.

[201] A. Siddique, A. K. Nayak, and J. Singh, "Synthesis of $FeCl_3$-activated carbon derived from waste Citrus limetta peels for removal of fluoride: An eco-friendly approach for the treatment of groundwater and bio-waste collectively," *Groundw. Sustain. Dev.*, vol. 10, no. January, p. 100339, 2020, doi: 10.1016/j.gsd.2020.100339.

[202] W. Chen, L. Yan, and P. R. Bangal, "JPC1011419885-NaHSO3-GO還元.pdf," pp. 19885–19890, 2010.

[203] C. Valencia, C. H. Valencia, F. Zuluaga, M. E. Valencia, J. H. Mina, and C. D. Grande-Tovar, "Synthesis and application of scaffolds of chitosan-graphene oxide by the freeze-drying method for tissue regeneration," *Molecules*, vol. 23, no. 10, 2018, doi: 10.3390/molecules23102651.

[204] D. M. Mahmudunnabi, M. Z. Alam, and M. Nurnabi, "Removal of TURQUOISE GN from aqueous solution using graphene oxide," *Desalin. Water Treat.*, vol. 174, pp. 389–399, 2020, doi: 10.5004/dwt.2020.24867.

[205] J. Wang and B. Chen, "Adsorption and coadsorption of organic pollutants and a heavy metal by graphene oxide and reduced graphene materials," *Chem. Eng. J.*, vol. 281, pp. 379–388, 2015, doi: 10.1016/j.cej.2015.06.102.

[206] P. Tan, J. Sun, Y. Hu, Z. Fang, Q. Bi, Y. Chen, and J. Cheng, "Adsorption of Cu^{2+}, Cd^{2+} and Ni^{2+} from aqueous single metal solutions on graphene oxide membranes,"

J. Hazard. Mater., vol. 297, pp. 251–260, 2015, doi: 10.1016/j.jhazmat.2015.04.068.

[207] W. Chen, L. Yan, and P. R. Bangal, "Preparation of graphene by the rapid and mild thermal reduction of graphene oxide induced by microwaves," *Carbon N. Y.*, vol. 48, no. 4, pp. 1146–1152, 2010, doi: 10.1016/j.carbon.2009.11.037.

[208] J. I. Paredes, S. Villar-Rodil, P. Solís-Fernández, A. Martínez-Alonso, and J. M. D. Tascón, "Atomic force and scanning tunneling microscopy imaging of graphene nanosheets derived from graphite oxide," *Langmuir*, vol. 25, no. 10, pp. 5957–5968, 2009, doi: 10.1021/la804216z.

[209] Y. Fei, Y. Li, S. Han, and J. Ma, "Adsorptive removal of ciprofloxacin by sodium alginate/graphene oxide composite beads from aqueous solution," *J. Colloid Interface Sci.*, vol. 484, pp. 196–204, 2016, doi: 10.1016/j.jcis.2016.08.068.

[210] R. Jabari, M. Jahanshahi, A. Rashidi, and A. Asghar, "Applied Surface Science Synthesize and characterization of graphene nanosheets with high surface area and nano-porous structure," *Appl. Surf. Sci.*, vol. 276, pp. 672–681, 2013, doi: 10.1016/j.apsusc.2013.03.152.

[211] S. Zhang, H. Wang, J. Liu, and C. Bao, "Measuring the specific surface area of monolayer graphene oxide in water," *Mater. Lett.*, p. 127098, 2019, doi: 10.1016/j.matlet.2019.127098.

[212] I. Sengupta, S. Chakraborty, and M. Talukdar, "Thermal reduction of graphene oxide : How temperature in fl uences purity," 2018, doi: 10.1557/jmr.2018.338.

[213] M. Rafatullah, O. Sulaiman, R. Hashim, and A. Ahmad, "Adsorption of copper (II), chromium (III), nickel (II) and lead (II) ions from aqueous solutions by meranti sawdust," *J. Hazard. Mater.*, vol. 170, no. 2–3, pp. 969–977, 2009, doi: 10.1016/j.jhazmat.2009.05.066.

[214] S. Lv, Q. Zhou, Y. Li, Y. He, and H. Zhao, "Tanning performance and environmental effects of nanosized graphene oxide tanning agent," *Clean Technol. Environ. Policy*, no. Table 1, 2016, doi: 10.1007/s10098-016-1128-9.

[215] R. Rojas, "Effect of particle size on copper removal by layered double hydroxides," *Chem. Eng. J.*, no. June, 2016, doi: 10.1016/j.cej.2016.06.007.

[216] S. Z. N. Ahmad, W. N. Wan Salleh, A. F. Ismail, N. Yusof, M. Z. Mohd Yusop, and F. Aziz, "Adsorptive removal of heavy metal ions using graphene-based nanomaterials: Toxicity, roles of functional groups and mechanisms,"

Chemosphere, vol. 248, p. 126008, 2020, doi: 10.1016/j.chemosphere.2020.126008.

[217] B. I. Olu-owolabi, P. N. Diagboya, and W. C. Ebaddan, "Mechanism of Pb^{2+} removal from aqueous solution using a nonliving moss biomass," *Chem. Eng. J.*, vol. 195–196, pp. 270–275, 2012, doi: 10.1016/j.cej.2012.05.004.

[218] R. P. Mohubedu, P. N. E. Diagboya, C. Y. Abasi, E. D. Dikio, and F. Mtunzi, "Magnetic valorization of biomass and biochar of a typical plant nuisance for toxic metals contaminated water treatment," *J. Clean. Prod.*, 2018, doi: 10.1016/j.jclepro.2018.10.215.

[219] P. N. Diagboya, E. D. Dikio, and E. D. Dikio, "Accepted Manuscript," 2018, doi: 10.1016/j.eti.2018.01.002.

[220] J. Torres, P. Santos, C. Ferrari, C. Kremer, and E. Kremerv, "Solution Chemistry of Arsenic Anions in the Presence of Metal Cations," *J. Solution Chem.*, 2017, doi: 10.1007/s10953-017-0699-3.

[221] P. N. Diagboya and E. D. Dikio, "Scavenging of aqueous toxic organic and inorganic cations using novel facile magneto-carbon black-clay composite adsorbent," *J. Clean. Prod.*, vol. 180, pp. 71–80, 2018, doi: 10.1016/j.jclepro.2018.01.166.

[222] Y. Abshirini, R. Foroutan, and H. Esmaeili, "Cr(VI) removal from aqueous solution using activated carbon prepared from Ziziphus spina-christi leaf," *Mater. Res. Express*, vol. 6, no. 4, 2019, doi: 10.1088/2053-1591/aafb45.

[223] H. Patel, "Fixed-bed column adsorption study: a comprehensive review," *Appl. Water Sci.*, vol. 9, no. 3, 2019, doi: 10.1007/s13201-019-0927-7.

[224] S. Raghav and D. Kumar, "Adsorption Equilibrium, Kinetics, and Thermodynamic Studies of Fluoride Adsorbed by Tetrametallic Oxide Adsorbent," *J. Chem. Eng. Data*, vol. 63, no. 5, pp. 1682–1697, 2018, doi: 10.1021/acs.jced.8b00024.

[225] T. Bohli, A. Ouederni, and I. Villaescusa, "Simultaneous adsorption behavior of heavy metals onto microporous olive stones activated carbon: analysis of metal interactions," *Euro-Mediterranean J. Environ. Integr.*, vol. 2, no. 1, 2017, doi: 10.1007/s41207-017-0030-0.

[226] P. R. Sera, P. N. Diagboya, S. O. Akpotu, F. M. Mtunzi, and T. B. Chokwe, "Bioresource Technology Reports Potential of valourized Moringa oleifera seed waste modified with activated carbon for toxic metals decontamination in conventional water treatment," *Bioresour. Technol. Reports*, vol. 16, no. November,

p. 100881, 2021, doi: 10.1016/j.biteb.2021.100881.

[227] M. K. Rai, B. Giri, Y. Nath, H. Bajaj, S. Soni, R. P. Singh, R. S. Singh, and B. N. Rai, "Adsorption of hexavalent chromium from aqueous solution by activated carbon prepared from almond shell: Kinetics, equilibrium and thermodynamics study," *J. Water Supply Res. Technol. - AQUA*, vol. 67, no. 8, pp. 724–737, 2018, doi: 10.2166/aqua.2018.047.

[228] W. J. Weber, P. M. Mcginley, and E. K. Lynn, "A Distributed Reactivity Model for Sorption by Soils and Sediments. 1. Conceptual Basis and Equilibrium Assessments," *Envlron. Sci. Technol.*, vol. 26, no. 10, pp. 1955–1962, 1992.

[229] I. Ali, A. Basheer, X. Y. Mbianda, A. Burakov, E. Galunin, I. Burakova, E. Mkrtchyan, A. Tkachev, and V. Grachev, "Graphene based adsorbents for remediation of noxious pollutants from wastewater," *Environ. Int.*, vol. 127, no. January, pp. 160–180, 2019, doi: 10.1016/j.envint.2019.03.029.

[230] A. Tajiki and M. Abdouss, "Synthesis and characterization of graphene oxide nano-sheets for effective removal of copper phthalocyanine from aqueous media," *Iran. J. Chem. Chem. Eng.*, vol. 36, no. 4, pp. 1–9, 2017.

[231] P. D. Alka Shukla, Yu-Hui Zhang and S. S. S. J. L. Margrave, "The role of sawdust in the removal of unwanted materials from water," *J. Hazard. Mater.*, vol. 95, no. 1–2, pp. 137–152, 2002, doi: 10.1016/s0304-3894(02)00089-4.